To the Graduate Council:

I am submitting herewith a dissertation written by Stephen Edward Stasko entitled "A Dynamic Study of an Earth Orbiting Tether Propulsion System." I have examined the final electronic copy of this dissertation for form and content and recommend that it be accepted in partial fulfillment of the requirements for the degree of Doctor of Philosophy, with a major in Aerospace Engineering.

Gary Flandro

Major Professor

We have read this dissertation
and recommend its acceptance:

Joseph Majdalani

John Steinhoff

Kenneth Kimble

Acceptance for the Council:

Linda Painter

Interim Dean of Graduate Studies

(Original signatures are on file with official student records.)

A DYNAMIC STUDY OF AN EARTH ORBITING TETHER PROPULSION SYSTEM

A Dissertation
Presented for the
Doctor of Philosophy
Degree
The University of Tennessee, Knoxville

Stephen Edward Stasko
May 2007

Copyright © 2007 by Stephen Edward Stasko
All rights reserved.

Dedication

To my loving wife,

Molly

Acknowledments

I would like to thank my advisor, Dr. Gary Flandro, for the guidance and encouragement he provided throughout my graduate education at UTSI. I am very privileged to have had the opportunity to learn from such an insightful and inspiring teacher. I would like also to extend my appreciation to the other members of my committee, Dr. Jopseph Majdalani, Dr. John Steinhoff, and Dr. Kenneth Kimble, whose suggestions and input helped greatly in the preparation of this dissertation. I would also like to express my gratitude for all the support I received from my family and friends. And finally I am grateful to my wife for her patience and love, without which I could not have accomplished this work.

Abstract

Commercial expansion beyond Earth orbit demands efficient, low cost and regular access to space that is not given by current launch systems. An alternative to rocketry has been proposed in the use of tethers as a method of in-space propulsion. One possible implementation of tether propulsion involves the use of a long, vertically oriented tether orbiting the Earth. A suborbital launch vehicle will deliver a payload to the tether's lower tip, which will then be carried up its length by an elevator car to the upper tip, where the payload is released on a transfer orbit. The orbiting space elevator represents a reusable second stage of a launch system designed to place payloads in high Earth orbit or trans-lunar trajectories.

This study investigates several dynamics problems encountered in an Earth orbiting tether propulsion system. In addition to calculating the structural requirements for the tether to safely bear the payload mass, several analytical estimation methods of the tether's orbital response to loading have been developed and compared to previous studies. A detailed mathematical simulation of the tether's orbital stability has been created, accounting for natural perturbations to the tether's orbit. With the dynamic simulation of the elevator's orbit, predictions of the total tether mass required to handle a payload with out degrading its orbit have been quantified.

The performance required by the suborbital launch vehicle's operation has also been examined. Minimum propellant trajectories to the elevator's lower tip are found using a Hamiltonian based trajectory optimization routine. The launch vehicle maneuvering requirements needed for rendezvous with the orbiting elevator have also

been explored. The margins of performance needed for a launch vehicle to deliver a payload to the elevator lower tip have been calculated to be roughly equivalent to a single stage to orbit mission profile.

The usefulness of the tether within the context of a trans-lunar transportation system has also been investigated. It has been shown that elevator-based transit to the Moon offers significant savings in Δv over a traditional rocket-based transportation scheme.

Table of Contents

Chapter			Page
1.	**Introduction**		1
	1.1	The Need for a Frontier	1
	1.2	Economics of Spaceflight	11
		1.2.1 The Space Shuttle	15
	1.3	Alternatives to Rocketry	18
2.	**History of Space Tether Propulsion**		26
3.	**Elevator Sizing**		37
	3.1	Stepwise Integration Method	37
	3.2	Alternate Method of Determining Elevator Cross Sectional Area	44
	3.3	Previous Methods of Determining Response to Loading	49
	3.4	New Methods of Estimating Orbital Response to Loading	55
		3.4.1 Shifting Center of Gravity Method	55
		3.4.2 CG Shift with Momentum Conservation Methods	59
	3.5	Elevator Sizing Results	60
4.	**Dynamic Tether Simulation**		65
	4.1	Previous Efforts	65
	4.2	Problem Description	66
		4.2.1 Definition of Coordinate Systems	67
	4.3	Tether Segment Equations of Motion	69
	4.4	Forces Acting Upon the Tether	73

4.4.1 Earth's Gravity 74

4.4.2 Tension 75

4.4.3 Atmospheric Drag 82

4.4.4 Earth Oblateness 86

4.4.5 Electrodynamic Propulsion 88

4.5 Method of Solution 93

4.6 Dynamic Tether Simulation Results 95

5. Launch Vehicle Ascent Analysis 105

5.1 Suborbital Ascent Requirements 105

5.2 History of Trajectory Optimization 106

5.3 Equations of Motion for an Ascending Spacecraft 109

5.4 Pontryagin Maximum Principle 117

5.5 Trajectory Optimization 119

5.6 Ascent Results 128

6. Rendezvous Analysis 137

6.1 Equations of Relative Motion 137

6.2 Solution Method 141

6.3 Rendezvous Analysis Results 145

6.3.1 Launch Vehicle Relative Motion 145

6.3.2 Launch Vehicle Hovering 148

6.3.3 Terminal Rendezvous 151

6.3.4 Total Rendezvous Requirements 154

7. Elevator Launched Trajectories 160

7.1 Lunar Destination 160

7.2 Trajectories to Lunar Orbit 163

7.2.1 Patched Conic Approximation 164

7.3 Trajectories to L1 Point 172

7.4 Trajectories to Lunar Elevator 173

7.5 Trajectory Results 173

7.5.1 Lunar Orbit Results 173

7.5.2 L1 Results 177

7.5.3 Lunar Elevator Results 177

7.5.4 Comparison of Trajectory Results 181

8. Summary and Recommendations for Further Study 185

List of References 191

Appendices 198

Appendix A: Dynamic Tether Simulation Code 199

Appendix B: Ascent Optimization Code 231

Appendix C: Rendezvous Code 241

Vita 250

List of Tables

Table	Page
Table 1.1: Yearly Production of the Mark II Miner	10
Table 1.2: LEO Launch Costs	12
Table 1.3: GTO Launch Costs	13
Table 3.1: Tether Material Properties	38
Table 4.1: Characteristics of Three Selected Elevators with 2000 km Center of Gravity Altitude	98
Table 4.2: Tether Mass Comparison	98
Table 5.1: Boundary Value Conditions for Ascent Trajectory Optimization	125
Table 5.2: Comparison of Different Launch Trajectories	129
Table 6.1: Boundary Value Conditions for Rendezvous Problem	144
Table 7.1: Apollo 16 Δv Budget	162
Table 7.2: Selected Tether Trajectory Data for Lunar Orbit Destination	174
Table 7.3: Selected Tether Trajectory Data for L1 Destination	179
Table 7.4: Selected Tether Trajectory Data for Lunar Elevator Destination	180
Table 7.5: Minimum Total Δv to the Lunar Surface for Selected Tethers	183
Table 7.6: Maximum Total Flight Time from Departure to the Lunar Surface for Selected Tethers	183
Table 8.1: Δv Budget for a Tether Assisted Mission to Lunar Orbit Compared to the Apollo Reference Mission	190

Table 8.2: Flight Time for a Tether Assisted Mission to Lunar Orbit 190
Compared to the Apollo Reference Mission

List of Figures

Figure	Page
Figure 1.1: Earth Orbiting Space Elevator	22
Figure 2.1: Momentum eXchange Electrodynamic Reboost System	33
Figure 3.1: Tether Upper and Lower Tip Velocities	43
Figure 3.2: Tether Cross Sectional Area versus Length	48
Figure 3.3: Tether Mass versus Length (Zubrin)	52
Figure 3.4: Tether Mass versus Length (Bridge to Space)	54
Figure 3.5: Tether Mass versus Length (CG Shift)	58
Figure 3.6: Tether Mass versus Length (CG Shift with Momentum Conservation)	61
Figure 3.7: Mass Ratio versus Handoff Velocity for All Estimation Methods	63
Figure 3.8: Mass Ratio versus Handoff Velocity	63
Figure 4.1: Earth Centric Cartesian Coordinate Systems	68
Figure 4.2: Earth-Centric Polar Coordinate System	70
Figure 4.3: Segment Centered Coordinate System	70
Figure 4.4: Relation Between Earth-Centric and Segment-Centric Coordinate Systems	80
Figure 4.5: Atmospheric Density versus Altitude	85
Figure 4.6: Elevator Mass versus Center of Gravity Altitude	96
Figure 4.7: Lower Tip Altitude versus Time for 200 km Handoff Altitude	100
Figure 4.8: Lower Tip Altitude versus Time for 300 km Handoff Altitude	100

Figure 4.9: Lower Tip Altitude versus Time for 400 km Handoff Altitude 101

Figure 4.10: Lower Tip Relative Position versus Time for 200 km Handoff Altitude 103

Figure 4.11: Lower Tip Relative Position versus Time for 300 km Handoff Altitude 103

Figure 4.12: Lower Tip Relative Position Versus Time for 400 km Handoff Altitude 104

Figure 5.1: Launch Vehicle Velocity and Energy versus Tether Length 107

Figure 5.2: Free Body Diagram of an Ascending Spacecraft 110

Figure 5.3: Powered Trajectory for Launch to 200 km Circular Orbit 131

Figure 5.4: Powered Trajectory for Launch to 200 km Apogee Altitude 131

Figure 5.5: Powered Trajectory for Launch to 300 km Apogee Altitude 132

Figure 5.6: Powered Trajectory for Launch to 400 km Apogee Altitude 132

Figure 5.7: Control Angle History for Launch to 200 km Circular Orbit 134

Figure 5.8: Control Angle History for Launch to 200 km Apogee Altitude 134

Figure 5.9: Control Angle History for Launch to 300 km Apogee Altitude 135

Figure 5.10: Control Angle History for Launch to 400 km Apogee Altitude 135

Figure 6.1: Rendezvous Coordinate System Diagram 138

Figure 6.2: Relative Motion Between the Launch Vehicle and 200 km Lower Tip 146

Figure 6.3: Relative Motion Between the Launch Vehicle and 300 km Lower Tip 146

Figure 6.4: Relative Motion Between the Launch Vehicle and 400 km Lower Tip 147

Figure 6.5: Δv versus Time for Launch Vehicle Hovering at the 200 km Lower Tip 149

Figure 6.6: Δv versus Time for Launch Vehicle Hovering at the 300 km Lower Tip 149

Figure 6.7: Δv versus Time for Launch Vehicle Hovering at the 400 km Lower Tip 150

Figure 6.8: Δv versus Time Until Rendezvous at the 200 km Lower Tip 152

Figure 6.9: Minimum Δv versus Rendezvous Error Time at the 200 km Lower Tip 152

Figure 6.10: Minimum Δv versus Rendezvous Error Time at the 300 km Lower Tip 153

Figure 6.11: Minimum Δv versus Rendezvous Error Time at the 400 km Lower Tip 153

Figure 6.12: Total Δv versus Rendezvous Error Time at the 200 km Lower Tip at 0° Inclination 155

Figure 6.13: Total Δv versus Rendezvous Error Time at the 200 km Lower Tip at 5° Inclination 155

Figure 6.14: Total Δv versus Rendezvous Error Time at the 300 km Lower Tip at 0° Inclination 157

Figure 6.15: Total Δv versus Rendezvous Error Time at the 300 km Lower Tip at 5° Inclination 157

Figure 6.16: Total Δv versus Rendezvous Error Time at the 400 km Lower Tip at 0° Inclination 158

Figure 6.17: Total Δv versus Rendezvous Error Time at the 400 km Lower Tip at 5° Inclination 158

Figure 7.1: Trans-lunar Patched Conic Trajectory 165

Figure 7.2: Entry Point into Lunar Sphere of Influence 167

Figure 7.3: Flight Time versus Departure Δv for Lunar Orbit Trajectories 176

Figure 7.4: Inclination Change Δv versus Departure Δv for Lunar Orbit Trajectories 178

Figure 7.5: Lunar Orbit Circularization Δv versus Departure Δv 178

Figure 7.6: Flight Time versus Departure Δv for L1 Trajectories 179

Figure 7.7: L1 Rendezvous Δv versus Departure Δv 180

Figure 7.8: Flight Time versus Departure Δv for Lunar Elevator Trajectories 182

Figure 7.9: Lunar Elevator Rendezvous Δv versus Departure Δv 182

Nomenclature

A,B,C	Geocentric equatorial Cartesian coordinate system
a	Acceleration
A_f	Facial Area
A_x	Cross sectional area
alt	Altitude
B	Magnetic field intensity
BEO	Beyond Earth Orbit
C	Kepler Area Constant
C_d	Coefficient of Drag
CG	Center of Gravity
Dia	Diameter
Dist	Distance
e	Eccentricity
E	Young's Modulus
EA	Eccentric Anomaly
F	Force
f_i	State equations
f_s	Factor of safety
g	Acceleration due to gravity
GEO	Geostationary orbit
GM	Gravitational constant
GSO	Geosynchronous orbit
GTO	Geostationary transfer orbit
H	Hamiltonian
HASTOL	Hypersonic Airplane Space Tether Orbital Launch
HEA	Hyperbolic Eccentric Anomaly
h	Angular momentum
i	Orbital inclination
I	Electrical current
ISS	International Space Station
J	Cost Function
J_2	Earth oblateness harmonic coefficient
l	Length
l_{nat}	Natural length
LEO	Low Earth Orbit
LOI	Lunar Orbit Insertion
K	Constant of integration
k	Spring constant
m	Mass
$\dot{m}$	Mass flow rate
$\overline{\mathbf{m}}$	Magnetic dipole moment
MXER	Momentum eXchange Electrodynamic Reboost

n	Summation number
NASA	National Aeronautics and Space Administration
OEC	Orbital Energy Constant
p	Pressure
po	Parameter of the orbit
q	Generalized coordinate
Q	Generalized forces
sa	Semi-major axis
r, θ, φ	Tether orbital plane centered spherical coordinate system
SPS	Solar Power Satellite
SSTO	Single Stage to Orbit
t	Time
T	Kinetic energy
Temp	Temperature
Tex	Temperature of the exosphere
TLI	Trans-lunar injection
TSS	Tethered satellite system
u	Argument of the latitude
v	Velocity
x	State vector
x_i	State variable
x,y,z	Tether segment centered Cartesian coordinate system
X,Y,Z	Geocentric tether orbital plane Cartesian coordinate system
z_i	Costate variable
α	Engine thrust control angle
β	Flight path angle
γ	Geocentric phase angle
Δ	Difference operator
δ	Complementary angle of lunar-centric flight path angle
ε	Strain
λ	Lunar-centric phase angle
μ_o	Permeability of free space
π	Ratio of a circle's circumference to its diameter
ρ	Density
σ	Tensile Stress
Φ	Gravitational potential function
ω	Angular velocity

Subscripts

apo	Apogee
atm	Atmospheric property
c	Centrifugal
cg	Center of gravity property

cgL	Center of gravity of tether with attached payload
con	Electrical conductor
cut	Engine cutoff property
D	Drag
E	Earth property
ED	Electrodynamic
g	Gravity
i	Generalized coordinates
j	Tether segment number
L	Loaded
L1	Lagrange point 1
le	Tether lower end
LV	Launch vehicle property
m	Moon
mo	Moon's orbit
p	Payload property
peri	Perigee
Rel	Relative
r	Radial direction
seg	Segment property
SOI	Sphere of Influence
stat	Central power Station property
T	Tether property
Ten	Tension
Th	Thrust
total	Payload and tether combined property
ue	Tether upper end
UL	Unloaded
v_r	Radial velocity
v_θ	Tangential velocity
x	x direction in tether segment centered coordinate system
y	y direction in tether segment centered coordinate system
z	z direction in tether segment centered coordinate system
θ	Tangential direction
φ	Direction perpendicular to orbital plane

Superscripts

*	Dimensional variable
0	Initial state
f	Final state
^	Unit vector

Chapter 1

Introduction

1.1 The Need for a Frontier

Throughout the history of the space age, humanity has possessed grandiose dreams of expanding beyond the Earth. The father of modern rocketry, Konstantin Tsiolkovsky, applying the theories he developed on the use of liquid rockets for space propulsion, outlined a sixteen step strategy in his 1926 work "Plan of Space Exploration" to expand the human presence into the solar system and beyond [1]. The first several steps of his plan are mainly demonstrations of space-related technologies that have already been accomplished, such as rocket powered aircraft, orbital space flight, and space suits enabling extravehicular activity. The use of solar radiation to grow plants in space to provide both food and artificial atmosphere, steps nine and eleven, have yet to be proven on a large scale; however, the idea of utilizing space-based resources has been since considered an integral enabling technology for long duration human presence in space independent of the Earth [2]. Interestingly, step fourteen of his plan, "Achievement of individual and social perfection", comes after steps calling for the colonization of the asteroid belt and the outer solar system, illustrating that Tsiolkovsky obviously would not agree with the popular modern idea of "Why spend money on space when we have enough problems here on Earth?" Rather, the careful ordering of his plan shows that the frontier represented by space, and the innovation and fortitude needed to face its challenges, can also provide the impetus for creative solutions to humanity's troubles and avoid the stagnation of society. Just as the New World offered the opportunity for

political experimentation free from the interference of stagnant European monarchies so will the frontier of space give us a venue to explore technologies that have the capability to reinvigorate our society. This more, than scientific knowledge or national prestige, is the true value of expanding civilization beyond the closed system of the Earth.

Access to space offers a solution to one particular problem facing the Earth today in the form of limited sources of energy. Energy usage is the most basic measurement of a civilization, and correlates directly to the wealth and welfare of its populace. A rise in the cost of energy, caused by a dwindling supply, has a negative impact throughout all levels of society. Increases in energy prices will drive up the cost of transportation, in turn raising the consumer prices of manufactured goods and food products. Forced to rebudget their limited income, consumers' spending will stagnate. An upwardly spiraling energy cost will eventually grind economic growth to a halt.

The largest single source of energy in the world is from fossil fuel combustion, in the form of coal, crude oil, and natural gas. While fossil fuels are widespread throughout the Earth, in most cases, such as oil shale, it is not economically feasible to extract them. In many situations, the energy required to process the diffuse deposits of fossil fuels is greater than the energy output of the recovered fuel. The majority of the world's energy comes from the crude oil reserves of the Middle East, with secondary sources in North America, Russia, and Venezuela, where the density of the fossil fuel deposits makes extraction economically feasible.

There is some degree of disagreement over how long the resources of crude oil will last, largely because of the different accounting methods used in determining the actual amount of available oil. For example, in 2004, the Saudi Aramco oil company

predicted that their total reserve of oil amounted to 900 billion barrels. Out of this total 200 billion barrels are unsubstantiated and unexplored. Their addition to the estimated reserve is based on an optimistic fact that the previous 20 years of exploration had increased Saudi Arabia's oil reserves by 17%, and that a similar increase could be expected in the next 20 years [3]. Another optimistic outlook on the supply of oil comes from the United States Geological Survey, who in a study performed in 2000, estimate a mean value of 3,021 billion barrels of oil in the world, including probable deposits not yet explored [4]. At a projected world daily use rate of 100 million barrels a day this supply will be totally exhausted in just under 84 years. Before the supply is totally exhausted the Hubbert Peak, the point where oil production reaches its maximum value, will occur, with predictions placing this event anywhere from the present day to two decades hence. Upon reaching the Hubbert Peak increased oil usage will drive the price of the dwindling supply upwards, beginning the deceleration of economic growth.

It has been pointed out that coal and natural gas reserves could be used in place of oil. Economically exploitable reserves around the world could last up to 300 years at current rates of use. Coal can be converted to liquid fuel by several different methods. An example of this is the Fischer-Tropsch process, used by Germany and Japan, two historically petroleum poor countries, with some success during World War II to convert their coal reserves into synthetic petroleum [5]. There are several drawbacks to using coal as an oil substitute. While the effect of humanity's actions on the environment is a matter of great debate between environmentalists, private industry, and government, the mechanism by which the introduction of carbon dioxide into the atmosphere raises global temperatures is well understood and production of carbon dioxide, inherent in the

combustion of fossil fuels, should be limited as much as possible. Coal fired power plants are the largest producer of carbon dioxide, due to the high carbon content of coal. Besides, the supply of coal, like petroleum, is a limited resource, and would be consumed at a far greater rate than it is replenished. Because of their non-renewability fossil fuels represent an economic dead end, and an alternative to their use should be sought.

In the 1970s a movement began, which direly predicted the reverse of societal growth based on the consumption of limited natural resources. Led by the Club of Rome and publicized in the book "The Limits to Growth", this movement used computer models, based on resource consumption and population growth, to predict a pessimistic view of the 21st century, marked by a decline in the Earth's resources, industrial output and food production, and a leveling of population growth. The solution presented in "The Limits to Growth" to the problem of limited resources is simple retrenchment, to reduce economic growth in the future until a state of static equilibrium is reached. Despite having used an analysis method based on computer simulation the book shuns technology-based solutions as a distraction from the all overriding problem of growth in a finite system [6]. Considering the Earth as a closed system and dismissing technology as a solution are two flaws that limit the usefulness of their analysis. Fossil fuels, the decayed remains of biologic matter of past ages, are properly viewed as the converted form of energy originating from the source of all energy on Earth, the Sun. A possible solution to the dwindling supply of fossil fuels lies in finding methods of utilizing the energy output of the Sun directly.

In the late 1970s the work of Gerard O'Neill and the L5 Society revitalized the old ideas of Tsiolkovsky's space colonization and cast it in the form of a possible

solution to the energy shortage problems facing the Earth. O'Neill envisioned large cylindrical space stations in Earth orbit, 2 miles in radius and 20 miles long, rotating to provide artificial gravity to the inhabitants living on the inner surface of the cylinder. Each space colony would be self-sufficient with the enclosed agricultural environments supporting the inhabitants and manufacturing facilities providing for the industrial needs of the colony [7]. O'Neill's colonies would be economically sustained by the manufacture and operation of Solar Power Satellites (SPS) from materials mined on the Moon. As detailed in a 1979 study, these satellites would be large in size, using five to ten square kilometers of collecting area to harvest approximately five gigawatts of solar energy, which would be beamed via microwaves back to the surface of the Earth [8]. At O'Neill's estimate of the SPS massing ten kilograms per kilowatt of power generated, this would lead to a total mass of 50,000 tonnes, obviously too large to be launched from the Earth, justifying O'Neill's ideas regarding manufacture from material in space [9]. A more modern estimate of SPS mass per energy is one kilogram per kilowatt, based on improved efficiency of solar cells. This produces a total system mass of 5,000 tonnes, representing the payload capacity of over 200 flights of the Space Shuttle, and is still beyond our current launch capabilities [10]. The high cost of launching payloads to space is a damning criticism against a project as ambitious as the SPS, which would not become economical until launch prices are lowered to the order of $100 per pound [11]. While not technically feasible in the forseeable future O'Neill's work on space colonization and solar power generation, developed as a counter to the Malthusian predictions of that period, represents the idea that the future of humanity on Earth lies with its ability to exploit resources off of the planet Earth.

A less ambitious solution to energy shortages lies in combining Earth based energy production with resources culled from space. In his 2003 State of the Union Address, President George W. Bush announced the government's Hydrogen Fuel Initiative, couched in geopolitical terms as a tool to lessen our dependence on foreign sources of oil. Key to this plan was the development of fuel cells for mobile uses such as personal transportation. Fuel cells are an alternative to combustion engines, and function on the principle of electrolysis. The polymer electrolyte fuel cell has been identified as the best for small applications like automobiles. It functions with the introduction of hydrogen fuel through a platinum anode, which acts as a catalyst, stripping the electrons from the hydrogen. The positively charged proton continues through an electrolyte membrane to the cathode, where it combines with oxygen to form water. The electrons stripped in the anode flow through an electrical circuit to the cathode outside of the electrolyte membrane, generating a voltage. Not being a combustion based process, fuel cells are not bound by the Carnot cycle efficiency limits and can generate efficiencies around 50%, compared to approximately 30% for gasoline fueled internal combustion engines. With water and unused oxygen as the only byproducts of the reaction fuel cells are also much cleaner than internal combustion engines.

Fuel cells are a proven technology, having first been constructed in 1839 by the English scientist Sir William Grove. Polymer exchange membranes fuel cells have already been used in American manned spacecraft since the Gemini program of the 1960s [12]. Despite their feasibility, there are drawbacks to the widespread use of fuel cells for transportation needs, first and foremost being the need for the platinum catalyst. Platinum is one of the rarest of the precious metals and its current rates of supply just

barely exceed the yearly demand [13]. Providing platinum catalysts for the millions of automobiles will far exceed the projected world reserve of platinum. An alternative source of platinum may exist on the Moon. In 1963, the geologist Robert Dietz put forth evidence that the Sudbury Basin in Canada, with its rich platinum deposits, was the product of a meteoric collision [14], and the platinum located there were in fact carried here to the Earth on a colliding meteorite. Following this logic, it has been postulated that with no environmental erosion or tectonic activity to disturb lunar impact sites, and no oxidation to degrade the metallic ores, platinum deposits on the Moon may be more easily recovered than on Earth [15]. An additional benefit of mining lunar platinum is the negligible environmental effects. On Earth, platinum deposits are widely dispersed, with a few grams recovered for every ton of rock processed, and processing the ore produces much waste. Moving platinum production facilities to the lifeless, sterile Moon would eliminate the pollution on Earth by the increased mining needed to support fuel cell manufacturing.

In addition to the lack of platinum, another weakness of the plan to adapt widespread use of fuel cells is the means of production of the hydrogen fuel. The most economical means of hydrogen production is steam reformation of natural gas, performed at high temperatures in excess of 700° C and represented by the chemical reactions

$$CH_4 + H_2O \rightarrow CO + 3H_2 \qquad (1.1)$$

$$CO + H_2O \rightarrow CO_2 + H_2 \qquad (1.2)$$

The end result of the process is the desired hydrogen fuel, along with the production of CO_2, a greenhouse gas. It has been estimated that to produce the required

hydrogen to power all the vehicles in the United States would create more greenhouse gases than continuing to run them on their original internal combustion engines [16].

An alternative to producing hydrogen by steam reformation is offered through the use of electrolysis to separate water into hydrogen and oxygen. Again, this is an energy intensive process and the electrical energy needed to convert enough hydrogen to power all the vehicles in the United States would currently be more than the nations total electrical power consumption [16]. An increase in fission nuclear reactors could meet the power requirements for hydrogen production, but suffers from political drawbacks due to public perceptions of nuclear power. There is currently enough uranium to power the world's total energy needs for 46 years using current light water reactors. A more efficient method would be the use of breeder reactors, which in addition to generating energy also produce plutonium which can be refined and used in a nuclear reactor to produce further power. With breeder reactors the current uranium supply would adequately power the world for over 2,000 years; but breeder reactors are an even more politically untenable solution, due to the use of plutonium in nuclear weapons. In order for hydrogen to be practical, a vast new source of energy must be developed.

A possible solution to this problem is offered by recent advances in nuclear fusion research. Of particular interest is the fusion reaction between deuterium and helium-3 as reactants, shown by the chemical equation

$$D + {}^{3}He \rightarrow {}^{4}He + p + 18.4\,MeV \qquad (1.3)$$

The appeal to this reaction, in comparison to other fusion reactions involving deuterium and tritium, is that no neutrons are produced and the reactor chamber is not rendered radioactive. The energetic protons can be directly converted to energy via

electrostatic fields, bypassing the steam cycle and its associated inefficiencies required in other power plants. The drawback to helium-3 fusion is its relative scarcity, naturally occurring on Earth only in miniscule amounts through the radioactive decay of tritium.

Again, as in the shortage of platinum, a possible source of helium-3 is offered by the Moon. In samples returned by the Apollo missions, minute concentrations of the isotope helium-3 have been found in the lunar soil, embedded there by the solar wind. Helium-3 represents a form of energy coming directly from the Sun. While its concentration is thinly dispersed, on the order of a few parts per billion, its relative value in the energy market could make its extraction economically feasible. One kilogram of helium-3 contains the energy equivalent of 157,480 barrels of oil. At current oil prices around $60 per barrel, the kilogram of helium-3 has an economic worth of $9,448,800.

Researchers at the University of Wisconsin have designed a machine to mine helium-3 on the Moon. Their Mark II Miner is an 18 ton crawler mounting a bucket conveyor system that scoops up the first three meters of lunar regolith. A solar concentrator dish mounted on the miner is used to heat the soil until the gases in it boil off and are collected. The crawler moves forward a leisurely 23 meters per hour, processing 1258 tonnes of regolith in that time [17]. Accounting for the fact that half of every 27.3 days is spent in lunar night, the Mark II Miner will excavate an area of 1 square kilometer in a year, producing the resources outlined in Table 1.1 [18].

There are many useful byproducts produced by Mark II Miner. The hydrogen and methane collected represent more than enough rocket propellant required to return the helium-3 to Earth. The water produced would be key to supporting the human presence on the Moon required to maintain the fleet of mining machinery. While the 33 kilograms

Table 1.1: Yearly Production of the Mark II Miner

Product	Mass
Hydrogen	201 tonnes
Water	109 tonnes
Helium	102 tonnes
Carbon Monoxide	63 tonnes
Carbon Dioxide	56 tonnes
Methane	53 tonnes
Nitrogen	16 tonnes
Helium-3	33 kg

of helium-3 mined in one year may seem miniscule, it has the energy equivalent of 5,196,840 barrels of oil. To supply the world's electrical energy needs alone would require approximately 100 tonnes of helium-3 per year, requiring over 3000 miners. These miners represent 54,000 tonnes of equipment that need to be lifted to the moon, requiring heavy lift boosters to place them in Earth orbit. Space stations in Earth orbit and lunar orbit are needed as way stations, with orbital transfer vehicle plying the space between them. Transit between the lunar space station and the surface of the Moon would require a reusable lunar lander vehicle. Bases on the moon would house the human presence required to maintain the fleet of miners. It has been estimated that the total infrastructure cost to deliver the mining equipment and crews to the Moon and return the helium-3 to Earth would run a cost of $1 trillion [19].

1.2 Economics of Spaceflight

This extensive idea of space development falls short of reality when confronted with the hard realities of economics. The main bottleneck to expansion into and exploitation of outer space is the high costs involved in launching payloads to orbit. Table 1.2 gives the low Earth orbit (LEO) payload and launch prices for current launch vehicles, with launch costs normalized to dollars for the year 2000 [20 & 21]. The Saturn V, having last been used in 1973, is included in this data only for the purposes of comparison.

Prices increase even more for destinations beyond Earth orbit (BEO). Table 1.3 shows the payload capacity and price per kilogram to launch payloads on a geostationary transfer orbit (GTO) for several different launch vehicles, again normalized to the value of the dollar in the year 2000 [20 & 21]. It should be noted that the useful payload

Table 1.2: LEO Launch Costs

Launch Vehicle	LEO Payload (kg)	Launch Cost ($M)	Cost per kg ($K)
Saturn V	118,000	2000	16.95
Space Shuttle	24,400	350	14.34
Ariane IV (44L)	10,200	120	11.76
Ariane V	16,000	180	11.25
Atlas IIIA	8,640	110	12.73
Atlas V 401	12,500	125	10.00
Delta III	8,292	93	11.22
Delta IV Medium	11,700	125	10.68
Delta IV Heavy	25,800	230	8.91
Titan IV	17,700	270	15.25
Proton	19,760	75	3.80
Soyuz	7,200	27	3.75
Pegasus XL	460	13	28.26
Taurus	1,363	22	16.14
Zenit 3SL	13,740	90	6.55

Table 1.3: GTO Launch Costs

Launch Vehicle	GTO Payload (kg)	Cost per kg ($K)
Space Shuttle	5,900	67.80
Ariane IV (44L)	4,520	26.55
Ariane V	6,800	26.47
Atlas IIIA	4,055	27.13
Atlas V 401	5,000	25.00
Delta III	3,810	24.41
Delta IV Medium	5,300	23.58
Delta IV Heavy	10,843	24.90
Titan IV	8,620	31.32
Taurus	430	51.16
Zenit 3SL	5,250	17.14

arriving at geostationary orbit (GEO) will be even less, as an orbit circularization maneuver is required at the apogee of the GTO.

The science fiction author Robert Heinlein had been quoted as saying "Once you get to Earth Orbit, you're halfway to anywhere in the solar system." This statement may be seen as a description of the engineering difficulties involved in accelerating a payload from standstill to 7.78 kilometers per second, but it is not an accurate description of the economics involved in current launch vehicles. It can be seen from the data in the Tables 1.2 and 1.3 that the ratio of GEO to LEO prices for a particular launch vehicle is on the average 2.6, with a low value of 2.05 for the Titan IV, and as high as 4.13 for the Space Shuttle. As the usable payload for each launch vehicle decreases for destinations beyond GEO, the prices are driven even higher. For example, the Saturn V can launch a 47,000 tonne payload on a trans-lunar trajectory, for a price of approximately $42,500 per kilogram. As a point of comparison, current plans to mine lunar helium-3 require a payload cost to the Moon of around $3000 per kilogram to be economically feasible [22].

It can be shown from the cost data that the relationship between payload capacity and the launch cost also scales poorly for different vehicles. It is expected that for a small vehicle like the Pegasus rocket prices to LEO will be high at $28,260 per kilogram. Proponents of the "big dumb booster" concept may point to the savings afforded by the Delta IV Heavy, with a relatively low cost to LEO of $8,910 per kilogram, but a similarly large vehicle like the Titan IV has a cost to LEO of $15,250 per kilogram.

The majority of current launch systems have been derived from vehicles that were designed as military missiles. The development process of these vehicles was dominated more by matters of national security than by economic concerns. In their militaristic

incarnation, these vehicles were viewed as being analogous to rounds of ammunition, whose sole purpose was to be expended in combat. This expendability and the prioritizing of mission over economics means that military missiles translate poorly as a means of mass transportation. By simple analogy, the economic value of an automobile or an airliner increases as its operational lifetime lengthens. The average age of an aircraft in the five largest US passenger carriers is 11.5 years and is 19.7 years for the cargo carrier Federal Express [23]. These aircraft are maintained in good condition precisely because a long service life will defray their large initial costs. In order for a space launch system to be economical, it must break away from the "artillery-round" archetype by being both reusable and able to perform on a regular schedule.

1.2.1 The Space Shuttle

Reusable launch systems offer the chance to lower the cost of placing objects in orbit, but require a regularity of flight rate that has not yet been approached. The only reusable space launch system to date is the space shuttle, which while technically impressive, fails to provide cheap access to space, primarily because of economic and technical compromises made in its design process.

As originally envisioned by the National Aeronautics and Space Administration (NASA) in the late 1960s, the space shuttle was only one component of a comprehensive Space Transportation System (STS), which also consisted of a space station, nuclear powered orbital transfer vehicles or "space tugs". With the shuttle's role of surface to orbit transportation combined with the space station and the orbital construction capability of the space tugs, these three components were to form the foundational infrastructure for an eventual manned mission to Mars scheduled for the 1980s. This

expansive program quickly died with cuts to NASA's 1971 budget, the shuttle being the only surviving component [24].

To justify the shuttle's development, advocates began to promote it as a manned space vehicle not only for NASA, but also a launch vehicle for the Air Force and the commercial satellite market. It was hoped that the large costs associated with shuttle development in the 1970s would be defrayed by the benefits of regular cheap access to space in the 1980s. This argument was key to the economic justification for the space shuttle. At the heart of this contention was the issue of shuttle launch frequency. In a 1970 cost benefit study comparing the space shuttle against an existing launch vehicle, the Titan III, the shuttle represented a savings of only $500 million for a projected flight rate of 28 flights a year. Savings would grow to six billion dollars when the flight rate was increased to 55 flights per year. A further study by an independent corporation found that the launch savings afforded by the space shuttle would pay for itself with 506 flights in the period of 1978-1990, for an average of 39 flights per year [25]. For comparison, the highest actual rate of shuttle flights in one year has been nine launches in 1985 [26].

NASA's original vision of the space shuttle was a fully reusable two stage system, consisting of a large manned first stage which would fly back to the launch site, and a smaller orbital vehicle with its own propulsion and fuel tanks. With meager funding to develop a fully reusable space launch system, design compromises quickly eliminated the fly-back booster, replacing it with a large expendable fuel tank and solid rocket boosters. On each flight, the shuttle hauls the reusable orbiter and its associated weight to orbit and back. A more economical launch system would reuse the first stage, the stage that

operates in the Earth's atmosphere, and have an expendable upper stage. The weight saved in heat shielding for the re-entry and wings for atmospheric maneuvering required by the orbiter could be applied to payload delivered to orbit. The reusability of the final stage represents the backward design of the shuttle [27].

An additional compromise stemming from the shuttle's perceived role was made in the configuration of the orbiter, which was originally designed with straight stubby wings and would act as a blunt body during reentry, allowing for a limited glide path in the Earth's atmosphere after reentry. The Air Force's requirement of the orbiter to have a large cross range maneuverability, based on their desire to use the shuttle in polar orbital operations, led to the large delta wings on the shuttle. With the improved lift from the large delta wing, the cross range requirements of the Air Force could be met by the shuttle by gliding during the hypersonic phase of atmospheric reentry, leading to higher vehicle temperatures for longer periods of time, necessitating the design of heavy and complex thermal protection systems for the orbiter.

As a result of the compromises made in its design, the space shuttle is not capable of a turn around time of less than several months. As can be seen in the Table 1.2, the shuttle has ended up as one of the more expensive launch systems, with its launch cost based on a 1988 cost estimate, normalized to year 2000 dollars, which assumes an average of six flights per year. The actual price of a shuttle launch is highly dependent on its flight rate, because in addition to defraying the original development cost, part of the launch cost includes a portion of the yearly large fixed expenditure for upkeep of the launch and processing facilities. In the late 1990s, the U.S. General Accounting Office assigned a nominal value of $400 million per flight, which would correspond to a LEO

payload cost of about $16,400 per kilogram [20]. This value is also misleading in regard to the shuttle's current primary mission, which is to support operations aboard the International Space Station (ISS). Because the ISS in a 51.6° inclined orbit, in order to accommodate the Russian launch complex at Baikonur cosmodrome, the shuttle's useful payload to this orbit is only 12,500 kilograms, driving the LEO payload price up to $28,000 per kilogram (by 1988 estimate) or $32,000 per kilogram (by GAO estimate). These prices of course disregard the shuttle's sporadic flight rate in the wake of the February 2003 *Columbia* accident.

The space shuttle, while technically impressive, fails to live up to its design purpose of providing low cost, regular access to space. Conflicts in its development led to a murky definition of its purpose, resulting in a vehicle that could do every technical task it was designed to do, but not for an economical price. Technological challenges and economic limitations similar to those experienced by the shuttle in its development process, has caused the cancellation of further projects promising cheap access to space, such as the Single Stage to Orbit (SSTO) National Aerospace Plane and the X-33/VentureStar.

1.3 Alternatives to Rocketry

For as long as rockets have been considered as the practical method to go into space, a theoretical alternative has existed in the form of the space elevator. One of the space elevator's earliest incarnations was visualized by the father of modern rocketry, Konstantin Tsiolkovsky. At a radial distance of 42,164 kilometers, an object in a circular orbit around the Earth will have the same orbital period as the sidereal rotation period of the Earth and is said to be in a geosynchronous orbit (GSO). In an equatorial orbit this

object will appear fixed over a point on the Earth's surface and is said to be in a geostationary orbit. Tsiolkovsky observed that a cable reaching down from a satellite in GEO to the surface of the Earth would allow the trip into space to be made solely by elevator car, at the expense of electrical energy only.

In order for the entire system to be balanced around its center of gravity, a similar cable would extend outwards from the cable center at GEO and would in effect, because of centrifugal acceleration, be hanging away from the Earth. Objects released from the cable at GEO altitude would remain in the same orbit. Payloads traversing the cable beyond GEO orbit would not require any energy to be lifted beyond the cable's center of gravity. Because of the centrifugal acceleration outwards, they would be effectively "lowered" away from the Earth. Payloads released along the upper cable length would be placed either in a high Earth elliptical orbit or, for altitudes greater than 47,000 kilometers, on an Earth-escape trajectory. The space elevator allows for the placement of payloads into high orbit without the use of chemical rocket engines, eliminating gravity losses and aerodynamic drag losses. With mass as the dominating concern of space travel, a space elevator would eliminate the vast quantities of fuel needed to achieve orbit, and would literally be a bridge to orbit, making cheap access to space a reality. The energy required to move a payload from the Earth's surface to GEO would be 14.8 kilowatt-hours per kilogram. With an energy cost of $0.10 per kilogram, a payload could be lifted to GEO for only $1.48 per kilogram. While this price only includes the energy cost and disregards the cost involved in development and construction, it should be noted that most mass transportation systems operate today at only a fraction above their energy cost [28]. One optimistic estimate provides a total development cost for the space

elevator a low value of $6.2 billion, providing the system with the economic potential of lowering the cost of placing payloads in GEO to as low as $100 per kilogram [29].

Despite the attractiveness of this prospect, there are daunting physical problems involved with such a huge structure. The first and foremost of these problems is the material used to construct the elevator. The structural demands are far beyond the capabilities of the strongest and lightest materials currently in use. Using graphite epoxy composites, a GEO space elevator would weigh in excess of $65x10^{20}$ tonnes and would be over two kilometers thick at the GEO center. The GEO space elevator does not become a feasible construction project without the use of ultra high strength materials, such as carbon nanotubes, which are not currently produced in industrial quantities.

An additional problem is the near Earth space environment. Atomic oxygen present in the thin upper atmosphere will quickly erode carbon materials. This effect could be mitigated with metallic coating of the elevator, where the oxygen would form a protective oxide layer on certain metals. Ultraviolet radiation would also slowly degrade the integrity of the elevator structural materials. Also protection must be provided for the length of elevator and any payload that traverses the region of the Van Allen Belts.

In addition to the natural effects of the space environment, the large preponderance of objects currently in orbit around the Earth must be accounted for. The United States Air Force currently tracks over 8,000 objects ten centimeters or larger in size in orbit around the Earth, representing a total estimated mass of 2,000,000 kilograms. The vast majority of these objects are not active satellites, but debris from expended launchers, anti-satellite weapons tests, and non-functional spacecraft. For untracked objects smaller than ten centimeters, the estimated population is in the tens of millions.

Thankfully, the lifetime of these objects in low orbits are brief and are measured in months. For debris in GEO altitudes, the orbital lifetime can last millions of years. In addition to man-made orbital debris, micrometeoroids pose a threat to the space elevator. An estimated 40,000 tonnes of micrometeoroids enter the Earth's atmosphere each year, moving at an average velocity of ten kilometers per second [30]. Both the man-made debris and the naturally occurring micrometeoroids pose a significant hazard to a GEO elevator.

Due to these problems, the space elevator remains for the time being confined to the dreams of visionaries and the pages of science fiction. There is another alternative to the problem of cheap access to space, an interim concept between rocketry and the space elevator. Launching payloads to space may be achieved through the use of a two stage system, consisting of a suborbital launch vehicle that will rendezvous with a vertically oriented, gravitational gradient stabilized, orbiting tether. The tether center of gravity acts as the orbital center of the system. The lower end of the tether travels, with respect to the Earth, at a velocity lower than circular orbit velocity for its altitude. Similarly the upper end of the tether is traveling at greater than circular orbit velocity for its altitude. The basic configuration of this system is shown in Figure 1.1.

After launch of the suborbital transfer vehicle, near the apex of its trajectory, it performs a rendezvous with the tether's lower end. When the position and velocity of the launch vehicle and the tether end are matched, the payload will be handed off to the tether. The payload then travels up the tether by elevator car, being released at a point along the upper length of the tether. Similar to the GEO elevator, lifting the payload beyond the tether's center of gravity actually involves lowering it away from the Earth,

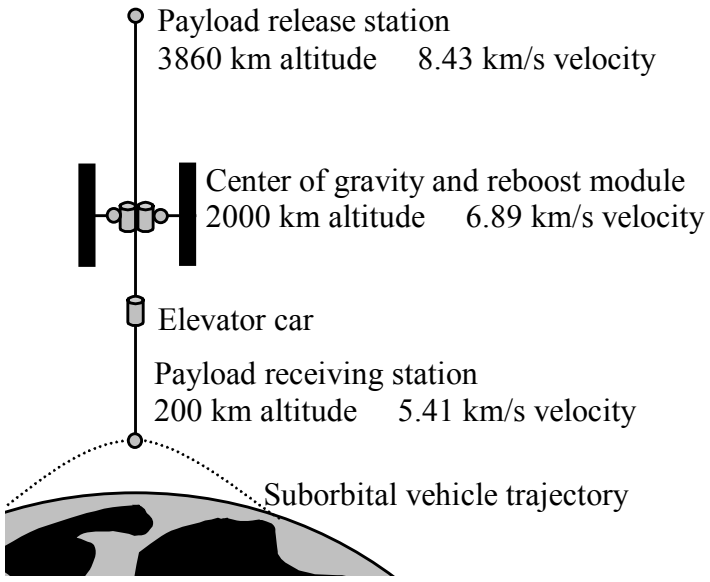


Figure 1.1: Earth Orbiting Space Elevator

due to the centrifugal acceleration. Since the payload is traveling at greater than circular orbit velocity at its altitude, when released it will travel in an elliptical orbit with its perigee at the release point. The overall effect of this is to place the payload into a higher orbit, while only expending enough fuel to reach a suborbital trajectory. With tether lengths of 2,700 kilometers, payloads which are released from the upper tip of the tether will be on a geostationary transfer trajectory, and possess over 90% of escape velocity at the upper tip altitude. The tether will have its orbit lowered by handling the payload, according to conservation principles. It can be reboosted into its initial orbit by an appropriate high efficiency system such as ion propulsion or electrodynamic tether propulsion. Electrodynamic propulsion is an especially attractive solution to this problem, as it taps the Earth's magnetic field to provide thrust to the tether through the Lorentz force. This method requires no propellant mass to be expended, only that an electrical current be run along the tether.

The Earth orbiting tether and sub-orbital launch vehicle offer several advantages over both conventional rocketry and the full ground to orbit space elevator. The required launch vehicle performance is only approximately 60% to 75% of that required for launch to orbit. This allows a vehicle to be built similar in size to past designs for an SSTO vehicle, and still be able to carry a useful payload at a reasonable mass fraction. The simplicity of the single stage design will increase the frequency of its flight rate, positively affecting its operational cost.

The orbiting tether itself is much shorter and much less massive than the GEO elevator, and its structural requirements allow it to be built from commercially available materials. The tether's shorter length significantly reduces the probabilities of contact

with space debris when compared to the space elevator. Unlike the full space elevator, which was limited to equatorial placement, the orbiting tether can be placed in an inclined orbit to allow it to deploy payload on lunar or ecliptic plane trajectories. More importantly, the freedom of its orbital placement can allow the tether to be placed in a resonant orbit that will have it pass over a launch site on a regular schedule.

Passage to the Moon, identified earlier in this chapter as the likely first goal in the utilization of space-based resources, could be greatly facilitated by an orbiting tether. Launch to Earth orbit and lunar transfer by rocket alone cost approximately 17,000 kilometers per second of Δv. For an Earth orbiting tether of length greater than 4,000 kilometers, the payload released at its upper end will already be on a translunar trajectory. The net effect of the tether and launch vehicle is to launch a payload to the Moon for approximately half the Δv required by pure rocketry.

The orbiting tether and suborbital launch vehicle have the potential to offer significant savings in launch cost. It represents a two stage system to high Earth orbit and beyond in which both stages are fully reusable. The propellant mass required for the second stage can be as low as zero with the use of electrodynamic reboost. The launch vehicle has the potential to be a much simpler vehicle to operate than the space shuttle. With these benefits, it is estimated that the Earth orbiting tether could lower costs of payload to high earth orbit to the order of $1,000 per kilogram.

This study will address several problems related to the Earth orbiting tether propulsion system. The design challenges examined in this study are primarily of a dynamical nature with some attention paid to the material structure of the tether. The initial problem addressed in this study is general structural design: determining the

interrelationships between the tether's baseline dimensions, mass, length, and payload size. Once in place, the tether's orbital position and stability will be under constant assault from disturbances. These perturbing factors may be operational, such as the addition of cargo at the lower end of the tether, or natural, such as atmospheric drag and Earth oblateness effects. Conservation principles can lead to estimates and guidelines of the tether's response to perturbation, but a dynamic model is needed to accurately describe its behavior.

In addition to suggesting a tether design, the suborbital launch vehicle will also be addressed in some detail. The tether's lower end will be moving at approximately 70% of orbital speed at an altitude of several hundred kilometers above the Earth, requiring a vehicle with similar performance to rendezvous with it. Due to the ballistic trajectory of the launch vehicle, the rendezvous must occur within a constrained time window. Times and maneuvers required for a rendezvous between the launch vehicle and the tether will be quantified through the study of their relative motion. Finally, the system's usefulness in a lunar transportation system will be assessed through a study of elevator launched trajectories.

Chapter 2

History of Space Tether Propulsion

The idea of a structure reaching from the surface of the Earth to the sky is one of human race's oldest ambitions. It has been recorded in different forms in some of the earliest know writings, which center upon a structure called the Tower of Babel, built around 2000 BC in ancient Mesopotamia. Recorded in the eleventh chapter of Genesis, the story of the tower of Babel borrows elements from an older Sumerian myth. The Sumerian myth is thought to have been based upon an incomplete ziggurat dedicated to the god Marduk, located in the city of Babylon, abandoned because of damage caused by earthquakes and lightning. When rebuilt by King Nebuchadnezzar around 560 B.C., it reached a height of approximately 100 meters, lending a sense of scale to the ambitions of the ancients. Both the Biblical and Sumerian versions of the tower story are cautionary tales warning of the dangers of hubris, sharing a common plot point of humanity's different languages being a punishment for its godlike aspirations.

The first modern technical description of a structure reaching the heavens was born from the same mind that formulated the first academic theories on the use of rocketry for space exploration. Konstantin Tsiolkovsky first wrote about a tower that extended from the Earth's surface to a "celestial castle" above geostationary orbit in a work entitled "Speculations about Earth and Sky on Vesta" written in 1895. Tsiolkovsky determined that his "orbital tower" would be in overall tension, with Earth's gravity pulling the section of the tower below geostationary altitude downward, while centrifugal force would pull the section of the tower above geostationary altitude upwards [31].

In unpublished work performed in the early 1950s, Dr. John McCarthy studied the idea of a cable extendeding in both directions from a satellite in geostationary orbit. The cable length extending upwards from the satellite was sized to balance the center of gravity of the whole system around the satellite. McCarthy realized that the cross section of the cable would have to increase as it rose higher from the surface of the Earth, in order to support the weight of the cable carried below it. This led him to posit the idea of a "taper ratio", describing the cable cross sectional area in relation to its radial position.

The taper ratio is derived from a material's self support length which is equal to its tensile strength divided by its density. For the strongest available material at the time of McCarthy's study, steel wire, the support length is 53.8 kilometers. To support the weight of the cable extending beyond 58.3 kilometers would require a gradual increase in the cross sectional area of the cable. The cable would start at the ground with a slender cross section, thickening as it approached geostationary altitude, and growing thinner as the cable extended out beyond its balance point. Working with steel wire McCarthy's interest in the problem ended when he calculated that at geostationary altitude, the cable would be $1x10^{50}$ times as thick as the diameter of the base [19].

Working from the basis of Tsiolkovsky's theories and independent of McCarthy's work, Russian engineer Yuri Artsutanov also discovered the idea of taper ratio. He is also the first to address the practical considerations of constructing such a massive structure. Artsutanov's suggestion was to use geostationary orbit as a construction base, building the cable lengths out in upwards and downwards directions to keep the entire structure balanced in its orbit [32]. He also devised what has come to be known as the "bootstrap" method of construction, whereby an initial cable is extended with a low

design payload weight. The addition of parallel cables gradually strengthen the design. Artsutanov is also responsible for the first exposure to the public of the idea of a space elevator, when he wrote a charmingly titled article "Into the Cosmos by Electric Locomotive" for the magazine supplement of *Pravda* in 1960. This article described the salient points of the Earth-based space elevator in layman's terms, describing the basic physics involved, its construction techniques, and its use, coupled with a Moon-based elevator, as a trans-lunar transportation system. While noting that no material currently existed to make the construction practical, the article ended on the hopeful note that "science and technology are swiftly moving ahead" [33].

Several American oceanographers working at the Woods Hole Institute in the early 1960s, without knowledge of Artsutanov or McCarthy's earlier work, independently derived the taper ratio for a third time. They noted that while a payload would have to be raised to the geostationary point of the cable, traversing the cable beyond the geostationary point involved lowering a payload away from the Earth. They described that the energy imparted to the payload would have to be taken, by conservation principles, away from the rotational rate of the Earth [34].

In 1975, Jerome Pearson published an article in the journal *Acta Astronautica* in which he reworked McCarthy's concepts using graphite whiskers as the construction material. Pearson was also the first to address the issue of vibrations in the cable caused by payload movement and tidal forces from the Moon. He found critical velocities at which cargo traversing the cable would excite resonant buildup. He also studied using the extension of the cable above geostationary altitude as a method of launching payloads on Earth-escape trajectories. Realizing the orbital elevator cable built of currently

available materials would have a mass measured in the billions of kilograms, Pearson concluded it would require over 24,000 flights of the space shuttle to construct [35].

The geostationary space elevator received its first widespread exposure in the West by way of Arthur C. Clarkes novel, "The Fountains of Paradise", published in 1979. In Clarke's tale of the construction of a space elevator, he describes it being built from diamond crystal filaments [36]. Clarke has further shown to be a proponent of the idea in an article published in *Advanced Earth Oriented Applications of Space Technology*. The nonfiction article reviews the work of previous engineers and scientists, with particular credit given to the work of Artsutanov [37].

There has been, in recent years, a blossoming interest in the full ground to orbit elevator, stimulated mainly by recent advances in the manufacture of high strength materials. Following a 2000 workshop on the idea of space tether propulsion NASA published the report "Space Elevators: An Advanced Earth-Space Infrastructure for the New Millenium". This work outlined the status and limitations of technologies involved with building a space elevator. Several near term paths of technological development are suggested, most importantly for this study the use of smaller orbiting tethers. Particular attention was given to several objections against building a space elevator, including the idea that long term project planning fails to incorporate technological advancements made in the interim [28].

Despite the cautious tone of the NASA report, work on the ground to orbit space elevator has continued, spurred on by the discovery of carbon nanotubes in 1991, cylindrical carbon molecules with a tensile strength two orders of magnitude better than currently available commercial materials. In his 2000 work on the space elevator,

Bradley Edwards outlines the feasibility of constructing an orbital elevator from carbon nanotube material. With its high strength to weight ratio, carbon nanotubes allow for the total tether mass to be measured in the hundreds of tonnes, rather than the thousands calculated by Pearson. Edwards goes into detail on the deployment, operation and design of a space elevator, addressing problems such as weather effects, space environment effects, and impact damage [38].

One company, LiftPort Group of Bremerton Washington, has optimistically announced their intention to build a space elevator by 2018, and are performing serious work in producing industrial scale quantities of carbon nanotube [39]. NASA, in conjunction with private companies, has sponsored X-Prize style competitions in 2005 and 2006 involving tether materials strength and elevator climber vehicle design.

Despite this newfound interest in the full ground to orbit elevator, several more near term applications of space tether propulsion exist involving tethers of much lesser length than the ground to geostationary space elevator. Scaling back from the massive geostationary cable, Hans Moravec, a colleague of John McCarthy's, published an article in 1977, involving a satellite in low earth orbit with two cables extending outward. This satellite would rotate in its orbital plane at a rate at which when the cable lower tip contacted the surface of the Earth, their relative velocities would be momentarily zero, allowing payload to be transferred to the cable. This rolling skyhook system would be much less massive than the ground to orbit elevator. Moravec's study neglected drag and aerodynamic heating caused by the tether moving through the Earth's atmosphere, which makes such a system impossible for use on the Earth, but a potential application exists on the airless Moon [40].

The rolling skyhook idea was modified later to have the tether end reach just above the earth's atmosphere, where cargo would be transferred to it by a high altitude, hypersonic aircraft. Work has continued on this configuration in a study conducted by Boeing along with Tethers Unlimited, Inc., called the Hypersonic Airplane Space Tether Orbital Launch system (HASTOL), addressing both the problems of tether design and also launch vehicle rendezvous with the spinning tether [41]. The rendezvous represents one of the most daunting problems involved with the spinning tether; a carefully timed arrangement is required between the tether's orbital position, its rotational position, and the hypersonic aircraft to allow the transfer of cargo. The dynamics of the system combine to force the transfer of payload to occur in a space of a few seconds [42] . Similarly to the rendezvous, the periods at which a payload could be released at the upper end of the tether's spin were limited, restricting its usefulness as a method to launch payload beyond LEO. Further study of the orbital response of handling a payload drove the system mass upwards towards several thousand tonnes for a spinning tether of length 600 kilometers, on the same order of magnitude of the non-spinning tethers addressed in this study [43].

Another application of tethers as an in-space propulsion system is currently being pursued in a joint study being conducted by NASA along with Lockheed Martin and Tethers Unlimited. This project, the Momentum eXchange Electrodynamic Reboost (MXER), is somewhat more modest than HASTOL, consisting of a 100 kilometer long spinning tether. This tether is in a 400 kilometer by 8000 kilometer elliptical orbit. The tether's spin rate and length are configured in such a manner that at its perigee point, the

lower tip will be traveling at the equivalent circular orbit velocity for its altitude, shown in Figure 2.1.

This system has difficulties similar to HASTOL in the short rendezvous time between the payload and the tether, but creative efforts have led to the design of a large deployable net used to capture the payload in its original orbit [44]. Having picked up its payload from LEO, the tether proceeds in its orbit towards the apogee point, where the payload is released when the it is on the upward side of the tether's spin, imparting to the payload not only the tether's orbital velocity but also its rotational velocity. The payload at release is on a geostationary transfer orbit. Momentum lost in raising the orbit of the tether is regained by electrodynamic means, whereby a current applied through the tether interacts with the Earth's magnetic field to regain orbital velocity. Work on the MXER has identified electrodynamic propulsion utilizing the Earth's magnetic field to be a key factor that makes tether based space propulsion attractive in the LEO environment, as well as addressed the dangers posed by orbital debris by suggesting the use of redundant lines separated by several meters [45]. Work on MXER had been proceeding with the goal of flying related experiments as technology demonstrators on the space shuttle, but the 2003 *Columbia* accident has postponed this schedule.

Actual flight experience with tethers has been very limited. A tether experiment was conducted between the Gemini IX spacecraft and its Agena docking target in 1966, when the two were linked by a 36 meter long Dacron tether. The Gemini IX experiments attempted to study both gravitational gradient stabilized and spinning tether dynamics. Data was inconclusive on the gravitational gradient and while the artificial gravity

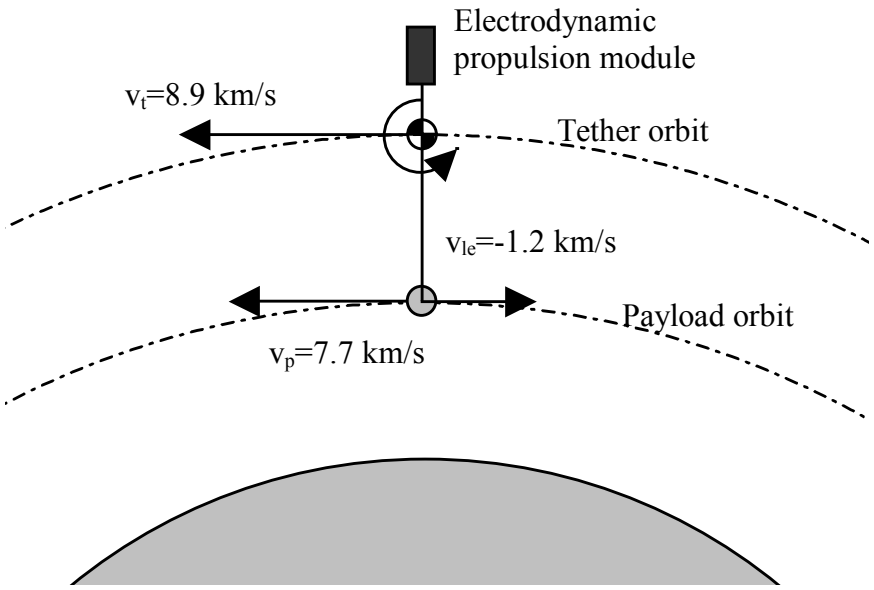


Figure 2.1: Momentum eXchange Electrodynamic Reboost System

generated in spin mode was too low to be felt by the crew, experiments confirmed its existence [46].

Several tether experiments have been conducted on board the space shuttle. In 1992 on STS-46, and in 1996, on STS-75, the Tethered Satellite System (TSS) was flown, successfully demonstrating the use of long gravitationally stabilized tethers and the generation of electrical current from the Earth's ionosphere. On its second flight, the TSS was deployed to a length of 19.7 kilometers, making it the longest electrodynamic structure ever built. For a period of five hours, the tethered satellite collected data on the extraction of current from the Earth's ionosphere before the tether broke. Despite its loss, the TSS did much to influence design and planning of further electrodynamic tether systems [47].

One of the earliest applications for non-spinning, gravitationally stabilized tether was first put forth by two engineers, A.R. Collar and J.W. Flower, in the *Journal of the British Interplanetary Society* in 1969. Their study concerned a twin satellite system, with one satellite in GEO while a long lightweight tether extended downwards approximately 35,000 kilometers to a satellite at a lower altitude. This system was proposed not as a propulsion device, but as a benefit to the communications industry. The low altitude 24 hour satellite system combined the advantage of geostationary altitude, primarily remaining fixed with respect to a point on the Earth's surface , with the lower signal strength needed to contact a satellite in LEO. Collar and Flower's study addressed similar concepts as the early work done on the full space elevator, and expanded work done on the orbital stability of the system [48].

The first mention of the orbiting space elevator came in 1994 when Eagle Sarmont published a paper on a concept that combined the concepts of the rotating skyhook and the orbital tower. Sarmont claims to have invented the concept in 1988 while working at Lockheed Missile and Space Corporation, and was promptly told by his manager he "was never to waste another moment of company time on the idea by even so much as mentioning it again" [49]. Sarmont's structure was a tether that would be in a low Earth Orbit about its center of gravity, with the lower end at an altitude just above the atmosphere, around 150 kilometers. It would be held vertical to the horizon by gravity gradient forces and payload would be transferred to it by a suborbital launch vehicle. Reboosting the system due to energy losses was accomplished by a high efficiency ion propulsion system. Sarmont's paper was primarily a cost balance study between using the Earth orbiting tether versus traditional rocketry and showed the potential of such a system to lower launch costs to several hundred dollars per pound [50].

A similar idea was put forward by Robert Zubrin in 1995. Calling his system the Hypersonic Skyhook, Zubrin paid particular attention to the materials strength required for such a system, developing an equation for the taper ratio of an orbiting elevator. He also estimated the drop in the tether's orbit, caused by handling a payload, by employing a momentum conservation routine, and outlined the use of electrodynamic systems to reboost the skyhook. Noting previous idea's originating with Artsutanov, he put forth the bootstrap method of construction as a way to eventually strengthen and lengthen the skyhook until payload deliveries could be made to the skyhook lower tip by hypersonic air breathing vehicles [51].

The Earth orbiting elevator was studied in one final incarnation by Lockheed Martin on a project they named the "Bridge to Space" during the period from of 1999 to 2001. A 3,200 kilometer long tether was used as the baseline model studied, allowing objects to be launched from the tether with 95% of escape velocity. The Lockheed study contained a serious effort to quantify the dangers posed by orbital debris, and found that redundant cables significantly extend the lifetime of the tether in the face of small scale space debris. Modeling the tether's interaction with larger tracked particles found that the frequency of encounters between the tether and other objects in orbit would be of the order of several per year [52]. An economic model was developed which predicted that once the system was running at full capacity costs to place payloads in GEO could be as low as $100 per pound. Although none of the technical aspects of the Bridge to Space were viewed as ahead of its time, the economic predictions were largely met with incredulity [53]. The perceived lack of interest in the concept led to work on it stopping in 2001.

Chapter 3

Elevator Sizing

3.1 Stepwise Integration Method

The primary design variables involved in sizing an Earth orbiting space elevator are the material used to construct the tether, the altitude of the tether's center of gravity, and the payload it is designed to carry. From these three choices, the length and overall mass of the tether are found. The length of the tether determines its usefulness as a payload launching system, while its mass is a measure of the investment required in its construction and placement in Earth orbit.

The selection of material balances three factors: its density, its tensile strength, and its tensile modulus. The density and tensile strength primarily affect the overall final mass of the tether, while its tensile modulus is important in determining its behavior when loaded. Table 3.1 lists the main materials considered for space tether applications with their respective material properties. Carbon nanotubes have been included in this list only for purposes of comparison, as production levels have not yet reached industrial quantities needed for a space tether system. Their tensile strength listed here is a theoretical maximum, and differs from what is observed in laboratory tensile tests. Experimental methods of measuring the tensile strength of carbon nanotube strands have yielded values ranging 1 to 63 gigapascals [54]. T-650/35 carbon fiber was used in Lockheed Martin's Bridge to Space study as the main structural material, with redundant lines made of Vectran and Kevlar. Spectra 2000 was the material proposed for use in the HASTOL study. Although Spectra has a good strength to weight ratio, its suffers

Table 3.1: Tether Material Properties

Material	Density (kg/m^3)	Tensile Strength (Pa)	Tensile Modulus (Pa)
T-650/35 Carbon	1770	4.55E+09	2.55E+11
Spectra 2000	970	3.50E+09	1.13E+11
Zylon HM	1560	5.80E+09	2.80E+11
Vectran	1440	3.02E+09	6.90E+10
Kevlar	1440	3.60E+09	8.30E+10
Carbon Nanotube	1300	1.30E+11	1.00E+12

problems with creep when undergoing long term loading [53]. For the purposes of this study, Zylon, with its high tensile strength and modulus, will be the material proposed for the construction of the Earth orbiting space elevator. Regardless of material choice, the actual tether will require some treatment and or coating to deal with the monatomic oxygen and ultraviolet radiation present in the LEO environment.

A program has been written for this study that, given a specific center of gravity altitude, tether material and payload mass, calculates the overall length and mass of the tether. This is achieved through breaking the tether into discrete segments of equal length. Starting with the lowest segment, an iterative process is used to calculate the required cross sectional area needed to support the mass of the tether and payload hanging beneath each segment. A similar method has been developed to calculate the size of a full ground to geostationary orbit space elevator [55].

The first step in this program is to calculate the downward acceleration at each segment of the tether. The acceleration is made up of two components, a downward component caused by the attraction to the Earth, and an upward centrifugal component caused by the rotation of the tether expressed as

$$a_j = \frac{GM_E}{r_j^2} - r_j \omega_T^2 \qquad (3.1)$$

A lower tip altitude of 250 kilometers has been selected for this portion of the study. This number was chosen to place the end of the tether above the denser portions of the Earth's upper atmosphere in order to minimize the effects of atmospheric drag and heating on the tether's lower end.

The angular velocity of the tether, ω, is found from the chosen value of the tether's center of gravity. The selection of tether's center of gravity determines its orbital speed, according to the equation

$$v_{cg} = \sqrt{\frac{GM_E}{r_{cg}}} \tag{3. 2}$$

The tether, being in a circular orbit, moves at a constant velocity. The orbital speed of the center of gravity is equal to the angular velocity of the tether multiplied by the radial distance of the center of gravity

$$v_{cg} = \omega_T \, r_{cg} \tag{3. 3}$$

The relation between the tether's angular velocity and the radius of the center of gravity is found to be

$$\omega_T = \sqrt{\frac{GM_E}{r_{cg}^{\,3}}} \tag{3. 4}$$

By plugging the value for the tether angular velocity back into the gravity equation, it can be shown that for a tether segment at the center of gravity the acceleration is zero. This supports the assumption that the tether can be treated as a satellite in free fall with cable lengths "hanging" from the center of gravity in both upwards and downwards directions [56].

The tension in the lowermost segment of the tether, caused by the attachment of the payload, is calculated by multiplying the payload mass by the gravitational and centrifugal acceleration at the tether's lower tip, by the equation

$$F_{Ten\,1} = m_p\left(\frac{GM_E}{r_{le}^{\,2}} - r_{le}\omega_T^{\,2}\right) \tag{3. 5}$$

From the tension, the cross sectional area of the lowermost tether segment can be found to be

$$A_{x1} = \frac{F_{Ten\,1}\, f_s}{\sigma} \tag{3. 6}$$

The mass of the lowermost cable segment is calculated by multiplying the density of the tether material by the volume of the lower segment

$$m_1 = \rho_T\, l_{seg}\, A_{x1} \tag{3. 7}$$

This process is repeated for the next segment, where the tension is found to be the sum of the tension in the previous segment plus the mass of the previous segment times its acceleration. For a general segment j, this takes the form

$$F_{Ten\,j} = F_{Ten\,j\text{-}1} + m_{j-1}\left(\frac{GM_E}{r_{j-1}^{\,2}} - r_{j-1}\omega_T^{\,2}\right) \tag{3. 8}$$

The cross section and mass of the general segment j is calculated exactly as the first segment was, according to the equations

$$A_{x\,j} = \frac{F_{Ten\,j}\, f_s}{\sigma} \tag{3. 9}$$

$$m_j = \rho_T\, l_{seg}\, A_{x\,j} \tag{3. 10}$$

This stepwise integration goes on for n number of iterations. As each step is added to the length of the tether, the center of gravity is computed according to the equation

$$r_{cg} = \sum_{j=n}^{1} \frac{m_j\, a_j\, r_j}{m_j\, a_j} \tag{3. 11}$$

When the calculated value of the radius of the center of gravity equals the design value chosen at the start of the program, the process stops. The total length of the tether is calculated by the number of iterations times the individual segment length. The total mass of the tether is the sum of the mass of each segment shown by

$$m_T = \sum_{j=1}^{n} \rho_T \, l_{seg} \, A_{x\,j} \tag{3. 12}$$

From the total length of the tether, the upper and lower velocities can be calculated by the equations

$$v_{le} = \omega_T \, r_{le} \tag{3. 13}$$

$$v_{ue} = \omega_T \, r_{ue} \tag{3. 14}$$

These tether tip velocity values are critical to sizing the suborbital launch vehicle and determining elevator launched trajectories. Figure 3.1 shows the upper and lower tip velocities, expressed as percentages of the escape velocity and the circular orbit velocity at their respective altitudes.

Tether lengths of interest to this study lie in the range of 2,700 to 4,300 kilometers. At the lower end of this range, a 2,700 kilometer long tether allows an object released from its upper end to be placed in a Hohmann trajectory with an apogee at the altitude required for geosynchronous orbit. This example illustrates the usefulness of the Earth orbiting tether system as a tool for launching payload beyond LEO. For tethers of 2,700 kilometers of length the lower tip will only be traveling at approximately 76% of circular orbit velocity at that altitude. This allows a payload to be placed on a geosynchronous transfer orbit for a Δv of only 76% of that required to reach LEO. Similarly, tether lengths of approximately 4,050 kilometers allow objects released from

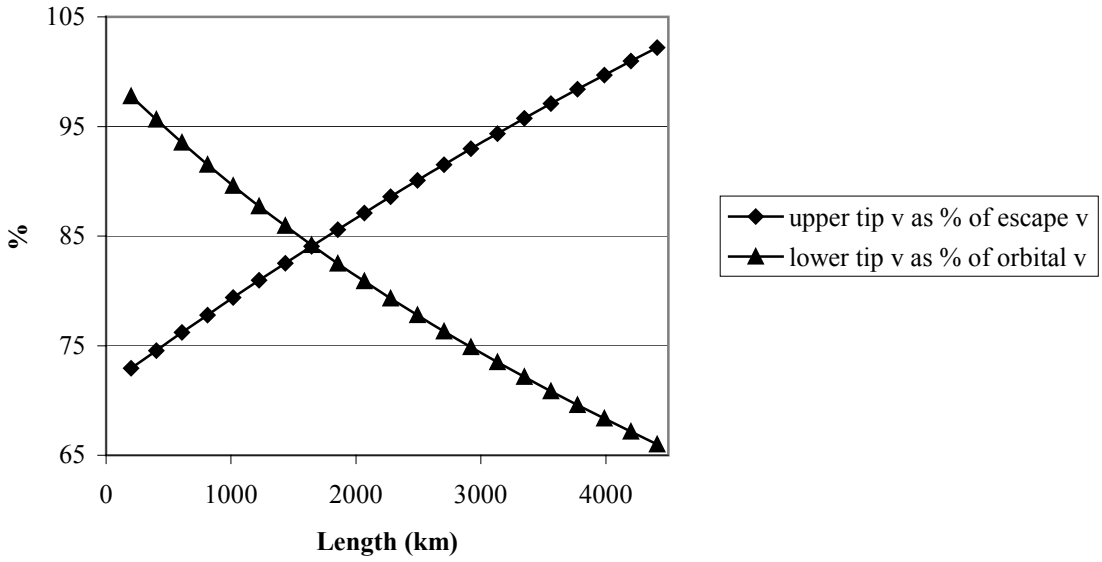


Figure 3.1: Tether Upper and Lower Tip Velocities

the upper tip to be placed in a Hohmann trajectory which will take them to an apogee of 384,400 kilometers, the orbital altitude of the moon. This allows a payload to be placed on a minimum energy lunar transfer orbit for the Δv expenditure of only 68% of that required to reach LEO. Finally for lengths of approximately 4,300 kilometers an object released from the tether's upper tip is traveling at greater than escape speed at that altitude, while only requiring the Δv equal to 66% of orbital velocity to reach the lower tip.

3.2 Alternate Method of Determining Elevator Cross Sectional Area

In place of the stepwise integration method detailed above, an explicit equation describing the cross sectional area at any point along the tether can be derived. This is accomplished by integrating the forces on a tether over its entire length [35]. This process begins by summing the forces on a differential element of the tether, according to the equation

$$\sum F = 0 = F_g + F_c + F_{Ten} \tag{3. 15}$$

where the forces involved are gravity caused by attraction to the Earth, centrifugal force caused by the tether rotation, and tension in the tether. The gravitational acceleration caused by the Earth is found by the equation

$$a_g = -\frac{GM_E}{r^2} \tag{3. 16}$$

while the centrifugal acceleration term is expressed as the radial position multiplied by the rotation rate of the tether, according to the equation

$$a_c = r\,\omega_T^{\,2} \tag{3. 17}$$

The tension force in the tether is expressed as the tensile strength of the tether material multiplied by the cross sectional area, divided by the design factor of safety, as shown in the equation

$$F_{Ten} = -\frac{\sigma A_x}{f_s} \tag{3. 18}$$

By multiplying the gravitational and centrifugal accelerations by the mass of the element dm their respective forces can be inserted into the force summation equation. Also by noting that the tension force is acting on the differential element with cross sectional area $dA_{x,}$ the force summation equation can be written in the following form

$$\sum F = 0 = -dm\frac{GM_E}{r^2} + dm\, r\, \omega_T{}^2 - \frac{\sigma}{f_s}\frac{dA_x}{dr}dr \tag{3. 19}$$

In order to produce an expression in terms of the cross sectional area, the differential element mass can be expressed as the product of the tether material density multiplied by the cross sectional area multiplied by the differential length of the element, shown by the expression

$$dm = \rho_T\, A_x\, dr \tag{3. 20}$$

Inserting this back into the force summation equation and combining the gravity and centrifugal terms allows it to take the form

$$\sum F = 0 = \rho_T\, A_x\, dr\left(-\frac{GM_E}{r^2} + r\, \omega_T{}^2\right) - \frac{\sigma}{f_s}dA_x \tag{3. 21}$$

Terms containing the cross sectional area are gathered together producing the following equation

$$\frac{dA_x}{A_x} = \frac{f_s}{\sigma}\rho_T \, dr\left(-\frac{GM_E}{r^2} + r\,\omega_T{}^2\right) \tag{3. 22}$$

Both sides of this equation can be integrated, the left with respect to cross sectional area, while the right with respect to the differential radial position dr, according to

$$\int \frac{dA_x}{A_x} = \int \frac{f_s\,\rho_T}{\sigma} A_x \left(-\frac{GM_E}{r^2} + r\omega^2\right) dr \tag{3. 23}$$

Integrating this expression produces the natural logarithm of the cross sectional area of the tether in terms of its radial position, shown by

$$\ln(A_x) = -\frac{f_s\,\rho_T}{\sigma}\left(\frac{GM_E}{r} + \frac{1}{2}r^2\omega_T{}^2\right) + K_1 \tag{3. 24}$$

By taking the exponential function of both sides of the equation, the cross sectional area of the tether can be expressed as a function of the radial position

$$A_x(r) = \exp\left[-\frac{f_s\,\rho_T}{\sigma}\left(\frac{GM_E}{r} + \frac{1}{2}r^2\omega_T{}^2\right)\right]\exp(K_1) \tag{3. 25}$$

The constant of integration, K_1, can be solved for by evaluating the equation at the tether's lower end. The cross sectional area of the tether's lower tip is a function of the material tensile strength, the design payload mass, the design factor of safety, and the acceleration felt at the lower tip of the tether, shown by the equation

$$A_{x\,le} = \frac{m_p\,a_{le}\,f_s}{\sigma} \tag{3. 26}$$

where the downward acceleration felt at the lower tip is a combination of gravitational attraction from the Earth and the outward centrifugal component induced by the tether's rotation, shown by the relation

$$a_{le} = \frac{GM_E}{r_{le}^2} - r_{le}\omega_T^2 \tag{3. 27}$$

Inserting this expression for the lower tip cross sectional area back into the integrated force summation equation, evaluated at the tether's lower tip, produces the equation

$$\frac{m_p f_s}{\sigma}\left(\frac{GM_E}{r_{le}^2} - r_{le}\omega_T^2\right) = A_x(r_{le}) = \exp\left[-\frac{f_s \rho_T}{\sigma}\left(\frac{GM_E}{r_{le}} + \frac{1}{2}r_{le}^2\omega_T^2\right)\right]\exp(K_1) \tag{3. 28}$$

This equation can be rearranged to isolate the exponential function of the constant of integration, allowing it to be expressed as

$$\exp(K_1) = \frac{\frac{m_p f_s}{\sigma}\left(\frac{GM_E}{r_{le}^2} - r_{le}\omega_T^2\right)}{\exp\left[-\frac{f_s \rho_T}{\sigma}\left(\frac{GM_E}{r_{le}} + \frac{1}{2}r_{le}^2\omega_T^2\right)\right]} \tag{3. 29}$$

This value of the integration constant is then inserted into the general expression of cross sectional area as a function of radial position producing the equation

$$A_x(r) = \exp\left[-\frac{f_s \rho_T}{\sigma}\left(\frac{GM_E}{r} + \frac{1}{2}r^2\omega_T^2\right)\right]\frac{\frac{m_p f_s}{\sigma}\left(\frac{GM_E}{r_{le}^2} - r_{le}\omega_T^2\right)}{\exp\left[-\frac{f_s \rho_T}{\sigma}\left(\frac{GM_E}{r_{le}} + \frac{1}{2}r_{le}^2\omega_T^2\right)\right]} \tag{3. 30}$$

This equation allows for the calculation of the cross sectional area at any point along the length of a tether, given its rotational rate, found from the design center of gravity altitude, its material properties, its lower tip altitude, and its design payload. Figure 3.2 shows typical cross sectional area profiles along several tethers of varying

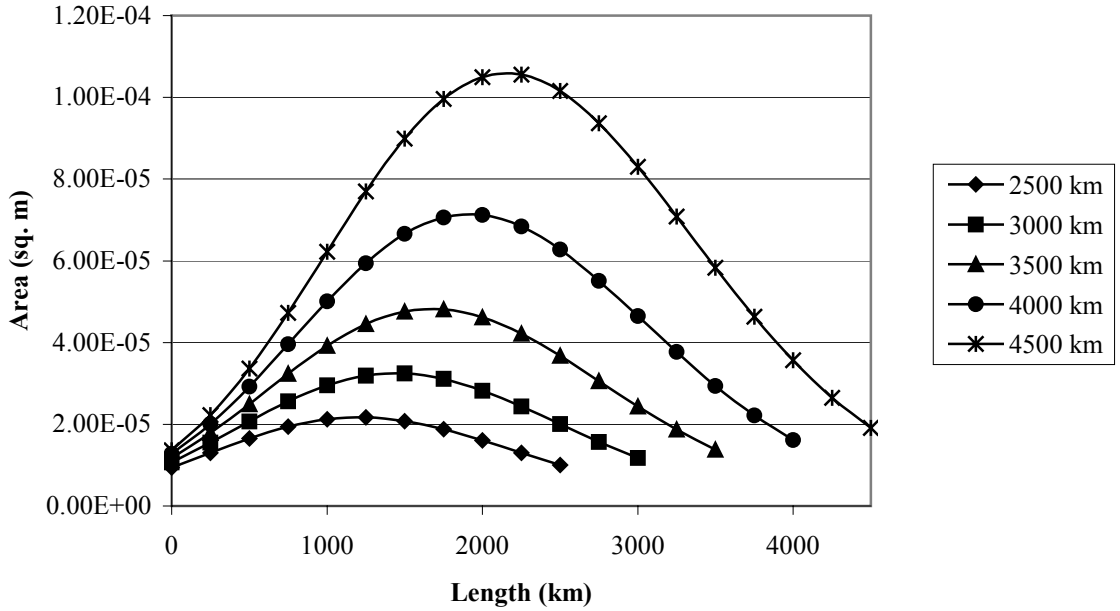


Figure 3.2: Tether Cross Sectional Area versus Length

length. Each tether shown in this figure is made of Zylon HM and designed to carry 10 tonnes with a safety factor of 1.5 and a lower tip altitude of 250 kilometers.

3.3 Previous Methods of Determining Response to Loading

Functioning as a free flying object in orbit around the Earth and used to impart energy to a payload, the Earth-orbiting tether will loose orbital speed and altitude each time it handles a payload. The stability of the Earth orbiting space elevator remains one of the most serious uncertainties regarding its feasibility [28]. Quantifying this loss of altitude and velocity has been attempted in previous studies by several different methods. Previous work done on this problem relies upon one of two physical schemes, the conservation of momentum, and the calculation of the tether center of mass. Both methods involve simplifications and assumptions that ignore certain aspects of the tether-payload behavior.

In the case of Dr. Robert Zubrin's Hypersonic Skyhook, the effect of handling a payload was modeled as a momentum exchange. In Zubrin's analysis, it was assumed that the launch vehicle had successfully transferred its payload to the tether's lower tip. At that instant, the payload angular momentum was calculated to be the product of the payload mass multiplied by the radius and velocity of the tether's lower tip, according to the equation

$$h_p = m_p r_{le} v_{le} \tag{3. 31}$$

By raising the payload to the tether's upper end, its angular momentum will be increased by the value

$$\Delta h_p = m_p r_{ue} v_{ue} - m_p r_{le} v_{le} \tag{3. 32}$$

The principle of conservation of momentum dictates that this increase in the angular momentum of the payload must be taken from the angular momentum of the tether, resulting in a loss of tether velocity. Zubrin's analysis treats the tether as a point mass at its center of gravity. The tether's original angular momentum is calculated by the equation

$$h_{T0} = m_T r_{cg} v_{cg0} \tag{3. 33}$$

From this total, the angular momentum that had been imparted to the payload is subtracted, calculating the corrected tether angular momentum according to the expression

$$h_{Tf} = h_{T0} - \Delta h_p \tag{3. 34}$$

The final velocity of the tether center of gravity can be calculated by the expression

$$v_{cgf} = \frac{(m_T + m_{stat}) r_{cg} v_{cg} - m_p r_{ue} v_{ue} + m_p r_{le} v_{le}}{(m_T + m_{stat}) r_{cg}} \tag{3. 35}$$

The Δv needed to sustain the tether in its original altitude is the difference between its original and final velocities. Because this analysis treats the momentum lost from the tether as a gradual process dependent on the payload climbing speed along the tether, the speed of elevator cars along the tether could be tailored to keep the whole system from lowering its altitude so much that it entered the upper portions of the Earth's atmosphere. Zubrin concludes his analysis by outlining the specifics of a 20 tonne tether, of approximately 3,450 kilometers length handling a 1.5 tonne payload. Raising a payload to the tether center of mass will cause the tether to loose 134 meters per second

of velocity. A 30 kilowatt electrodynamic reboost system will produce approximately 2.1 Newtons of force, allowing the tether to be reboosted to its original orbit in 15 days [51]. Zubrin's analysis does not take into account the drop experienced by the tether caused by the addition of payload weight. In his analysis, any drop in tether orbital altitude is caused by the raising of the payload along the tether. Implicit in this analysis is the idea that a payload added to the tether's lower end will not cause a drop in orbital altitude unless it is carried up the elevator car, an assumption that defies physical reasoning.

Using Zubrin's method for a tether made of Zylon HM material carrying a payload of 1.5 tonnes, the required total tether mass required can be calculated for varying tether lengths. In Zubrin's initial analysis no mention was made of the mass required for the reboost propulsion system. A 100 tonne reboost system has been added at the central station, providing the total system masses seen in Figure 3.3.

A similar method of elevator sizing based on momentum conservation principles was also used in the Lockheed Martin Bridge to Space project. Again, the tether was treated as a point mass at its center of gravity. A velocity deficit was computed from the difference between the angular momentum for the tether alone and the angular momentum of the combined tether and payload. In this method, it should be noted that movement of payload up the tether does not cause any drop in the tether's orbit. Any change in the system is caused by the addition of payload at the tether's lower end. This method also ignores any shift in the center of gravity of the tether payload system. All analysis has been performed treating the system as a point mass at the original unloaded tether center of gravity. The Bridge to Space project was based on a tether made of carbon fiber designed to carry a 10,000 kilogram payload. Using this conservation

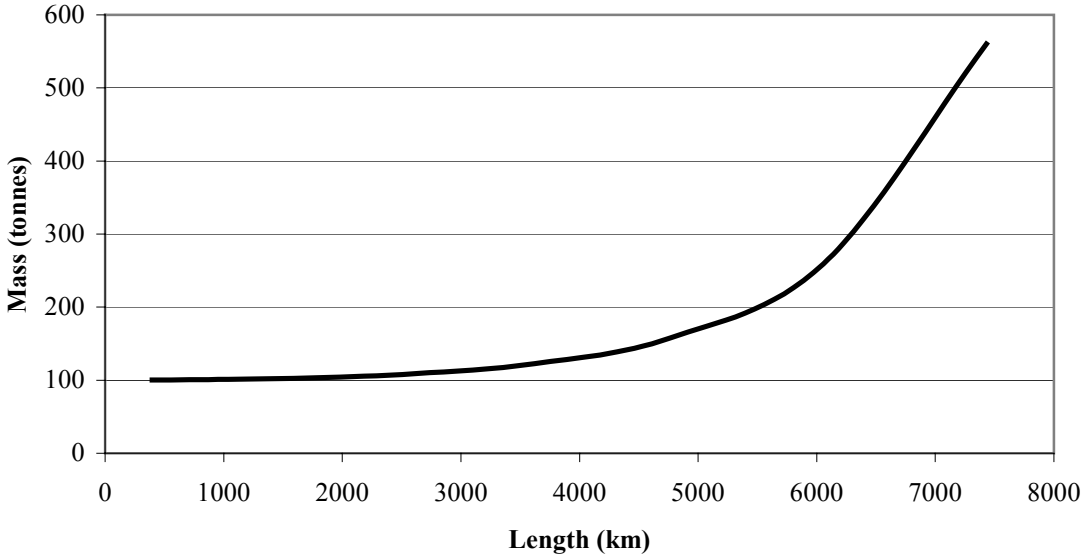


Figure 3.3: Tether Mass versus Length (Zubrin)

momentum procedure on a tether massing 500 tonnes, a modest drop of only 16 kilometers in the tether's orbital altitude was observed when the payload was added [53]. Figure 3.4 shows the required tether mass for varying lengths using this momentum conservation sizing methods [57].

A third method of determining the required mass of a tether was outlined in Eagle Sarmont's work on his Earth orbiting tether. This method, based on the shifting of the center of gravity that occurs with the addition of the payload, is relatively straightforward but mechanically complex. Utilizing the stepwise integration method, a tether model is developed. The center of gravity of the loaded tether is found by the equation

$$r_{cgL} = \sum_{j=n}^{1} \frac{m_j\, a_j\, r_j + m_p\, a_{le}\, r_{le}}{m_j\, a_j + m_p\, a_{le}} \tag{3. 36}$$

The velocity of the new tether-payload center of gravity is calculated by multiplying the loaded center of gravity by the angular rotation rate of the tether, shown by the expression

$$v_{cgL} = \omega_T\, r_{cgL} \tag{3. 37}$$

The velocity of the loaded center of gravity is less than the circular orbit velocity at its altitude, so the tether center of gravity is treated as being at the apogee of an elliptical orbit. Starting from the velocity and radial position of the loaded center of gravity, the parameters of its new elliptical orbit are calculated.

Sarmont's tether system differed in design from the others in that it carried a large 40 tonne manned space station on its lower tip. At the lower tip, the Earth's gravity and the centrifugal acceleration combine to produce an acceleration of 3.1 meters per second in the downward direction. While this is attractive from the point of view of space

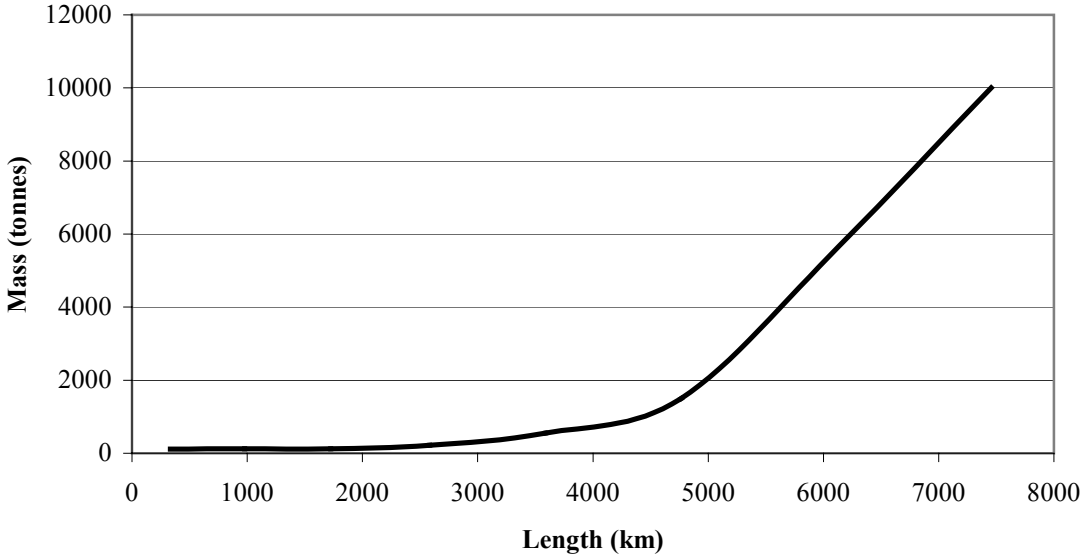


Figure 3.4: Tether Mass versus Length (Bridge to Space)

biology, it requires the tether to be strengthened to permanently bear the weight of this heavy station. With the payload added to the lower end, Sarmont's Earth orbiting tether then undergoes several actions to minimize the shift in the center of gravity of the tether payload system. The first step taken to decrease the center of gravity shift is to quickly reel in the lower length of the tether, raising the altitude of the lower manned station and the payload. He speculates that by also reeling in the upper end of the tether and by lowering the central power station along the tether length, the center of gravity can be controlled to a degree that the tether payload system will end up in a circular orbit 30 to 60 kilometers lower in altitude than when it started. Accounting for the mechanical adjustments made to the tether, Sarmont calculates that for a tether of length of 2,188 kilometers and lower tip altitude of 150 kilometers, which requires the launch vehicle to achieve 80% of orbital velocity and payloads to be released with 87.274% of escape velocity, the total mass of the system would be 825,000 kilograms [50].

3.4 New Methods of Estimating Orbital Response to Loading

For this study two new methods have been used to determine the tether's orbital response at the moment the payload is attached. Both of these involve measuring the shift in the center of gravity of the payload-tether system when the payload is added. For the first the new orbit is simply calculated from the velocity of the new center of gravity, while in the second the total angular momentum is used to calculate the altered trajectory of the tether-payload system.

3.4.1 Shifting Center of Gravity Method

If the moveable masses along the tether length employed by Sarmont are disregarded, a simplified method of studying shifts in the center of gravity of the tether-

payload system can be used to estimate the required mass of the tether. The center of gravity of the tether-payload system is again calculated according to the equation

$$r_{cgL} = \sum_{j=n}^{1} \frac{m_j\, a_j\, r_j + m_p\, a_{le}\, r_{le}}{m_j\, a_j + m_p\, a_{le}} \tag{3. 38}$$

The velocity of the new tether-payload center of gravity is calculated by the expression

$$v_{cgL} = \omega_T\, r_{cgL} \tag{3. 39}$$

This velocity will be less than the circular orbit velocity at the loaded center of gravity, so the tether-payload is treated as being at the apogee of a new elliptical orbit. The parameters of this new elliptical orbit are calculated, using a series of common relations from orbital mechanics [58].

This process begins with the calculation of the Kepler area constant of the new orbit, by the equation

$$C_{cgL} = v_{cgL}\, r_{cgL} \tag{3. 40}$$

The orbital energy constant of the loaded center of gravity's orbit is found by the expression

$$OEC_{cgL} = v_{cgL}^{\,2} - \frac{2\,GM_E}{r_{cgL}} \tag{3. 41}$$

From the values of the Kepler area constant and the orbital energy constant, the eccentricity of the tether's loaded center of gravity is found according to the equation

$$e_{cgL} = \sqrt{1 + \frac{C_{cgL}^{\,2}}{GM_E^{\,2}} OEC_{cgL}} \tag{3. 42}$$

The parameter of the orbit of the tether's loaded center of gravity is found from the relation

$$po_{cgL} = \frac{C_{cgL}^{\ 2}}{GM_E} \tag{3. 43}$$

From the eccentricity and the orbit parameter, the perigee altitude of the tether's loaded center of gravity is found by the expression

$$r_{peri\,cgL} = \frac{po_{cgL}}{1 + e_{cgL}} \tag{3. 44}$$

The distance between the tether's lower tip and the loaded center of gravity is subtracted from the perigee radius to find the radial position of the lower tip at perigee. In order to minimize the drag and heating effects of entering the Earth's atmosphere, it is desired to keep the tether's lower end from descending below an altitude of 100 kilometers. Rather than use a complex set of movable masses and extendable tethers that Sarmont employs, it has been observed that the shift can be minimized by increasing the tether's overall mass. This is achieved in the analysis by increasing the factor of safety in the stepwise integration process, thus increasing the cross sectional area throughout the tether length. The higher safety factor, while increasing the total mass of the system, has several practical advantages. If the tether structure is made up of multiple lines, the higher factor of safety allows for the redundant lines of the tether to absorb some damage from small scale orbital debris and still retain its original payload capability. Figure 3.5 shows the tether mass, for varying lengths, calculated using the method of shifting center of gravity. These calculations involve a tether made of Zylon, with a starting lower tip

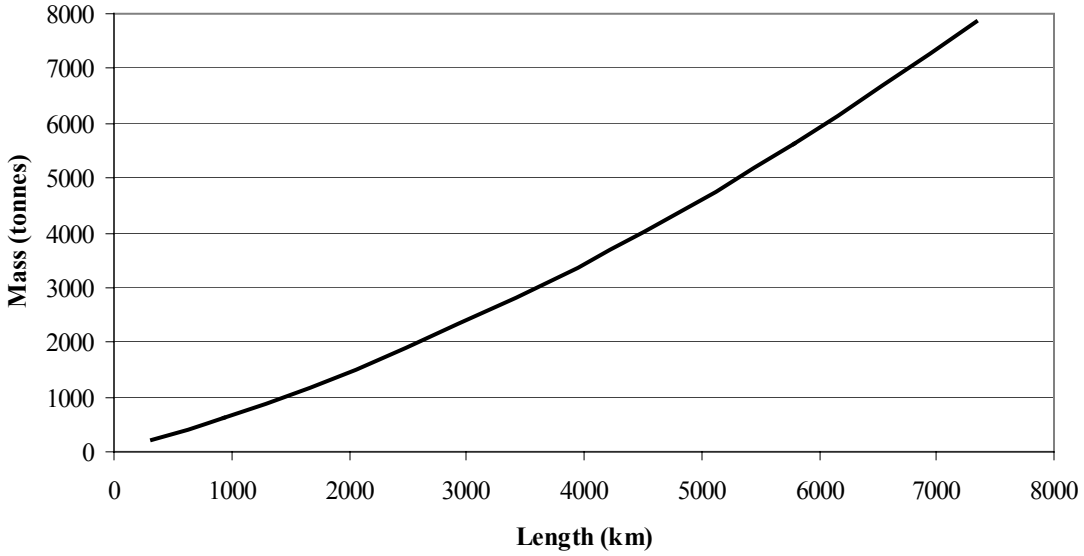


Figure 3.5: Tether Mass versus Length (CG Shift)

altitude of 250 kilometers, a payload of 10,000 kilograms and a central reboost station mass of 100 tonnes.

It can be observed that while the methods used in Zubrin's and Lockheed Martin's analysis produced an exponential growth in tether mass as the length increased, by the method of shifting center of gravity the relation between length and mass is more linear. The drawback to this method is that the response of the tether to loading is entirely independent of the mass of the central station, where the tether propulsion system is located. Because of its location at the center of gravity where the centrifugal and gravitational forces cancel each other out, the mass of the central station contributes nothing to the calculation of the loaded center of gravity. Because of the central station's nonexistent role in determining the tether's orbital response by center of gravity analysis, an additional estimation method based on momentum conservation was investigated.

3.4.2 CG Shift with Momentum Conservation Method

For this study, a fourth method of estimating the effect of payload addition on the tether's orbit has been developed, combining elements of the center of gravity shift employed by Sarmont with the conservation principles that are used by Zubrin and the Lockheed Martin Bridge to Space study. This allows for the accounting of the central reboost propulsion module mass to enter in the analysis.

This method shares a common trait with all of the others, in that the tether is treated as a point mass at its center of gravity. This new center of gravity is calculated by the equation

$$r_{cgL} = \sum_{j=n}^{1} \frac{m_j\, a_j\, r_j + m_p\, a_{le}\, r_{le}}{m_j\, a_j + m_p\, a_{le}} \qquad (3.45)$$

The total angular momentum of the tether, with the mass of the reboost propulsion station included is calculated by the equation

$$h_T = (m_{stat} + m_T) r_{cg} v_{cg} \tag{3. 46}$$

The total angular momentum of the payload-tether orbit is calculated by adding to this the angular momentum of the payload , shown by

$$h_{total} = (m_{stat} + m_T) r_{cg} v_{cg} + m_p r_{le} v_{le} \tag{3. 47}$$

The velocity of the new loaded center of gravity is found by dividing the product of the total angular momentum of the system by the product of the total mass, including tether, reboost station and payload, and the radius of the loaded center of gravity, as detailed in the expression

$$v_{cgL} = \frac{h_{total}}{(m_t + m_{stat} + m_p) r_{cgL}} \tag{3. 48}$$

With the value of the new velocity of the loaded tether-payload system center of gravity obtained, the orbit is calculated with the standard orbital mechanics equations similar to the method employed above in the shifted center of gravity analysis. Also, as in the center of gravity shift analysis, the tether's lower tip is prevented from entering the Earth's atmosphere by increasing the total mass of the tether, again accomplished by increasing its factor safety. Figure 3.6 represents the tether length plotted against its total mass, for a tether with an initial lower tip altitude of 250 kilometers, a payload mass of 10 tonnes and a reboost module weight of 100 tonnes.

3.5 Elevator Sizing Results

A comparison can be made of the five different methods of elevator sizing explained in this chapter: Zubrin, Bridge to Space, Sarmont, CG shift and CG

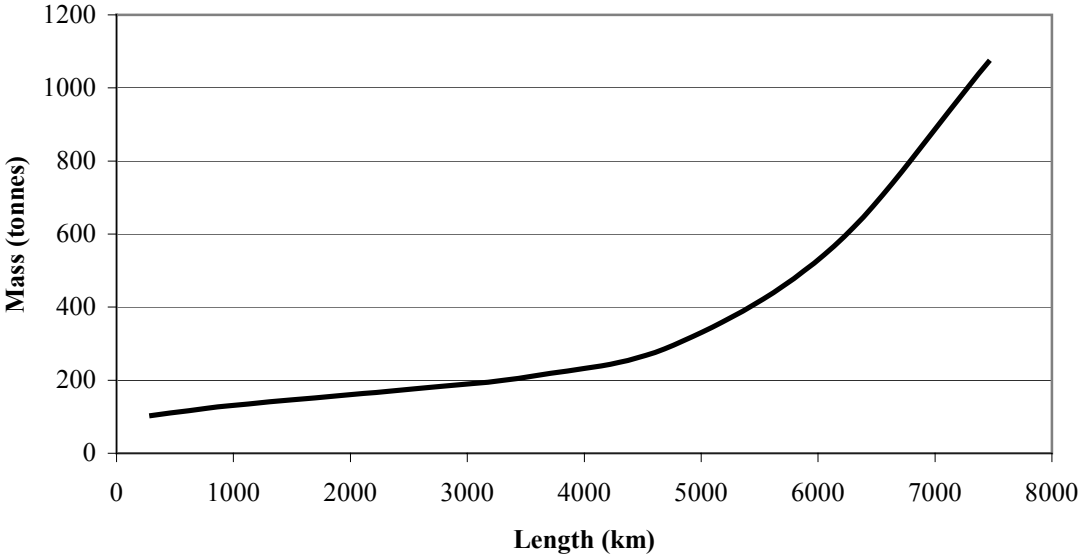


Figure 3.6: Tether Mass versus Length (CG Shift with Momentum Conservation)

Momentum Conservation. Instead of comparing the total system mass for each method, the mass ratio, equal to the total tether and reboost station mass divided by the payload mass, is used to normalize the data. Also, instead of plotting for varying tether lengths, the data is plotted for varying values of the lower tip velocity, the velocity at which the launch vehicle hands off its payload to the tether, recasting the results in terms of the required launch vehicle performance. With orbital velocity at the lower tip altitude of 250 kilometers equal to 7.75 kilometers per second, the lower tip velocity gives some measure as to the relaxed performance requirements of the suborbital launch vehicle, as afforded by the tether. Figure 3.7 shows the mass ratios calculated by the four detailed orbital response methods for varying handoff velocities, along with the single data point generated in Sarmont's writings.

The technique of center of gravity shift developed for this study produces the largest required mass ratios, while the method of center of gravity shift with momentum conservation scheme is the lowest. For tethers with a handoff velocity of approximately 5.25 kilometers per second, the upper tip velocity is fast enough to allow payloads to be released on a Hohmann trajectory to the Moon. Figure 3.8 disregards the high values provided by the shifted center of gravity analysis and provides a more detailed view of the mass ratios generated by methods of Zubrin, Lockheed Martin, and the CG shift with momentum conservation.

It should be noted that the methods of Zubrin and Bridge to Space and the method of center of gravity shift with momentum conservation are somewhat in agreement for handoff velocities of less than 6 kilometers per second, corresponding to tether lengths of around approximately 2,600 kilometers in length, depending upon material properties.

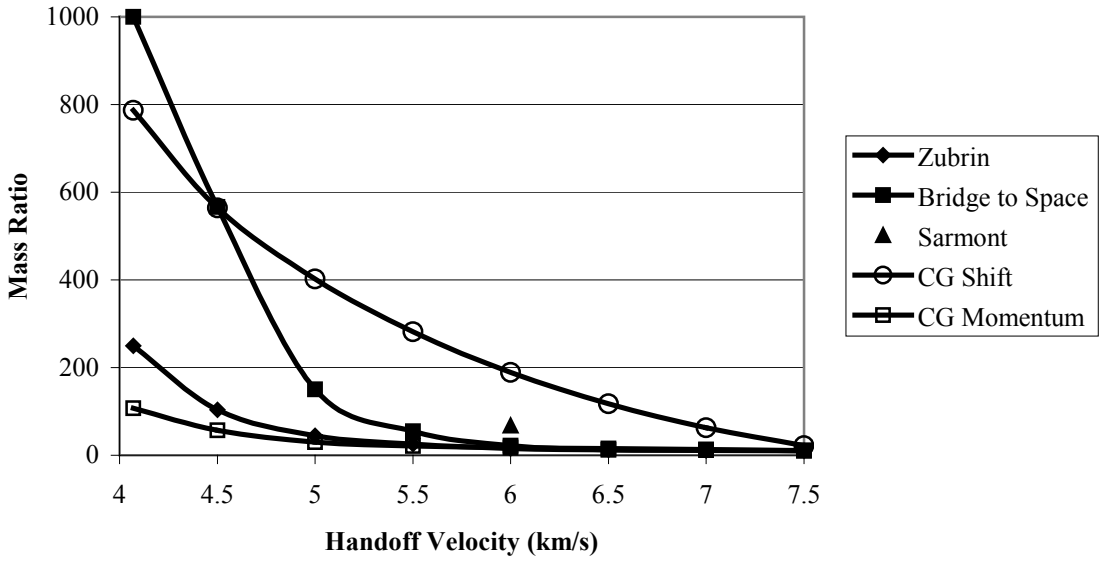


Figure 3.7: Mass Ratio versus Handoff Velocity for All Estimation Methods

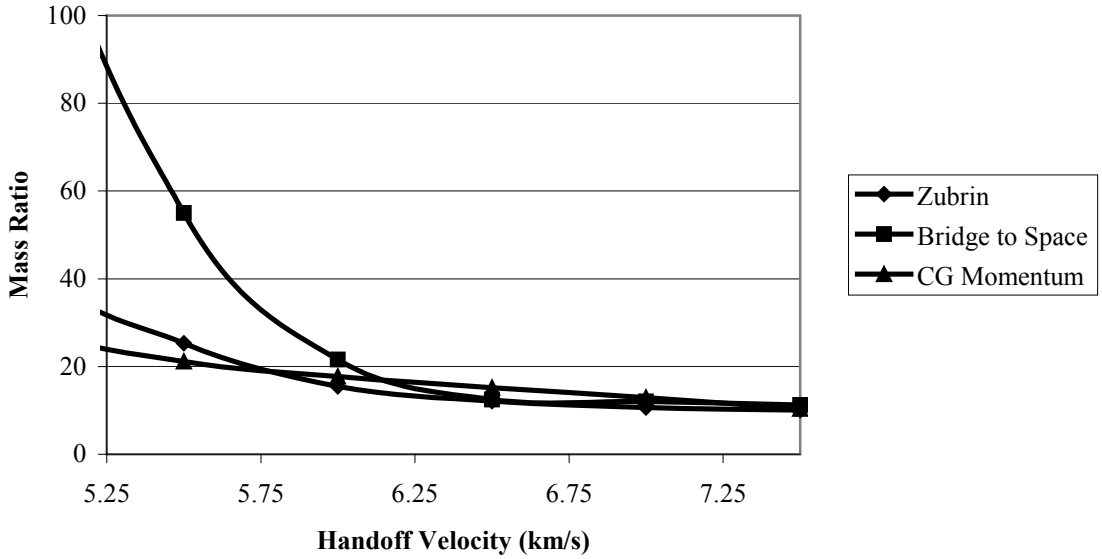


Figure 3.8: Mass Ratio versus Handoff Velocity

Lunar transport tethers are approximately 4,000 kilometers long, corresponding to a handoff velocity of 5.25 kilometers per second, while escape trajectory tethers are around 4,300 kilometers in length and correspond to a handoff velocity of 5.17 kilometers per second. Both of these lengths fall in the range where the results of the various methods begin to deviate from each other. Because of the divergent results of the different methods, these techniques should only be seen as an approximation of the behavior of the tether while bearing the payload. To truly understand the behavior of the tether-payload system, it is necessary to devise an accurate dynamic simulation of its behavior.

Chapter 4

Dynamic Tether Simulation

4.1 Previous Efforts

In order to understand the dynamics involved with loading the orbiting elevator with a payload, a detailed mathematical model of the system must be developed. Past efforts to model the behavior of tethered satellite systems have used various methods. The simplest models involve the tether being treated as a massless and rigid rod connecting two end masses in a dumbbell configuration [59]. This approach is attractive because in treating the tether satellite system as a dumbbell structure, it simplifies the equations of motion to describing the movement of the two end masses with 3 degrees of freedom each. The drawback to this approach is that it neglects any strain deformation experienced by the tether and yields a simplified model of any pendular motion experienced by the tether. The tether has also been modeled as a continuum, allowing for the coupling of the orbital and pendular motion of the tether [60]. This analysis is appealing in that the tether is not simplified by assumptions of being massless, however this method has only been used to study tethers of constant cross section and relatively short length.

Both the dumbbell and the continuum models have been used primarily to simulate the motion of a small satellite tethered to a relatively larger end mass, in most cases a tethered satellite operating from the space shuttle. The tether lengths in these studies are typically on the order of ten kilometers, far short of the lengths needed for an orbiting space elevator. The dumbbell approach has in the past been used in a limited

number of cases to study the behavior of larger tethers and it has been shown that such a system is not stable in the radial direction when the length of the tether approaches the same order of magnitude of the orbital radius of the satellite [61]. Further studies using energy momentum techniques applied to a continuous string have shown that a full ground to geosynchronous space elevator made of carbon nanotubes is stable when a mass of approximately 6,000 kilograms is added to the geosynchronous point [62].

Another method developed to simulate the motion of a tether in space is to treat the tether as a collection of point masses connected by springs. Individual equations of motion for each point mass are derived and integrated through time to provide a description of the tether's motion. Such an approach lends itself to the pursuit of a numerical solution to the problem of tether orbital dynamics. A program named BeadSim was written by Joseph Carroll of Tether Applications, Inc. in the late 1980s that used the point mass collection method to describe the tether's orbital motion. This program was a simplified two dimensional representation of the mechanical motion of a tether in a central gravity field with some account given to atmospheric drag.

4.2 Problem Description

This study will pursue the point mass and springs approach to describe the tether orbital motion. In addition to the central gravity force exerted by the Earth that dominates the tether's motion, the perturbing forces caused by atmospheric drag, Earth oblateness and electrodynamic propulsion will be included in this study. The tether is divided into one hundred equidistant segments. Each segment is treated as a point mass occupying the midpoint of each segment length. All forces acting on an individual tether segment are assumed to act on the segment's point mass. The collection of point masses

are connected by massless springs which are mathematically modeled to simulate the elasticity of the material comprising the tether. The payload is also modeled as a point mass, attached by a spring to the lowest tether segment point mass. The mass of each segment point mass is calculated by the product of the tether material density, the cross sectional area at the position of the point mass, calculated by the equation derived in Chapter 3, and the segment length, according to the equation

$$m_j = \rho_T \, A_{x\,j} \, l_{seg} \tag{4. 1}$$

At the segment occupying the tether center of gravity, an additional mass of 100 tonnes has been added to simulate the tether power supply and the mass of any equipment used in the maintenance of the tether.

4.2.1 Definition of Coordinate Systems

Spherical polar coordinates with their origin at the Earth's center are used in the derivation of the equations of motion for each tether segment point mass. Spherical coordinates are useful because they accurately describe the motion of the orbiting tether, with r and θ coordinates lying in the original orbital plane of the tether, and φ describing angular position inclined to the orbital plane. In addition to the spherical polar coordinates used in the equations of motion, several other coordinate systems are used to describe the various forces acting on the tether. The first coordinate system, A,B,C, shown in Figure 4.1, is centered on the Earth with A and B axes in the Earth's equatorial plane and Z axis pointing north along the Earth's polar axis. The second coordinate system, X,Y,Z, also shown in Figure 4.1, is centered on the Earth with X axis lying along the intersection of the tether's orbital plane with the Earth's equatorial plane, coinciding

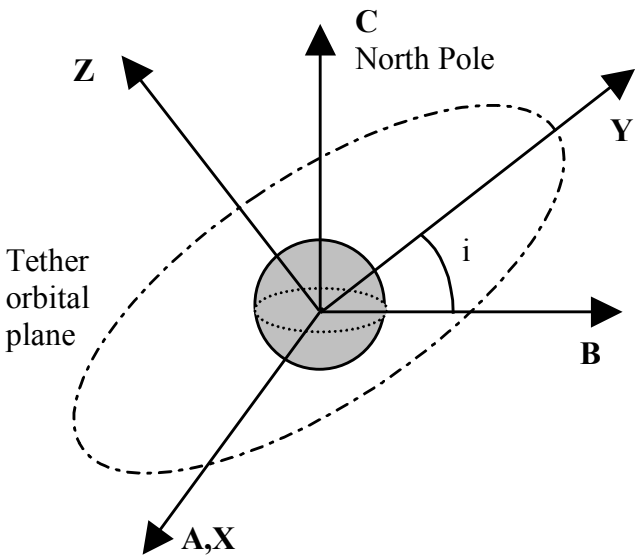


Figure 4.1: Earth Centric Cartesian Coordinate Systems

with the A axis, the Z axis perpendicular to the tether's orbital plane and Y axis orthogonal to the other two. Converting from spherical polar coordinates to Earth centered orbital plane coordinate system is accomplished by the set of equations

$$\begin{bmatrix} X \\ Y \\ Z \end{bmatrix} = \begin{bmatrix} r\cos(\varphi)\cos(\theta) \\ r\cos(\varphi)\sin(\theta) \\ r\sin(\theta) \end{bmatrix} \tag{4. 2}$$

as can be seen from Figure 4.2.

A third coordinate system, x,y,z, shown in Figure 4.3, is centered on a particular tether segment point mass j with the x axis lying along the outward radial direction, the y axis in the direction of orbital motion and z axis perpendicular to the orbital plane with northwards being positive. This allows distances and accelerations in the tether segment centered coordinate system to be easily transferred to the spherical polar coordinates in which the equations of motion are written in. The segment centered x direction corresponds to the spherical polar r direction, while the y axis is pointing in the positive θ direction, and the z axis is in the positive φ direction.

4.3 Tether Segment Equations of Motion

The first step in this analysis is to develop equations of motion for each tether segment. This is accomplished through the use of Lagrange's equation for non-conservative forces, expressed as

$$\frac{d}{dt}\left(\frac{\partial T}{\partial \dot{q}_i}\right) - \frac{\partial T}{\partial q_i} = Q_j \tag{4. 3}$$

where T is the total kinetic energy of all the tether segments, Q is the set of generalized forces acting on the tether segment, and q is the set of generalized coordinates describing

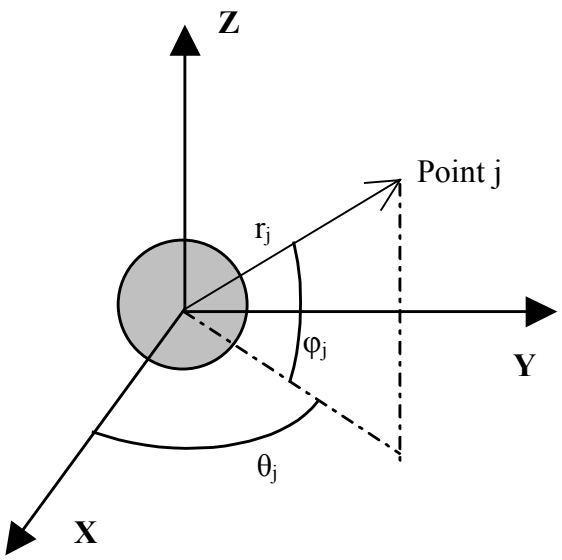


Figure 4.2: Earth-Centric Polar Coordinate System

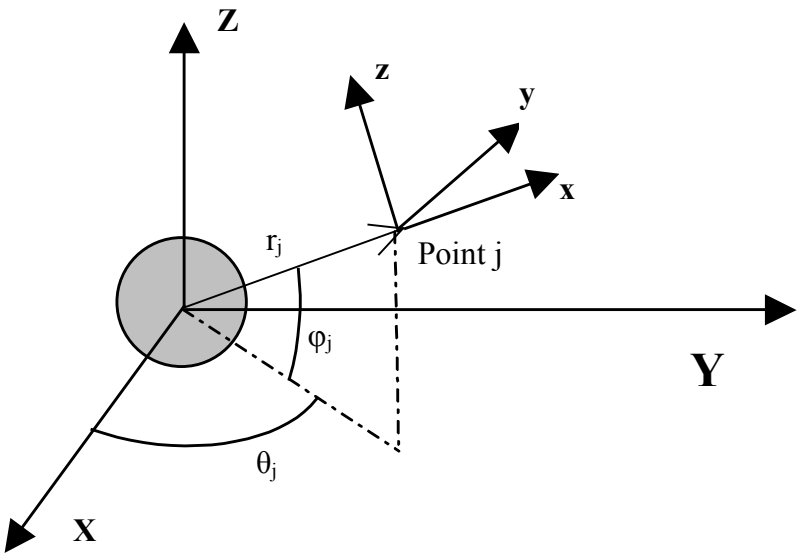


Figure 4.3: Segment Centered Coordinate System

the segment's motion. The kinetic energy of the tether is described by summing the products of the mass of each segment multiplied by its respective velocity, shown by the equation

$$T = \sum_{j=1}^{n} \frac{1}{2} m_j \left[\dot{r}_j^{\,2} + \left(r_j \dot{\theta}_j \right)^2 + \left(r_j \dot{\varphi}_j \right)^2 \right] \tag{4. 4}$$

For a specific segment, the equation of motion corresponding to the radial coordinate can be found by the equation

$$\frac{d}{dt}\left(\frac{\partial T}{\partial \dot{r}_j} \right) - \frac{\partial T}{\partial r_j} = Q_{r\,j} \tag{4. 5}$$

The partial derivative of the tether segment kinetic energy with respect to the radial velocity is expressed as

$$\frac{\partial T}{\partial \dot{r}_j} = m_j \dot{r}_j \tag{4. 6}$$

while the partial derivative of the tether kinetic energy with respect to radial position is

$$\frac{\partial T}{\partial r_j} = m_j r_j \dot{\theta}_j^{\,2} \tag{4. 7}$$

Inserting these relations back into LaGrange's equation produces the radial coordinate equation of motion for a specific tether segment, shown by

$$\ddot{r}_j - r_j \dot{\theta}_j^{\,2} = \frac{Q_{r\,j}}{m_j} \tag{4. 8}$$

Rearranging the equation produces an expression for acceleration in the radial direction, shown by

$$\frac{dv_{r\,j}}{dt} = r_j \dot{\theta}_j^{\,2} + \frac{Q_{r\,j}}{m_j} \tag{4. 9}$$

The equation of motion in the θ direction can also be derived through Lagrange's equation starting with the expression

$$\frac{d}{dt}\left(\frac{\partial T}{\partial \dot{\theta}_j}\right) - \frac{\partial T}{\partial \theta_j} = Q_{\theta j}\, r_j \tag{4. 10}$$

where the term on the right hand side of the equation, $Q_{\theta j}\ r_j$, is a generalized torque expressed as the product of the generalized force and the radial position of the point mass. The partial derivative of the tether kinetic energy with respect to angular velocity in the θ direction is

$$\frac{\partial T}{\partial \dot{\theta}_j} = m_j\, r_j^{\,2} \dot{\theta}_j \tag{4. 11}$$

while the partial derivative of the tether kinetic energy with respect to the θ coordinate is zero, shown by

$$\frac{\partial T}{\partial \theta_j} = 0 \tag{4. 12}$$

By noting that the velocity of the tether segment in the θ direction is equal to the product of the radius of the segment with its tangential velocity, the partial derivative of the tether kinetic energy can be rewritten in the form of

$$\frac{\partial T}{\partial \dot{\theta}_j} = m_j\, r_j\, v_{\theta j} \tag{4. 13}$$

Inserting this expression back into Lagrange's equation produces the expression

$$\frac{d}{dt}\left(r_j\, v_{\theta j}\right) = \frac{Q_{\theta j}}{m_j}\, r_j \tag{4. 14}$$

By evaluating the derivative on the left hand side according to the chain rule, the Lagrange equation can be rearranged to produce an expression for acceleration in the θ direction, shown by

$$\frac{dv_{\theta j}}{dt} = -\frac{\dot{r}_j v_{\theta j}}{r_j} + \frac{Q_{\theta j}}{m_j} \tag{4. 15}$$

The same process can be used to derive the equation for acceleration in the φ direction, producing the expression

$$\frac{dv_{\varphi j}}{dt} = -\frac{\dot{r}_j v_{\varphi j}}{r_j} + \frac{Q_{\varphi j}}{m_j} \tag{4. 16}$$

4.4 Forces Acting Upon the Tether

The major force acting on a tether in orbit of the Earth is internal tension, generated by gravitational attraction between the Earth and the tether. The smaller perturbing forces acting on the tether fall into four separate categories. The first of these are gravitational perturbations caused by Earth oblateness, lunar gravitation, solar gravitation, and relativistic effects. This study accounts for the Earth oblateness effects but disregards the third body attraction of the Sun and Moon and relativistic effects, which are extremely small, on the order of 10^{-8} when compared to the internal tension force in the tether [61].

The second group of perturbing forces are generated by the material structure and properties of the tether material. These perturbing forces can be created by the bending stiffness of the material, residual stresses in the material if it has been stored in a spooled configuration for long periods of time, and internal friction of the material fibers. These

forces are all typically small, on the order of 10^{-9} when compared to the internal tether tension, and are disregarded in this study [61].

The third set of perturbing forces are related to the Earth's magnetic field and its interaction with the tether. The collision between an orbiting tether and the ion in the upper atmosphere will induce a small plasma drag, typically on the order of $2x10^{-4}$ Newtons. For a conducting tether with no applied current, electrostatic charge will produce a Lorentz force that will slowly decelerate the tether. With a current applied across the tether from an external force, the direction of this Lorentz force can be reversed and consequently will increase the speed of the tether. The use of electrodynamic reboosting of the tether is modeled in this study.

The fourth and final set of perturbations are caused by the upper atmospheric environment in which the tether resides. These perturbations are caused by atmospheric drag, solar pressure on the tether, and meteor impacts. Atmospheric drag has been modeled in this simulation of tether behavior. Solar pressure is relatively small, on the order of 10^{-4} Newtons, and is disregarded in this study, as are the effects of meteor impacts, with an even smaller typical force of 10^{-7} Newtons [61].

4.4.1 Earth's Gravity

With the use of polar spherical coordinates, the gravitational attraction of the Earth acts only in the radial direction. The acceleration due to Earth's gravity felt by the tether segment is calculated by the expression

$$a_{gj} = -\frac{GM}{r_j^{\,2}} \tag{4. 17}$$

where GM is the gravitational constant of the Earth, assumed to have the value of 398,601 km^3/s^2. The value of the acceleration is negative because it acts against the positive radial outward direction.

4.4.2 Tension

With the treatment of the tether as a collection of point masses connected by springs, accounting must be made for the accelerations felt by each point mass caused by the springs. For this study, the springs are assumed to behave linearly, allowing the formulation of the spring forces to be based on based on Hooke's law, which states that the strain experienced by a material body is linearly related to the stress causing the deformation, shown by the expression

$$\sigma = E\varepsilon \tag{4. 18}$$

where E is the Young's modulus of the tether material. By noting that the stress of the spring is equal to the loading force over the cross sectional area and that the strain is equal to the change in length of the spring divided by the natural length of the spring, Hooke's law can be written as

$$\frac{F_{Ten}}{A_x} = E\frac{l - l_{nat}}{l_{nat}} \tag{4. 19}$$

Rearranging the expression to solve for the tension force provides the expression

$$F_{Ten} = \frac{E\,A_x}{l_{nat}}\left(l - l_{nat}\right) \tag{4. 20}$$

The value of the Young's modulus multiplied by the cross sectional area divided by the natural length of the spring can be viewed as the spring constant, producing the alternate formulation of Hooke's law

$$F_{Ten} = k(\Delta l) \tag{4. 21}$$

which states that the change in the spring's length is linearly proportional to the tension force.

For this study it should be carefully noted that the natural length of the springs between each tether segment are not simply equal to the distance between point masses. When the tether is in its orbit and is not loaded with a payload, it is still stretched by the combination of Earth's gravity and centrifugal forces. Because the tether cross sectional area changes with radial position the natural lengths of each spring are not equal, and it is necessary to calculate the natural length of the each springs between every tether segment.

The tether cross sectional area was derived in Chapter 3 to allow for constant stress in the tether when loaded with its design payload. This assumption forms the basis of the derivation of each spring's natural length. The constant stress experienced at a generalized point along the tether when loaded with the payload is the sum of the stress in the unloaded tether and the additional stress caused by the payload shown by the expression

$$\sigma_L = \sigma_{UL} + \frac{m_p g_p}{A_x} \tag{4. 22}$$

where m_p is the mass of the payload and g_p is the gravitational acceleration at the tether lower tip where the payload is attached. The numerical value for the loaded stress in the tether is the value of the material's tensile strength divided by the design factor of safety, shown by the equation

$$\sigma_L = \frac{\sigma}{f_s} \tag{4. 23}$$

The formulation of Hooke's law for the unloaded tether is expressed as

$$\sigma_{UL} = E\frac{l_{seg} - l_{nat}}{l_{nat}} \tag{4. 24}$$

where l_{seg} is the distance between each tether segment point mass. By noting that the unloaded stress is the difference between the loaded stress and the stress caused by the payload the expression can be rewritten as

$$\sigma_L - \frac{m_p g_p}{A_x} = E\frac{l_{seg} - l_{nat}}{l_{nat}} \tag{4. 25}$$

This can be solved to produce an equation for the natural length of the tether, shown by the expression

$$l_{nat} = \frac{E\, l_{seg}}{E + \sigma_L - \dfrac{m_p g_p}{A_x}} \tag{4. 26}$$

The equation can be generalized to express the natural length of any spring along the segmented tether of this study, shown by the equation

$$l_{nat,j} = \frac{E\, l_{seg}}{E + \sigma_L - \dfrac{2\, m_p g_p}{A_{x\,j} + A_{x\,j+1}}} \tag{4. 27}$$

which corresponds to the spring between tether point mass j and point mass j+1.

With the natural length of each spring known, the tension forces and accelerations acting on each segment can be calculated according to the equation

$$a_{Ten} = \frac{F_{Ten}}{m} = \frac{E\, A_x}{m}\frac{(Dist - l_{nat})}{l_{nat}} \tag{4. 28}$$

For a general tether segment point mass j, the acceleration caused by the spring between point mass j and point mass j+1, is shown by the equation

$$a_{Ten,(j,j+1)} = \frac{E\left(A_{x\,j} + Ax_{j+1}\right)}{2\,m_j}\frac{\left(Dist_{j,j+1} - l_{nat,j}\right)}{l_{nat,j}} \tag{4. 29}$$

It can be observed that the tension acceleration experienced by a point mass is dependent upon the position of the adjacent point masses. This dependency couples the equations of motion of a point mass to that of its adjacent point masses. By noting that the mass of the tether segment is the product of the material density, the segment cross sectional area, and the segment length, the tension acceleration can be written as

$$a_{Ten,(j,j+1)} = \frac{E\left(A_{x\,j} + A_{x\,j+1}\right)}{2\,\rho_T\,A_{x\,j}\,l_{seg}}\frac{\left(Dist_{j,j+1} - l_{nat,j}\right)}{l_{nat,j}} \tag{4. 30}$$

Similarly, the tension acceleration acting on point mass j caused by the spring in between point mass j and point mass j-1 can be written as

$$a_{Ten,(j,j-1)} = \frac{E\left(A_{x\,j} + A_{x\,j-1}\right)}{2\,\rho_T\,A_{x\,j}\,l_{seg}}\frac{\left(Dist_{j,j+1} - l_{nat,j-1}\right)}{l_{nat,j-1}} \tag{4. 31}$$

The tension acting on the payload attached at the tether lower tip caused by the spring between the first point mass and the payload is calculated by the equation

$$a_{Ten,(p,1)} = \frac{E\left(A_{x\,0} + A_{x\,1}\right)}{2\,m_p}\frac{\left(Dist_{p,1} - l_{seg}/2\right)}{l_{seg}/2} \tag{4. 32}$$

while the tension acting on the first tether segment caused by the spring between it and the payload is written as

$$a_{Ten,(1,p)} = \frac{E\left(A_{x0} + A_{x1}\right)}{2\,\rho_T\,A_{x1}\,l_{seg}} \frac{\left(Dist_{p,1} - l_{seg}/2\right)}{l_{seg}/2} \tag{4. 33}$$

Each of these equations depends on the distance between a segment point mass and the point mass adjacent to it on the tether. This distance is calculated by converting the values of their position in the Earth-centered r,θ, φ coordinate frame to the Earth-centered X,Y,Z orbital plane coordinate system, shown by Figure 4.4. Once converted into the Cartesian planetocentric coordinates the distance between two segment centers is found by the equation

$$Dist_{j,j+1} = \sqrt{\left(X_j - X_{j+1}\right)^2 + \left(Y_j - Y_{j+1}\right)^2 + \left(Y_j - Y_{j+1}\right)^2} \tag{4. 34}$$

In order to insert the tension acceleration into the individual segments' equations of motion it is necessary to break the tension acceleration into x,y,z components of the segment-centric coordinate system. The first step is to calculate the distance between a segment point mass and its adjacent point mass in separate coordinates. This is accomplished by performing a coordinate rotation on the Earth-centric distance coordinates. For example, the coordinates of segment j+1 in the segment j-centric coordinate system is found by the following coordinate transfer

$$\begin{bmatrix} x \\ y \\ z \end{bmatrix}_{j,j+1} = \begin{bmatrix} \cos(\varphi_j)\cos(\theta_j) & \cos(\varphi_j)\sin(\theta_j) & \sin(\varphi_j) \\ -\sin(\theta_j) & \cos(\theta_j) & 0 \\ -\sin(\varphi_j)\cos(\theta_j) & -\sin(\varphi_j)\sin(\theta_j) & \cos(\varphi_j) \end{bmatrix} \begin{bmatrix} X_{j+1} - X_j \\ Y_{j+1} - Y_j \\ Z_{j+1} - Z_j \end{bmatrix} \tag{4. 35}$$

The directional cosines of segment j+1 in the segment j centered coordinate system can then be expressed by the set of ratios

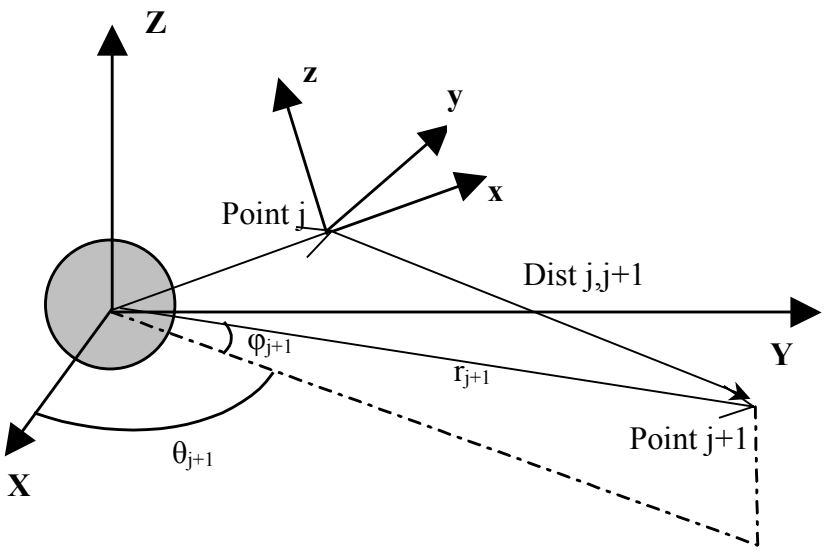


Figure 4.4: Relation Between Earth-Centric and Segment-Centric Coordinate Systems

$$\frac{x_{j,j+1}}{Dist_{j,j+1}}\hat{\mathbf{x}} \tag{4. 36}$$

$$\frac{y_{j,j+1}}{Dist_{j,j+1}}\hat{\mathbf{y}} \tag{4. 37}$$

$$\frac{z_{j,j+1}}{Dist_{j,j+1}}\hat{\mathbf{z}} \tag{4. 38}$$

With the directional cosines calculated the tension acceleration can be written in components of the point mass centered coordinate system, allowing for their inclusion in the r,θ,φ equations of motion. For example, the tension acceleration acting on point mass j caused by the spring between point mass j and j+1 is written in the x,y,z coordinate system as

$$a_{Ten,(j,j+1),x} = \frac{E\left(A_{x\,j} + A_{x\,j+1}\right)}{2\,\rho_T\,A_{x\,j}\,l_{seg}}\frac{\left(Dist_{j,j+1} - l_{nat,j}\right)}{l_{nat,j}}\frac{x_{j,j+1}}{Dist_{j,j+1}} \tag{4. 39}$$

$$a_{Ten,(j,j+1),y} = \frac{E\left(A_{x\,j} + A_{x\,j+1}\right)}{2\,\rho_T\,A_{x\,j}\,l_{seg}}\frac{\left(Dist_{j,j+1} - l_{nat,j}\right)}{l_{nat,j}}\frac{y_{j,j+1}}{Dist_{j,j+1}} \tag{4. 40}$$

$$a_{Ten,(j,j+1),z} = \frac{E\left(A_{x\,j} + A_{x\,j+1}\right)}{2\,\rho_T\,A_{x\,j}\,l_{seg}}\frac{\left(Dist_{j,j+1} - l_{nat,j}\right)}{l_{nat,j}}\frac{z_{j,j+1}}{Dist_{j,j+1}} \tag{4. 41}$$

Similarly, the tension acceleration acting on point mass j caused by the spring between point mass j and j-1 is expressed in point mass centered coordinates x,y,z as

$$a_{Ten,(j,j-1),x} = \frac{E\left(A_{x\,j} + A_{x\,j-1}\right)}{2\,\rho_T\,A_{x\,j}\,l_{seg}}\frac{\left(Dist_{j,j-1} - l_{nat,j-1}\right)}{l_{nat,j-1}}\frac{x_{j,j-1}}{Dist_{j,j-1}} \tag{4. 42}$$

$$a_{Ten,(j,j-1),y} = \frac{E\left(A_{x\,j} + A_{x\,j-1}\right)}{2\,\rho_T\,A_{x\,j}\,l_{seg}}\frac{\left(Dist_{j,j-1} - l_{nat,j-1}\right)}{l_{nat,j-1}}\frac{y_{j,j-1}}{Dist_{j,j-1}} \tag{4. 43}$$

$$a_{Ten,(j,j-1),z} = \frac{E\left(A_{x\,j} + A_{x\,j-1}\right)}{2\,\rho_T\ A_{x\,j}\ l_{seg}} \frac{\left(Dist_{j,j-1} - l_{nat,j-1}\right)}{l_{nat,j-1}} \frac{z_{j,j-1}}{Dist_{j,j-1}} \tag{4. 44}$$

4.4.3 Atmospheric Drag

The lower length of the tether will undergo a small deceleration due to aerodynamic drag caused by the upper reaches of the Earth's atmosphere. This drag force is calculated by the equation

$$F_D = \frac{1}{2}\rho_{atm}\ v^2\ C_D\ A_f \tag{4. 45}$$

where v is the velocity of the tether, C_D is its coefficient of drag and A_f is the surface area of the tether exposed to the direction of travel. The velocities of the tether segments in the radial direction are on the order of a few meters per second, while in the θ direction velocity at the tether lower tip is approximately 5 kilometers per second, depending on the tether overall length. Because of the tether's limited radial velocity, atmospheric drag on the segment point mass in the radial direction is not calculated for this study. For a particular segment point mass, the exposed surface area in the θ or φ direction is dependent upon the cross sectional area of the segment, which is calculated by the equation derived in Chapter 3. The cross sectional area of the segment is related to its thickness by the expression

$$A_x = \pi\ rad^2 \tag{4. 46}$$

assuming that the tether's cross sectional shape is circular. The diameter of an individual line in the tether segment is calculated by the equation

$$Dia = \sqrt{\frac{4\,A_x}{n\,\pi}} \tag{4. 47}$$

where n is the number of lines making up the multiple line tether. The exposed surface area for a particular segment is then calculated by the product of the individual line diameter, the segment length, and the number of lines, and is written as

$$A_f = l_{seg} \sqrt{\frac{4 A_x n}{\pi}} \tag{4. 48}$$

The drag equation requires the total velocity of the particular tether segment, which is expressed as the sum of its components by the equation

$$v = \sqrt{\dot{r}^2 + \left(r \dot{\theta}\right)^2 + \left(r \dot{\varphi}\right)^2} \tag{4. 49}$$

The atmospheric density is calculated for the radial position of each tether segment point mass. A simplified model is used that separates the atmosphere into three zones, each governed by a different relation between atmospheric density and altitude [63]. The first zone is valid for altitudes between 70 and 118 kilometers; within this zone the atmospheric density decays exponentially with increasing altitude according to the relation

$$\rho_{atm} = 11 e^{-Alt/6} \tag{4. 50}$$

The second region of the atmosphere is between 118 and 200 kilometers, where the atmospheric density is governed by the expression

$$\rho_{atm} = \frac{(alt - 95)^{-3}}{2600} \tag{4. 51}$$

The third zone of the atmosphere is above altitudes of 200 kilometers, where the atmospheric density is dependent on both the altitude and the temperature of the exosphere, shown by the equation

$$\rho_{atm} = \frac{1.47 \times 10^{-16}\ \mathrm{Tex}\left(3000 - \mathrm{Tex}\right)}{\left[1 + 2.9(\mathrm{alt} - 200)/\mathrm{Tex}\right]^{10}} \tag{4. 52}$$

Figure 4.5 shows the atmospheric density versus altitude for several different values of exosphere temperature. The actual temperature of the exosphere is highly dependent upon solar activity levels and can vary between 600 K and 2000 K, depending upon the particular time within the solar cycle. For this study an average value of 1100 K has been used in the computer model.

The drag force can be broken into y and z components of the segment point mass centered coordinate system, corresponding to the θ and φ directions, respectively, by using the velocity directional cosines, which are

$$\frac{r\,\dot{\theta}}{v}\hat{\mathbf{y}} \tag{4. 53}$$

$$\frac{r\,\dot{\varphi}}{v}\hat{\mathbf{z}} \tag{4. 54}$$

For a general tether segment point mass j, the y and z component drag accelerations are calculated by dividing the drag force equation by the mass of the particular segment, and are written as

$$a_{D\,j\,y} = \frac{\rho_{atm\,j}\ v_j^{\,2}\ C_D\ l_{seg}}{2\,\rho_T\ A_{x\,j}\ l_{seg}} \sqrt{\frac{4\,A_{x\,j} n}{\pi}}\ \frac{r_j\ \dot{\theta}_j}{v_j} \tag{4. 55}$$

$$a_{D\,j\,z} = \frac{\rho_{atm\,j}\ v_j^{\,2}\ C_D\ l_{seg}}{2\,\rho_T\ A_{x\,j}\ l_{seg}} \sqrt{\frac{4\,A_{x\,j} n}{\pi}}\ \frac{r_j\ \dot{\varphi}_j}{v_j} \tag{4. 56}$$

These expressions can be algebraically simplified and expressed in terms of the r, θ and φ coordinates of the tether segment, resulting in the final form

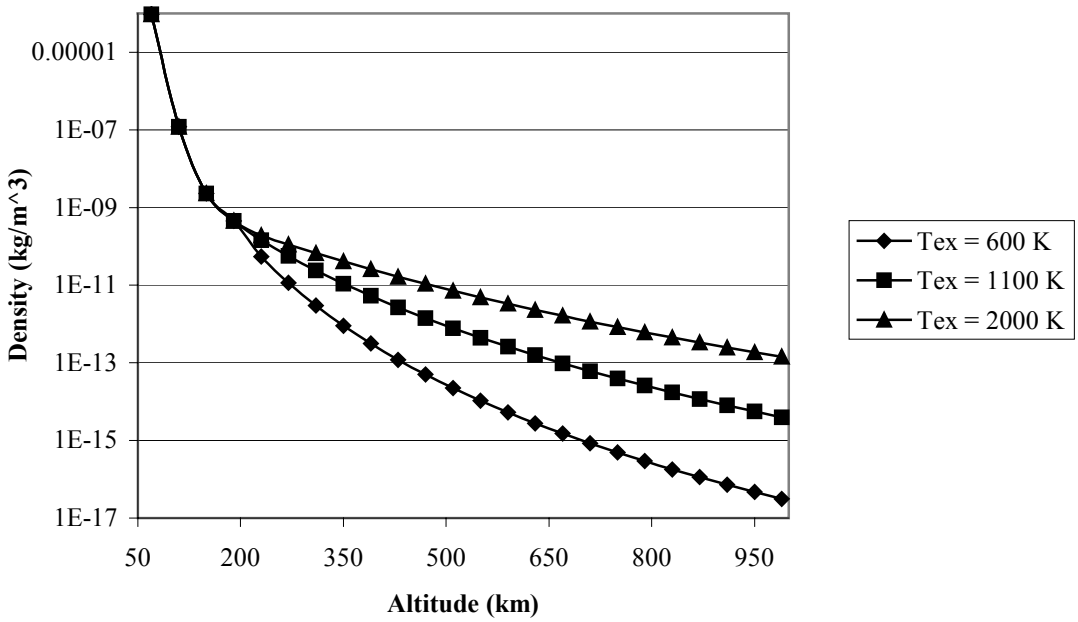


Figure 4.5: Atmospheric Density versus Altitude

$$a_{Djy} = \frac{\rho_{atmj} C_D r_j \dot{\theta}_j}{2\rho_T} \sqrt{\frac{4n\left[\dot{r}_j^2 + \left(r_j \dot{\theta}_j\right)^2 + \left(r_j \dot{\varphi}_j\right)^2\right]}{\pi A_{xj}}} \tag{4. 57}$$

$$a_{Djz} = \frac{\rho_{atmj} C_D r_j \dot{\varphi}_j}{2\rho_T} \sqrt{\frac{4n\left[\dot{r}_j^2 + \left(r_j \dot{\theta}_j\right)^2 + \left(r_j \dot{\varphi}_j\right)^2\right]}{\pi A_{xj}}} \tag{4. 58}$$

4.4.4 Earth Oblateness

The oblateness of the Earth produces a harmonic perturbation to the tether's orbit. Expressions for this small acceleration are derived using potential theory. The radial and tangential equations of motion for an object in orbit are expressed in terms of the Earth's gravitational potential as

$$\ddot{r} - r\dot{\theta}^2 = \frac{\partial \Phi}{\partial r} \tag{4. 59}$$

$$r\ddot{\theta} + 2r\dot{\theta}^2 = \frac{1}{r}\frac{\partial \Phi}{\partial \theta} \tag{4. 60}$$

where the potential function for a perfectly spherical gravity field is

$$\Phi = \frac{GM_E}{r} \tag{4. 61}$$

In order to account for the oblateness of the Earth an additional term must be added to the potential function, producing the form

$$\Phi = \frac{GM_E}{r} + \frac{GM_E J_2 r_E^2}{2r^3}\left\{1 - \frac{3}{2}\sin^2(i)\left[1 - \cos(2u)\right]\right\} \tag{4. 62}$$

where J_2 is the oblateness harmonic coefficient with a value of 1082.630×10^{-6} and u is the argument of the latitude, the tangential position of the tether segment with respect to the Earth's equatorial plane [64]. For the equation of motion corresponding to radial

position, the partial derivative of the new potential function with respect to radial position is calculated to be

$$\frac{\partial \Phi}{\partial r} = -\frac{3}{2}\frac{GM_E J_2 r_E^2}{r_j^4}\left\{1-\frac{3}{2}\sin^2(i)\left[1-\cos(2u)\right]\right\} \tag{4. 63}$$

The partial derivative of the potential function with respect to tangential position, needed for the second orbital equation of motion is computed to be

$$\frac{1}{r}\frac{\partial \Phi}{\partial \theta} = -\frac{3}{2}\frac{GM_E J_2 r_E^2}{r_j^4}\sin^2(i)\sin(2u) \tag{4. 64}$$

The out-of-plane acceleration in the φ direction caused by oblateness is found by taking the partial derivative of the potential function with respect to the orbital inclination, divided by the product of the radial position and the sine of the argument of the latitude, shown by

$$\frac{1}{r\sin(u)}\frac{\partial \Phi}{\partial i} = -\frac{3}{2}\frac{GM_E J_2 r_E^2}{r_j^4}\sin(i)\sin(i)\sin(u) \tag{4. 65}$$

The derived accelerations in the radial, tangential, and out-of-plane directions correspond, respectively, to the x, y and z directions in the segment-centric coordinate system. It is also noted that for an object in a circular orbit, the argument of the latitude can be equal to the true anomaly, if the origin of the true anomaly measurement occurs at the intersection of the orbital plane with the Earth's equatorial plane.. This allows the oblateness perturbing accelerations on a general tether segment point mass j to be written in terms of the angular position of the segment, shown by the expressions

$$a_{Obj\,x} = -\frac{3}{2}\frac{GM_E J_2 r_E^2}{r_j^4}\left\{1-\frac{3}{2}\sin^2(i)\left[1-\cos(2\theta_j)\right]\right\} \tag{4. 66}$$

$$a_{Obj\,y} = -\frac{3}{2}\frac{GM_E\,J_2\,r_E^{\,2}}{r_j^{\,4}}\sin^2(i)\sin(2\theta_j) \tag{4.67}$$

$$a_{Obj\,z} = -\frac{3}{2}\frac{GM_E\,J_2\,r_E^{\,2}}{r_j^{\,4}}\sin(i)\cos(i)\sin(\theta_j) \tag{4.68}$$

4.4.5 Electrodynamic Propulsion

In order to compensate for the drop in tether orbital altitude caused by the handling of payloads, it is necessary to apply a thrust force to raise the orbital altitude of the tether. Adjustments to the tether's orbital velocity can be accomplished through the use of a high efficiency, low thrust propulsion system, such as electric propulsion. For this study, an electrodynamic tether propulsion system is used for orbital maneuvering of the tether. Such a system has the benefit of requiring no fuel to be expended; rather the particles comprising the Earth's magnetosphere act as the reaction mass. When a current is applied to the tether, it acts as a wire in the presence of a magnetic field, producing a Lorentz force on the tether by the equation [65]

$$F_{ED} = \int I\left(d\bar{\mathbf{l}} \times \bar{\mathbf{B}}\right) \tag{4.69}$$

For this study, the Earth's magnetic field is able to be modeled as a dipole magnetic field, running along the geographic polar axis of the Earth [66]. In reality, the Earth's magnetic axis is tilted with respect to the geographical polar axis by approximately 11.3°. The geographical polar axis was chosen as the magnetic axis in this study to allow the magnetic field to be time independent, and not contingent upon the hourly position of the Earth, as the Earth's true magnetic field is. This produces a calculated difference in the magnetic field intensity that varies between 0% and 10%, depending upon the latitude position at which the measurement is taken. As the actual

electrodynamic force is a small acceleration acting over a long time, and the time spent at the actual extreme latitudes was small for an orbiting object, this assumption was considered acceptable for this study. The equation for the magnetic field intensity for a dipole field in polar spherical coordinates is

$$\overline{\mathbf{B}} = \frac{\mu_o}{4\,\pi\,r^3}\left(3\left(\overline{\mathbf{m}}\cdot\hat{\mathbf{r}}\right)\hat{\mathbf{r}} - \overline{\mathbf{m}}\right) \tag{4. 70}$$

where $\hat{r}$ is the unit vector in the radial position. In the Earth-centric, equatorial coordinate system, the z axis points towards the geographic north pole. In this coordinate system the vector expression of the magnetic dipole moment of the earth is

$$\overline{\mathbf{m}} = \begin{bmatrix} 0 \\ 0 \\ 8.1\times10^{22} \end{bmatrix} \begin{matrix} \hat{\mathbf{A}} \\ \hat{\mathbf{B}} \\ \hat{\mathbf{C}} \end{matrix} \text{Am}^2 \tag{4. 71}$$

This vector is transferred to the Earth-centric, tether orbital plane coordinate system through a rotation about the A axis by the inclination angle of the tether orbit, shown in the equations

$$\overline{\mathbf{m}} = \begin{bmatrix} 1 & 0 & 0 \\ 0 & \cos(i) & -\sin(i) \\ 0 & \sin(i) & \cos(i) \end{bmatrix} \begin{bmatrix} 0 \\ 0 \\ 8.1\times10^{22} \end{bmatrix} \begin{matrix} \hat{\mathbf{X}} \\ \hat{\mathbf{Y}} \\ \hat{\mathbf{Z}} \end{matrix} \text{Am}^2 \tag{4. 72}$$

The dot product between the magnetic dipole moment vector and the unit vector of the tether segment point mass is expressed in the segment polar spherical coordinates as

$$\overline{\mathbf{m}}\cdot\hat{\mathbf{r}} = -\sin(i)\left(8.1\times10^{22}\right)\cos(\theta)\sin(\varphi) + \cos(i)\left(8.1\times10^{22}\right)\sin(\varphi) \tag{4. 73}$$

With these expressions the magnetic field intensity can be written in vector components within the Earth-centric, tether orbital plane coordinate system as

$$\overline{\mathbf{B}} = \frac{\mu_o}{4\,\pi\,r^3}\left\{\begin{array}{l} 3\left(8.1\times10^{22}\right)\left[-\sin(i)\cos(\theta)\sin(\varphi)+\cos(i)\sin(\varphi)\right]\begin{bmatrix}\cos(\theta)\cos(\varphi)\\ \cos(\theta)\sin(\varphi)\\ \sin(\varphi)\end{bmatrix}\hat{\mathbf{X}} \\ -\begin{bmatrix}0\\ -\sin(i)\left(8.1\times10^{22}\right)\\ \cos(i)\left(8.1\times10^{22}\right)\end{bmatrix}\hat{\mathbf{Y}} \\ \hat{\mathbf{Z}}\end{array}\right. \tag{4. 74}$$

The values for magnetic field intensity at a specific tether segment are then transferred into the point mass-centric coordinate system by two successive coordinate rotations dependent upon the point mass' tangential and out of plane coordinates θ and φ, represented by the matrix expression

$$\begin{bmatrix}B_x\\ B_y\\ B_z\end{bmatrix}_j = \begin{bmatrix}\cos(\varphi_j)\cos(\theta_j) & \cos(\varphi_j)\sin(\theta_j) & \sin(\varphi_j)\\ -\sin(\theta_j) & \cos(\theta_j) & 0\\ -\sin(\varphi_j)\cos(\theta_j) & -\sin(\varphi_j)\sin(\theta_j) & \cos(\varphi_j)\end{bmatrix}\begin{bmatrix}B_X\\ B_Y\\ B_Z\end{bmatrix} \tag{4. 75}$$

The cross product between the individual tether segment length and the local magnetic field intensity is dependent upon the orientation of the tether length, which is calculated to be equal to one half the distance from the segment point mass to either of its adjacent point masses, expressed in the vector equation

$$\left(d\bar{\mathbf{l}}\times\overline{\mathbf{B}}\right)_j = \left(\frac{1}{2}\begin{bmatrix}x\\ y\\ z\end{bmatrix}_{j+1}\times\begin{bmatrix}B_x\\ B_y\\ B_z\end{bmatrix}\right)+\left(\frac{1}{2}\begin{bmatrix}x\\ y\\ z\end{bmatrix}_{j-1}\times\begin{bmatrix}B_x\\ B_y\\ B_z\end{bmatrix}\right) \tag{4. 76}$$

This expression is expanded to the form

$$\left(d\bar{\mathbf{l}}\times\overline{\mathbf{B}}\right)_j = \frac{1}{2}\begin{vmatrix}\hat{\mathbf{x}} & \hat{\mathbf{y}} & \hat{\mathbf{z}}\\ x_{j+1} & y_{j+1} & z_{j+1}\\ B_{x\,j} & B_{y\,j} & B_{z\,j}\end{vmatrix}+\frac{1}{2}\begin{vmatrix}\hat{\mathbf{x}} & \hat{\mathbf{y}} & \hat{\mathbf{z}}\\ x_{j-1} & y_{j-1} & z_{j-1}\\ B_{x\,j} & B_{y\,j} & B_{z\,j}\end{vmatrix} \tag{4. 77}$$

In this study several small angle assumptions were used to simplify the calculation of the field intensity cross product. In initial executions of the program, the angular difference in positions between a point mass and its adjacent point mass was never observed to go above $1x10^{-4}$ radians. This allows a small angle assumption to be applied, stating that the major difference in position between adjacent point masses is solely in the radial direction, allowing the cross product of segment length and field intensity to be written as

$$\left(d\bar{l} \times \overline{\mathbf{B}}\right)_j = \frac{1}{2}\begin{bmatrix} 0 \\ -x_{j+1} B_{z\,j} - x_{j-1} B_{z\,j} \\ x_{j+1} B_{y\,j} + x_{j-1} B_{y\,j} \end{bmatrix} \begin{matrix} \hat{\mathbf{x}} \\ \hat{\mathbf{y}} \\ \hat{\mathbf{z}} \end{matrix} \qquad (4.\ 78)$$

For the supply of current in the tether, it is assumed that a power supply is located at the central station of the tether. The power supplied is assumed to be constant over time, requiring the power supply to be either a combination of solar and battery power, or nuclear in nature. With power supplied from one location, it should be noted that the current, required by the equation dictating electrodynamic force, is not constant throughout its length. The current in the conducting line will decrease as the distance from the power station increases. Based upon the basic design parameter of the reactor design, namely power supplied, the current at each tether segment is calculated. This process starts with the equation describing the relationship between power, current and voltage, written as

$$P = I\,V \qquad (4.\ 79)$$

By noting Kirchoff's law, the relation between voltage, current, and resistance, written as

$$V = I\,R \tag{4. 80}$$

the power expression can be rewritten in terms of the power supplied, producing the equation

$$P = I^2 R \tag{4. 81}$$

which can be solved for the current, producing the expression

$$I = \sqrt{\frac{P}{R}} \tag{4. 82}$$

The resistance in the line is dependent upon several factors, namely the resistance of the material conducting the current, the cross sectional area of the conducting line, and the distance measured from the power supply, written as

$$R = \frac{\text{Dist}\,\rho_{elec}}{A_{x\,con}} \tag{4. 83}$$

This expression can be placed back into the current equation, producing a relation for current at each segment point mass, written as

$$I_j = \sqrt{\frac{P\,A_{x\,con}}{\left| r_j - r_{stat} \right| \rho_{elec}}} \tag{4. 84}$$

For this study a power station producing 50 kilowatts was selected. This level of power is of the same order as supplied by the solar arrays of the International Space Station. A platinum conductor of 1 square millimeter with resistivity of 10.6×10^{-8} Ohm meters was assumed to be part of the multiline tether system. This allows the components of the electrodynamic acceleration upon a tether segment point mass to be written in the segment centric coordinate system as

$$a_{ED\,j\,x} = 0 \tag{4. 85}$$

$$a_{ED\,j\,y} = \sqrt{\frac{P\,A_{x\,con}}{\left| r_j - r_{stat} \right| \rho_{elec}}} \frac{\left(- x_{j+1}\,B_{z\,j} - x_{j-1}\,B_{z\,j} \right)}{2\,\rho_T\,A_{x\,j}\,l_{seg}} \tag{4. 86}$$

$$a_{ED\,j\,z} = \sqrt{\frac{P\,A_{x\,con}}{\left| r_j - r_{stat} \right| \rho_{elec}}} \frac{\left(x_{j+1}\,B_{y\,j} + x_{j-1}\,B_{y\,j} \right)}{2\,\rho_T\,A_{x\,j}\,l_{seg}} \tag{4. 87}$$

4.5 Method of Solution

With the derivation of the forces acting on each tether segment, a solution can be sought to their equations of motion. Due to the very limited out-of-plane angular displacement between adjacent segment point masses observed in the initial numerical simulations, the full program with all perturbing forces included is run in only two dimensions, radial position r and in-plane angular position θ. Out of plane positions, which were typically on the order of $1x10^{-4}$ radians, were disregarded in further iterations of the program. This led to the tether segment point mass equations of motion to be written as

$$\frac{dv_{r\,j}}{dt} = r_j \dot{\theta}_j^{\,2} + a_{g\,j} + a_{Ten,(j,j+1),x} + a_{Ten,(j,j-1),x} + a_{Ob\,j\,x} \tag{4. 88}$$

$$\frac{dv_{\theta\,j}}{dt} = -\frac{\dot{r}_j v_{\theta\,j}}{r_j} + a_{Ten,(j,j+1),y} + a_{Ten,(j,j-1),y} + a_{D\,j\,y} + a_{Ob\,j\,y} + a_{ED\,j\,y} \tag{4. 89}$$

The computer program integrates each of the equations of motion for all one hundred of the point masses and the payload point mass simultaneously using a fourth order Runge Kutta routine. This requires expanding the equations of motion into a collection of first order differential equations. For a general point mass j, the set of expanded first order equations are written fully as

$$\frac{dr_j}{dt} = v_{r\,j} \tag{4.90}$$

$$\begin{aligned}\frac{dv_{r\,j}}{dt} = {} & r_j \dot{\theta}_j^{\,2} - \frac{GM}{r_j^{\,2}} + \frac{E\left(A_{x\,j} + A_{x\,j+1}\right)}{2\,\rho_T\,A_{x\,j}\,l_{seg}} \frac{\left(Dist_{j,j+1} - l_{nat,j}\right)}{l_{nat,j}} \frac{x_{j,j+1}}{Dist_{j,j+1}} \\ & + \frac{E\left(A_{x\,j} + A_{x\,j-1}\right)}{2\,\rho_T\,A_{x\,j}\,l_{seg}} \frac{\left(Dist_{j,j-1} - l_{nat,j-1}\right)}{l_{nat,j-1}} \frac{x_{j,j-1}}{Dist_{j,j-1}} \\ & - \frac{3}{2} \frac{GM\,J_2\,r_E^{\,2}}{r_j^{\,4}} \left(1 - \frac{3}{2}\sin^2(i)\left[1 - \cos(2\theta_j)\right]\right)\end{aligned} \tag{4.91}$$

$$\frac{d\theta_j}{dt} = \frac{v_{\theta\,j}}{r_j} \tag{4.92}$$

$$\begin{aligned}\frac{dv_{\theta\,j}}{dt} = {} & -\frac{\dot{r}_j v_{\theta\,j}}{r_j} + \frac{E\left(A_{x\,j} + A_{x\,j+1}\right)}{2\,\rho_T\,A_{x\,j}\,l_{seg}} \frac{\left(Dist_{j,j+1} - l_{nat,j}\right)}{l_{nat,j}} \frac{y_{j,j+1}}{Dist_{j,j+1}} \\ & + \frac{E\left(A_{x\,j} + A_{x\,j-1}\right)}{2\,\rho_T\,A_{x\,j}\,l_{seg}} \frac{\left(Dist_{j,j-1} - l_{nat,j-1}\right)}{l_{nat,j-1}} \frac{y_{j,j-1}}{Dist_{j,j-1}} \\ & + \frac{\rho_{atm\,j}\,C_d\,r_j\,\dot{\theta}_j}{2\,\rho_T} \sqrt{\frac{4\,n\left(\dot{r}_j^{\,2} + \left(r_j\,\dot{\theta}_j\right)^2 + \left(r_j\,\dot{\varphi}_j\right)^2\right)}{\pi\,A_{x\,j}}} \\ & - \frac{3}{2} \frac{GM\,J_2\,r_E^{\,2}}{r_j^{\,4}} \sin^2(i)\sin(2\theta_j) \\ & + \sqrt{\frac{P\,A_{x\,con}}{\left|r_j - r_{stat}\right|\rho_{elec}}} \frac{\left(-x_{j+1}\,B_{z\,j} - x_{j-1}\,B_{z\,j}\right)}{2\,\rho_T\,A_{x\,j}\,l_{seg}}\end{aligned} \tag{4.93}$$

The four initial conditions needed for each generalized segment point mass are its radial position and velocity, and tangential position and velocity. The initial radial velocity is set to zero, as well as the initial tangential position. This simulates the tether "hanging" in orbit perpendicular to the Earth's local horizon with no vertical speed. The radial position of a generalized segment is based on the number and length of segments

used in the program. The initial tangential velocity is calculated by the product of the initial radial position and the tether angular velocity, as shown by

$$v_{r\,j}^{o} = r_{j}^{o}\omega_{T} \tag{4. 94}$$

4.6 Dynamic Tether Simulation Results

Numerical simulations were run for a tether made of Zylon with a 100 tonne reboost module, which produces 50,000 watts of energy for the electrodynamic reboost system. The elevator is assumed to be composed of four independent lines with a platinum conductor one square millimeter in cross sectional area built into its structure.

The program was run for varying altitudes of the tether's center of gravity and for different values of lower tip altitudes, where the payload handoff between the launch vehicle and the tether occurs. The mass of the tether was adjusted for each run of the program by altering the structural factor of safety, in order to produce a lower tip perigee altitude of 100 kilometers. Figure 4.6 shows the total tether mass versus center of gravity altitude for tethers with handoff altitudes at 200, 300 and 400 kilometers. As can be seen in the graph, the tether mass increases in a manner approximating a shallow exponential growth. The higher handoff altitudes of 300 and 400 kilometers produce lower overall elevator masses than the 200 kilometer handoff altitude tether. The savings in total system mass have to be weighed against the increased launch vehicle performance needed to reach these higher altitudes.

Three elevators of particular interest have been identified in this study. Each has a center of gravity altitude of 2,000 kilometers and a handoff altitude of 200, 300 and 400 kilometers, respectively. The center of gravity altitude is chosen to be 2,000 kilometers

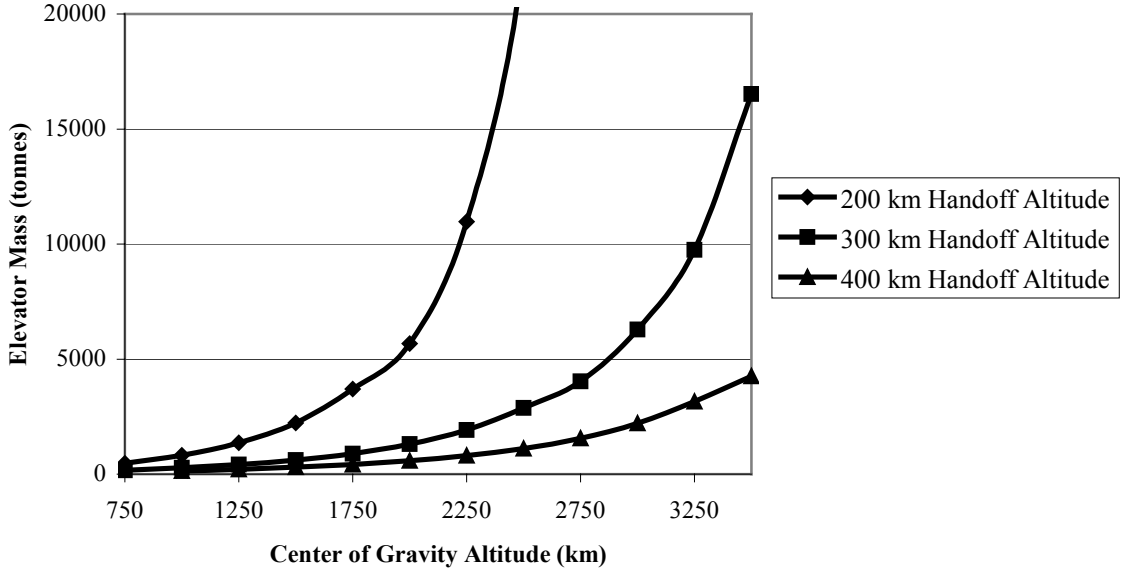


Figure 4.6: Elevator Mass versus Center of Gravity Altitude

because it leads to upper tip velocities that are approximately 95% of the required velocity for a trans-lunar trajectory. Each of the three tethers has an orbital period of 2.119 hours. Table 4.1 gives a comparison of these three tethers with their pertinent characteristics. Table 4.2 shows the comparison of the required elevator masses calculated by the three methods developed in this study: the estimation methods explained in Chapter 3, composed of the center of gravity shift and center of gravity shift with momentum conservation, and the dynamic simulation developed in this chapter.

As can be seen from Table 4.2, the shifting center of gravity method with momentum conservation provided masses that were much lower than those found in dynamic simulation. The required elevator masses generated by the numerical program at least approach the same order of magnitude as those calculated by the shifting center of gravity method. There are still large differences between the data yielded by the numerical program and that from the center of gravity shift method, which can at best be viewed as a very rough estimate of required elevator mass.

The required masses of the three selected elevators, as found by dynamic simulation, are significantly larger than the International Space Station, which at 195 tonnes is the largest structure constructed in space [67]. The use of modular multiple line structures means that much of the elevator's mass is composed of identical tether segments, which will significantly ease development costs. Nevertheless, the large masses required for the elevator still represents a sizeable investment in placing the tether components in orbit.

In order to find the orbital response of the tether to being loaded with the payload, the equations of motion for each tether segment and the payload attached at the lower end

Table 4.1: Characteristics of Three Selected Elevators with 2000 km Center of Gravity Altitude

Handoff Altitude (km)	200	300	400
Handoff Velocity (km/s)	5.415	5.498	5.580
As % of Orbital Velocity	69.57%	71.16%	72.76%
As % of Orbital Energy	51.54%	55.06%	58.48%
Elevator mass (tonnes)	5725.047	1307.625	582.390
Safety Factor	4.00	3.10	2.63
Tether Length (km)	3558	3468	3300
Upper Tip Altitude (km)	3758	3768	3700
Upper Tip Velocity (km/s)	8.344	8.352	8.296
As % of Escape Velocity	94.10%	94.23%	93.28%
As % of Lunar Velocity	95.33%	95.46%	94.49%

Table 4.2: Tether Mass Comparison

Handoff Altitude (km)	200	300	400
CG Shift	4711.873	2024.197	1198.178
CG Shift with Momentum Conservation	256.839	190.629	165.585
Dynamic Simulation	5725.047	1307.625	582.390

are integrated over time for each of the three selected tethers. Figures 4.7, 4.8 and 4.9 show the time history of the altitude of the tether lower tip for the first 12 hours after payload transfer for each of the three selected tethers, respectively.

For each case, it can be observed that the attachment of the payload causes the tether to enter into an elliptical orbit, with the payload and lower tip altitude varying between its initial altitude and the 100 kilometers deemed necessary to avoid atmospheric heating and drag. With each orbital revolution, an increase in lower tip altitude over time can be observed. This increase is due to the thrust applied by the electrodynamic reboost system and is more pronounced in the lighter tethers with higher lower tip altitudes. The tether with the 200 kilometer handoff altitude underwent an average 1.8 kilometers increase in perigee altitude with each revolution. The tether with the 300 kilometer handoff altitude experienced a 7.1 kilometer average increase in perigee altitude with each orbital revolution, while the tether with the 400 kilometer handoff altitude experienced an average perigee altitude increase of 16.5 kilometers per revolution. The increase in orbital speed applied by the electrodynamic reboost system also has the effect of shortening the elevator's orbital period by approximately 1.1 minutes for each orbital revolution. To effectively return the elevator to its initial circular orbit would require the development of a control law for the electrodynamic reboost system. This control law would dictate its operation only during certain portions of the elevator's orbit, specifically during the half of the orbit centered around the apogee of the tether. This would keep the tether at its original orbital altitude at apogee while decreasing the perigee altitude with each successive revolution. In the absence of deriving this control law the

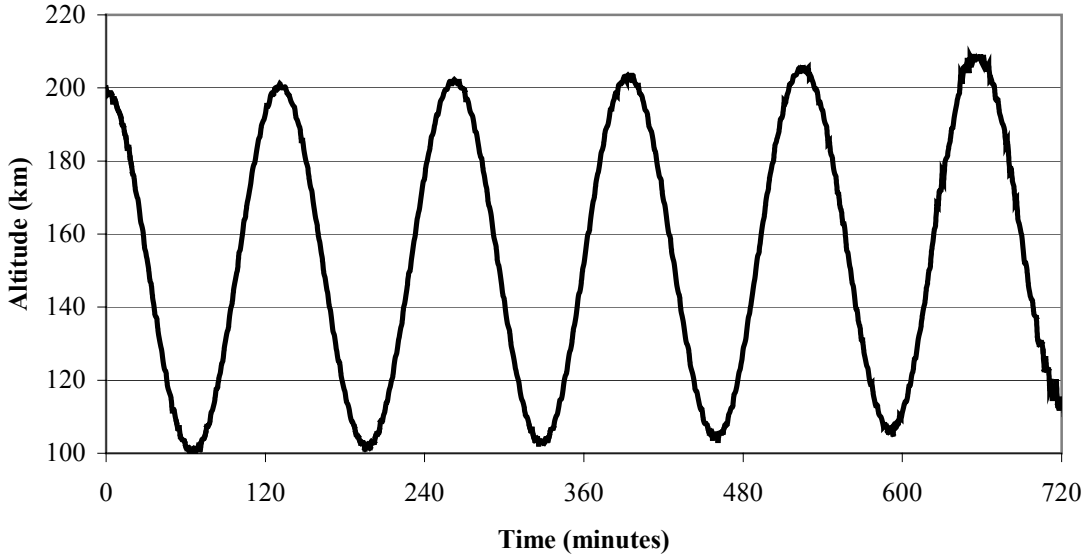


Figure 4.7: Lower Tip Altitude versus Time for 200 km Handoff Altitude

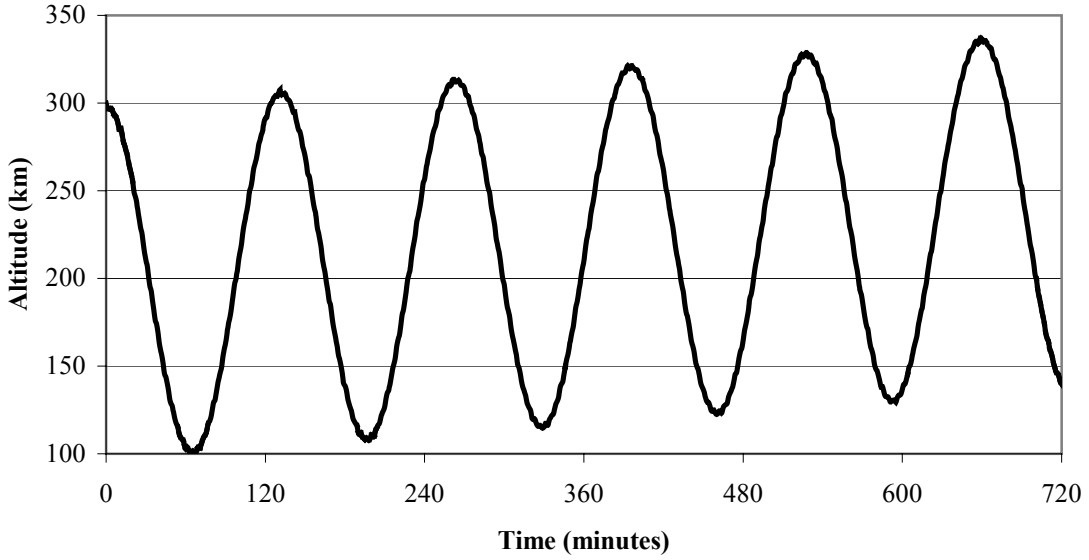


Figure 4.8: Lower Tip Altitude versus Time for 300 km Handoff Altitude

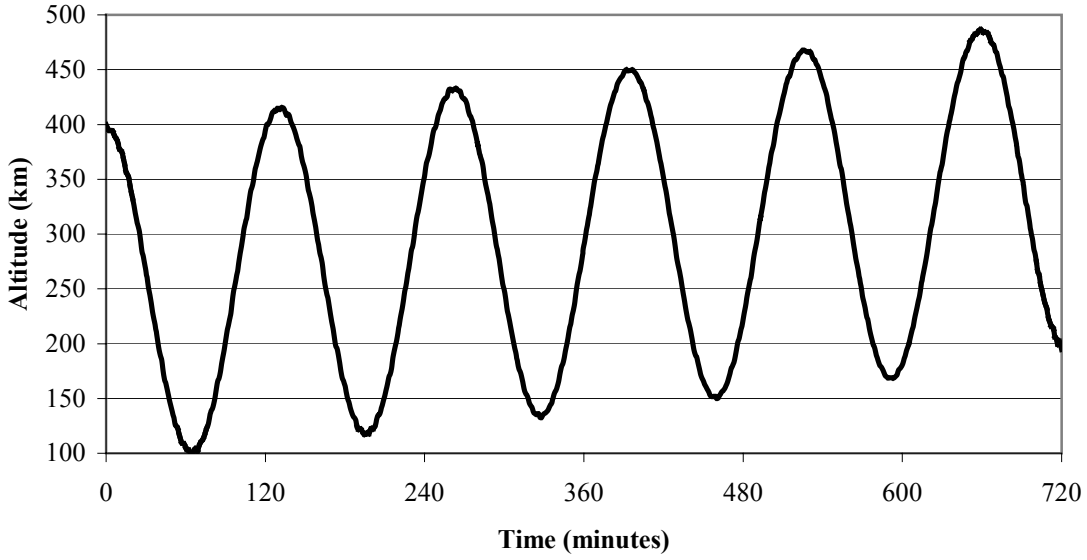


Figure 4.9: Lower Tip Altitude versus Time for 400 km Handoff Altitude

numerical simulation performed proves that it is possible to “fly” the tether it its orbit solely by electrodynamic means, with no expenditure of propellant.

In order for the launch vehicle to rendezvous with the tether and transfer its payload, it is necessary to define the pendular motion of the lower tip of the tether. To achieve this, the equations of motion are run for the tether alone, with no payload attached and the electrodynamic reboost system turned off. This is done to represent the motion of the tether in a stable circular orbit prior to payload handoff. The y coordinate position of the lower tip in the coordinate system attached to tether’s center of gravity segment is recorded. This produces the amount of distance in the tether’s orbital plane by which the lower tip either leads ahead of or follows behind the line between the Earth and the tether’s center of gravity. Figures 4.10, 4.11 and 4.12 show the lower tip relative position plotted over two hours, approximately one orbital revolution, for the three selected tethers in this study.

It can be seen for each of the tethers that the lower tip position relative to the elevator’s center of gravity is roughly sinusoidal, varying between approximately eight kilometers ahead of or behind the line between the tether’s center of gravity and the Earth. For each of the three selected elevators, the relative velocity of the lower tip in the y direction of the coordinate system attached to the tether center of gravity was never observed to exceed 11 meters per second. This value is relatively small compared to the lower tip velocity of approximately 5.4 kilometers per second. The slow relative speed between the tether lower tip and the local vertical allows for the assumption made in the rendezvous portion of the study to represent the lower tip as a stationary point hanging straight down from the elevator’s center of gravity.

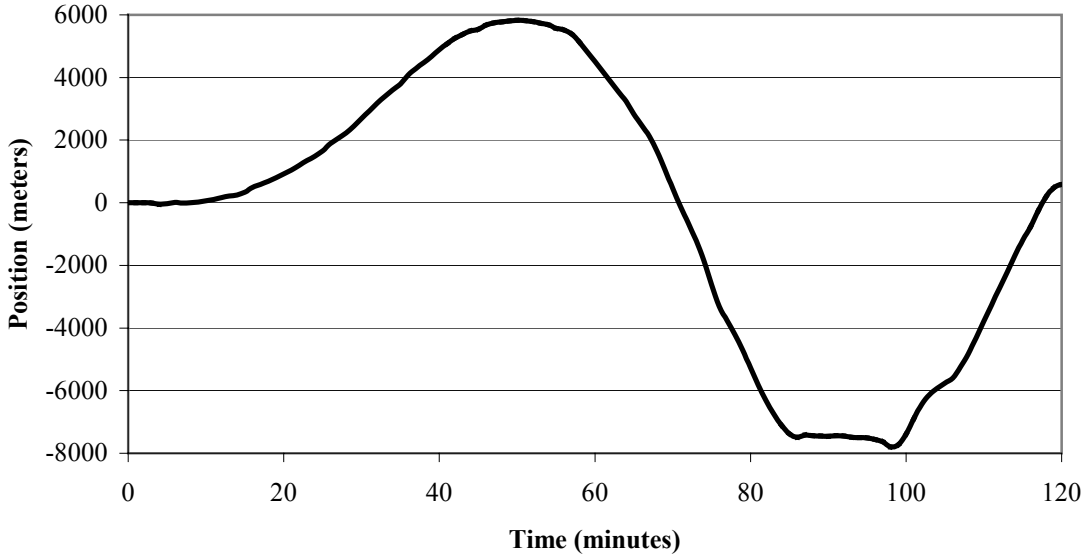


Figure 4.10: Lower Tip Relative Position versus Time for 200 km Handoff Altitude

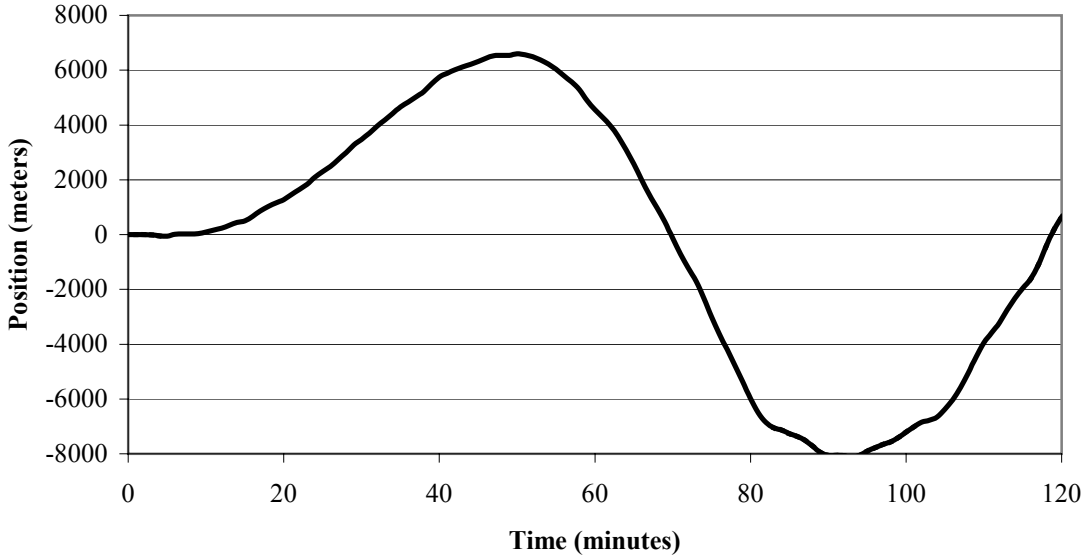


Figure 4.11: Lower Tip Relative Position versus Time for 300 km Handoff Altitude

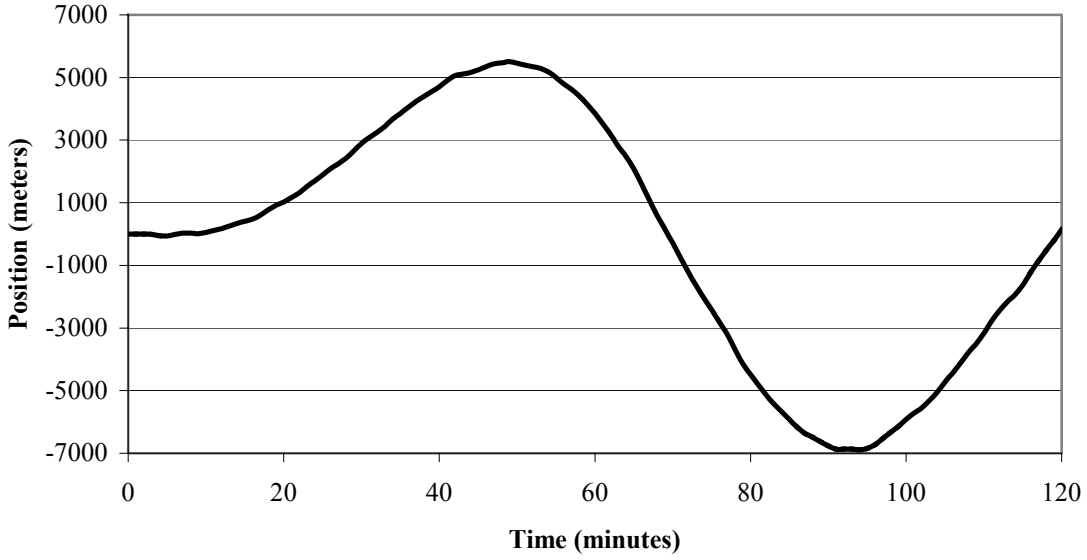


Figure 4.12: Lower Tip Relative Position Versus Time for 400 km Handoff Altitude

Chapter 5

Launch Vehicle Ascent Analysis

5.1 Suborbital Ascent Requirements

In order for the payload to be transferred from the launch vehicle to the elevator's lower tip, a rendezvous must occur between the two. The launch vehicle must be on a trajectory that will place it in the location of the tether's lower tip altitude with matching velocity. For a tether moving in a circular orbit this requires the launch vehicle, at the apogee of its ballistic trajectory, to possess no radial velocity and a ground track velocity matching the tether lower tip, according to the equation

$$v_{LV\,apo} = \omega_T \, r_{le} \tag{5. 1}$$

Because the tether's lower tip travels at a velocity less than the circular orbit velocity at the corresponding altitude, the Δv requirements for the launch vehicle are much less stringent than those of a vehicle achieving orbit. The savings in launch vehicle performance are impressive when cast in terms of required energy. For example, an object launched into a circular orbit of 250 kilometers altitude has a kinetic energy of 30.069 megajoules per kilogram and a potential energy of 2.45 megajoules per kilogram, for a total of 32.519 megajoules per kilogram. For a tether with its center of gravity at 2,000 kilometers altitude, its lower tip at 250 kilometers altitude will be traveling at 5.456 kilometers per second. A vehicle that will rendezvous with the lower tip, matching its position and velocity, will have a kinetic energy of 14.889 megajoules per kilogram and a potential energy of 2.45 megajoules per kilogram, for a total energy imparted to the launch vehicle of 17.339 megajoules per kilogram. This means a payload launched to

rendezvous with the tether will only possess 53.317% of the energy needed to place it in a low earth orbit. Figure 5.1 shows the required launch vehicle velocity and energy expressed as a percentage of the circular orbit velocity and energy for varying lengths of tether.

For this study it has been assumed that the launch vehicle will be a vertical take-off vehicle powered by conventional rockets. No aerodynamic lifting will be used in the ascent phase. The trajectory of the launch vehicle has been studied by modeling its equations of motion and applying a Hamiltonian-based optimization scheme.

5.2 History of Trajectory Optimization

The problem of trajectory optimization was first identified with the introduction of the guided missile as a weapon of war. The earliest numerical solutions to the problem of powered ascent grew out of the V-2 rocket program undertaken by the Germans during World War II. As the ranges of early guided missiles were relatively small, these calculations were in a Cartesian format with corrections for the earth's curvature inserted into longer range trajectories.

These earliest methods of range optimization involved establishing conditions for the vehicle's position and velocity at the end of its vertical climb. These predetermined flight conditions at the end of the climb formed the initial values to be inserted into the non-controlled equations of motion for the vehicle. This method therefore is not a continuously controlled system, as control forces were exerted on the vehicle only at the end point of the vertical climb when pitchover occurred. Once it entered its post-climb attitude, the equations of motion were integrated through time to determine its final position at the end of its trajectory.

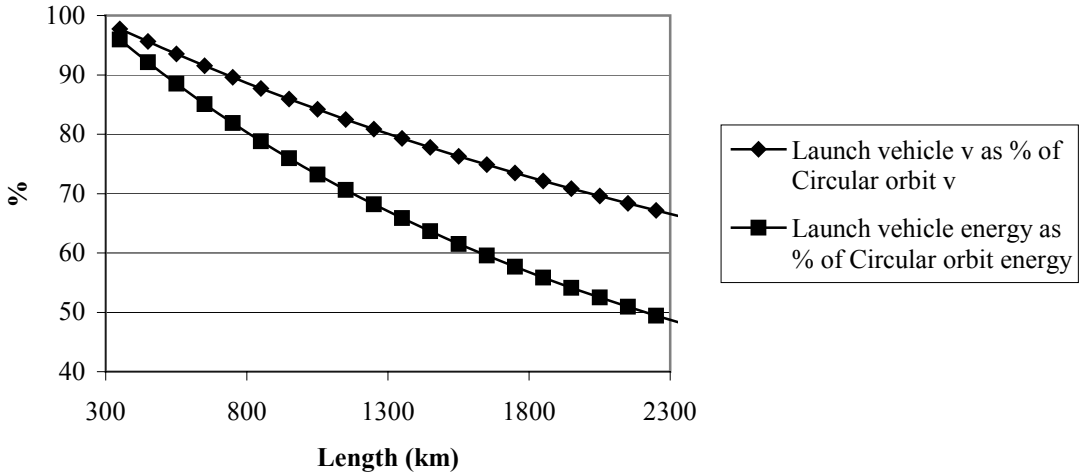


Figure 5.1: Launch Vehicle Velocity and Energy versus Tether Length

A graphical method, accounting for the vector changes of velocity caused by vehicle thrust, aerodynamic forces, and gravitational losses, can be used to calculate the optimum continuously controlled pitch program for an ascending space vehicle. Such a method can be easily used to determine a controlled trajectory for a vehicle ascending into orbit, but this analysis is again performed in Cartesian format, necessitating the addition of correction factors for the curvature of the earth. This method grew out of the work originally performed for the V-2 program and remained in use in missile range calculations during the 1950s [68].

An analytic solution can be found to the optimal ascent problem if several assumptions are made. The first of these assumptions states that the thrust of the ascending vehicle, and thus its mass flow rate, must be constant. The second assumption states that the gravity acting on the vehicle is a linear function of its radial position. These assumptions reduce the representation of the problem to that of a harmonic oscillator with a forcing function. A solution can therefore be found through the method of variation of parameters [69].

A solution to a continuously controlled trajectory problem can be sought through the method of calculus of variations. In this approach a particular performance parameter of a vehicle is minimized by enforcing the Euler-Lagrange condition. This generally reduces the trajectory problem to a two point boundary value problem, which can be solved by several numerical techniques, including steepest ascent and the Newton-Raphson method [70].

The Euler-Lagrange condition, which is the basis of the calculus of variations approach, becomes inconvenient as the number of parameters in the problem increase.

The cases when these equations can be integrated in closed form are limited [71]. An alternative to the calculus of variations method lies in the study of the Hamiltonian of a dynamic system. Hamiltonian-based optimization techniques, an example of which is the Pontryagin maximum principle used in this study, have been utilized for trajectory calculations on the upper stages of Saturn boosters in the 1960s and early space shuttle trajectory studies since the 1970s [72].

5.3 Equations of Motion for an Ascending Spacecraft

The equations of motion for a powered ascent vehicle can be derived by the use of Lagrange's equation for non-conservative forces,

$$\frac{d}{dt}\left(\frac{\partial T}{\partial \dot{q}_i}\right) - \frac{\partial T}{\partial q_i} = Q_i \tag{5. 2}$$

where T is the kinetic energy of the spacecraft, q is an appropriate set of generalized coordinates and Q_i is the generalized force on the spacecraft. The equations of motion for this problem will be derived for polar coordinates with the origin located at the center of the planet. This is done to eliminate any correcting terms for trajectory curvature that are inherent to rectangular derivation of the equations [73]. Expressing the equations of motion in polar coordinates is also beneficial in that they take the form of the equations of orbital motion with the addition of a thrusting force. The coordinate system and a free body diagram of the forces on the vehicle are illustrated in Figure 5.2.

The generalized coordinates for the problem are radial and angular position of the spacecraft with respect to the center of the Earth. For this study it is assumed that the thrust vector always passes through the vehicle's center of gravity. For a vehicle with a gimballing engine, this assumes the pitching moments produced by the gimballed engine

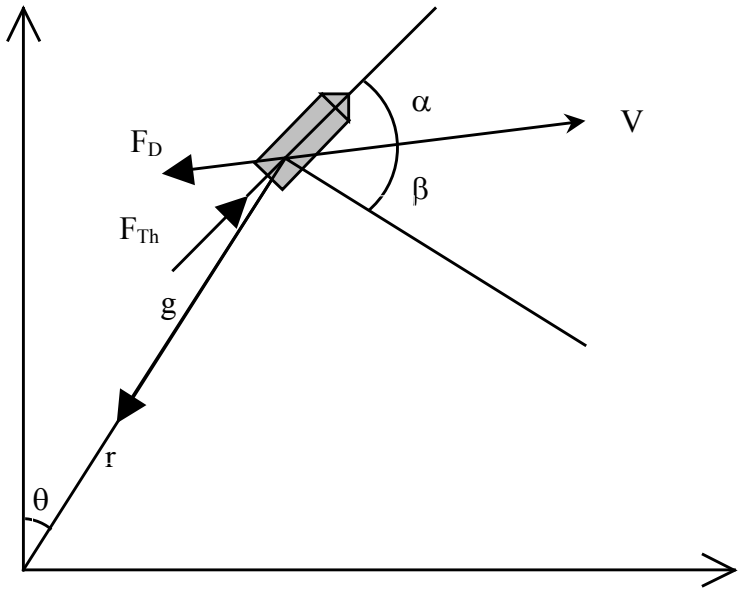


Figure 5.2: Free Body Diagram of an Ascending Spacecraft

are small. For a vehicle without engine gimballing ability, this assumption reflects reality, as steering changes are made by maneuvering the entire vehicle at a desired angle to its velocity vector. This study also neglects the aerodynamic effects of lift on the vehicle and only accounts for the drag as it ascends through the atmosphere.

The first step in using Lagrange's equations is to express the kinetic energy of the launch vehicle as

$$T = \frac{1}{2} m\left[\dot{r}^2 + \left(r\dot{\theta}\right)^2\right] \tag{5. 3}$$

Lagrange's equation for the first generalized coordinate, radial position, is

$$\frac{d}{dt}\left(\frac{\partial T}{\partial \dot{r}}\right) - \frac{\partial T}{\partial r} = Q_r \tag{5. 4}$$

The generalized force in the radial direction is made up of the radial components of gravity, engine thrust, and aerodynamic drag and is expressed as

$$Q_r = m\left[-\frac{GM_E}{r^2} + \frac{F_{Th}}{m}\sin(\beta+\alpha) - \frac{F_D}{m}\sin(\beta)\right] \tag{5. 5}$$

The partial derivatives of the kinetic energy expression with respect to radial position and time rate of change of radial position are

$$\frac{\partial T}{\partial \dot{r}} = m\dot{r} \tag{5. 6}$$

$$\frac{\partial T}{\partial r} = mr\dot{\theta}^2 \tag{5. 7}$$

The above expressions are inserted into Lagrange's equation and the common mass variable present in each term can be divided out, producing the following relation

$$\ddot{r} - r\dot{\theta}^2 = -\frac{GM_E}{r^2} + \frac{F_{Th}}{m}\sin(\beta+\alpha) - \frac{F_D}{m}\sin(\beta) \tag{5. 8}$$

Since the tangential component of velocity is the product of the radius and the angular rate of change, the differential equation for the radial rate of change can be expressed as

$$\frac{dv_r}{dt} = \frac{v_\theta^{\,2}}{r} - \frac{GM_E}{r^2} + \frac{F_{Th}}{m}\sin(\beta+\alpha) - \frac{F_D}{m}\sin(\beta) \tag{5. 9}$$

Lagrange's equation for the second of the two generalized coordinates, angular position, is

$$\frac{d}{dt}\left(\frac{\partial T}{\partial \dot{\theta}}\right) - \frac{\partial T}{\partial \theta} = Q_\theta \tag{5. 10}$$

The generalized torque in the angular direction is made up only of the angular component of engine thrust and aerodynamic drag, since gravity is only active in the radial direction, and is expressed as

$$Q_\theta = F_{Th}\ \cos(\beta+\alpha)\cdot r\ - F_D\ \cos(\beta)\cdot r \tag{5. 11}$$

The partial derivatives of the kinetic energy with respect to angular position and time rate of change of angular position are

$$\frac{\partial T}{\partial \dot{\theta}} = mr^2\dot{\theta} \tag{5. 12}$$

$$\frac{\partial T}{\partial \theta} = 0 \tag{5. 13}$$

By again noting that the tangential velocity is equal to the product of the radial position and the rate of change of angular position, the partial derivative of the kinetic energy with respect to rate of change of angular position can be expressed as

$$\frac{\partial T}{\partial \dot{\theta}} = mrv_\theta \tag{5. 14}$$

These expressions are inserted into Lagrange's equation and the common mass variable present in each term can be divided out, producing the following equation

$$\frac{d}{dt}\left(rv_{\theta}\right) = \frac{F_{Th}}{m}\cdot\cos\left(\beta+\alpha\right)\cdot r \; - \frac{F_D}{m}\;\cos\left(\beta\right)\cdot r \tag{5. 15}$$

By expanding the time derivative in the above equation the differential equation for the tangential velocity can be written as

$$\frac{dv_{\theta}}{dt} = -\frac{v_r v_{\theta}}{r} + \frac{F_{Th}}{m}\cos\left(\beta+\alpha\right) - \frac{F_D}{m}\;\cos\left(\beta\right) \tag{5. 16}$$

In order to perform Runge-Kutta integration upon the two derived equations, we must have a set of two differential equations to describe the radial and angular position, so that the total set can be treated as four first order differential equations. This produces the set of equations as follows

$$\frac{dr}{dt} = v_r \tag{5. 17}$$

$$\frac{d\theta}{dt} = \frac{v_{\theta}}{r} \tag{5. 18}$$

$$\frac{dv_r}{dt} = \frac{v_{\theta}^{\,2}}{r} - \frac{GM_E}{r^2} + \frac{F_{Th}}{m}\sin\left(\beta+\alpha\right) - \frac{F_D}{m}\sin(\beta) \tag{5. 19}$$

$$\frac{dv_{\theta}}{dt} = -\frac{v_r v_{\theta}}{r} + \frac{F_{Th}}{m}\cos\left(\beta+\alpha\right) \; - \frac{F_D}{m}\;\cos\left(\beta\right) \tag{5. 20}$$

It should also be noted that the aerodynamic drag on the vehicle is calculated according to the following equation

$$F_D = C_D\,\rho_{atm}\,\frac{v^2}{2}\,A_f \tag{5. 21}$$

The density of the air is calculated by modeling the atmosphere in three zones, the troposphere, the lower stratosphere and the upper stratosphere. The first zone encountered by the launch vehicle, the troposphere, is applied at altitudes ranging from sea level to 11,000 meters. In the troposphere the air temperature decreases linearly and the pressure decreases exponentially. The curve fit equations for the temperature and pressure in the troposphere are

$$\text{Temp} = 15.04 - (0.00649 \cdot \text{alt}) \tag{5. 22}$$

$$\text{p} = 101.29 \cdot \left(\frac{\text{Temp} + 273.1}{288.08} \right)^{5.256} \tag{5. 23}$$

where the temperature is given in degrees Celsius, the pressure in kilopascals, and alt is the altitude of the launch vehicle in meters.

The second atmosphere zone, the lower stratosphere, extends from altitudes of 11,000 meters up to 25,000 meters. In the lower stratosphere the air temperature is constant and the pressure decreases exponentially. The curve fit equations for the lower stratosphere are

$$\text{Temp} = -56.46 \tag{5. 24}$$

$$\text{p} = 22.65 \cdot \exp(1.73 - 0.000157 \cdot \text{alt}) \tag{5. 25}$$

The final atmosphere zone is used for altitudes greater than 25,000 meters and is valid up to LEO altitudes. In this zone the temperature increases slightly and the pressure decreases exponentially with altitude. The curve fit equations for the upper stratosphere are

$$\text{Temp} = -131.21 + (0.00299 \cdot \text{alt}) \tag{5. 26}$$

$$p = 2.488 \cdot \left(\frac{\text{Temp} + 273.1}{216.6} \right)^{-11.388} \tag{5. 27}$$

The density of the air in each zone, measured in kilograms per cubic meter, is found by the equation of state, written as

$$\rho_{atm} = \frac{p}{0.2869 \cdot (\text{Temp} + 273.1)} \tag{5. 28}$$

In order to carry out a numerical solution to the problem, while minimizing calculation times, it is useful to cast the equations in non-dimensional form. This would reduce the time taken for a computer to complete the numerical calculation. The non-dimensional values for velocity, length, and time can be calculated from the set of relations

$$r = \frac{r^*}{r_E} \tag{5. 29}$$

$$v = \frac{v^*}{\sqrt{\frac{GM_E}{r_E}}} \tag{5. 30}$$

$$t = \frac{t^*}{\sqrt{\frac{r_E^{\,3}}{GM_E}}} \tag{5. 31}$$

where the asterisk superscript denotes the dimensional variable. The scaling variable for radial position is the equatorial radius of the Earth, r_E. The circular orbit speed at the surface of the Earth is the velocity scaling variable. A time scaling variable is derived from dividing the distance scaling variable by the velocity scaling variable. The set of dimensionless equations of motion for an ascending launch vehicle is written as

$$\frac{r_E}{\sqrt{\frac{r_E^{\,3}}{GM_E}}}\frac{dr^*}{dt^*} = v_r^{\,*}\sqrt{\frac{GM_E}{r_E}} \tag{5. 32}$$

$$\frac{1}{\sqrt{\frac{r_E^{\,3}}{GM_E}}}\frac{d\theta^*}{dt^*} = \frac{v_\theta^{\,*}}{r^*}\frac{\sqrt{\frac{GM_E}{r_E}}}{r_E} \tag{5. 33}$$

$$\frac{\sqrt{\frac{GM_E}{r_E}}}{\sqrt{\frac{r_E^{\,3}}{GM_E}}}\frac{dv_r^{\,*}}{dt^*} = \frac{v_\theta^{\,*2}}{r^*}\frac{\left(\sqrt{\frac{GM_E}{r_E}}\right)^2}{r_E} - \frac{GM}{r^{*2}}\frac{1}{r_E^{\,2}} + \frac{F_{Th}}{m}\sin(\beta+\alpha) - \frac{F_D}{m}\sin(\beta) \tag{5. 34}$$

$$\frac{\sqrt{\frac{GM_E}{r_E}}}{\sqrt{\frac{r_E^{\,3}}{GM_E}}}\frac{dv_\theta^{\,*}}{dt^*} = -\frac{v_r^{\,*}v_\theta^{\,*}}{r^*}\frac{\left(\sqrt{\frac{GM_E}{r_E}}\right)^2}{r_E} + \frac{F_{Th}}{m}\cos(\beta+\alpha) - \frac{F_D}{m}\cos(\beta) \tag{5. 35}$$

Simplification of the above equations, and the dropping of the asterisk for clarity, as it is no longer needed, produces the dimensionless state equations in their final form

$$\frac{dr}{dt} = v_r \tag{5. 36}$$

$$\frac{d\theta}{dt} = \frac{v_\theta}{r} \tag{5. 37}$$

$$\frac{dv_r}{dt} = \frac{v_\theta^{\,2}}{r} - \frac{1}{r^2} + \frac{F_{Th}}{m\,g_E}\sin(\beta+\alpha) - \frac{F_D}{m\,g_E}\sin(\beta) \tag{5. 38}$$

$$\frac{dv_\theta}{dt} = -\frac{v_r v_\theta}{r} + \frac{F_{Th}}{m\,g_E}\cos(\beta+\alpha) - \frac{F_D}{m\,g_E}\cos(\beta) \tag{5. 39}$$

where g_E is the gravitational acceleration on the surface of the Earth. It is this set of equations to which the Pontryagin maximum principle will be applied in order to optimize the ascent trajectory for minimum fuel expenditure.

5.4 Pontryagin Maximum Principle

Considering a problem with an n-dimensional state vector x and state equations defined as

$$\dot{x}_i = f_i(\mathbf{x}, \mathbf{u}) \qquad i = 1, 2, \ldots, n \tag{5. 40}$$

where **u** is a control vector. A transfer is sought from an initial state $\mathbf{x}^0$ at time zero to a final desired state $\mathbf{x}^f$ at some unspecified time t^f. There exists a control as a function of time, **u**(t), that will accomplish this transfer while minimizing a cost function

$$J = \int_{t^0}^{t^f} f_0(\mathbf{x}, \mathbf{u})\, dt \tag{5. 41}$$

where $f_0(\mathbf{x}, \mathbf{u})$ is a state equation relatedg to an additional state variable x_0 by the equation

$$\dot{x}_0 = f(\mathbf{x}, \mathbf{u}) \tag{5. 42}$$

Added to the previous state vector **x** this additional state variable forms the state vector $\hat{\mathbf{x}}$ with dimension n+1 and corresponding state equations

$$\dot{\hat{x}}_i = \hat{f}_i(\mathbf{x}, \mathbf{u}) \qquad i = 0, 1, 2, \ldots, n \tag{5. 43}$$

From the extended state vector the Hamiltonian of the system, a function of the state variable, the costate variable, and the control, can be defined as

$$H = \hat{\mathbf{z}}^T \dot{\hat{\mathbf{x}}} = \sum_{i=0}^{n} z_i f_i \qquad i = 0, 1, 2, \ldots, n \tag{5. 44}$$

where $\hat{\mathbf{z}}$ represents an extended co-state vector with n+1 dimensions. The equations for both the state and costate variables can be defined by the equations

$$\frac{dx_i}{dt} = \frac{\partial H}{\partial z_i} \qquad i = 1, 2,\ldots, n \tag{5. 45}$$

$$\frac{dz_i}{dt} = -\frac{\partial H}{\partial x_i} \qquad i = 1, 2,\ldots, n \tag{5. 46}$$

Since the value of the Hamiltonian does not depend on the additional state variable x_0, the equation for its corresponding costate variable is

$$\dot{z}_0 = 0 \tag{5. 47}$$

Having stated the problem in terms of its Hamiltonian, with accompanying state and costate variables, the PMP can be applied to the problem. The four basic conditions of the PMP are as follows [74]:

1. The Pontryagin maximum principle states that an arbitrary value of negative one is assigned to z_0. This leads to the modified expression of the Hamiltonian as

$$H = -f_0 + \sum_{i=0}^{n} z_i f_i \qquad i = 1, 2,\ldots, n \tag{5. 48}$$

2. The optimum control function, according to the Pontryagin maximum principle, will maximize the Hamiltonian to a value greater than or equal to zero for all time during an optimal trajectory. The equation for the optimum control function is obtained using the following equation,

$$\frac{\partial H}{\partial u} = 0 \tag{5. 49}$$

3. There exists a set of initial values for the costate vector and state vector that will transfer the values of the state vector from their initial state to a desired final state.

4. Along an optimal trajectory the Hamiltonian exhibits a constant value. This constant value is positive if the final time is fixed and is zero if the final time is free.

The problem as stated now consists of 2n + 2 state and costate equations. These equations are solved by the n known initial and final values, the initial value of x_0, and the value of z_0. For problems with an unspecified final time, such as the one in this study, the unknown final time requires an additional known final condition. This condition is supplied by the fourth condition of the PMP.

5.5 Trajectory Optimization

The task of the launch vehicle is to ascend on a trajectory allowing it to rendezvous with the tether lower tip to facilitate a transfer of the payload. The problem undertaken in this study is to achieve a rendezvous trajectory while burning a minimum amount of propellant. The cost function for this problem is then stated as

$$J = \int_0^{t_f} (\dot{m})\, dt \tag{5. 50}$$

For this study, the launch vehicle propulsion system is assumed to have a constant mass flow rate. This allows us to treat the optimization of the trajectory as a minimum time problem, simplifying the cost function to the form

$$J = \int_0^{t_f} 1\, dt \tag{5. 51}$$

The state vector of the ascent vehicle is composed of the radial and tangential components of its position and velocity, a total of four state variables. It is observed that none of the state equations are dependent on the angular position of the launch vehicle, θ, nor is angular position a specified value in the desired final state of the system. The

angular position is therefore unimportant in terms of trajectory optimization and can be overlooked in the optimization process [75]. Disregarding the angular position of the launch vehicle allows the number of state equations to be reduced from four to three. The value of the angular position of the ascending launch vehicle will be of interest, however, in calculating the downrange distance covered by the launch vehicle and in timing the rendezvous. The corresponding state equations are written as

$$f_1 = \frac{dr}{dt} = v_r \tag{5. 52}$$

$$f_2 = \frac{dv_r}{dt} = \frac{v_\theta{}^2}{r} - \frac{1}{r^2} + \frac{F_{Th}}{m\, g_E}\sin(\beta+\alpha) - \frac{F_D}{m\, g_E}\sin(\beta) \tag{5. 53}$$

$$f_3 = \frac{dv_\theta}{dt} = -\frac{v_r v_\theta}{r} + \frac{F_{Th}}{m\, g_E}\cos(\beta+\alpha) - \frac{F_D}{m\, g_E}\cos(\beta) \tag{5. 54}$$

Optimization of the trajectory by the PMP is based upon maximizing the Hamiltonian of the system. The Hamiltonian of the ascent vehicle can be expressed as

$$\begin{aligned} H = -1 + z_r(v_r) + z_{v_r}\left[\frac{v_\theta{}^2}{r} - \frac{1}{r^2} + \frac{F_{Th}}{m\, g_E}\sin(\beta+\alpha) - \frac{F_d}{m\, g_E}\sin(\beta)\right] \\ + z_{v_\theta}\left[-\frac{v_r v_\theta}{r} + \frac{F_{Th}}{m\, g_E}\cos(\beta+\alpha) - \frac{F_d}{m\, g_E}\cos(\beta)\right] \end{aligned} \tag{5. 55}$$

The set of costate differential equations are derived from the partial derivatives of the Hamiltonian with respect to each state variable and are written as

$$\frac{dz_r}{dt} = -\frac{\partial H}{\partial r} = z_{v_r}\left(\frac{v_\theta{}^2}{r^2} - \frac{2}{r^3}\right) + z_{v_\theta}\left(-\frac{v_r v_\theta}{r^2}\right) \tag{5. 56}$$

$$\frac{dz_{v_r}}{dt} = -\frac{\partial H}{\partial v_r} = -z_r + z_{v_r}\left[-\frac{F_{Th}}{m\,g_E}\frac{\partial}{\partial v_r}\sin(\beta+\alpha)+\frac{F_D}{m\,g_E}\frac{\partial}{\partial v_r}\sin(\beta)\right] + z_{v_\theta}\left[\frac{v_\theta}{r}-\frac{F_{Th}}{m\,g_E}\frac{\partial}{\partial v_r}\cos(\beta+\alpha)+\frac{F_D}{m\,g_E}\frac{\partial}{\partial v_r}\cos(\beta)\right] \tag{5. 57}$$

$$\frac{dz_{v_\theta}}{dt} = -\frac{\partial H}{\partial v_\theta} = z_{v_r}\left[-\frac{2v_\theta}{r}-\frac{F_{Th}}{m\,g_E}\frac{\partial}{\partial v_\theta}\sin(\beta+\alpha)+\frac{F_D}{m\,g_E}\frac{\partial}{\partial v_\theta}\sin(\beta)\right] + z_{v_\theta}\left[\frac{v_r}{r}-\frac{F_{Th}}{m\,g_E}\frac{\partial}{\partial v_\theta}\cos(\beta+\alpha)+\frac{F_D}{m\,g_E}\frac{\partial}{\partial v_\theta}\cos(\beta)\right] \tag{5. 58}$$

The above equations contain derivatives of the sine and cosine of angle β, the angle between the launch vehicle's velocity vector and the local horizontal, and derivatives of the launch vehicles velocity. This angle can be expressed in terms of the radial and tangential components of the vehicle velocity by the relation

$$\beta = \tan^{-1}\left(\frac{v_r}{v_\theta}\right) \tag{5. 59}$$

The magnitude of the velocity vector can also be expressed in terms of the components of velocity by the following equation

$$v = \sqrt{{v_r}^2 + {v_\theta}^2} \tag{5. 60}$$

The partial derivatives of the trigonometric functions of the control angle and angle to local horizon can be written in the form

$$\frac{\partial}{\partial v_r}\sin(\beta+\alpha) = \cos(\beta+\alpha)\frac{\partial\varphi}{\partial v_r} = \frac{v_\theta}{v^2}\cos(\beta+\alpha) \tag{5. 61}$$

$$\frac{\partial}{\partial v_r}\cos(\beta+\alpha) = -\sin(\beta+\alpha)\frac{\partial\varphi}{\partial v_r} = -\frac{v_\theta}{v^2}\sin(\beta+\alpha) \tag{5. 62}$$

$$\frac{\partial}{\partial v_\theta}\sin(\beta+\alpha) = \cos(\beta+\alpha)\frac{\partial\varphi}{\partial v_\theta} = -\frac{v_r}{v^2}\cos(\beta+\alpha) \tag{5. 63}$$

$$\frac{\partial}{\partial v_\theta}\cos(\beta+\alpha) = -\sin(\beta+\alpha)\frac{\partial \varphi}{\partial v_\theta} = \frac{v_r}{v^2}\sin(\beta+\alpha) \tag{5. 64}$$

It should also be noted that the aerodynamic drag on the vehicle is dependent on the vehicle velocity, according to the equation

$$F_D = C_D\, \rho_{atm}\, \frac{v^2}{2} A_f \tag{5. 65}$$

Inserting this into the drag term and again noting that the velocity can be expressed in its radial and tangential components leads to the derivatives of the drag term being written as

$$\frac{\partial}{\partial v_r}\frac{C_D\, \rho_{atm}\left(v_r{}^2 + v_\theta{}^2\right)A_f}{2\, m\, g_E}\sin(\beta) = \frac{C_D\, \rho_{atm}\, A_f}{2\, m\, g_E}\left[2\, v_r \sin(\beta) + v_\theta \cos(\beta)\right] \tag{5. 66}$$

$$\frac{\partial}{\partial v_r}\frac{C_D\, \rho_{atm}\left(v_r{}^2 + v_\theta{}^2\right)A_f}{2\, m\, g_E}\cos(\beta) = \frac{C_D\, \rho_{atm}\, A_f}{2\, m\, g_E}\left[2\, v_r \cos(\beta) - v_\theta \sin(\beta)\right] \tag{5. 67}$$

$$\frac{\partial}{\partial v_\theta}\frac{C_D\, \rho_{atm}\left(v_r{}^2 + v_\theta{}^2\right)A_f}{2\, m\, g_E}\sin(\beta) = \frac{C_D\, \rho_{atm}\, A_f}{2\, m\, g_E}\left[2 v_\theta \sin(\beta) - v_r \cos(\beta)\right] \tag{5. 68}$$

$$\frac{\partial}{\partial v_\theta}\frac{C_D\, \rho_{atm}\left(v_r{}^2 + v_\theta{}^2\right)A_f}{2\, m\, g_E}\cos(\beta) = \frac{C_D\, \rho_{atm}\, A_f}{2\, m\, g_E}\left[2\, v_\theta \cos(\beta) + v_r \sin(\beta)\right] \tag{5. 69}$$

The equation for the optimal control of the steering angle is found by setting the partial derivative of the Hamiltonian with respect to the control equal to zero, yielding the expression

$$\frac{\partial H}{\partial \alpha} = 0 = z_{v_r}\left[\frac{F_{Th}}{m\, g_E}\frac{\partial}{\partial \alpha}\sin(\beta+\alpha)\right] + z_{v_\theta}\left[\frac{F_{Th}}{m\, g_E}\frac{\partial}{\partial \alpha}\cos(\beta+\alpha)\right] \tag{5. 70}$$

The partial derivatives of the sine and cosine of α, the angle between the velocity vector and the thrust vector of the launch vehicle, are expressed as

$$\frac{\partial}{\partial \alpha}\sin(\beta+\alpha)=\cos(\beta+\alpha) \tag{5. 71}$$

$$\frac{\partial}{\partial \alpha}\cos(\beta+\alpha)=-\sin(\beta+\alpha) \tag{5. 72}$$

Inserting these into the partial derivative of the Hamiltonian with respect to the control angle leads to the expression

$$z_{v_r}\left[\frac{F_{Th}}{m\,g_E}\cos(\beta+\alpha)\right]=z_{v_\theta}\left[\frac{F_{Th}}{m\,g_E}\sin(\beta+\alpha)\right] \tag{5. 73}$$

Simplifying the above equation yields a relation between the thrust control angle, the flight path angle, and the costate variables corresponding to velocity, and is written as

$$\tan(\beta+\alpha)=\frac{z_{v_r}}{z_{v_\theta}} \tag{5. 74}$$

Solving the above expression for α yields an expression for the control law of the thrust angle of the launch vehicle, as shown by

$$\alpha=\tan^{-1}\left(\frac{z_{v_r}}{z_{v_\theta}}\right)-\beta \tag{5. 75}$$

This expression for the engine control angle is inserted back into the equations of motion for the state and costate variables, resulting in the set of six differential equations, written as

$$\frac{dr}{dt}=v_r \tag{5. 76}$$

$$\frac{dv_r}{dt}=\frac{{v_\theta}^2}{r}-\frac{1}{r^2}+\frac{F_{Th}}{m\,g_E}\sin\left[\tan^{-1}\left(\frac{z_{v_r}}{z_{v_\theta}}\right)\right]-\frac{F_D}{m\,g_E}\sin(\beta) \tag{5. 77}$$

$$\frac{dv_\theta}{dt} = -\frac{v_r v_\theta}{r} + \frac{F_{Th}}{m g_E}\cos\left[\tan^{-1}\left(\frac{z_{v_r}}{z_{v_\theta}}\right)\right] - \frac{F_D}{m g_E}\cos(\beta) \tag{5. 78}$$

$$\frac{dz_r}{dt} = z_{v_r}\left(\frac{v_\theta{}^2}{r^2} - \frac{2}{r^3}\right) + z_{v_\theta}\left(-\frac{v_r v_\theta}{r^2}\right) \tag{5. 79}$$

$$\begin{aligned}\frac{dz_{v_r}}{dt} = -z_r + z_{v_r}&\left\{\begin{aligned}&-\frac{F_{Th}}{m g_E}\frac{v_\theta}{v^2}\cos\left[\tan^{-1}\left(\frac{z_{v_r}}{z_{v_\theta}}\right)\right]\\&+\frac{C_D\,\rho_{atm}\,A_f}{2\,m\,g_E}\left[2\,v_r\sin(\beta) + v_\theta\cos(\beta)\right]\end{aligned}\right\}\\ + z_{v_\theta}&\left\{\begin{aligned}&\frac{v_\theta}{r} + \frac{F_{Th}}{m g_E}\frac{v_\theta}{v^2}\sin\left[\tan^{-1}\left(\frac{z_{v_r}}{z_{v_\theta}}\right)\right]\\&+\frac{C_D\,\rho_{atm}\,A_f}{2\,m\,g_E}\left[2\,v_r\cos(\beta) - v_\theta\sin(\beta)\right]\end{aligned}\right\}\end{aligned} \tag{5. 80}$$

$$\begin{aligned}\frac{dz_{v_\theta}}{dt} = z_{v_r}&\left\{\begin{aligned}&-\frac{2v_\theta}{r} + \frac{F_{Th}}{m g_E}\frac{v_r}{v^2}\cos\left[\tan^{-1}\left(\frac{z_{v_r}}{z_{v_\theta}}\right)\right]\\&+\frac{C_D\,\rho_{atm}\,A_f}{2\,m\,g_E}\left[2v_\theta\sin(\beta) - v_r\cos(\beta)\right]\end{aligned}\right\}\\ + z_{v_\theta}&\left\{\begin{aligned}&\frac{v_r}{r} - \frac{F_{Th}}{m g_E}\frac{v_r}{v^2}\sin\left[\tan^{-1}\left(\frac{z_{v_r}}{z_{v_\theta}}\right)\right]\\&+\frac{C_D\,\rho_{atm}\,A_f}{2\,m\,g_E}\left[2\,v_\theta\cos(\beta) + v_r\sin(\beta)\right]\end{aligned}\right\}\end{aligned} \tag{5. 81}$$

This set of equations is treated as a boundary value problem and solved by fourth order Runge-Kutta integration. In order to solve the boundary value problem, the number of known final conditions must equal the number of unknown initial conditions. A list of the known and unknown conditions in this problem appears in Table 5.1. The three unknown initial values of the costate variables and the final time in which the ascent is performed are the four unknown initial values. The program written to solve this

Table 5.1: Boundary Value Conditions for Ascent Trajectory Optimization

Variable	Initial Condition	Final Condition
Radial position	known	known
Radial velocity	known	known
Tangential velocity	known	known
Radial position costate	unknown	unknown
Radial velocity costate	unknown	unknown
Tangential velocity costate	unknown	unknown
Hamiltonian	known	known
Time	known	unknown

problem analyzes the equations and provides a set of initial costate variables for each successive time step. This method eliminates time as an unknown and requires the specification of only three known final conditions. The three conditions that must be specified within the program are the final radial position, the final radial velocity, and the final value of the Hamiltonian, which is zero, according to the PMP. An algorithm, based on Newton's method, will produce guesses for the values of the unknown initial conditions for the costate vector that will, when the equations are integrated over time, generate the desired final conditions of radial position and velocity and Hamiltonian. As the program converges on the desired Hamiltonian, radial position and velocity requirements, the selection of final time, and its accompanying set of initial costate variables, is then made by choosing the time step at which the tangential velocity of the launch vehicle is equal to the tangential velocity calculated for the desired final trajectory of the vehicle.

The trajectory optimization was run using a vehicle based on the McDonnell Douglas Delta Clipper DC-I single stage to orbit vehicle. The DC-I was the larger production version of a concept demonstrated by the DC-X vehicle which flew from 1993 to 1995. The Delta Clipper was chosen for this study because it was designed to deliver a payload of 9,000 kilograms, similar to the 10,000 kilogram payload used in this study, to a 200 kilometer circular orbit. The DC-I was designed to be 9.15 meters in diameter and 38.72 meters tall. The dry mass of the vehicle was 36,000 kilograms and it carried 424,000 kilograms of propellant. The initial design was powered by a single plug nozzle variant of the J-2 rocket engine burning liquid oxygen and liquid hydrogen. This engine produces 6,864,600 Newtons of thrust in vacuum with an specific impulse of 425

seconds. At sea level, the engine produces 5,330,100 Newtons of force with an specific impulse of 330 seconds. At full throttle the engine consumes 1,646 kilograms per second of propellant.

The trajectory analysis program developed for this study is set up so that the launch vehicle is constrained to climb vertically to an altitude of one kilometer. At this point, pitchover occurs and the program begins to solve for a optimal powered trajectory with engine cutoff at a specified altitude. After engine cutoff the launch vehicle will coast on a ballistic trajectory to the tether lower tip. The desired conditions at engine cutoff are found from the apogee radius and velocity of the non-powered ballistic portion of the launch vehicle trajectory. The radius and velocity of the launch vehicle's apogee corresponds to the radial position and velocity of the elevator's lower tip. Defining the engine cutoff conditions begins with the calculation of the unpowered trajectory's Kepler Area Constant, according to the equation

$$C_{LV} = r_{le}\, v_{le} \tag{5. 82}$$

The orbital energy constant of the unpowered trajectory is also found by the values of the tether lower tip radius and velocity, according to the expression

$$OEC_{LV} = v_{le}^{\,2} - \frac{2\,GM_E}{r_{le}} \tag{5. 83}$$

From the values of the Kepler area constant and the orbital energy constant, the eccentricity of the ballistic trajectory is found through the equation

$$e_{LV} = \sqrt{1 + OEC_{LV}\left(\frac{C_{LV}}{GM_E}\right)^2} \tag{5. 84}$$

With the eccentricity of the launch vehicle trajectory known the semimajor axis can be found, as shown by

$$a_{LV} = \frac{r_{le}}{1 + e_{LV}} \tag{5. 85}$$

With these orbital parameters defined the velocity at the specified engine cutoff altitude can be found by the relation

$$v_{cut} = \sqrt{\frac{GM_E}{r_{cut}}} \sqrt{2 - \frac{r_{cut}}{a_{LV}}} \tag{5. 86}$$

For the purposes of this study, a cutoff altitude of 100 kilometers has been chosen to allow the launch vehicle to be powered to an altitude above which atmospheric drag during the ballistic climb can be disregarded.

5.6 Ascent Results

The program was run for each of the three tethers identified in Chapter 4, with launch vehicle apogee at 200, 300, and 400 kilometers. In addition the ascent to an circular orbit of 200 kilometers altitude was also calculated. This was accomplished by placing the launch vehicle, at the time of engine cutoff, on a ballistic trajectory with an apogee at 200 kilometers. At apogee, an impulsive maneuver of 100 meters per second was needed to circularize its orbit. This orbital trajectory approached the limit of the launch vehicle capability as defined in this study. Table 5.2 shows a comparison of several properties associated with the orbital and elevator bound trajectories. The first column of data corresponds to the orbital ascent trajectory, while the second, third and fourth represent suborbital tether bound trajectories to varying lower tip altitudes.

Table 5.2: Comparison of Different Launch Trajectories

Apogee Altitude (km)	200	200	300	400
Apogee Velocity (km/s)	7.684	5.415	5.498	5.580
Time of Engine Cutoff (s)	339	310	315	318
Velocity at Cutoff (km/s)	7.805	5.585	5.823	6.048
Radial Velocity at Cutoff (km/s)	0.183	0.978	1.338	1.580
Tangential Velocity at Cutoff (km/s)	7.803	5.499	5.668	5.838
Flight Path Angle at Cutoff (degrees)	1.347	10.093	13.283	15.140
Time from Cutoff to Apogee (s)	971	205	300	382
Propellant Remaining (kg)	4571	40187	34957	30225
Δv Remaining (km/s)	0.295	2.617	2.356	2.105
Peak Acceleration (g's)	10.337	6.089	6.482	6.885

Figure 5.3 shows a plot of the powered trajectory for an ascent to a 200 kilometer circular orbit with the origin at the launch site. The apparent drop in altitude, observed towards the end of the trajectory, is actually caused by the curvature of the Earth. Throughout the powered portion of the trajectory the launch vehicle is constantly climbing in altitude. As noted in Table 5.2, the ascent to a 200 kilometer altitude orbital trajectory requires a much larger cutoff velocity than trajectories bound for the elevator's lower tip. For an orbital trajectory, the flight path angle between the vehicle's velocity vector and the local horizontal is much smaller than that of the elevator bound trajectories. These two factors, the larger cutoff velocity and the smaller flight path angle, require that the launch vehicle powered trajectory must last 339 seconds to place it on its shallow high speed trajectory at cutoff. This value is somewhat larger than the burn times required for elevator bound trajectories, and leaves the launch vehicle with much less Δv remaining after engine shutdown. The low flight path angle also causes the launch vehicle to having a relatively long coasting time of 971 seconds until apogee is reached and the orbit is circularized.

Figures 5.4, 5.5, and 5.6 show the launch vehicle powered trajectories for an ascent to an elevator with a lower tip altitude, of 200, 300, and 400 kilometers, respectively. The launch vehicle's flight path angle with respect to the local horizontal is much higher than that involved with the orbital ascent. For an elevator bound trajectory, the launch vehicle at engine cutoff is in a much steeper ballistic climb than the shallow orbital trajectory. The steepness of the trajectory is more pronounced as the lower tip altitude is increased. The increased steepness of the elevator bound trajectories requires less time to "turn" the launch vehicle from its initial vertical climb. Combined with the

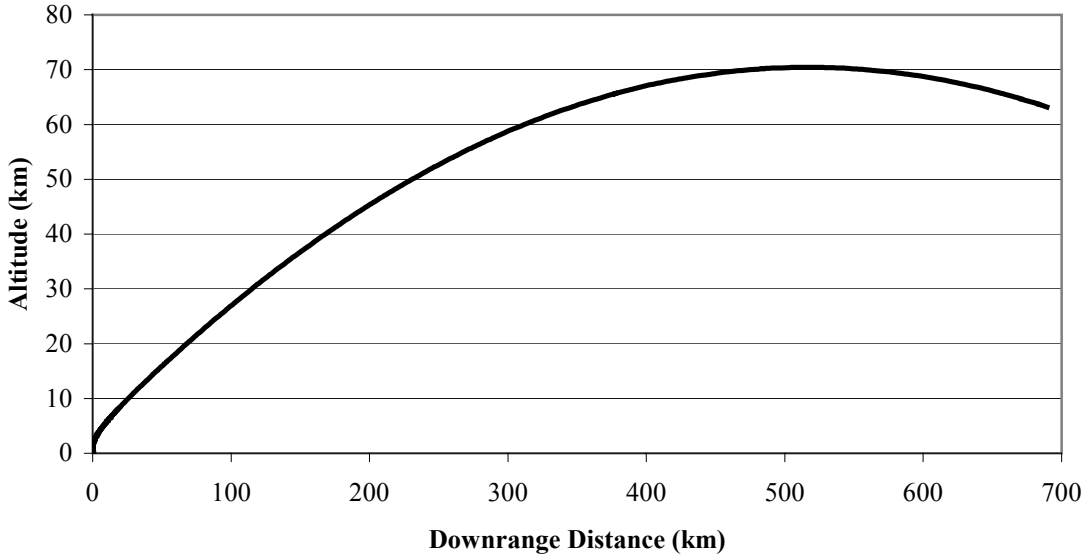


Figure 5.3: Powered Trajectory for Launch to 200 km Circular Orbit

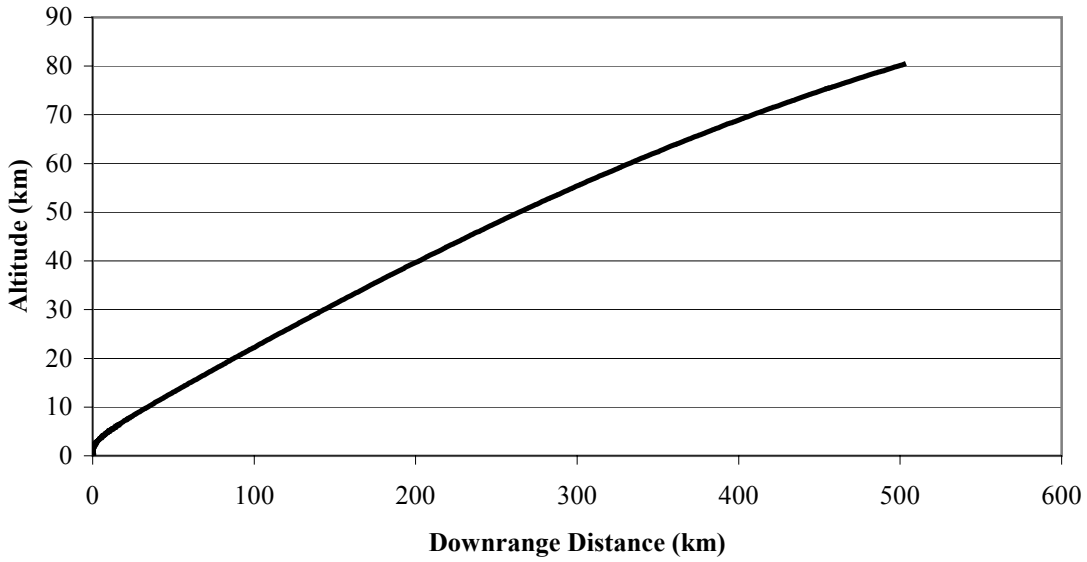


Figure 5.4: Powered Trajectory for Launch to 200 km Apogee Altitude

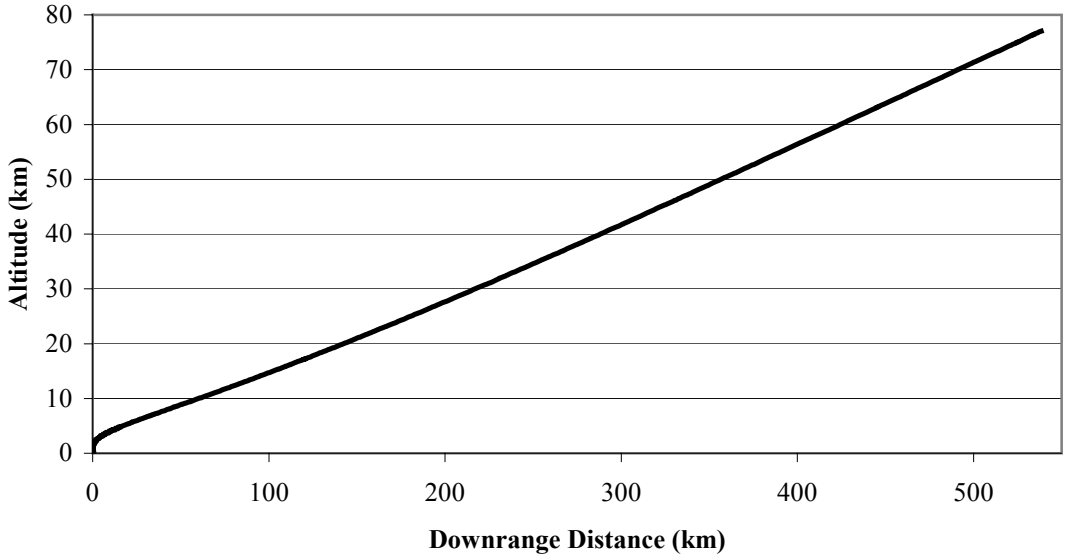


Figure 5.5: Powered Trajectory for Launch to 300 km Apogee Altitude

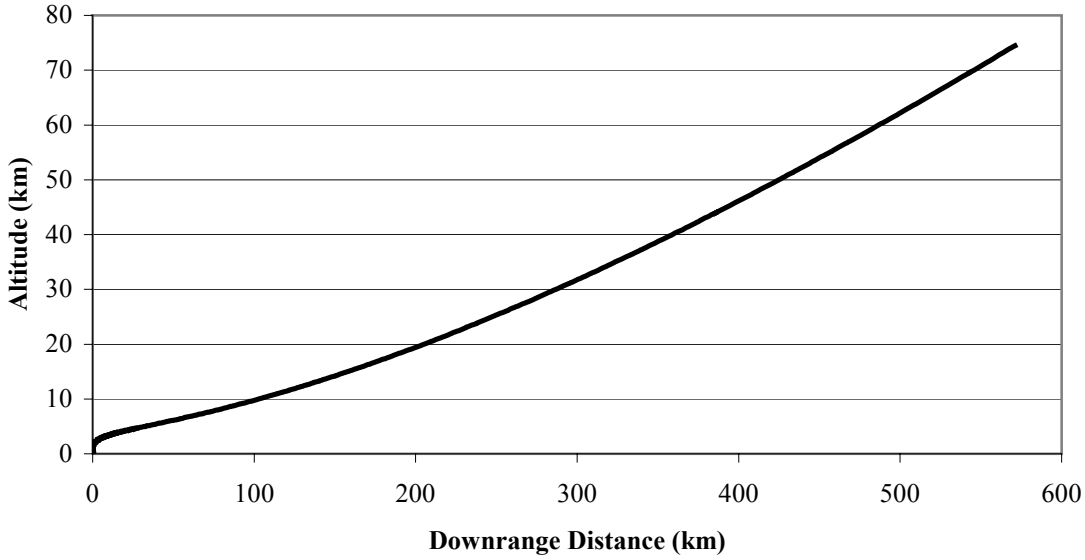


Figure 5.6: Powered Trajectory for Launch to 400 km Apogee Altitude

lower tangential velocity requirements this leads to shorter burn times for the elevator bound trajectories. Elevator bound launch vehicles are left with much more Δv available after engine cutoff.

Figures 5.7, 5.8, 5.9 and 5.10 show the time history of the engine control angle for the ascent to a 200 kilometer orbit, and to an elevator lower tip of 200, 300 and 400 kilometers, respectively. Each of these plots have a value of zero control angle for the first 37 seconds of ascent. This represents the constrained vertical climb held until the launch vehicle reaches one kilometer of altitude. At the point of pitchover the engine control angle jumps to a large negative value. This maneuver is dictated by the optimal control law to initially turn the vehicle from its vertical climb. Following the pitchover maneuver, the engine control angle quickly increases, reaching a maximum value between 30 and 40 degrees approximately 90 seconds after liftoff. This angle is somewhat high, and could not be accomplished through the use of a gimballing engine alone without producing large moments on the launch vehicle. The entire vehicle will have to be steered relative to its velocity vector, supporting the assumption made in the derivation of the vehicle equations of motion that the engine thrust always acts through the launch vehicle's center of gravity. After reaching its peak value at approximately 90 seconds into the flight, the engine control angle gradually decreases as the flight progresses. The negative values of engine control angle observed at the end of the orbital ascent occur during the portion of the ascent when the launch vehicle is flying nearly horizontally in a shallow climb, and building up the required 7.803 kilometers per second of tangential velocity at engine cutoff. The negative angle represents thrust directed down towards the Earth needed to hold the launch vehicle in its shallow climb. Negative

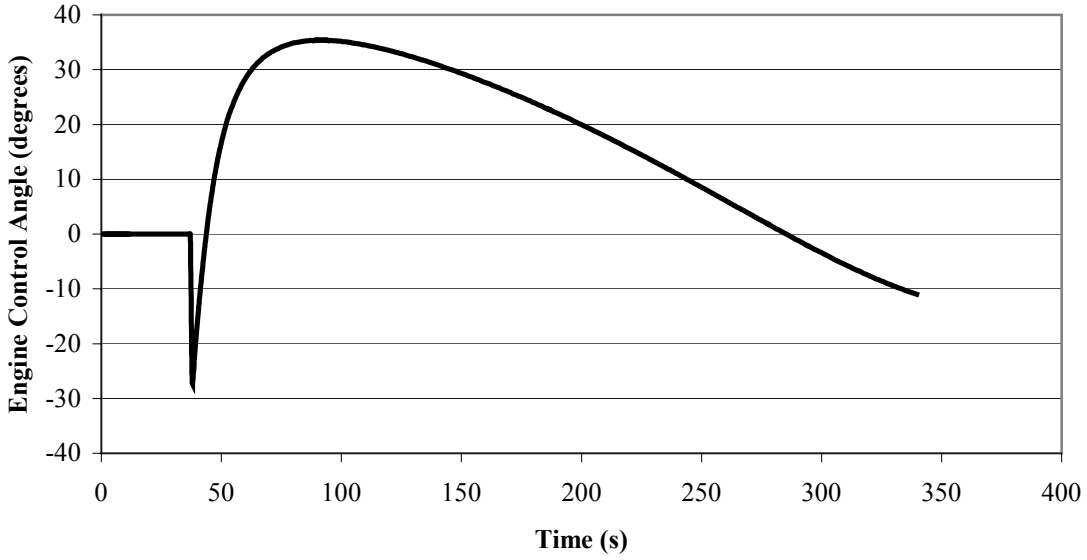


Figure 5.7: Control Angle History for Launch to 200 km Circular Orbit

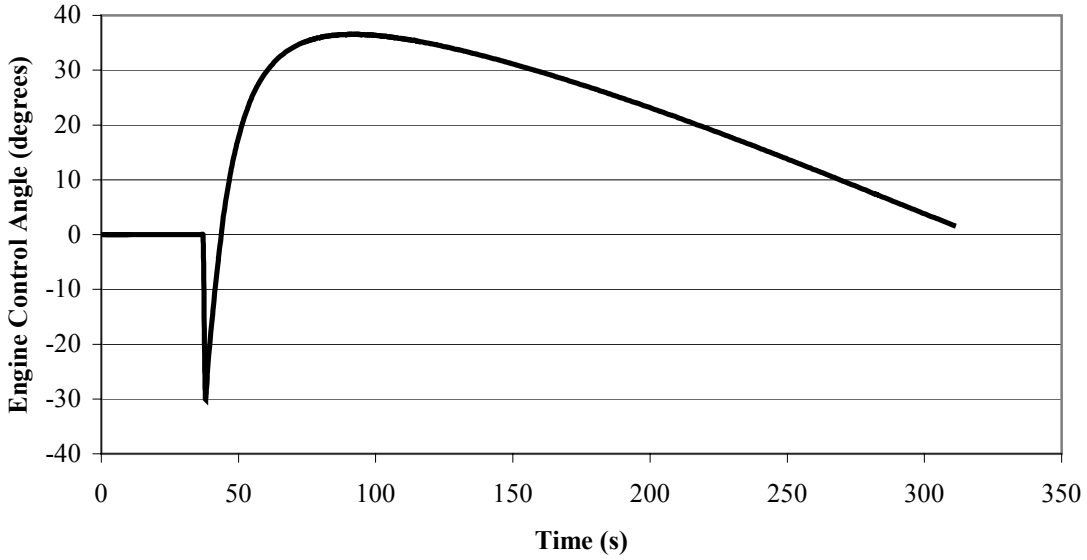


Figure 5.8: Control Angle History for Launch to 200 km Apogee Altitude

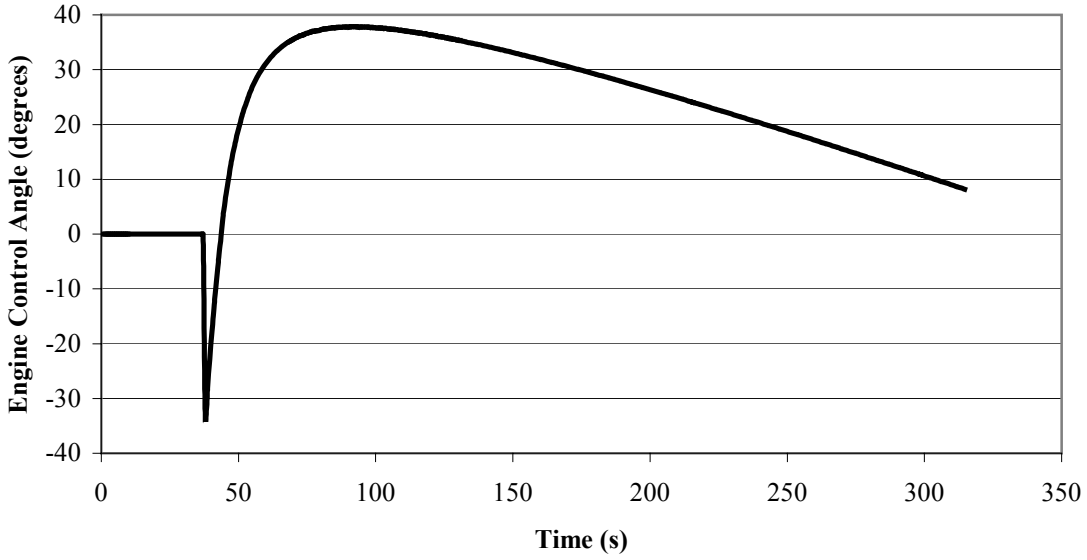


Figure 5.9: Control Angle History for Launch to 300 km Apogee Altitude

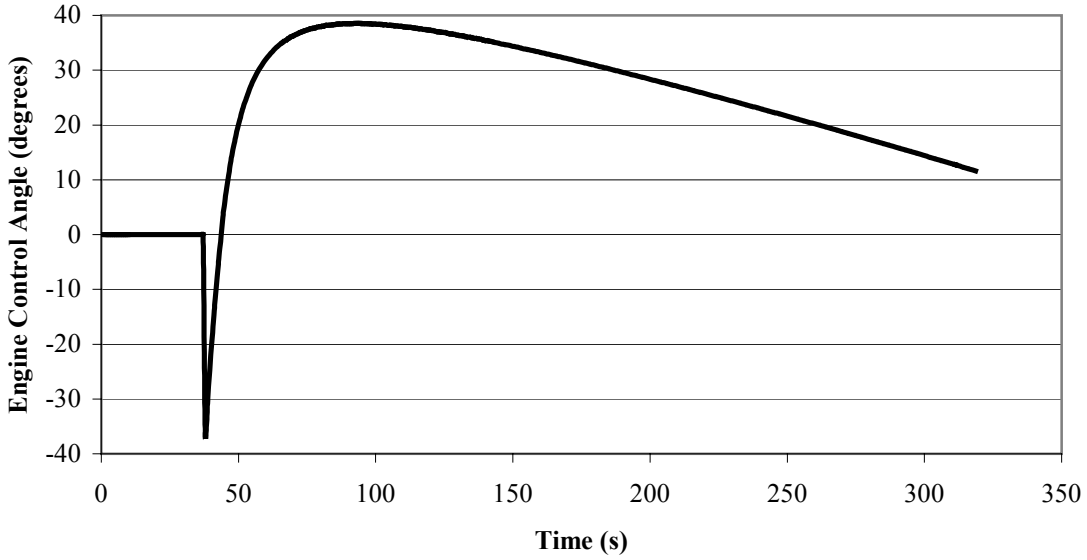


Figure 5.10: Control Angle History for Launch to 400 km Apogee Altitude

values of engine control angle are not observed in the elevator bound trajectories because the launch vehicle at engine shutdown was flying at a much steeper angle to the horizon and did not require the thrust to be directed downwards to support near horizontal flight.

Chapter 6

Rendezvous Analysis

6.1 Equations of Relative Motion

At the apex of its ballistic trajectory, the launch vehicle must rendezvous with the lower tip of the tether, allowing the transfer of the payload. Rendezvous between the launch vehicle and the lower tip is accomplished through matching the velocity and position of the two vehicles. This is performed through several maneuvers, the first of which takes the launch vehicle to the vicinity of the lower tip and the second of which nulls the relative velocity between the two. Additionally, some maneuvering capability is required of the launch vehicle to stay in formation with the elevator lower tip in order to allow the transfer of the payload. Determining the Δv needed to perform each of these maneuvers is achieved by a study of the relative motions of the two vehicles.

The first step in the analysis is to determine the relative position of the two spacecraft. A moving coordinate frame is attached to the tether center of gravity, which rotates at an angular rate equal to the tether's orbital angular rate. The coordinate frame originating at the center of the Earth is assumed to be inertial. It should be noted that the tether coordinate frame is attached to the center of gravity of the tether. This is done because the tether's center of gravity is moving in an orbital manner; the actual rendezvous target, the lower tip of the tether is traveling in a circular trajectory around the Earth, but is moving at less than orbital velocity. Figure 6.1 shows a diagram of the coordinate system used in the derivation of the equations of relative motion between the two spacecraft.

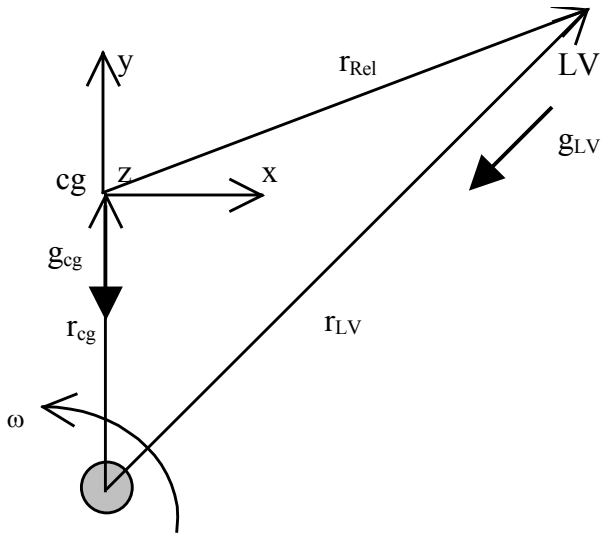


Figure 6.1: Rendezvous Coordinate System Diagram

The relative position of the launch vehicle to the elevator's center of gravity is represented by the vector equation

$$\bar{\mathbf{r}}_{LV} = \bar{\mathbf{r}}_{cg} + \bar{\mathbf{r}}_{Rel} \tag{6. 1}$$

where r_{LV} and r_T are the vector positions of the launch vehicle and the tether center of gravity in relation to the center of the Earth. This equation is differentiated with respect to the inertial coordinate system attached to the Earth, yielding the expression [64]

$$\ddot{\bar{\mathbf{r}}}_{LV} = \ddot{\bar{\mathbf{r}}}_{cg} + \ddot{\bar{\mathbf{r}}}_{Rel} + 2\left(\boldsymbol{\omega}_T \times \dot{\bar{\mathbf{r}}}_{Rel}\right) + \dot{\boldsymbol{\omega}}_T \times \bar{\mathbf{r}}_{Rel} + \boldsymbol{\omega}_T \times \boldsymbol{\omega}_T \times \bar{\mathbf{r}}_{Rel} \tag{6. 2}$$

where $\ddot{\bar{\mathbf{r}}}_{LV}$ is the inertial acceleration of the launch vehicle, $\ddot{\bar{\mathbf{r}}}_T$ is the inertial acceleration of the tether lower tip, $\ddot{\bar{\mathbf{r}}}_{Rel}$ is the acceleration of the launch vehicle relative to the tether center of gravity, $2\left(\boldsymbol{\omega}_T \times \dot{\bar{\mathbf{r}}}_{Rel}\right)$ is the Coriolis acceleration, $\dot{\boldsymbol{\omega}}_T \times \bar{\mathbf{r}}_{Rel}$ is the Euler acceleration and $\boldsymbol{\omega}_T \times \left(\boldsymbol{\omega}_T \times \bar{\mathbf{r}}_{Rel}\right)$ is the centripetal acceleration.

By neglecting the small gravitational acceleration between the launch vehicle and the tether, the inertial acceleration of the launch vehicle can be viewed as the sum of the gravitational acceleration caused by the Earth and the applied accelerations caused by powered maneuvers, shown in the expression

$$\ddot{\bar{\mathbf{r}}}_{LV} = \bar{\mathbf{g}}_{LV} + \bar{\mathbf{a}}_{LV} \tag{6. 3}$$

Inserting this relation into the inertial acceleration equation, resolving it into x, y, and z coordinates yields the set of equations

$$-g_{LV} + a_x = \ddot{x} - 2\omega_T \dot{y} - \dot{\omega}_T y - \omega_T{}^2 x \tag{6. 4}$$

$$-g_{LV}\left(\frac{y + r_{cg}}{r_{LV}}\right) + a_y = \ddot{y} - g_T + 2\omega_T \dot{x} + \dot{\omega}_T x - \omega_T{}^2 y \tag{6. 5}$$

$$-g_{LV}\left(\frac{z}{r_{LV}}\right)+a_z=\ddot{z} \tag{6. 6}$$

Solving for the relative accelerations between the launch vehicle and the tether allows the equations to be written as

$$\ddot{x}=-g_{LV}\left(\frac{x}{r_{LV}}\right)+a_x+2\omega_T\dot{y}+\dot{\omega}_T y+{\omega_T}^2 x \tag{6. 7}$$

$$\ddot{y}=-g_{LV}\left(\frac{y+r_{cg}}{r_{LV}}\right)+a_y-2\omega_T\dot{x}-\dot{\omega}_T x+{\omega_T}^2 y \tag{6. 8}$$

$$\ddot{z}=-g_{LV}\left(\frac{z}{r_{LV}}\right)+a_z \tag{6. 9}$$

The gravitational acceleration felt by the launch vehicle can be expressed as

$$g_{LV}=\frac{GM_E}{{r_{LV}}^2} \tag{6. 10}$$

It also should be noted that the tether is assumed to be in a circular or near circular orbit, allowing the terms containing angular acceleration $\dot{\omega}_T$ to be neglected. This allows the relative acceleration equation to be simplified to the form

$$\ddot{x}=-\frac{GM_E\,x}{{r_{LV}}^3}+a_x+2\omega_T\dot{y}+{\omega_T}^2 x \tag{6. 11}$$

$$\ddot{y}=-\frac{GM_E\left(y+r_{cg}\right)}{{r_{LV}}^3}+a_y-2\omega_T\dot{x}+{\omega_T}^2 y \tag{6. 12}$$

$$\ddot{z}=-\frac{GM_E\,z}{{r_{LV}}^3}+a_z \tag{6. 13}$$

The equations in their above form have been widely used for rendezvous applications in Earth orbit, as most spacecraft rendezvous occur in circular or nearly

circular orbits [76]. A simple solution can be sought to these equations through a harmonic oscillator approach [77]. This type of solution is useful in tracking relative drift between two closely flying satellite in similar orbits. The problem of rendezvous between the launch vehicle and the tether's lower end is complicated by the fact that the two objects are on very different trajectories. The launch vehicle is on a ballistic trajectory that will return it to the Earth if a rendezvous is not achieved. The rendezvous target, the tether lower tip, is moving in a non-orbital fashion on a circular trajectory at significantly lower speeds than the circular orbit velocity for its altitude. For these reasons, a numerical method presents itself as an alternative to seeking a solution to the rendezvous equations.

6.2 Solution Method

The equations for relative acceleration are second order derivatives, but they can be solved by Runge-Kutta integration by treating them as a set of six first order differential equations. The equations of relative motion are written as first order equations in the form of

$$\frac{dx}{dt} = \dot{x} \tag{6. 14}$$

$$\frac{d\dot{x}}{dt} = -\frac{GM_E\, x}{r_{LV}^{\,3}} + a_x + 2\omega_T \dot{y} + \omega_T^{\,2} x \tag{6. 15}$$

$$\frac{dy}{dt} = \dot{y} \tag{6. 16}$$

$$\frac{d\dot{y}}{dt} = -\frac{GM_E \left(y + r_{cg}\right)}{r_{LV}^{\,3}} + a_y - 2\omega_T \dot{x} + \omega_T^{\,2} y \tag{6. 17}$$

$$\frac{dz}{dt} = \dot{z} \tag{6. 18}$$

$$\frac{d\dot{z}}{dt} = -\frac{GM_E z}{r_{LV}^3} + a_z \tag{6. 19}$$

There are a total of six equations governing the spacecraft relative positions and velocities in three dimensions. This set of equations can be used to explore three different facets of rendezvous between the launch vehicle and the tether.

The first problem is to define the unconstrained relative motion between the launch vehicle and its target. For this case, the initial position and velocities are inputted for an ideal case in which the launch vehicle will pass by the tether lower end at the apex of its trajectory. This is useful in that it shows how much time the two spacecraft will be in relative position without any active maneuvering on the part of the launch vehicle. The amount of time spent in formation is a critical factor in determining the ease of payload transfer between the launch vehicle and the elevator.

The second problem addresses how much maneuvering capability will be needed by the launch vehicle to hover in the vicinity of the tether's lower end for a predetermined amount of time. It can be assumed that the transfer of payload from the launch vehicle to the elevator will not be instantaneous. By quantifying the constant thrust applied to the launch vehicle to hold it at the tether's lower end a better understanding is gained of its required maneuvering capability. Starting with zero relative distance and velocity between the elevator's lower tip and the launch vehicle, an unknown constant thrust is applied to the launch vehicle to hold it at the elevator's lower tip for a specified amount of time. The unknown applied thrust is found from solving the

equations of relative motion using the final conditions of zero distance between the lower tip and the launch vehicle. The Δv required to hold the launch vehicle at the tether lower tip is found by multiplying the constant acceleration by the desired time needed to transfer the payload from the launch vehicle to the tether.

The third and final problem studied is terminal rendezvous between the launch vehicle and the tether lower tip. The launch vehicle may reach the apogee of its trajectory at some moment before or after the tether end will travel by it. This can be caused by errors in guidance during the powered ascent or by issues involving the launch window of the vehicle. For this case it is assumed that the launch vehicle is on a trajectory that, with the absence of any active maneuvering, will not arrive at the elevator lower end at the apex of its ballistic trajectory, but will miss it by some measured amount of time. The data gained from this case is useful in sizing of the maneuvering capability required by the launch vehicle to affect a rendezvous under less than ideal conditions. For this case the positions of the launch vehicle and lower tip form the known initial condition of the problem. The required initial relative velocity to bring the two together to a rendezvous is unknown. The solution to this boundary value problem requires three known final conditions, which exist in the form of the x, y, and z coordinates of the desired final relative position between the two vehicles. Table 6.1 contains a list of the boundary value conditions for the terminal rendezvous problem.

These desired final distances between the launch vehicle and the tether are zero in the x and z directions. In the y direction, the desired final distance is equal to the length of the tether between its center of gravity and its lower end. These unknown initial

Table 6.1: Boundary Value Conditions for Rendezvous Problem

Variable	Initial Condition	Final Condition
Relative position x	known	known
Relative position y	known	known
Relative position z	known	known
Relative velocity x	unknown	unknown
Relative velocity y	unknown	unknown
Relative velocity z	unknown	unknown

conditions are solved for using a three dimensional shooting method, with the desired zero distance between the two forming the known final condition.

6.3 Rendezvous Analysis Results

6.3.1 Launch Vehicle Relative Motion

Figures 6.2, 6.3 and 6.4 show the relative motion of the launch vehicle with respect to the elevator's lower tip for a handoff altitude of 200, 300, and 400 kilometers, respectively. The relative motion shown in these graphs represents the ideal rendezvous condition, where the apex of the launch vehicle trajectory will meet with the lower tip of the elevator at the same point in space simultaneously. The trajectory for the launch vehicle is assumed to be coplanar with the orbit of the elevator. On each graph, the origin is at the elevator lower tip and each tick mark along the path of the launch vehicle's motion represents five seconds of elapsed time. As can be seen from these graphs of the relative motion, most of the movement between the launch vehicle and the tether's lower tip is in the vertical direction. The tangential velocity of the launch vehicle is closely matched with the tangential velocity of the tether lower tip, producing a relatively small lateral relative motion between them. The launch vehicle rapidly rises up to the apogee of its ballistic trajectory and very quickly descends away. For each of the handoff altitudes studied, the launch vehicle is within a range of 50 meters of the elevator lower tip for a period of time less than ten seconds. This short time would require a near instantaneous transfer of the payload from launch vehicle to elevator, which is impractical. To achieve a payload transfer, the launch vehicle must suspend itself along its trajectory and hover at the elevator lower tip for some specified period of time.

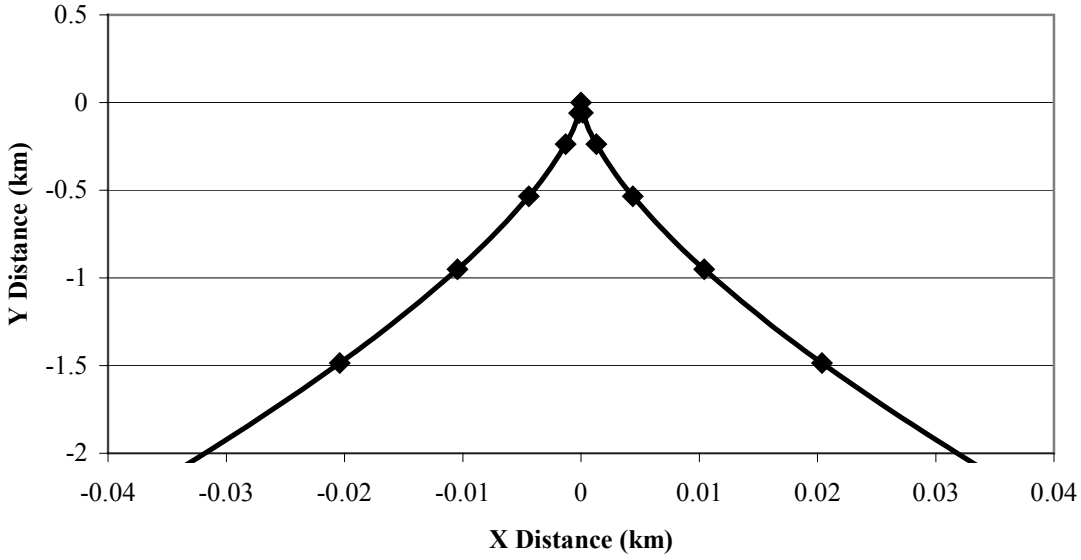


Figure 6.2: Relative Motion Between the Launch Vehicle and 200 km Lower Tip

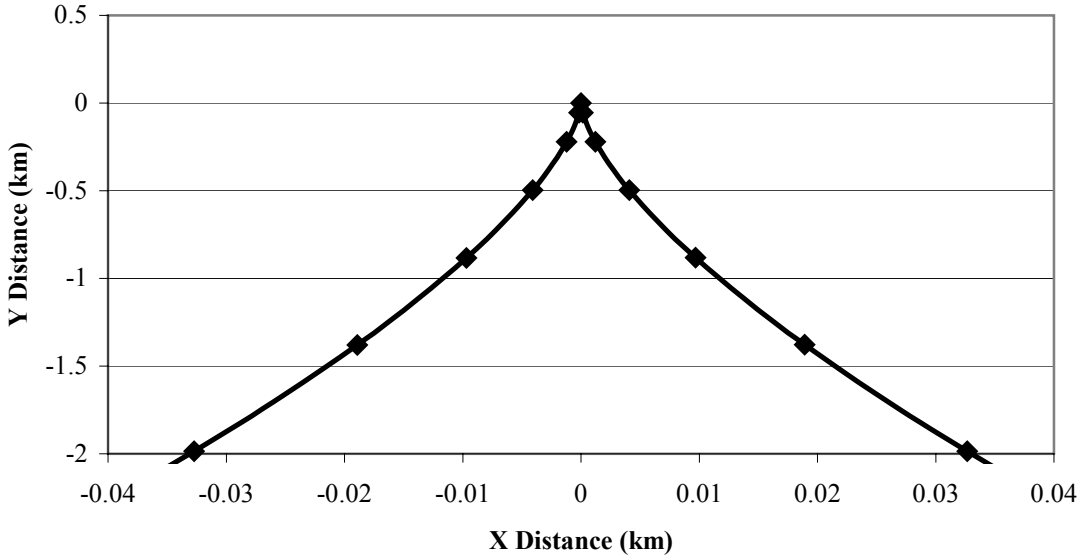


Figure 6.3: Relative Motion Between the Launch Vehicle and 300 km Lower Tip

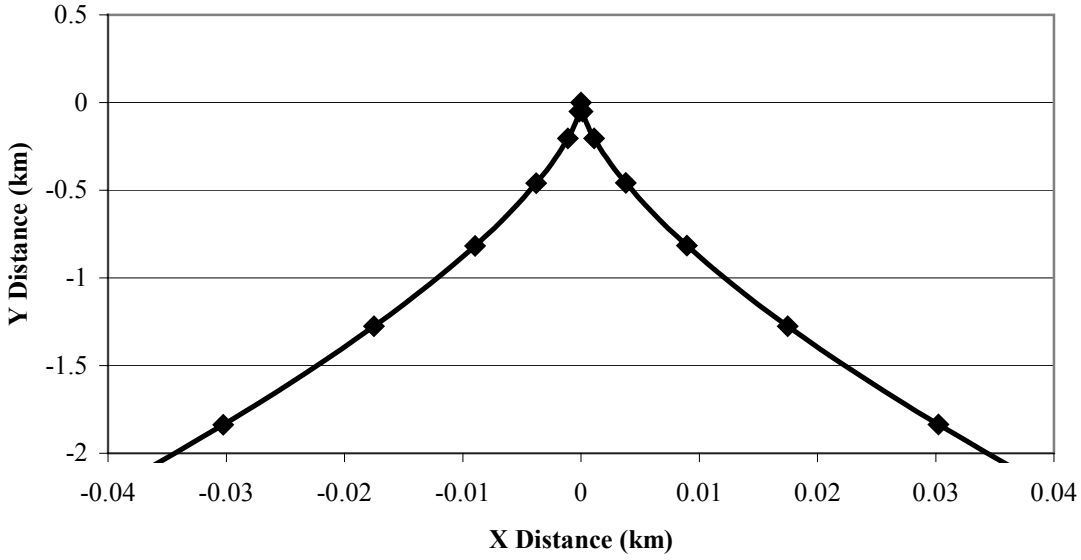


Figure 6.4: Relative Motion Between the Launch Vehicle and 400 km Lower Tip

6.3.2 Launch Vehicle Hovering

Figures 6.5, 6.6 and 6.7 show the required Δv needed to hold the launch vehicle at the elevator's lower tip for a handoff altitude of 200, 300, and 400 kilometers, respectively. For a launch vehicle trajectory that is coplanar with the elevator orbit, the hovering requirement is easily calculated by measuring the acceleration at the elevator's lower tip, which is composed of the gravitational attraction of the Earth and the centrifugal acceleration caused by the tether orbital rotation, as shown by the equation

$$a_g = \frac{GM_E}{r_{le}^2} - r_{le}\,\omega_T^2 \qquad (6.\ 20)$$

This equation produces a value of 4.753 meters per second of acceleration experienced at the handoff point for a tether with a lower tip of 200 kilometers. The acceleration felt at the handoff point is 4.411 meters per second and 4.082 meters per second for Elevator's with lower ends at 300 and 400 kilometers of altitude, respectively. These values are confirmed with the numerical program used in this study. For the non-coplanar cases, it can be seen from Figures 6.5, 6.6 and 6.7 that as the inclination between the launch vehicle trajectory and the tether orbital plane increases, the Δv required for hovering rapidly grows larger. For each handoff altitudes studied, a 10° inclination between the launch vehicle trajectory and the tether orbit leads to a required Δv of approximately 2,000 meters per second, with the value growing larger as the required hovering time increased. From Chapter 5 it has been shown that the launch vehicle retains enough propellant after the powered ascent to a 200 kilometer apogee to provide for 2,617 meters per second of Δv. Similarly, the propellant remaining on the launch vehicle launch vehicle allows for 2,356 meters per second and 2,105 meters per

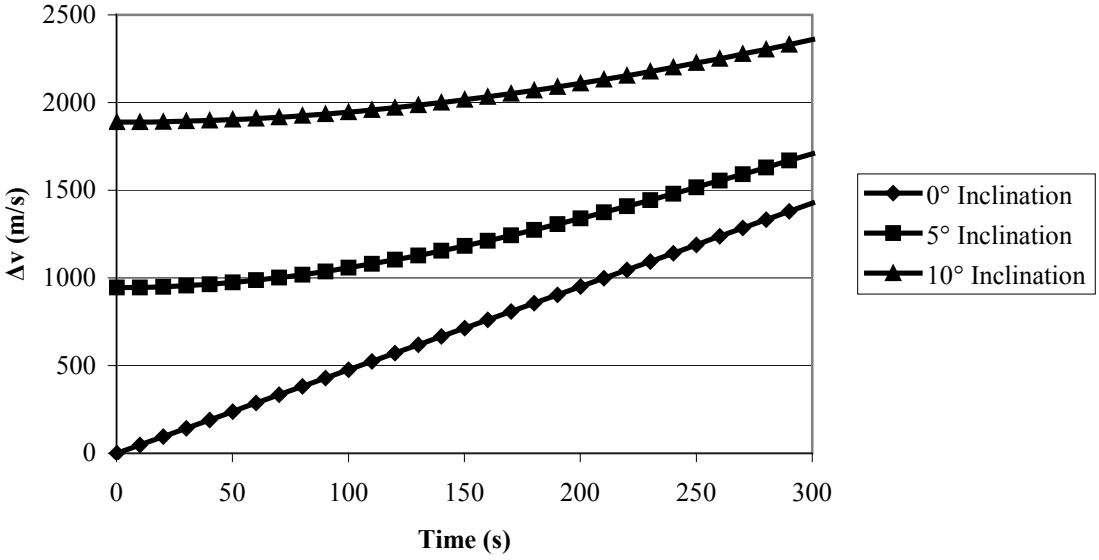


Figure 6.5: Δv versus Time for Launch Vehicle Hovering at the 200 km Lower Tip

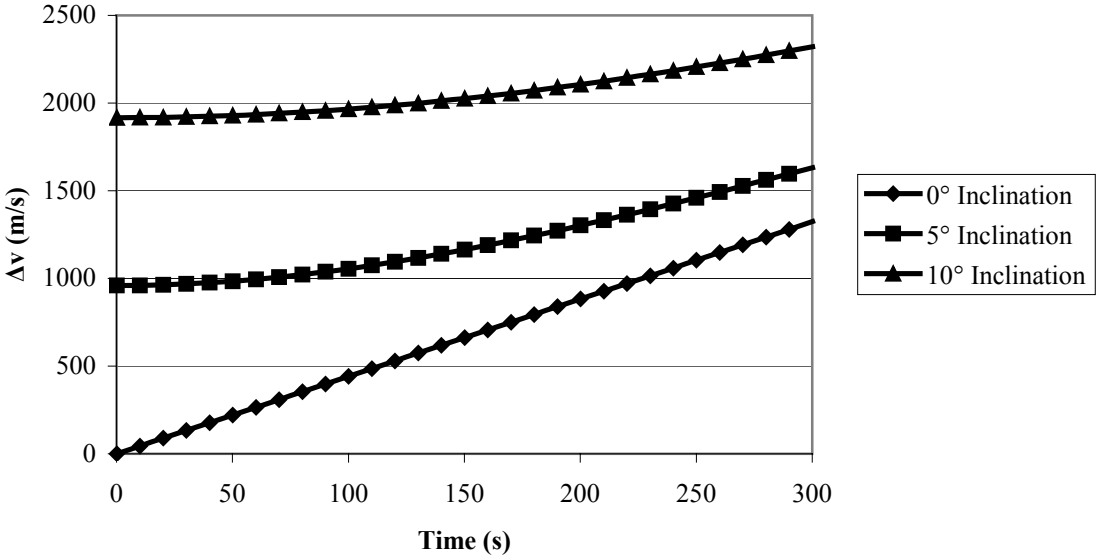


Figure 6.6: Δv versus Time for Launch Vehicle Hovering at the 300 km Lower Tip

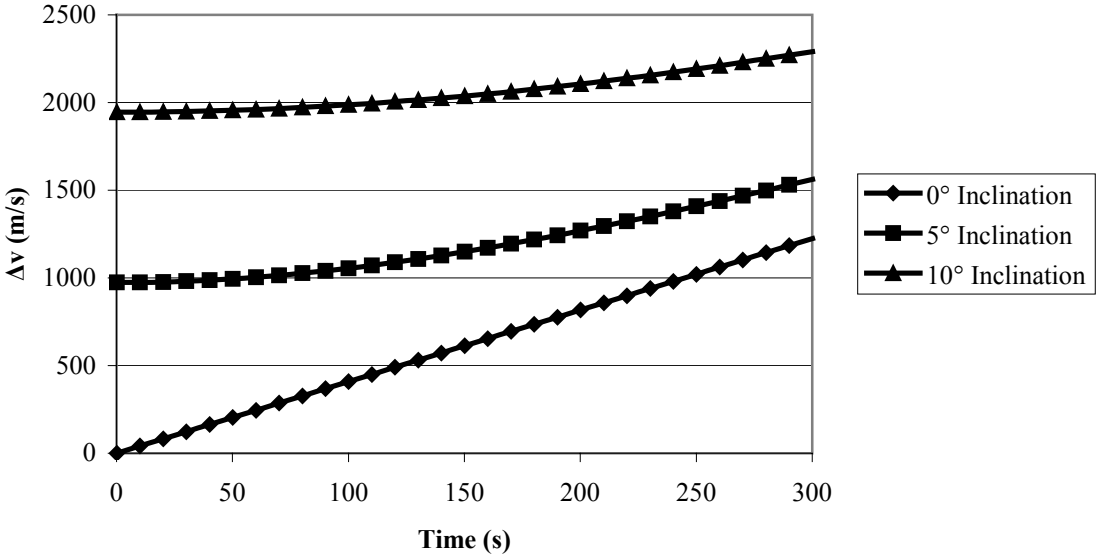


Figure 6.7: Δv versus Time for Launch Vehicle Hovering at the 400 km Lower Tip

second of Δv after the powered ascent to an apogee of 300 and 400 kilometers, respectively. The requirements for hovering at a tether inclined 10° to the launch vehicle trajectory represent a large portion of the Δv available after powered ascent, and would require near perfect timing of the terminal rendezvous between the two.

6.3.3 Terminal Rendezvous

Figure 6.8 shows a typical plot of the required Δv needed to achieve a terminal rendezvous between the launch vehicle and an elevator with a 200 kilometer lower tip altitude. For the particular case illustrated in this graph, the launch vehicle's unaltered trajectory places it at apogee 45 seconds before the tether is in position for rendezvous, with the launch vehicle trajectory on a coplanar trajectory with the tether orbit. For this case, the terminal rendezvous requiring the minimum Δv occurs at approximately 256 seconds after the engine cutoff, when 978.333 meters per second of maneuvering is required to place the launch vehicle at the elevator lower tip.

Multiple cases are run with varying rendezvous error times and the minimum Δv required for terminal rendezvous is determined for each case. Figures 6.9, 6.10 and 6.11 represent the minimal Δv calculated for each different rendezvous error time for handoff altitudes of 200, 300, and 400 kilometers, respectively. On these plots, the error time represents the number of seconds by which the launch vehicle misses the rendezvous point. For example, a value of negative 60 seconds means the launch vehicle is a minute late in reaching the handoff point. In other words, upon reaching its apogee the launch vehicle is a minute behind the actual position of the tether's lower tip. Conversely, a positive rendezvous error time corresponds to the launch vehicle reaching the handoff point before the tether lower tip has arrived. For each of the three elevators selected in

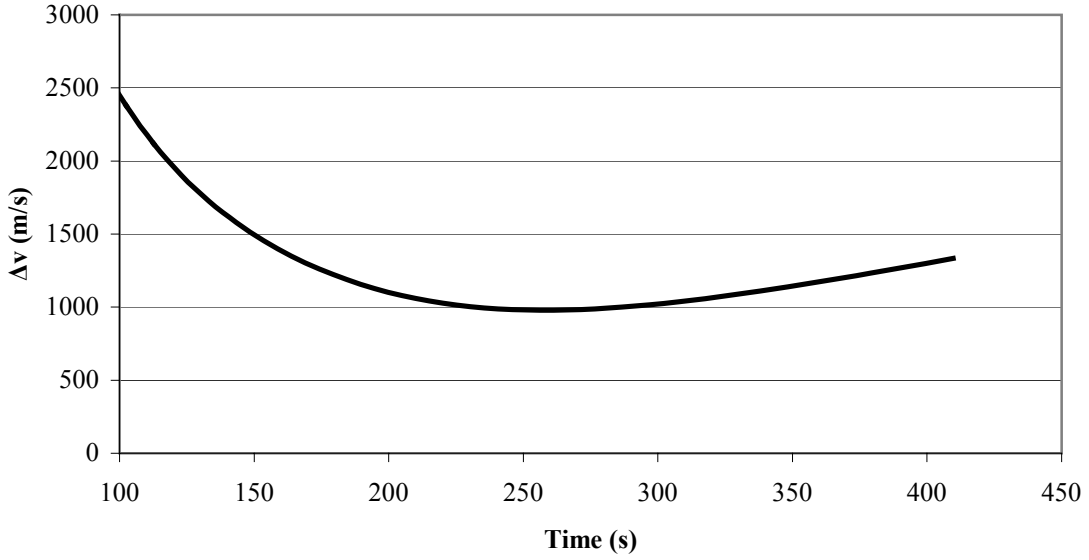


Figure 6.8: Δv versus Time Until Rendezvous at the 200 km Lower Tip

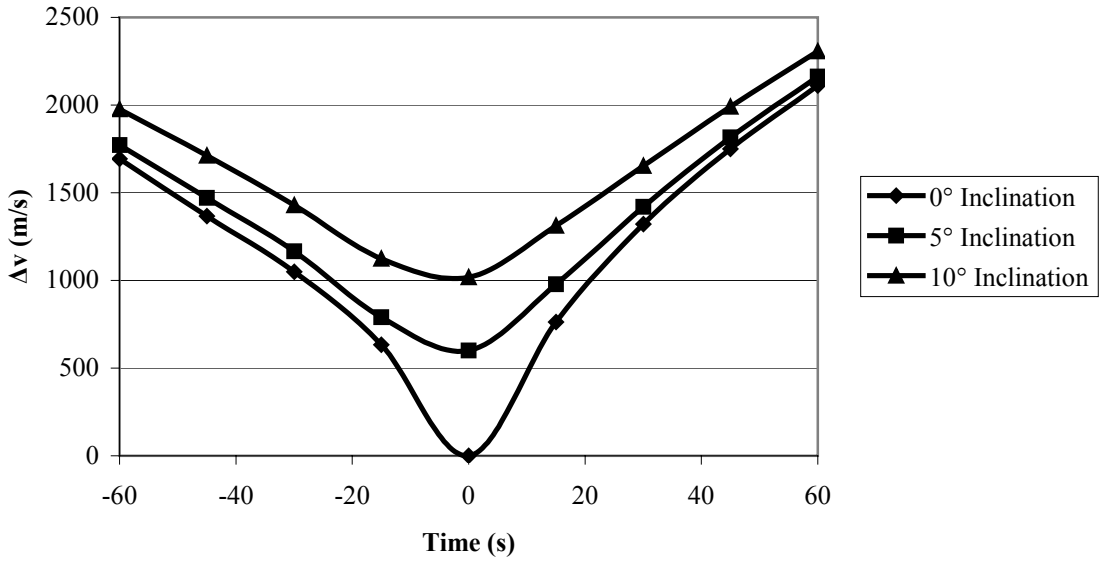


Figure 6.9: Minimum Δv versus Rendezvous Error Time at the 200 km Lower Tip

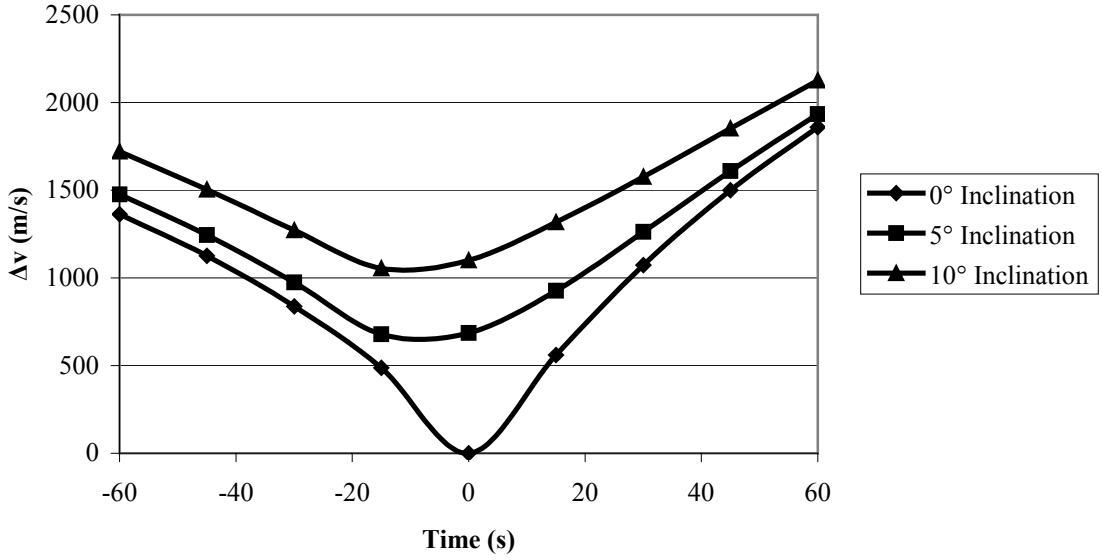


Figure 6.10: Minimum Δv versus Rendezvous Error Time at the 300 km Lower Tip

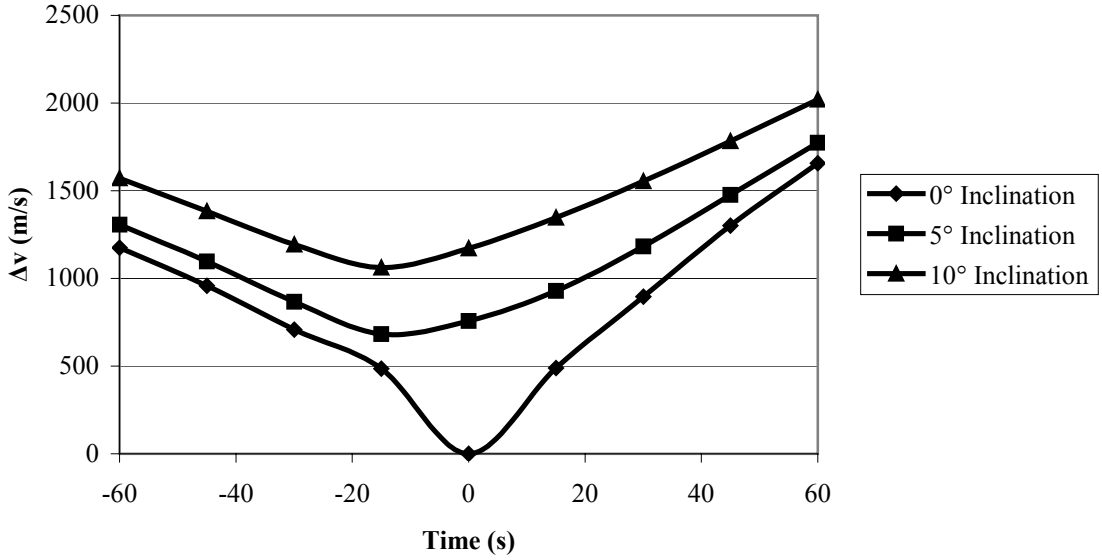


Figure 6.11: Minimum Δv versus Rendezvous Error Time at the 400 km Lower Tip

this study, these cases are run for 0°, 5°, and 10° of inclination between the launch vehicle trajectory and the orbital plane of the elevator. From each of the plots, it can be observed that the ideal case of no rendezvous time error and 0° of inclination produces a value of zero meters per second of Δv. The launch vehicle passes by the elevator's lower tip as the two meet at the launch vehicle apogee. As the rendezvous error times increase the required Δv also grows. In all cases the values for negative rendezvous error time are somewhat less than those with corresponding positive rendezvous time. In general, it can be observed that less Δv is required for the launch vehicle to catch up to a tether that is ahead of it in orbital position at the time of rendezvous than for the launch vehicle to slow down to meet a tether that is behind it in orbital position.

6.3.4 Total Rendezvous Requirements

By combining the required Δv needed for terminal rendezvous along with that needed for hovering at the tether's lower tip, the total required Δv for the entire rendezvous maneuver can be calculated. Figure 6.12 shows the minimum Δv required for the total rendezvous maneuver versus rendezvous error time between a launch vehicle on a coplanar trajectory with a tether at a handoff altitude of 200 kilometers, plotted with varying amounts of hover time. As the maximum value on the plot corresponds to the 2,617 meters per second of Δv left after powered ascent, this graph represents the window of rendezvous performance that the launch vehicle is capable of after powered ascent.

Figure 6.13 shows the minimum Δv required for the total rendezvous maneuver versus rendezvous error time for a launch vehicle on a trajectory inclined at 5° with the tether at a handoff altitude of 200 kilometers. Again the maximum plotted value of Δv is

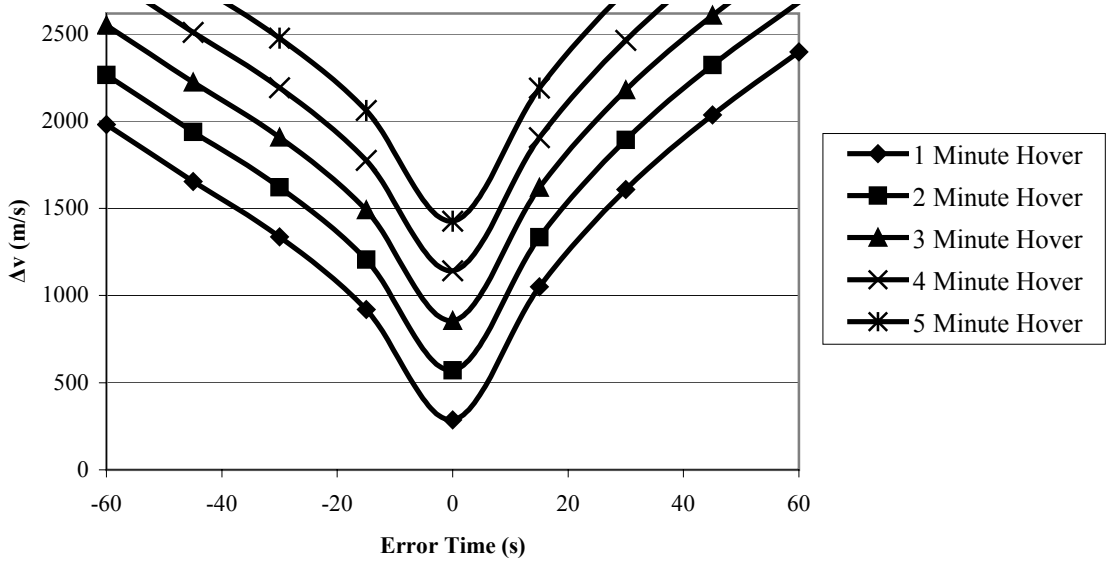


Figure 6.12: Total Δv versus Rendezvous Error Time at the 200 km Lower Tip at 0° Inclination

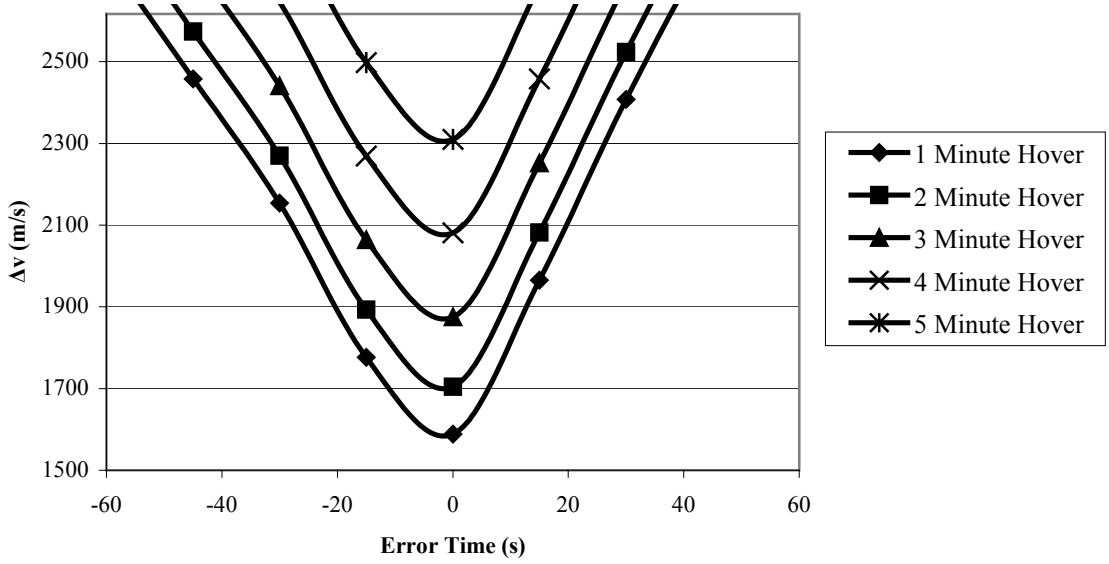


Figure 6.13: Total Δv versus Rendezvous Error Time at the 200 km Lower Tip at 5° Inclination

2,617 meters per second, representing the window of rendezvous performance within the capabilities of the launch vehicle. For each of the three tethers included in this study, the total Δv required to achieve rendezvous between the launch vehicle and an elevator at a relative inclination of 10° exceeds the maneuvering capability remaining with the launch vehicle after the completion of the powered ascent.

Figures 6.14 and 6.15 show the minimum Δv required for the total rendezvous maneuver versus rendezvous error time between a launch vehicle and the elevator at a handoff altitude of 300 kilometers, for inclinations of 0° and 5°, respectively. The maximum plotted value of these graphs corresponds to the 2,356 meters per second of Δv left with the launch vehicle following powered ascent.

Figures 6.16 and 6.17 show the minimum Δv required for the total rendezvous maneuver versus rendezvous error time between a launch vehicle and the elevator at a handoff altitude of 400 kilometers, for inclinations of 0° and 5°, respectively. The maximum plotted value of these graphs corresponds to the 2,105 meters per second of Δv left with the launch vehicle following powered ascent. It should be noted that for an inclination of 5°, a hover time of five minutes produces a minimum total Δv of 2,318 meters per second, outside of the launch vehicle capability.

From each of these graphs it can be seen that the required rendezvous performance is somewhat similar irregardless of the particular handoff altitude. For coplanar trajectories the minimum Δv curves are more shallow as the handoff altitude is increased. For example, a coplanar rendezvous at an altitude of 200 kilometers altitude with –60 seconds of rendezvous error time and one minute of hovering requires 1,979 meters per second Δv, while the corresponding case at 400 kilometers of altitude only

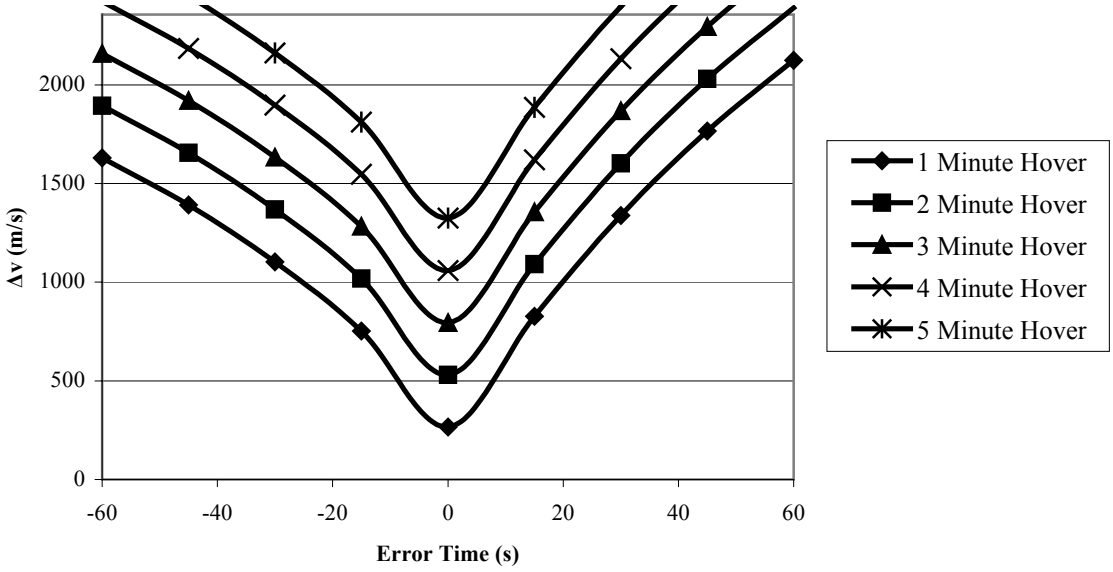


Figure 6.14: Total Δv versus Rendezvous Error Time at the 300 km Lower Tip at 0° Inclination

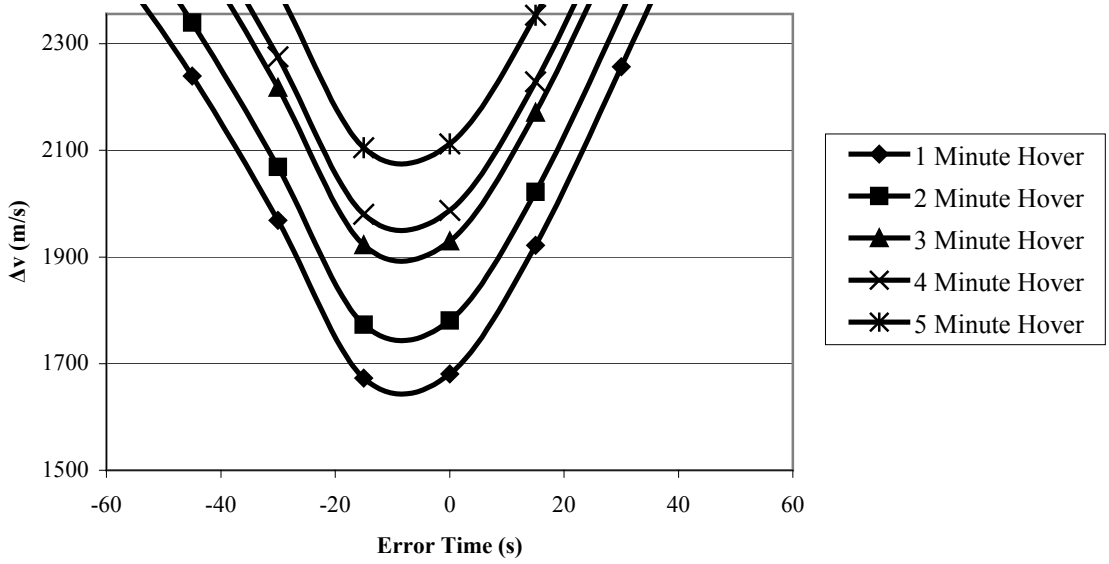


Figure 6.15: Total Δv versus Rendezvous Error Time at the 300 km Lower Tip at 5° Inclination

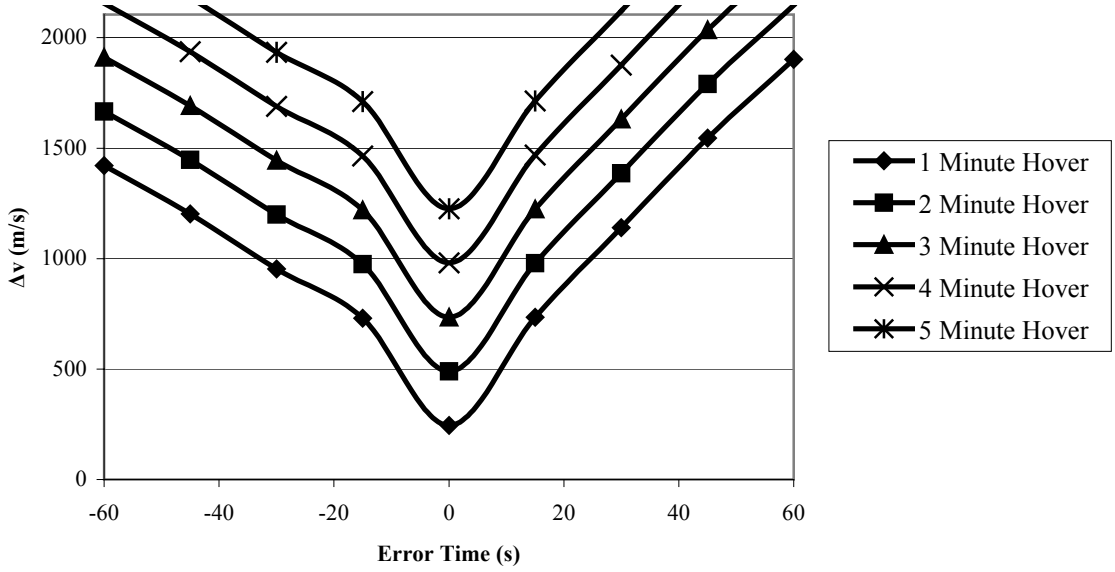


Figure 6.16: Total Δv versus Rendezvous Error Time at the 400 km Lower Tip at 0° Inclination

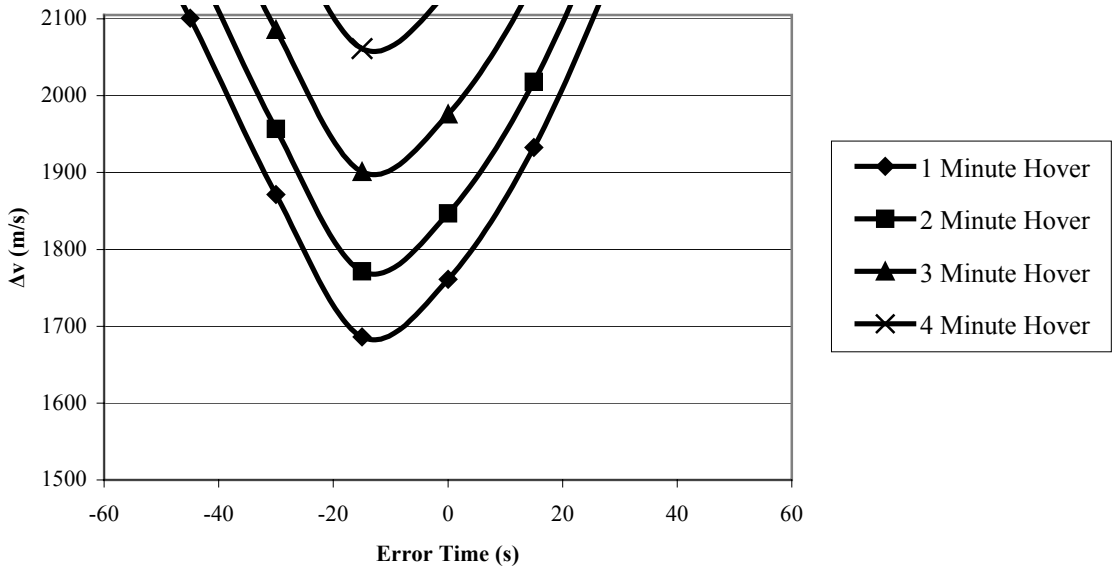


Figure 6.17: Total Δv versus Rendezvous Error Time at the 400 km Lower Tip at 5° Inclination

requires 1,420 meters per second of Δv. In conclusion, it has been shown that a vehicle designed for a single stage to orbit mission has enough performance to achieve a rendezvous with the orbiting space elevator in a reasonably sized window of time when launched on a coplanar or nearly coplanar trajectory.

Chapter 7

Elevator Launched Trajectories

7.1 Lunar Destination

The orbiting space elevator primarily serves as a system to launch payloads into high Earth orbit, or on trans-lunar and interplanetary trajectories. In Chapter 1, the Moon is identified as a location of particular interest in future space development, due to its possession of platinum and helium-3. Both of these materials could offer possible solutions to energy shortages in the future. This section will analyze trans-lunar trajectories originating from the upper end of the orbiting space elevator.

The Moon orbits around the Earth with a period of 27.321 days, an eccentricity of 0.0554, and a semi-major axis of 384,400 kilometers. The lunar orbital plane's inclination to the Earth's equatorial plane varies between 28.6° and 18.4° over a period of 18.6 years [78]. For the purposes of this study, the Moon is assumed to be in a circular orbit with a radius of 384,400 kilometers with the lunar orbital plane's inclination to the Earth at an average value of 23.5°. The Earth orbiting elevator is assumed to be in an orbital inclination of 35° with respect to the Earth's equatorial plane. This value is chosen to allow access to the elevator from launch sites in approximately the lower third of the continental United States.

The three types of trajectories included in this study will be classified by their destination: lunar orbit, the L1 Lagrange point, and a lunar elevator. The trajectory analysis for a destination in lunar orbit is accomplished through the use of the patched conic method. This approximation treats a spacecraft as being in orbit around a single

central body, either the Earth or the Moon, when it lies within that body's sphere of influence. The radius of the lunar sphere of influence is calculated from the values of the radius of its orbit around the Earth and the ratio of the masses of the Moon and Earth, by the equation

$$r_{SOI} = r_{mo}\left(\frac{m_m}{m_E}\right)^{2/5} \qquad (7.\ 1)$$

This equation yields a value of 66,183.7 kilometers for the radius of the lunar sphere of influence, within which the Moon's gravity dominates the motion of a space craft.

The Apollo missions to the Moon will serve as a reference against which the elevator launched trajectories will be compared. An Apollo mission to the Moon begins with a launch from Cape Canaveral to a parking orbit in LEO. To depart from LEO, a trans-lunar injection (TLI) maneuver is made to place the spacecraft on a trajectory to intersect the Moon after approximately three days of travel. During the coasting phase after TLI, while the spacecraft is on a lunar-transfer orbit, several small mid-course corrections could be made to fine tune its arrival at the Moon. Entry into the lunar sphere of influence places the Apollo spacecraft on a trajectory that took it around the Moon and back out of its sphere of influence, unless a maneuver is made at the time of close lunar approach. This Lunar Orbit Insertion (LOI) maneuver decelerates the spacecraft enough to allow it to enter into a low lunar orbit, from which a descent could be made. Typical values for these maneuvers are shown in Table 7.1, which contains the Δv budget for the Apollo 16 mission flown in April of 1972.

Table 7.1: Apollo 16 Δv Budget

Maneuver	Δv (m/s)
Launch to LEO	11,600
TLI	3,050
Midcourse Correction	0
LOI	940
Descent	2,040
Total	17,630

Launch opportunities for the Apollo spacecraft occur twice per day, when the launch site, and consequently the low Earth parking orbit, is within the plane of the lunar transfer orbit. In actual practice, the launch window for an Apollo mission is further limited to one opportunity every 28 days, once per lunar "day", due to mission constraints of lighting conditions at the landing site.

7.2 Trajectories to Lunar Orbit

Of the three trajectory types included in this study, an elevator-launched trajectory to lunar orbit is the most similar to the Apollo mission. However, trajectories bound for lunar orbit differ from Apollo in several important respects. With the orbiting space elevator, the Δv required to launch a payload to orbit is reduced, due to the lower velocity of the tether's bottom tip. Because the tether's upper tip possesses a large tangential velocity approximately 95% of that required to reach the Moon, the TLI maneuver can be achieved with limited expenditure of propellant. With the minimum Δv applied to the spacecraft at release, an elevator launched spacecraft would have a flight path angle of 0° relative to the local Earth horizontal and would be on a Hohmann trajectory to the Moon, arriving in approximately five days. While this prospect is attractive, it limits the available launch opportunities to only two per every 28 days, when the Moon crosses the plane of the elevator's orbit. This also requires careful timing of the elevator's position in its orbit to allow it to be at the proper insertion point for trans-lunar trajectory. If some additional maneuvering capability is provided to the spacecraft at the time of launch from the elevator, the spacecraft could be launched with some inclination to the original elevator orbit and at flight path angles other than 0°. This allows the launch window

constraints on orbital inclination and elevator positioning to be relaxed, and facilitate quicker flight times to the Moon.

7.2.1 Patched Conic Approximation

Figure 7.1 shows a diagram of the patched conic trajectory used in this study to analyze trajectories bound for lunar orbit. The first step in the patched conic approach is to specify the departure velocity, radius, and flight path angle. The departure radius of the elevator launched spacecraft is equal to the radius of the upper tip of the orbiting space elevator. Because the upper tip of the elevator travels with only 95% of the velocity required for a Hohmann transfer to the Moon, the departure velocity must be specified to be a value greater than the upper tip velocity. The Δv required at departure is calculated by the law of cosines relation between the tether's upper tip velocity, the departure velocity, and the departure flight path angle, according to the equation

$$\Delta v_0 = \sqrt{v_0^{\,2} + v_{ue}^{\,2} - 2\, v_0\, v_{ue} \cos(\beta_0)} \tag{7.2}$$

The departure flight path angle was held to be zero in this study, in order to take full advantage of the tangential velocity imparted to the spacecraft by the Earth orbiting tether. If, at the point of departure from the elevator, a maneuver is made to match the inclination of the departing spacecraft with the lunar orbital plane, the Δv equation must include a second term to account for the difference in inclination between the two, and would then take the form

$$\Delta v_0 = \sqrt{v_0^{\,2} + v_{ue}^{\,2} - 2\, v_0\, v_{ue} \cos(\beta_0)} + 2\, v_0 \sin\left(\frac{i_T - i_m}{2}\right) \tag{7.3}$$

From the departure conditions at the elevator's upper tip, several characteristics of the elevator launched spacecraft's transfer orbit can be calculated, which will be useful

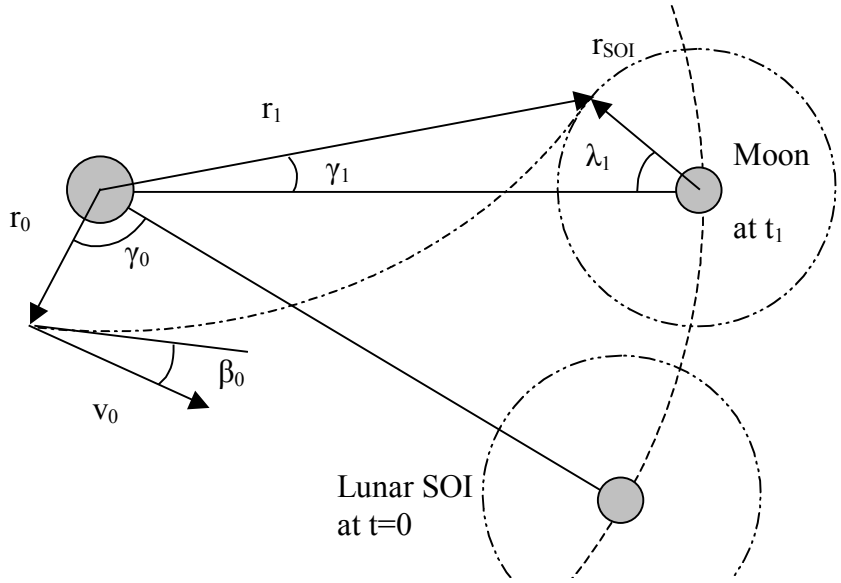


Figure 7.1: Trans-lunar Patched Conic Trajectory

later in computing the flight time involved in the lunar transfer. The value of the departure trajectory's orbital energy constant is given by the relation

$$OEC_E = v_0^{\,2} - \frac{2\,GM_E}{r_{ue}} \tag{7.4}$$

The Kepler area constant of the transfer orbit is found by the equation

$$C_E = r_{ue}\; v_0 \cos(\beta_0) \tag{7.5}$$

while the parameter of the transfer orbit is found to be the ratio of the Kepler area constant and the gravitational parameter of the Earth, as shown by the equation

$$po_E = \frac{C_E}{GM_E} \tag{7.6}$$

With the orbital energy constant and the Kepler area constant known, the eccentricity of the transfer orbit is calculated according to the expression

$$e_E = \sqrt{1 + OEC_E \left(\frac{C_E}{GM_E} \right)^2} \tag{7.7}$$

and the semimajor axis of the transfer orbit is described by the equation

$$sa_E = \frac{-GM_E}{OEC_E} \tag{7.8}$$

In addition to the departure conditions, another variable must be specified, the angle λ_l, which is the angle between the Earth-Moon line and the point of entry into the lunar sphere of influence, with the Moon at the vertex of the angle. By varying the value of the angle λ_l the altitude of closest lunar approach can be controlled. Figure 7.2 shows the diagram of the transfer trajectory at the point of entry into the lunar sphere of influence. The radial position of the spacecraft, with relation to the Earth, at the point of

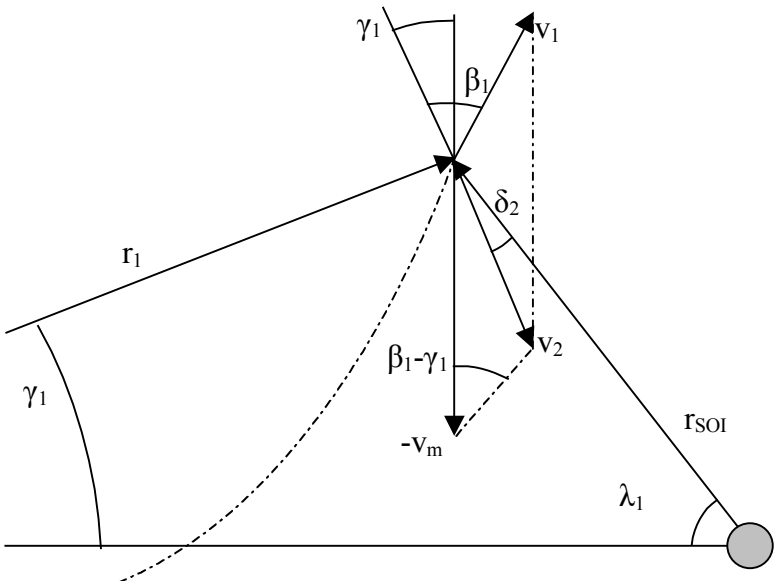


Figure 7.2: Entry Point into the Lunar Sphere of Influence

entry into the lunar sphere of influence is calculated by the law of cosines relation between the radius of the Moon's orbit, the radius of the lunar sphere of influence, and the angle between the point of entry and the Earth-Moon line, shown by the equation

$$r_1 = \sqrt{{r_{mo}}^2 + {r_{SOI}}^2 - 2\, r_{mo}\, r_{SOI} \cos(\lambda_1)} \tag{7. 9}$$

The spacecraft's velocity with respect to the Earth at the point of entry is calculated by the expression

$$v_1 = \sqrt{OEC_E + \frac{2\, GM_E}{r_1}} \tag{7. 10}$$

If the maneuver to match the inclination between the transfer orbit and the lunar orbital plane is made at the point of entry into the lunar sphere of influence, then the magnitude of that maneuver can found from the expression

$$\Delta v_1 = 2\, v_1 \sin\left(\frac{i_T - i_m}{2}\right) \tag{7. 11}$$

The flight path angle of the spacecraft with respect to the Earth is found by the relation

$$\beta_1 = \cos^{-1}\left(\frac{C_E}{r_1\, v_1}\right) \tag{7. 12}$$

The angle between the Earth-Moon line and the point of entry into the lunar sphere of influence with the Earth at the vertex, $\gamma 1$, is calculated from the expression

$$\gamma_1 = \sin^{-1}\left(\frac{r_{SOI}}{r_1} \sin \lambda_1\right) \tag{7. 13}$$

The spacecraft's velocity at the point of entry into the lunar sphere of influence, with respect to the Moon, is found by the law of cosines relation between the Moon's

orbital velocity, the spacecraft's Earth-centric velocity and the difference between the Earth-centric flight path angle and the entry point phase angle, shown by

$$v_2 = \sqrt{v_1^{\,2} + v_m^{\,2} - 2\, v_1\, v_m \cos(\beta_1 - \gamma_1)} \tag{7. 14}$$

With the lunar-centric velocity at the entry point known, the orbital characteristics of the spacecraft trajectory within the lunar sphere of influence can be calculated. The orbital energy constant of the lunar-centric trajectory is found by the equation

$$OEC_m = v_2^{\,2} - \frac{2\,GM_m}{r_{SOI}} \tag{7. 15}$$

while the Kepler area constant of the lunar-centric trajectory is found by the product of the velocity and radius at the entry point, and the sine of the lunar-centric flight path angle, shown by the expression

$$C_m = r_{SOI}\, v_2 \sin(\delta_2) \tag{7. 16}$$

where the lunar-centric flight path angle is calculated by the trigonometric relation

$$\delta_2 = \sin^{-1}\left[\frac{v_m}{v_2}\cos(\lambda_1) - \frac{v_1}{v_2}\cos(\lambda_1 - \gamma_1 - \beta_1)\right] \tag{7. 17}$$

The orbital parameter and eccentricity of the spacecraft's lunar-centric trajectory are found by equations similar to that of the Earth-centric trajectory, shown as

$$po_m = \frac{C_m}{GM_m} \tag{7. 18}$$

$$e_m = \sqrt{1 + OEC_m\left(\frac{C_m}{GM_m}\right)^2} \tag{7. 19}$$

The radius and velocity of the spacecraft at the point of closest approach to the Moon are found by the equations

$$r_{peri} = \frac{po_m}{1 + e_m} \tag{7. 20}$$

$$v_{peri} = \sqrt{OEC_m + \frac{2\,GM_m}{r_{peri}}} \tag{7. 21}$$

with careful attention being paid to make sure that the perilune radius is greater than 1,738 kilometers, the surface radius of the Moon. For this study, a final lunar orbit altitude of 100 kilometers has been used. The Δv required to circularize the spacecraft's orbit around the Moon is calculated by the difference between its velocity at perilune and the circular orbit velocity corresponding to the perilune radius, shown by

$$\Delta v_{peri} = v_{peri} - \sqrt{\frac{GM_m}{r_{peri}}} \tag{7. 22}$$

With the trajectory characteristics calculated, the transfer time from release at the elevator's upper tip and entry into the lunar sphere of influence is found according to Kepler's law. The first step is to calculate the true anomaly of the spacecraft at the departure point and at the point of entry into the lunar sphere of influence by the expressions

$$\theta_0 = \cos^{-1}\left(\frac{po_E - r_{ue}}{e_E\, r_{ue}}\right) \tag{7. 23}$$

$$\theta_1 = \cos^{-1}\left(\frac{po_E - r_l}{e_E\, r_l}\right) \tag{7. 24}$$

The values for the eccentric anomaly at the departure and entry points are found by the relations

$$EA_0 = \cos^{-1}\left[\frac{e_E + \cos(\theta_0)}{1 + e_E \cos(\theta_0)}\right] \tag{7. 25}$$

$$EA_1 = \cos^{-1}\left[\frac{e_E + \cos(\theta_1)}{1 + e_E \cos(\theta_1)}\right] \tag{7. 26}$$

with the total travel time between the two points found by the equation

$$\Delta t = \sqrt{\frac{a_E^{\ 3}}{GM_E}}\{[EA_1 - e_E \sin(EA_1)] - [EA_0 - e_E \sin(EA_0)]\} \tag{7. 27}$$

Because the upper tip of the elevator is traveling with a high percentage of escape velocity, the addition of enough Δv to the spacecraft will propel it on an escape trajectory with respect to the Earth. This requires the use of a slightly different form of Kepler's law, formulated specifically for hyperbolic trajectories. The hyperbolic eccentric anomalies for the departure and entry points are calculated by the expressions

$$HEA_0 = 2\tanh^{-1}\left[\tan\left(\frac{\theta_0}{2}\right)\sqrt{\frac{e_E - 1}{e_E + 1}}\right] \tag{7. 28}$$

$$HEA_1 = 2\tanh^{-1}\left[\tan\left(\frac{\theta_1}{2}\right)\sqrt{\frac{e_E - 1}{e_E + 1}}\right] \tag{7. 29}$$

and the travel time between departure and entry into the lunar sphere of influence is found according to the equation

$$\Delta t = \sqrt{\frac{a_E^{\ 3}}{GM_E}}\{[e_E \sinh(HEA_1) - HEA_1] - [e_E \sinh(HEA_0) - HEA_0]\} \tag{7. 30}$$

Travel times between the point of entry into the lunar sphere of influence and the perilune point are found by a similar application of Kelper's law.

7.3 Trajectories to L1 Point

Located between the Earth and the Moon at a radial distance of 57,900 kilometers from the Moon, the L1 point is one of five Lagrangian points of equilibrium in the Earth-Moon System. The L1 point is attractive as a staging area for a trans-lunar transportation system, because the entire lunar surface is accessible from L1 without timing constraints. Additionally, the Δv requirements to de-orbit and land from L1 are independent of the landing site's location on the Moon, and are equal to approximately 2.5 kilometers per second. Rendezvous with the L1 point can be achieved by the use of an elliptical orbit that passes through Lagrange point's 362,500 kilometer radial distance, as measured from the Earth. The L1 moves in the Earth-Moon system with the same angular velocity of the Moon. For the assumption used in this study that the Moon is in a constant circular orbit the velocity of the L1 can be calculated to have a value of 868.061 meters per second with respect to the Earth, by the equation

$$v_{L1} = \omega_M r_{L1} \tag{7. 31}$$

where ω_M is the angular velocity of the Moon's assumed circular orbit around the Earth, with a value of 2.658×10^{-6} radians per second. The Δv required to rendezvous with the L1 point can be found by the expression

$$\Delta v_{L1} = \sqrt{v_r^{\,2} + (v_\theta - v_{L1})^2} + 2\, v_{L1} \sin\left(\frac{i_T - i_m}{2}\right) \tag{7. 32}$$

in which the first term calculates the Δv required to match the radial and tangential components of the spacecraft with that of the L1 point, and the second term matches the orbital inclination between the two.

7.4 Trajectories to Lunar Elevator

The third lunar transport strategy analyzed in this study involves a lunar elevator, that stretches from the Moon's surface towards the Earth. The lunar elevator extends past the L1 point, which acts as its center of balance, before it is ended with an appropriately sized counterweight. The advantages of a combined system of Earth and Moon based tethers was identified in Artsutanov's early writings on the space elevator [33]. Due to the Moon's weaker gravity, a full elevator stretching from the ground to beyond the L1 point is possible with current material. The benefit of the lunar elevator is that there is no expenditure of propellant for landing on the surface of the Moon, as the descent is made along the elevator. At lunar altitudes lower than the L1 point, no actual power has to be supplied to move the payload along the lunar elevator. Lunar gravitation will pull the payload down and the only input needed would be braking to control the speed of its descent. The drawback is that the only "landing site" accessible is the lower tip of the elevator. For this study, a lunar elevator length of 100,000 kilometers is assumed. The tip of the elevator is at a radial distance of 284,400 kilometers from the Earth. Rendezvous calculations with the lunar elevator are made using the same method as that used with the L1 point, but with the radius of the lunar elevator's upper tip replacing the L1 radius.

7.5 Trajectory Results

7.5.1 Lunar Orbit Results

The three tethers selected in Chapter 4 possess upper tip velocities that are each approximately 95% of the velocity required for a minimum energy transfer Hohmann velocity to the altitude of the Moon's orbit. Table 7.2 shows the upper tip velocity and

Table 7.2: Selected Tether Trajectory Data for Lunar Orbit Destination

Handoff Altitude (km)	200	300	400
Upper Tip Altitude (km)	3758	3768	3700
Upper Tip Velocity (km/s)	8.344	8.352	8.296
Moon Bound Hohmann Velocity (km/s)	8.754	8.750	8.780
Minimum Departure Δv (km/s)	0.410	0.398	0.484
Flight time (hrs)	79.130	79.128	79.138
Lunar Orbit Circularization Δv (km/s)	0.780	0.780	0.780

the required minimum Δv needed for a Hohmann transfer to a Lunar orbit of 100 kilometers.

The values in Table 7.2 assume that the inclination change between the departure orbit and the Moon's orbit around the Earth is not made at the point of departure. This is more economical, as inclination changes are proportional to the spacecraft's current velocity, according to the equation

$$\Delta v_i = 2\, v \sin\left(\frac{\Delta i}{2}\right) \tag{7. 33}$$

By postponing the inclination maneuver to a point higher out on the transfer orbit, where the spacecraft's velocity is lower, significant savings can be made in the Δv required for departure. For each of the three tethers, an inclination change made at the point of departure would cost approximately 1.755 kilometers per second. By performing the inclination change at the point of entry into the lunar sphere of influence, the inclination change maneuver is only 0.097 kilometers per second.

By applying modest amounts of Δv to increase the departure velocity, the trip time to lunar orbit can be lowered significantly. Figure 7.3 shows the decrease in flight time to lunar orbit for increasing values of departure Δv for the three selected tethers.

A tradeoff must be made in increasing the departure velocity with the goal of diminishing flight time. The higher release velocities at the elevator's upper tip lead to the spacecraft possessing a higher velocity at the entry into the lunar sphere of influence than that experienced in the minimum energy orbit. Because inclination changes are proportional to a spacecraft's current velocity, the faster transfer orbits lead to a higher required inclination change maneuver. The quicker transfer orbit also causes the

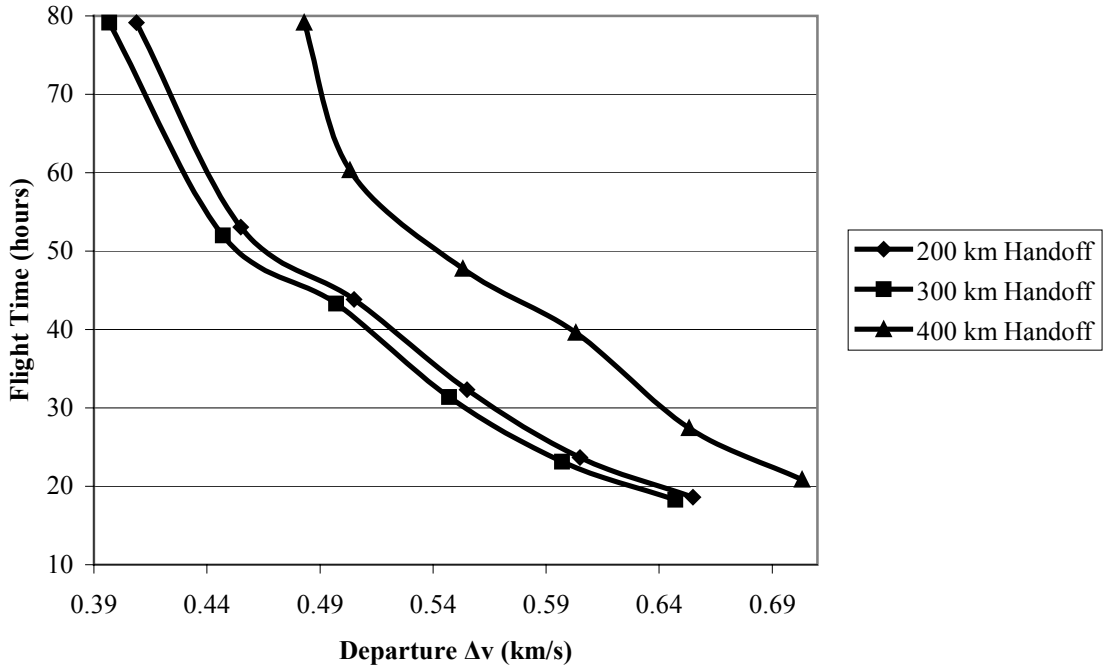


Figure 7.3: Flight Time versus Departure Δv for Lunar Orbit Trajectories

spacecraft to posses a higher velocity at the point of perilune, necessitating a larger orbit circularization maneuver. Figures 7.4 and 7.5 show the values of the inclination change and orbit circularization maneuvers plotted against differing values of departure Δv.

7.5.2 L1 Results

Table 7.3 shows the upper tip velocity and the required minimum Δv needed for departure on a Hohmann transfer to a rendezvous at the L1 point. The departure velocity requirements for reaching the L1 point are an average of 20 meters per second less than that needed for lunar orbit. The flight time is somewhat larger for L1 trajectories than for lunar orbit trajectories. The reason for this is that the final phase of lunar orbit trajectories are falling rapidly towards the Moon on a hyperbolic trajectory, while an L1 bound trajectory just skims the surface of the lunar sphere of influence.

As in the case of trajectories bound for lunar orbit, increasing the departure velocity produces quicker flight times to the L1 point. These quicker transit times must be balanced against the Δv required to rendezvous with the L1 point. Higher departure velocities cause the tether launched spacecraft to arrive at the L1 point with significant radial velocity, which must be cancelled to enter the L1 point's circular motion around the Earth. Figures 7.6 and 7.7 show the values of flight time and rendezvous Δv for increasing values of departure Δv.

7.5.3 Lunar Elevator Results

Table 7.4 shows the upper tip velocity and the required minimum Δv needed for departure on a Hohmann transfer to a rendezvous with a lunar elevator of 100,000 kilometers in length. The departure velocity requirements to reach a lunar elevator are 20 meters per second less than that for an L1 trajectory for each of the three selected tethers.

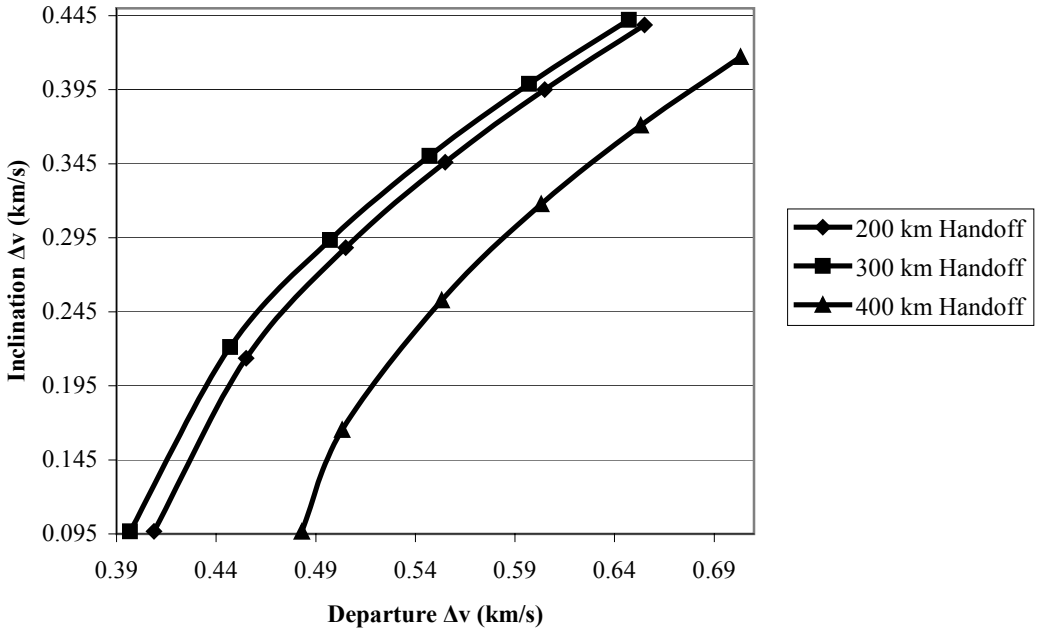


Figure 7.4: Inclination Change Δv versus Departure Δv for Lunar Orbit Trajectories

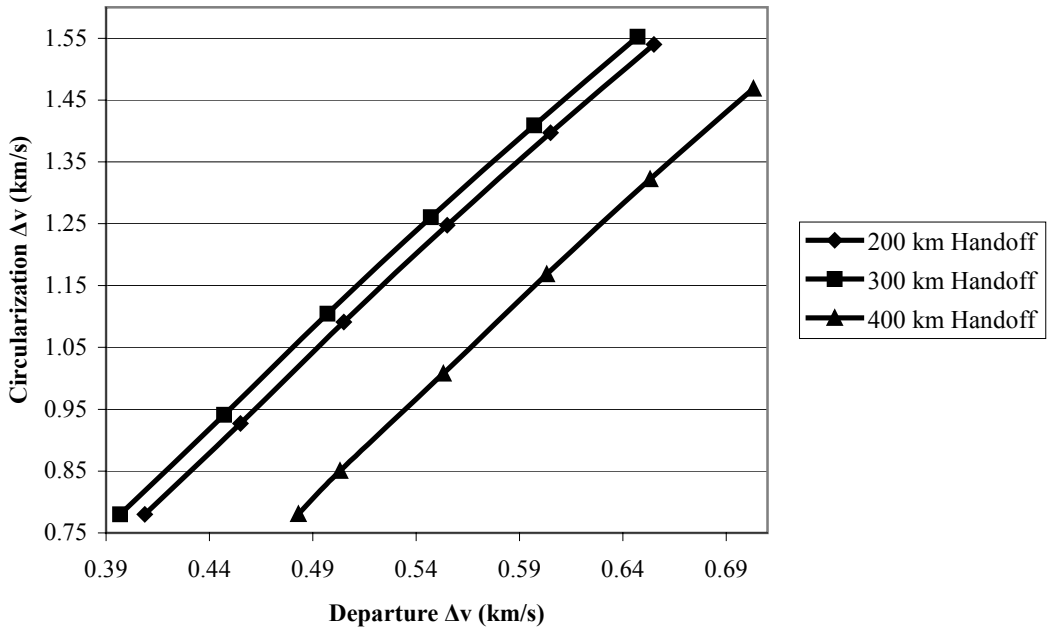


Figure 7.5: Lunar Orbit Circularization Δv versus Departure Δv

Table 7.3: Selected Tether Trajectory Data for L1 Destination

Handoff Altitude (km)	200	300	400
Upper Tip Altitude (km)	3758	3768	3700
Upper Tip Velocity (km/s)	8.344	8.352	8.296
L1 Bound Hohmann Velocity (km/s)	8.734	8.730	8.760
Minimum Departure Δv (km/s)	0.390	0.378	0.464
Flight Time (hours)	95.449	95.453	95.424
L1 Rendezvous Δv (km/s)	0.771	0.771	0.772

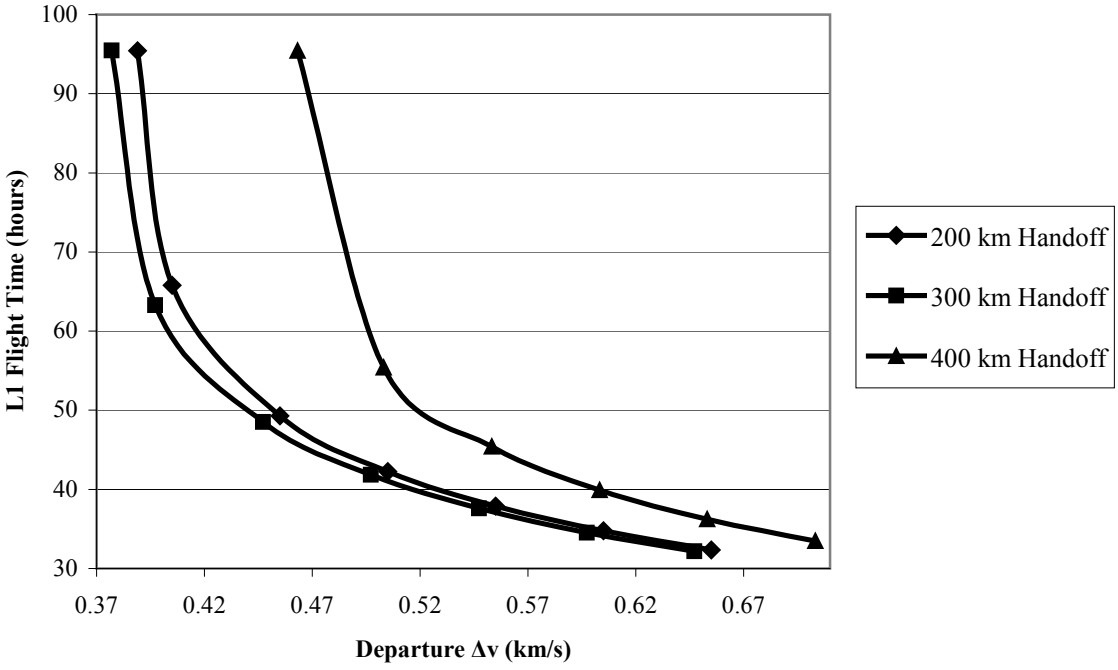


Figure 7.6: Flight Time versus Departure Δv for L1 Trajectories

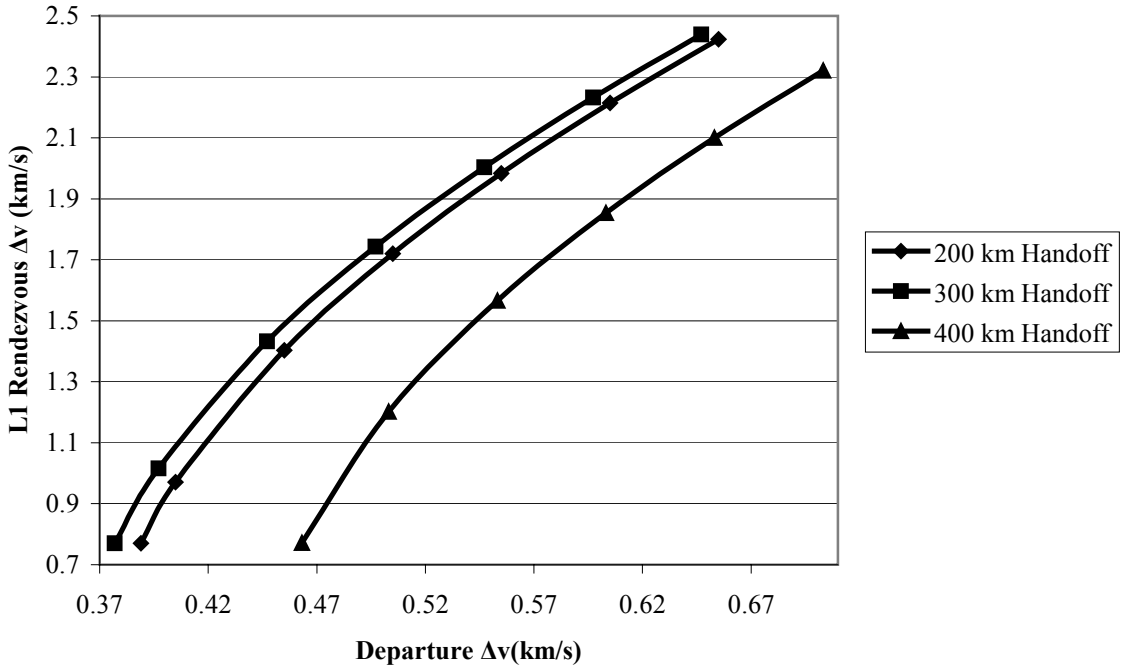


Figure 7.7: L1 Rendezvous Δv versus Departure Δv

Table 7.4: Selected Tether Trajectory Data for Lunar Elevator Destination

Handoff Altitude (km)	200	300	400
Upper Tip Altitude (km)	3758	3768	3700
Upper Tip Velocity (km/s)	8.344	8.352	8.296
Lunar Elevator Bound Hohmann Velocity (km/s)	8.715	8.710	8.740
Minimum Departure Δv Required (km/s)	0.371	0.358	0.444
Flight Time (hours)	78.116	78.119	78.092
Lunar Elevator Δv (km/s)	0.597	0.597	0.598

The flight time to the Lunar elevator is an average of 17.333 hours shorter than that to the L1 point, and an average of 1.023 hours shorter than a trajectory bound for lunar orbit.

Figure 7.8 shows the decrease in flight time afforded by adding departure Δv. As in the case of trajectories bound for the L1 point, increasing the departure Δv causes the rendezvous requirements at the Lunar Elevator to go up. The magnitudes of the rendezvous maneuver with the lunar elevator are very close in value to those of L1 rendezvous, and are shown in Figure 7.9.

7.5.4 Comparison of Trajectory Results

Table 7.5 gives the total minimum Δv required to reach the lunar surface for the three different transfer scenarios for each of the three selected tether lengths. Table 7.6 gives the corresponding total flight time from release at the lunar elevator until the payload reaches the lunar surface. Descent from lunar orbit is assumed to happen in just under one hour, while descent from the L1 point is assumed to take 72 hours and requires 2.5 kilometers per second of Δv. Descent along the lunar elevator includes a large block of time spent traveling down from its upper tip, which is assumed to be accomplished at an average speed of 44.704 meters per second and takes 621.371 hours.

As can be seen in Table 7.5, the Δv required for transfer from the Earth orbiting tether to the lunar surface is much lower for each of the elevator assisted scenarios than the 6.03 kilometers per second of Δv called for in the Apollo style mission. The flight time for direct elevator launched trajectories to lunar orbit is comparable to that of the Apollo missions, which involve a three day period between departure from the Earth until arrival at the Moon. The L1 trajectories offer a less attractive option compared to lunar orbit trajectories in terms of flight time and Δv; the flight times are over double that

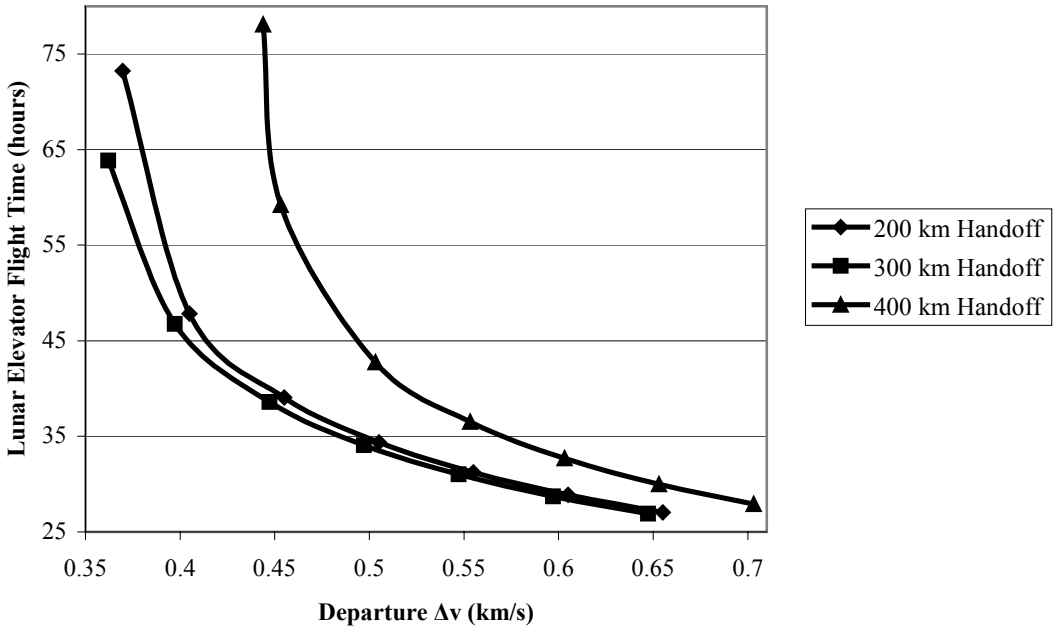


Figure 7.8: Flight Time versus Departure Δv for Lunar Elevator Trajectories

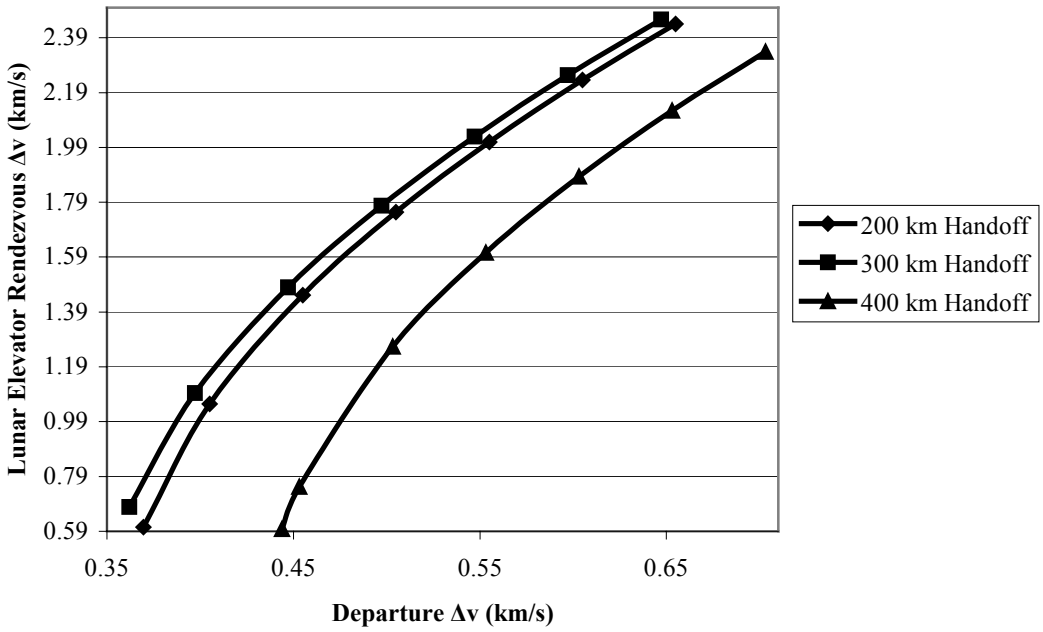


Figure 7.9: Lunar Elevator Rendezvous Δv versus Departure Δv

Table 7.5: Minimum Total Δv to the Lunar Surface for Selected Tethers

Handoff Altitude (km)	200	300	400
Lunar Orbit Δv (km/s)	3.230	3.218	3.304
L1 Point Δv (km/s)	3.661	3.649	3.736
Lunar Elevator Δv (km/s)	0.968	0.955	1.042

Table 7.6: Maximum Total Flight Time from Departure to the Lunar Surface for Selected Tethers

Handoff Altitude (km)	200	300	400
Lunar Orbit Flight Time (hours)	80.107	79.54	80.015
L1 Point Flight Time (hours)	167.449	167.453	167.424
Lunar Elevator Flight Time (hours)	699.487	699.49	699.463

required for an elevator launch to lunar orbit and come at a cost of slightly more total Δv. The lunar elevator trajectories involve the longest flight times, most of which are spent in descending along the lunar elevator, but these come with dramatically reduced Δv, an average of only 16% the Δv required by the Apollo mission. Each of the three transfer scenarios illustrates the value of the tether as a method to launch payloads beyond Earth orbit.

Chapter 8

Summary and Recommendations for Further Study

In this study, an effort was made to predict the sizing requirements of an orbiting space elevator, and its orbital stability with the handling of a payload. Additionally, the performance required for a launch vehicle to transfer a payload from Earth to a rendezvous with the tether has been quantified. Finally, the savings afforded by an Earth orbiting space elevator in the context of a lunar transportation system have been investigated. These problems were solved by modeling several different phases of operation of the space elevator, starting with its structural requirements. In Chapter 3, an expression was derived for the required elevator cross-sectional area to support an attached payload as a function of its radial position. Further efforts to predict the orbital motion of the elevator after payload attachment were outlined. Two estimation methods were developed to predict the required elevator mass to avoid having the structure re-enter the Earth's atmosphere after the payload had been attached. Values were found for tethers of varying lengths, which were compared against previous work done in the field. The first of these techniques was a simple routine of predicting a loaded elevator's orbital change based on the shift in the elevator-payload system's center of gravity. A more detailed scheme was developed which predicted the loaded elevator-payload orbital motion based on the principle of conservation of angular velocity. The estimation process involving conservation principles was found to produce elevator masses of the same order of magnitude as developed in previous work involving the orbiting space elevator. The method involving center of gravity shift produced required elevator masses

that were much larger than the momentum conservation scheme and any of the previously developed methods employed in other studies.

Because of the divergent results of the loaded tether's orbital response afforded by estimation methods, efforts were made to develop a dynamic simulation of the elevator's motion in orbit, as described in Chapter 4. A detailed model of the tether was created by breaking it into discrete segments and modeling the forces acting on each segment. The forces acting on the tether included the gravitational attraction of the Earth, tension in the tether with the addition of the payload, the aerodynamic drag caused by the Earth's atmosphere, minor accelerations caused by the Earth's oblateness, and electrodynamic interaction with the Earth's magnetic field. These perturbations were modeled because of their relative magnitude compared to the internal tension in the tether, and taken together, it was felt they would produce a relatively accurate description of the tether's motion.

It should be noted that the gravitational attraction of the Sun and Moon, the solar pressure on the tether, and the acceleration imparted by micrometeroid impacts were disregarded because of the relative small scale of these perturbations. Structural perturbations caused by the residual material stresses and internal fiber friction were also disregarded. There were two reasons for their exclusion: first, because of their relatively small magnitude, and second, because of their dependence on factors involving the construction of the tether, an issue which lay outside the scope of this study. A more detailed mathematical model of these perturbations should be included in future efforts made at studying the elevator's orbital motion.

In addition to the effect of micrometeroids on the tether's orbit, the threat they pose to the survivability of an Earth orbiting elevator was not accounted for in this study.

Natural and man made space debris is a serious hazard to any object in the low Earth orbit environment. Although this study accounts for a multiple line tether in the dynamic model, further investigation is needed in determining the interaction between the tether and small scale space debris. This problem has to be accounted for before any further judgement on the feasibility of an orbiting space elevator is made.

With the dynamic model developed in Chapter 4, values of tether mass were calculated with the goal of avoiding orbital decay with the addition of payload. Three tethers were identified for further investigation, with lower tip altitudes of 200, 300, and 400 kilometers. The mathematical model developed in Chapter 4 produces tether masses that varied significantly from those predicted by the estimation methods in Chapter 3; this places the value of their accuracy in further question. The masses required by the dynamic simulation were quite large, and varied between the 582 tonnes to over 5700 tonnes, depending upon the lower tip altitude. The relatively large mass of the elevator, and the requirement to construct it in orbit, could be seen as a strike against the economic feasibility of the concept. The elevator would have to handle payloads on a regular basis in order to defray the large investment costs in construction and transportation of the material to Earth orbit. For each of the three tethers, it was found that an approximately sized power system could influence the tether's orbit through electrodynamic interaction with the Earth's magnetic field.

The dynamic model developed in Chapter 4 could be further refined by accounting for the motion of payloads being raised along the length of the tether. Payload motion up the tether would produce a Coriolis acceleration that would slow the tether's orbital speed, causing it to drop in altitude. Because the deceleration would be

proportional to the speed that the payload is raised, it could be controlled by limiting the velocity at which payloads are moved along the tether. In view of these factors, the interaction between payload handling motion and tether orbital decay merits further study.

The launch vehicle performance required to deliver a payload to the tether was explored in Chapter 5. A dynamic model of the launch vehicle's suborbital trajectory was developed and optimized through the use of the Pontryagin maximum principle. In Chapter 6, rendezvous between the launch vehicle and the elevator's lower tip was investigated. The relative motion between the launch vehicle and the elevator's lower tip was described. The required performance of the launch vehicle to rendezvous with the elevator under less than ideal conditions was quantified. The amount of maneuvering required to allow a reasonable time to transfer the payload from the launch vehicle to the lower tip was also found. The requirements of rendezvous timing and hovering were calculated to be well within the operational capability of a vehicle originally designed for a single stage to orbit mission.

In Chapter 7, several different lunar transportation scenarios were examined using the Earth orbiting elevator and compared against the Apollo launch system. The three schemes examined were a direct transfer from the elevator's upper tip to lunar orbit, an elevator-launched transfer to the L1 staging point, and a trajectory from the Earth orbiting elevator to a corresponding lunar elevator. Each scenario involved a series of maneuvers: the first made at the upper tip of the Earth orbiting elevator to place it on an appropriate departure trajectory, a second made to match the departure orbital plane with the lunar orbital plane, and the third maneuver made to stabilize the trajectory upon arrival in the

vicinity of the Moon. For each of the scenarios it is found that tether assisted trajectories offer significant savings in Δv compared to an Apollo style mission to the Moon, but as some cost to the total flight time spent in transit.

When the data obtained in Chapter 7 is combined with that found in the investigations of the launch and rendezvous, contained in Chapters 5 and 6, a total account of the savings afforded by the tether can be formed. Table 8.1 gives a total Δv budget for an elevator launched mission to the Moon, via lunar orbit, compared to the Apollo 16 reference mission. The elevator assisted maneuvers included in Table 8.1 are for a tether with a handoff altitude of 400 kilometers. This particular tether was chosen because of its relatively low total mass of 582 tonnes led to its construction being judged the most feasible of the three. The Δv for rendezvous in Table 8.1 is for an ideal case of coplanar launch and tether trajectories, with an assumed hovering time of one minute needed to transfer the payload. From Table 8.1 the savings offered by the tether can be seen clearly in both the launch and trans-lunar injection phases of the mission.

Table 8.2 gives a total flight time for an elevator launched trajectory to lunar orbit compared to the Apollo reference mission. For this case, it can be seen that the Apollo style mission will place a payload on the Moon over twice as fast as a tether launched payload, but at a total cost of 1.58 times as much Δv.

Table 8.1: Δv Budget for a Tether Assisted Mission to Lunar Orbit Compared to the Apollo Reference Mission

Maneuver	Elevator	Apollo
Launch (km/s)	7.518	11.600
Elevator Rendezvous (km/s)	0.245	0
TLI (km/s)	0.484	3.050
LOI (km/s)	0.877	0.940
Descent (km/s)	2.040	2.040
Total (km/s)	11.164	17.630

Table 8.2: Flight Time for a Tether Assisted Mission to Lunar Orbit Compared to the Apollo Reference Mission

Maneuver	Elevator	Apollo
Launch (hours)	0.105	0.192
Elevator Ascent (hours)	91.667	0
Trans Lunar Coast (hours)	79.138	72.000
Descent (hours)	0.877	0.877
Total (km/s)	171.787	73.069

List of References

List of References

1. Tsiolkovsky, Konstantin E., 1995. Exploration of the Universe with Reaction Machines : Exploring the Unknown. The NASA History Series. NASA SP 4407, Washington, D.C.

2. http://www.informatics.org/museum/tsiol.html

3. http://www.saudi-us-relations.org/energy/saudi-energy-reserves.html

4. U.S. Geological Survey World Petroleum Assessment 2000, http://energy.cr.usgs.gov/WEcont/chaps/AR.pdf

5. http://www.fe.doe.gov/aboutus/history/ syntheticfuels_history.html

6. Meadows, D.H., Meadows, D.L., Randers, J., and Behrens, W.W., The Limits to Growth, University Books, New York, 1972.

7. O'Neill, Gerard K., *The High Frontier: Human Colonies in Space*. William Morrow & Company, 1977.

8. Mankins, J.C., "A Fresh Look at Space Solar Power: New Architectures, Concepts and Technologies", IAF-97-R.2.03, 38th International Astronautical Federation Conference, Turin, Italy, 1997.

9. Heppenheimer, T.A., Colonies in Space, Stackpole Books, Harrisburg, PA, 1977.

10. http://www.spacedaily.com/news/ssp-03b.html

11. Lewis, J.S., Mining the Sky, Persus Publishing, Reading, MA, 1997.

12. Ishii, R.K., "Stationary & Transportation Fuel Cell Applications", First International Conference on Energy Efficiency, Hong Kong, January 15-17, 2003.

13. http://www.platinum.matthey.com/ media_room/1084885203.html.

14. Dietz, R.S., "Sudbury Structure as an Astrobleme", Journal of Geology, v. 72, 1964, pp. 412–434.

15. Wingo, D., Moonrush: Improving Life on Earth with the Moon's Resources, Apogee Books, Burlington, Ontario, Canada, 2004.

16. Romm, J.J., The Hype about Hydrogen: Fact and Fiction in the Race to Save the Climate, Island Press, Washington D.C., 2004.

17. Sviatoslavsky, I.N., "The Challenge of Mining He-3 on the Lunar Surface: How All the Parts Fit Together", WCSAR-TR-AR3-9311-2, Wisconsin Center for Space Automation and Robotics, Madison lunar, WI, November, 1993.

18. Kulcinski, G.L., Ashley, R.P., Santarius, J.F., Piefer, G., and Subramanian, K.M., "The Development of Lunar ^{3}He Resources: Near-Term Applications and Long-Term Prospects", UWFDM-1128, 4th International Conference on Exploration and Utilisation of the Moon, Noordwijk, The Netherlands, July 10-15, 2000.

19. Edwards, B., and Westling, E.A., *The Space Elevator*, Spageo, San Francisco, CA, 2002.

20. Wertz, J. R., and Larson, W. J., *Space Mission Analysis and Design, Third Edition*, El Segundo, CA, 1999.

21. www.astronautix.com

22. Schmitt, H.H., Return to the Moon, Copernicus Books, New York, NY, 2006.

23. http://www.airfleets.net/home/index.php.

24. Smith, M., Space Shuttle: US Winged Spacecraft, X-15 to Orbiter, Haynes Publishing Group, Somerset England, 1986.

25. Heppenheimer, T.A., The Space Shuttle Decision: NASA's Search for a Reusable Space Vehicle, NASA SP-4221, 1999.

26. Curtis, A.R., ed., *Space Almanac*, *Second Edition*, Gulf Publishing, Houston, 1992.

27. Zubrin, R., Entering Space: Creating a Spacefaring Civilization, Tarcher/Putnam Publishing, New York, NY, 1999.

28. Smitherman, D.V. Jr., ed., "Space Elevators: An Advanced Earth-Space Infrastructure for the New Millenium", Advanced Space Infrastructure Workshop on Geostationary Orbiting Tether "Space Elevator" Concepts, NASA CP-2000-210429, Huntsville, Alabama, August, 2000.

29. Raitt, D., and Edwards, B., "The Space Elevator: Economics and Applications", IAC-040IAA.3.8.3, 55th International Astronautical Congress, Vancouver, Canada, October 4-8, 2004.

30. Belk, C.A., Robinson, J.H., Alexander, M.B., Cooke, W.J., and Pavelitz, S.D., "Meteoroids and Orbital Debris: Effects on Spacecraft", NASA Reference Publication 1408, August 1997.

31. Tsiolkovsky, K.E., "Speculations about Earth and Sky and on Vesta", Academy of Sciences, U.S.S.R., Moscow, 1959.

32. Artsutanov, Y., "Into Space Without Rockets: A New Idea for Space Launch", AFSC Foreign Technology Division Report, ADA084597, Air Force Systems Command, Wright Patterson AFB, 1969.

33. Artsutanov, Y., "Into the Cosmos by Electric Locomotive", *Konsomolaya Pravda*, July 31, 1960.

34. Isaacs, J.D., Vine, A.C., Bradner, H. and Bachus, G.E., "Satellite Elongation into a True "Sky-Hook", *Science*, Volume 151, February , 1966, pp. 682-683.

35. Pearson, J., "The Orbital Tower: A Spacecraft Launcher Using the Earth's Rotational Energy," *Acta Astronautica*, Vol. 2, 1975, pp. 785-799.

36. Clarke, A.C., The Fountains of Paradise, Harcourt Brace Jovanovich, New York, 1978.

37. Clarke, A.C., "The Space Elevator: Thought Experiment or Key to the Universe?", *Advanced Earth Oriented Applications of Space Technology*, Vol. 1, no. 1, 1981, pp. 39-48.

38. Edwards, B., "The Space Elevator: NIAC Phase I Final Report", NASA Institute of Advanced Concepts, October 31, 2000.

39. http://www.liftport.com/

40. Moravec, H., "A Non-Synchronous Orbital Skyhook," *Journal of the Astronautical Sciences.*, Vol. 25, 1977, pp.307-322.

41. Bogar, T.J., Bangham, M.E., Forward, R.L., and Lewis, J.L., "Hypersonic Airplane Space Tether Orbital Launch System: Interim Study Results,"AIAA Paper 99-4802, 1999.

42. Grant, J., Martin, J., Nowlan, D., Tillotson, B., and Hoyt, R., "The HASTOL Tether System Applied to Commerical Launch", AIAA-2001-3966, 37th AIAA/ASME/ SAE/ASEE Joint Propulsion Conference, Salt Lake City, Utah, 8-11 July 2001.

43. Grant, J. et. al., **"**Hypersonic Airplane Space Tether Orbital Launch (HASTOL) Architecture Study: Phase II Final Report", NASA Institute of Advanced Concepts Subcontract No. 07600-040, October 31, 2000.

44. Hoyt, R.P., Slostad, J.T., and Frank, S.S., "A Modular Momentum-Exchange/Electrodynamic-Reboost Tether System Architecture", AIAA-2003-5214, 39th AIAA/ASME/SAE/ASEE Joint Propulsion Conference, Huntsville, Alabama, 20-23 July 2003.

45. Sorensen, K., "Momentum eXchange Electrodynamic Reboost (MXER) Tether Technology Assessment Group Final Report", NASA In-Space Propulsion Technologies Program, Huntsville, Alabama, July 24, 2003.

46. Hacker, B.C., and Alexander A.C., *On the Shoulders of Titans: A History of Project Gemini*, NASA SP 4203, National Aeronautic and Space Administration, Washington D.C., 1977.

47. Cosmo, M.L., and Lorenzini, E.C., Tethers in Space Handbook, 3rd edition, Marshall Space Flight Center, Huntville Alabama, 1997.

48. Collar, A. R. and J. W. Flower, "A (Relatively) Low Altitude 24-hour Satellite", *Journal of the British Interplanetary Society,* Volume 22, 1969, pp. 442-469.

49. http://www.affordablespaceflight.com

50. Sarmont, E., "How an Earth Orbiting Tether Makes Possible an Affordable Earth-Moon Transportation System," SAE Paper 942120 Aerotech '94, Los Angeles, California, October 3-6, 1994.

51. Zubrin, R., "The Hypersonic Skyhook", *Jounal of the British Interplanetary Society*, Vol. 48, No. 3, March, 1995, pp.123-128.

52. Mottinger, T.A., and Marshall, L.S., "The Bridge to Space Launch System," CP552, Space Technology and Applications International Forum, American Institute of Physics, New York, 2001, pp. 514-518.

53. Personal communication with Dr. Robert Boyd of Lockheed Martin.

54. Li, Y., Kunlin, W., Wei, J., Gu, Z. Wang, Z.,Luo, J.and Wu, D., "Tensile Properties of Long Aligned Double-walled Carbon Nanotube Strands", *Carbon, the Journal of the American Carbon Society*, Vol. 43, September, 2004, pp. 31-35.

55. Edwards, B., "The Space Elevator: NIAC Phase II Final Report", NASA Institute of Advanced Concepts, March 1, 2003.

56. Colombo, G., "Study of Certain Launching Techniques Using Long Orbiting Tethers", NASA CR-164060, March, 1981.

57. Marshall, L.S., Ladner, D.R., and McCandless II, B., "The Bridge to Space: Elevator Sizing & Performance Analysis," CP608, Space Technology and Applications International Forum, American Institute of Physics, New York, 2002, pp. 286-290.

58. Ehricke, K. A., Spaceflight, Volume I: Environment and Celestial Mechanics, D. Van Nostrand Company, Inc., Princeton, NJ, 1962.

59. Rajan, M. and Anderson, T.J., "First Integrals of Motion in the Dynamics of Tethered Satellites", *Journal of the Astronautical Sciences*, Vol. 34, No. 3, July-September 1986, pp. 331-339.

60. Modi, V.J. and Misra, A.K., "Orbital Perturbations of Tethered Satellite Systems", *Journal of the Astronautical Sciences*, Vol. 25, No. 3, July-September 1977, pp. 271-278.

61. Beletsky, V.V. and Levin, E.M., Dynamics of Space Tether Systems, Advances in the Astronautical Sciences, Volume 83, American Astronautical Society, San Diego, CA, 1993.

62. Steindl, A. and Troger, H., "Is the Sky-Hook Configuration Stable?", *Nonlinear Dynamics*, Vol. 40, No. 4, June 2005, pp. 419-431.

63. Cosmo, M.L., and Lorenzini, E.C., Tethers in Space Handbook, 3rd edition, Marshall Space Flight Center, Huntsville Alabama, 1997.

64. Chabotov, V. A. (editor), Orbital Mechanics: Second Edition, AIAA Inc., New York, NY, 1996.

65. Furhop, K.R., Gilchrist, B.E., Bilen, S.G., and Voronka, N.R., "System Analysis of the Expected Electrodynamic Tether Performance for the ProSEDS Mission", AIAA-2003-5096, 39th AIAA/ASME/SAE/ASEE Joint Propulsion Conference, Huntsville, Alabama, 20-23 July 2003.

66. Olsen, R.C., Introduction to the Space Environment, Naval Postgraduate School, 2003.

67. http://www.spaceflight.nasa.gov/station/isstodate.html

68. Ehricke, K. A., Spaceflight, Volume II: Dynamics, D. Van Nostrand Company, Inc., Princeton, NJ, 1962.

69. Jezewski, D. J., "An Optimal, Analytic Solution to the Linear Gravity, Constant-Thrust Trajectory Problem", *AIAA Journal of Spacecraft and Rockets*, Vol. 8, No. 1, July, 1971, pp. 793-796.

70. McIntyre, J. E., "Guidance, Flight Mechanics, and Trajectory Optimization", NASA CR-1012, March, 1968.

71. Schindler, G. M., "Minimum Flight Time Paths", *Journal of the American Rocket Society*, Vol. 30, No. 4, April, 1960, pp. 352-355.

72. Sinha, S., "A Study to Evaluate STS Heads-Up Performance Employing a Minimum-Hamiltonian Optimization Strategy", NASA TP-2793, February, 1988.

73. Lewallen, J. M., Scwausch, O. A., and Tapley, B.D., "Coordinate System Influence on the Regularized Trajectory Optimization Problem", *AIAA Journal of Spacecraft and Rockets*, Vol. 8, No. 1, January, 1971, pp. 15-20.

74. Hocking, L. M., Optimal Control: An Introduction to the Theory with Applications, Oxford University Press, New York, NY, 1991.

75. Marec, J. P., Optimal Space Trajectories, Elsevier Scientific Publishing Company, Amsterdam, The Netherlands, 1979.

76. Houbolt, J. C., "Problems and Potentialities of Space Rendezvous", A*stronautica Acta*, Vol. 7, 1961, pp. 406-429.

77. Wiesel, W. E., Spaceflight Dynamics, McGraw-Hill Inc., New York, NY, 1989.

78. Eckart, P, et al, *The Lunar Base Handbook*, 1st edition, McGraw-Hill Primis Custom Publishing, New York, 1999.

Appendices

Appendix A: Dynamic Tether Simulation Code

```
{-------------------------------------------------------------------------------------------------}
program Propagation;
{Goal: Calculates the orbital propagation of the tether
Assumptions:  Payload attached at lower end
                                Tether initially in circular orbit
                                Tether made of Zylon HM
                                Forces calculated on each segment:
                                        Tension, Gravity, Electrodynamic, Earth
                                        Oblateness,Atmosphereic Drag
{-------------------------------------------------------------------------------------------------}
USES SIOUX;
Type    vec = array[1..650] of extended;
                mat = array[1..600,1..600] of extended;
Var     x,z,w,dw,       {Segment specific values}
        R               {Tether radial position}: vec;
OutputFile  : TEXT;
        GM,                     {Gravitational parameter of the Earth}
        Pi,                     {Pi are round}
        rEarth,                 {Radius of the Earth}
        magang,                 {Angle between magnetic and geographic north pole}
        MuNought,               {Permeability of free space}
        M,                      {Magnitude of Earth's magnetic dipole moment}
        Tex,                    {Temperature of the exosphere}
        Tincl,                  {angle of tether orbital inclination}
        CGalt,                  {Intitial CG altitude of tether}
        TethLength,             {Total length of tether}
        aLowPt,                 {Altitude of tether lower pt}
        aHighPt,                {Altitude of tether higher pt}
        Vcg,                    {design cg initial velocity}
        angvelCG,               {design angular velocity of the tether CG}
        massPLdes,              {design mass of attached payload}
        massPLact,              {actual mass of attached payload}
        massStation,            {mass of the tether central station}
        NoLines,                {Number of Tether lines}
        YoungMod,               {Tether spring constant}
        rho,                    {Tether material density}
        sigma,                  {Tether material Tensile Strength}
        FacSaf,                 {Tether Structural Factor of Safety}
        Power,                  {Tether Power station output}
        diaCon,                 {diameter of conducting wire}
        Resistivity,            {Resisitvity of conducting wire}
        Cd,                     {Tether Coefficient of Drag}
```

```
        NoLines,            {Number of multiple lines in tether}
        Ao,                 {X sec area of tether lower end}
        AreaConst,          {Constant used in determining X-sec area of each segment}
        natleng0,           {natural length of tether lower end}
        correction,         {Tangential speed correction factor}
        NoSegments,         {Number of tether segments}
        SegLength,          {Length of each segment}
        StationSeg,         {Segment which contains the power station}
        Mx,                 {Magnetic dipole moment x component in tether orbital
                            plane coord system}
        My,                 {Magnetic dipole moment y component in tether orbital
                            plane coord system}
        Mz,                 {Magnetic dipole moment z component in tether orbital
                            plane coord system}
        t,                  {time in runge kutta}
        Time                {time in solution time step}
        :extended;
{-------------------------------------------------------------------------------------------}
function arctan2(r,s : extended) : extended;
var q: extended;
begin
        if s= 0.0 then
                if r>0 then q:=3.14159265358979323846264 3/2
                else q:=-3.14159265358979323846264 3/2
        else
        q:= arctan(r/s);
        if s<0.0 then
                if r<0.0 then q:=q-3.14159265358979323846264 3
                else q:= q+3.14159265358979323846264 3;
        if r=0.0 then q:= 0.0;
        arctan2:= q;
end;
{-------------------------------------------------------------------------------------------}
function arcsin(r : extended) : extended;
        var q: extended;
        begin
                if r= 0.0 then q:=0.0
                else
                        if r = 1.0 then q:=3.14159265358979323846264 3/2
                        else
                        if r =-1.0 then q:=-3.14159265358979323846264 3/2
                        else q:= arctan(r/sqrt (1-(r*r)));
                arcsin:= q;
        end;
{-------------------------------------------------------------------------------------------}
```

```
function xsecArea(r : extended) : extended;
        var q: extended;
        begin
                q:=AreaConst*exp((-rho*FacSaf*1000.0*1000.0*((GM/r) +
                (0.5*r*r*angvelCG*angvelCG)))/sigma);
                xsecArea:= q;
        end;
{-------------------------------------------------------------------------------------------------}
function Dist(a,b,c,d : extended) : extended;
{This function calculates the distance between two segment points along the tether}
        var q: extended;
        begin
                q:=sqrt( (((a*cos(b))-(c*cos(d)))*((a*cos(b))-(c*cos(d)))) + (((a*sin(b))-
                (c*sin(d)))*((a*sin(b))-(c*sin(d)))));
                Dist:= q;
        end;
{-------------------------------------------------------------------------------------------------}
function XPTcen(a,b,c,d : extended) : extended;
{This function calculates the radial coord of pt c,d (r, theta) in a coord system centered on
a,b (r, theta)}
        var q: extended;
        begin
                q:=(cos(b)*((c*cos(d))-(a*cos(b)))) + (sin(b)*((c*sin(d))-(a*sin(b))));
                XPTcen:= q;
        end;
{-------------------------------------------------------------------------------------------------}
function YPTcen(a,b,c,d : extended) : extended;
{This function calculates the tangential coord of pt c,d in a coord system centered on a,b}
        var q: extended;
        begin
                q:=(cos(b)*((c*sin(d))-(a*sin(b)))) - (sin(b)*((c*cos(d))-(a*cos(b))));
                YPTcen:= q;
        end;
{-------------------------------------------------------------------------------------------------}
function natLength(a: extended): extended;
{This function calculates the natural length of an unloaded tether segment in meters for
an inputted radius in km}
        var q : extended;
        begin
                q:=YoungMod*1000.0*SegLength/(YoungMod+(sigma/FacSaf)-
                (massPLdes*1000.0*((GM/((rEarth+aLowPt)*(rEarth+aLowPt)))-
        (angvelCG*angvelCG*(rEarth+aLowPt)))/xsecArea(a+(SegLength/2.0))));
                natLength:= q;
        end;
```

```
{-------------------------------------------------------------------------------------------------}
function aTenRadUp(a,b,c,d,e : extended) : extended;
{This function calculates the acceleration due to tension between two segment points
along the tether in the radial direction of pt a,b
a,b are radial and tangential positions of the segment under acceleration, c,d are radial
and tangential positions of the upper segment, e is the segment number}
        var q: extended;
        begin
                if Dist(a,b,c,d) < natLength(e) then    q:=0.0
                else q:= (YoungMod*xsecArea(e+(SegLength/2.0))*(Dist(a,b,c,d)-
                (natLength(e)))/(rho*xsecArea(e)*SegLength*1000.0*natLength(e))) *
                 XPTcen(a,b,c,d)/Dist(a,b,c,d);
                aTenRadUp:= q;
        end;
{-------------------------------------------------------------------------------}
function aTenRadDown(a,b,c,d,e : extended) : extended;
{This function calculates the downward acceleration due to tension between two segment
points along the tether in the radial direction of pt a,b
a,b are radial and tangential positions of the segment under acceleration, c,d are radial
and tangential positions of the lower segment, e is the segment number}
        var q: extended;
        begin
                if Dist(a,b,c,d) < natLength(e) then    q:=0.0
                else q:= (YoungMod*xsecArea(e-(SegLength/2.0))*(Dist(a,b,c,d)-
                (natLength(e-SegLength)))/(rho*xsecArea(e)*SegLength*1000.0*
                natLength(e-SegLength)))* XPTcen(a,b,c,d)/Dist(a,b,c,d);
                aTenRadDown:= q;
        end;
{-------------------------------------------------------------------------------}
function aTenTangUp(a,b,c,d,e : extended) : extended;
{This function calculates the upward acceleration due to tension between two segment
points along the tether in the tangential direction of pt a,b
a,b are radial and tangential positions of the segment under acceleration, c,d are radial
and tangential positions of the upper segment, e is the segment number}
        var q: extended;
        begin
                if Dist(a,b,c,d) < natLength(e) then    q:=0.0
                else q:= (YoungMod*xsecArea(e+(SegLength/2.0))*(Dist(a,b,c,d)-
                (natLength(e)))/(rho*xsecArea(e)*SegLength*1000.0*natLength(e)))
                * YPTcen(a,b,c,d)/Dist(a,b,c,d);
                aTenTangUp:= q;
        end;
{-------------------------------------------------------------------------------}
function aTenTangDown(a,b,c,d,e : extended) : extended;
{This function calculates the downward acceleration due to tension between two segment
```

```
points along the tether in the tangential direction of pt a,b
a,b are radial and tangential positions of the segment under acceleration, c,d are
radial and tangential positions of the lower segment, e is the segment number}
        var q: extended;
        begin
                if Dist(a,b,c,d) < natLength(e) then    q:=0.0
                else q:= (YoungMod*xsecArea(e-(SegLength/2.0))*(Dist(a,b,c,d)-
                (natLength(e-SegLength)))/(rho*xsecArea(e)*SegLength*1000.0*
                natLength(e-SegLength)))* YPTcen(a,b,c,d)/Dist(a,b,c,d);
                aTenTangDown:= q;
        end;
{-------------------------------------------------------------------------------}
function payloadTension(a,b,c,d : extended) : extended;
        var q: extended;
        begin
                if Dist(a,b,c,d) < ((SegLength*1000.0/2.0)) then q:=0.0
                else q:= (YoungMod*Ao*(Dist(a,b,c,d)-
                (1000.0*SegLength/2.0))/(1000.0*SegLength/2.0));
                payloadTension:=q;
        end;
{-------------------------------------------------------------------------------}
function Density(a : extended) : extended;
{This function calculates the atmospheric density for a given radial position}
        var q: extended;
        begin
                if a < ((rEarth+118.0)*1000.0) then q:=10000.0*11.0*exp(-(a-
                6378000.0)/6000.0);
                if a > ((rEarth+118.0)*1000.0) then q:=10000.0*(exp(-3.0*ln(((a-
                6378000.0)/1000.0)-95.0))) / 2600.0;
                if a > ((rEarth+200.0)*1000.0) then q:=10000.0*1.47e-16*Tex*(3000.0-
                Tex)/(exp(10.0*ln( 1.0 + ((2.9*(((a-6378000.0)/1000.0)-200))/Tex))));
                if a > ((rEarth+1200.0)*1000.0) then q:= 0.0;
                Density:=q;
        end;
{-------------------------------------------------------------------------------}
function aDragTang(a,b,c,d : extended) : extended;
{This function calculates the tangential acceleration due to aerodynamic drag
a is radial position, b is radial velocity, c is tangential velocity d is segment number}
        var q: extended;
        begin
        q:=0.5*Density(a)*Cd*c*sqrt(4.0*NoLines*((b*b)+(c*c))/(Pi*xsecArea(d)))/
        (10000.0*rho);
                aDragTang:=q;
        end;
{-------------------------------------------------------------------------------}
```

```
function aOblRad(a,b: extended) : extended;
{This function calculates the radial acceleration due to earth oblateness
        a is radial position,
        b is tangential position}
        var q: extended;
        begin
                q:=(-1.5*GM*1000.0*1000.0*1000.0*0.00108263*1000.0*rEarth*1000.0
                *rEarth/(a*a*a*a))*(1.0-(1.5*sin(Tincl)*sin(Tincl)*(1.0-cos(2.0*b))));
                aOblRad:=q;
        end;
{-------------------------------------------------------------------------------}
function aOblTang(a,b: extended) : extended;
{This function calculates the tangential acceleration due to earth oblateness
a is radial position, b is tangential position}
        var q: extended;
        begin
                q:=(-1.5*GM*1000.0*1000.0*1000.0*0.00108263*1000.0*rEarth*1000.0
                *rEarth/(a*a*a*a))*(sin(Tincl)*sin(Tincl)*sin(2.0*b));
                aOblTang:=q;
        end;
        {-------------------------------------------------------------------------------}
function aEdtTang(a,b: extended) : extended;
{This function calculates the tangential acceleration due to electrodynamic tether effects
a is radial position, b is the segment number}
        var q: extended;
        begin
                if b = StationSeg then
                        q:=(sqrt(Power/(Resistivity*1000.0*(0.2*SegLength))))*Pi*
                        diaCon*MuNought*M*cos(Tincl)/(rho*xsecArea(b)*8.0*a*a*a)
                else q:=(sqrt(Power/(Resistivity*1000.0*(abs(b-StationSeg)))))*Pi*
                diaCon*MuNought*M*cos(Tincl)/(rho*xsecArea(b)*8.0*a*a*a);
                aEdtTang:=q;
        end;
{-------------------------------------------------------------------------------}
function aTotRad(a,b,c,d,e,f,g: extended) : extended;
{This function calculates the sum of Radial accelerations due to tension up and tension
down, and electrodynamic tether effects
a is radial position of the segment, b is tangential position of the segment, c is radial
position of the next lower segment, d is tangential position of the next lower segment, e is
radial position of the next upper segment, f is tangential position of the next upper
segment, g is the segment number     }
        var q: extended;
        begin
                if g = StationSeg then q:=((aTenRadUp(a,b,e,f,g) +
                aTenRadDown(a,b,c,d,g))*rho*SegLength*1000.0*xsecArea(g)/
```

```
            (massStation+(rho*SegLength*1000.0*xsecArea(g))))+aOblRad(a,b)
            else q:=aTenRadUp(a,b,e,f,g) + aTenRadDown(a,b,c,d,g) + aOblRad(a,b);
            aTotRad:=q;
        end;
{--------------------------------------------------------------------------------}
function aTotTang(a,b,c,d,e,f,g,h,i: extended) : extended;
{This function calculates the sum of Radial accelerations due to tension up and tension
down, and electrodynamic tether effects
a is radial position of the segment, b is tangential position of the segment, c is radial
position of the next lower segment, d is tangential position of the next lower segment, e is
radial position of the next upper segment, f is tangential position of the next upper
segment, g is the segment number, h is the radial velocity,i is the tangential velocity}
        var q: extended;
        begin
            if g= StationSeg then q:=((aTenTangUp(a,b,e,f,g)+
            aTenTangDown(a,b,c,d,g) + aEdtTang(a,g) -
            aDragTang(a,h,i,g))*rho*SegLength*1000.0*xsecArea(g)/(massStation+(r
            ho*SegLength*1000.0*xsecArea(g))))+ aOblTang(a,b)
            else q:=aTenTangUp(a,b,e,f,g) + aTenTangDown(a,b,c,d,g) +
            aEdtTang(a,g) - aDragTang(a,h,i,g) + aOblTang(a,b);
            aTotTang:=q;
        end;
{--------------------------------------------------------------------------------}
Procedure Parameters;
        begin
        SIOUXSettings.tabspaces := 0;
        Pi := 3.14159265358979323846 2643;
        GM := 398601.0;                     {Gravitational Parameter (Earth), km3/s2}
        rEarth := 6378.0;                   {Radius of Earth, km}
        magang := 11.3*Pi/180.0;            {radians}
        M:= 8.1E22;                         {Amp m^2}
        MuNought:=0.00000125663706144; {Hentry/meter}
        Tex:=1100.0;                        {K}
        {Tether Characteristics}
        Tincl:=35.0*Pi/180.0;               {radians}
        CGalt:=2100.0;                      {km}
        TethLength:=  3838.0;               {km}
        aLowPt:=200.0;                      {km}
        aHighPt:=aLowPt+TethLength;         {km}
        Vcg:=sqrt(GM/(CGalt+rEarth));       {km/s}
        angvelCG:=Vcg/(CGalt+rEarth);       {radians/s}
        massPLdes:=   10000.0;              {kg}
        massPLact:=   10000.0;              {kg}
        massStation:= 50000.0;              {kg}
```

```
        NoLines:=     4.0;                  {number of tether lines}
        {Material Properties}
        YoungMod:=  180.0E9;                {Pa, N/M^2}
        rho:=         1560.0;               {kg/m^3}
        sigma:=       5.80E9;               {Pa, N/m^2}
        FacSaf:=      3.5;                  {Factor of Safety}
        Cd:=          2.2;                  {Coefficient of drag}
        {Electrodynamic power generation properties}
        Power:=       75000.0;              {Watts}
        diaCon:=      0.001;                {meters}
        Resistivity:= 0.0000000159;         {Ohm meters, resistivity of Silver}

        Ao:=   massPLdes*FacSaf*1000.0*((GM/((rEarth+aLowPt)*(rEarth+aLowPt)))-
        (angvelCG*angvelCG*(rEarth+aLowPt)))/sigma;
        AreaConst:=   Ao/exp(-rho*FacSaf*1000.0*1000.0*((GM/(rEarth+aLowPt)) +
        (0.5*(rEarth+aLowPt)*(rEarth+aLowPt)*angvelCG*angvelCG))/sigma);
        natleng0:= Ao*YoungMod*(1000.0*SegLength/2.0)/((massPLdes*1000.0*
        ((GM/((rEarth+aLowPt)*(rEarth+aLowPt)))-(
        angvelCG*angvelCG*(rEarth+aLowPt))))
        +(Ao*YoungMod));
        correction:=  1.000;                {tangential speed correction factor}
        end;
{-------------------------------------------------------------------------------}
Procedure Segment;              {Segment definitions}
        begin
        NoSegments:= 100.0; {Number of tether segments}
        SegLength:=TethLength/NoSegments;
        R[1]:=rEarth+aLowPt+(SegLength/2.0);      {km}
        R[2]:=rEarth+aLowPt+(3.0*SegLength/2.0);{km}
        R[3]:=rEarth+aLowPt+(5.0*SegLength/2.0);{km}
        R[4]:=rEarth+aLowPt+(7.0*SegLength/2.0);{km}
        R[5]:=rEarth+aLowPt+(9.0*SegLength/2.0);{km}
        R[6]:=rEarth+aLowPt+(11.0*SegLength/2.0);{km}
        R[7]:=rEarth+aLowPt+(13.0*SegLength/2.0);{km}
        R[8]:=rEarth+aLowPt+(15.0*SegLength/2.0);{km}
        R[9]:=rEarth+aLowPt+(17.0*SegLength/2.0);{km}
        R[10]:=rEarth+aLowPt+(19.0*SegLength/2.0);{km}
        R[11]:=rEarth+aLowPt+(21.0*SegLength/2.0); {km}
        R[12]:=rEarth+aLowPt+(23.0*SegLength/2.0);{km}
        R[13]:=rEarth+aLowPt+(25.0*SegLength/2.0);{km}
        R[14]:=rEarth+aLowPt+(27.0*SegLength/2.0);{km}
        R[15]:=rEarth+aLowPt+(29.0*SegLength/2.0);{km}
        R[16]:=rEarth+aLowPt+(31.0*SegLength/2.0);{km}
        R[17]:=rEarth+aLowPt+(33.0*SegLength/2.0);{km}
        R[18]:=rEarth+aLowPt+(35.0*SegLength/2.0);{km}
```

```
R[19]:=rEarth+aLowPt+(37.0*SegLength/2.0);{km}
R[20]:=rEarth+aLowPt+(39.0*SegLength/2.0);{km}
R[21]:=rEarth+aLowPt+(41.0*SegLength/2.0);{km}
R[22]:=rEarth+aLowPt+(43.0*SegLength/2.0);{km}
R[23]:=rEarth+aLowPt+(45.0*SegLength/2.0);{km}
R[24]:=rEarth+aLowPt+(47.0*SegLength/2.0);{km}
R[25]:=rEarth+aLowPt+(49.0*SegLength/2.0);{km}
R[26]:=rEarth+aLowPt+(51.0*SegLength/2.0);{km}
R[27]:=rEarth+aLowPt+(53.0*SegLength/2.0);{km}
R[28]:=rEarth+aLowPt+(55.0*SegLength/2.0);{km}
R[29]:=rEarth+aLowPt+(57.0*SegLength/2.0);{km}
R[30]:=rEarth+aLowPt+(59.0*SegLength/2.0);{km}
R[31]:=rEarth+aLowPt+(61.0*SegLength/2.0);{km}
R[32]:=rEarth+aLowPt+(63.0*SegLength/2.0);{km}
R[33]:=rEarth+aLowPt+(65.0*SegLength/2.0);{km}
R[34]:=rEarth+aLowPt+(67.0*SegLength/2.0);{km}
R[35]:=rEarth+aLowPt+(69.0*SegLength/2.0);{km}
R[36]:=rEarth+aLowPt+(71.0*SegLength/2.0);{km}
R[37]:=rEarth+aLowPt+(73.0*SegLength/2.0);{km}
R[38]:=rEarth+aLowPt+(75.0*SegLength/2.0);{km}
R[39]:=rEarth+aLowPt+(77.0*SegLength/2.0);{km}
R[40]:=rEarth+aLowPt+(79.0*SegLength/2.0);{km}
R[41]:=rEarth+aLowPt+(81.0*SegLength/2.0);{km}
R[42]:=rEarth+aLowPt+(83.0*SegLength/2.0);{km}
R[43]:=rEarth+aLowPt+(85.0*SegLength/2.0);{km}
R[44]:=rEarth+aLowPt+(87.0*SegLength/2.0);{km}
R[45]:=rEarth+aLowPt+(89.0*SegLength/2.0);{km}
R[46]:=rEarth+aLowPt+(91.0*SegLength/2.0);{km}
R[47]:=rEarth+aLowPt+(93.0*SegLength/2.0);{km}
R[48]:=rEarth+aLowPt+(95.0*SegLength/2.0);{km}
R[49]:=rEarth+aLowPt+(97.0*SegLength/2.0);{km}
R[50]:=rEarth+aLowPt+(99.0*SegLength/2.0);{km}
R[51]:=rEarth+aLowPt+(101.0*SegLength/2.0);{km}
R[52]:=rEarth+aLowPt+(103.0*SegLength/2.0);{km}
R[53]:=rEarth+aLowPt+(105.0*SegLength/2.0);{km}
R[54]:=rEarth+aLowPt+(107.0*SegLength/2.0);{km}
R[55]:=rEarth+aLowPt+(109.0*SegLength/2.0);{km}
R[56]:=rEarth+aLowPt+(111.0*SegLength/2.0);{km}
R[57]:=rEarth+aLowPt+(113.0*SegLength/2.0);{km}
R[58]:=rEarth+aLowPt+(115.0*SegLength/2.0);{km}
R[59]:=rEarth+aLowPt+(117.0*SegLength/2.0);{km}
R[60]:=rEarth+aLowPt+(119.0*SegLength/2.0);{km}
R[61]:=rEarth+aLowPt+(121.0*SegLength/2.0);{km}
R[62]:=rEarth+aLowPt+(123.0*SegLength/2.0);{km}
R[63]:=rEarth+aLowPt+(125.0*SegLength/2.0);{km}
```

```
        R[64]:=rEarth+aLowPt+(127.0*SegLength/2.0);{km}
        R[65]:=rEarth+aLowPt+(129.0*SegLength/2.0);{km}
        R[66]:=rEarth+aLowPt+(131.0*SegLength/2.0);{km}
        R[67]:=rEarth+aLowPt+(133.0*SegLength/2.0);{km}
        R[68]:=rEarth+aLowPt+(135.0*SegLength/2.0);{km}
        R[69]:=rEarth+aLowPt+(137.0*SegLength/2.0);{km}
        R[70]:=rEarth+aLowPt+(139.0*SegLength/2.0);{km}
        R[71]:=rEarth+aLowPt+(141.0*SegLength/2.0);{km}
        R[72]:=rEarth+aLowPt+(143.0*SegLength/2.0);{km}
        R[73]:=rEarth+aLowPt+(145.0*SegLength/2.0);{km}
        R[74]:=rEarth+aLowPt+(147.0*SegLength/2.0);{km}
        R[75]:=rEarth+aLowPt+(149.0*SegLength/2.0);{km}
        R[76]:=rEarth+aLowPt+(151.0*SegLength/2.0);{km}
        R[77]:=rEarth+aLowPt+(153.0*SegLength/2.0);{km}
        R[78]:=rEarth+aLowPt+(155.0*SegLength/2.0);{km}
        R[79]:=rEarth+aLowPt+(157.0*SegLength/2.0);{km}
        R[80]:=rEarth+aLowPt+(159.0*SegLength/2.0);{km}
        R[81]:=rEarth+aLowPt+(161.0*SegLength/2.0);{km}
        R[82]:=rEarth+aLowPt+(163.0*SegLength/2.0);{km}
        R[83]:=rEarth+aLowPt+(165.0*SegLength/2.0);{km}
        R[84]:=rEarth+aLowPt+(167.0*SegLength/2.0);{km}
        R[85]:=rEarth+aLowPt+(169.0*SegLength/2.0);{km}
        R[86]:=rEarth+aLowPt+(171.0*SegLength/2.0);{km}
        R[87]:=rEarth+aLowPt+(173.0*SegLength/2.0);{km}
        R[88]:=rEarth+aLowPt+(175.0*SegLength/2.0);{km}
        R[89]:=rEarth+aLowPt+(177.0*SegLength/2.0);{km}
        R[90]:=rEarth+aLowPt+(179.0*SegLength/2.0);{km}
        R[91]:=rEarth+aLowPt+(181.0*SegLength/2.0);{km}
        R[92]:=rEarth+aLowPt+(183.0*SegLength/2.0);{km}
        R[93]:=rEarth+aLowPt+(185.0*SegLength/2.0);{km}
        R[94]:=rEarth+aLowPt+(187.0*SegLength/2.0);{km}
        R[95]:=rEarth+aLowPt+(189.0*SegLength/2.0);{km}
        R[96]:=rEarth+aLowPt+(191.0*SegLength/2.0);{km}
        R[97]:=rEarth+aLowPt+(193.0*SegLength/2.0);{km}
        R[98]:=rEarth+aLowPt+(195.0*SegLength/2.0);{km}
        R[99]:=rEarth+aLowPt+(197.0*SegLength/2.0);{km}
        R[100]:=rEarth+aLowPt+(199.0*SegLength/2.0);{km}
        StationSeg:=R[50];
        end;
{-------------------------------------------------------------------------------}
procedure Runge( procedure de(t:extended; var y,dy:vec); n :integer; h :extended;
                                        var t :extended; var y :vec );
        var     y1,f1,f2,f3,f4 :vec;
                i : integer;
                h2 : extended;
```

```
        begin
                h2:= h/2;
                de( t,y,f1 );
                for i:=1 to n do y1[i]:= y[i] + h2*f1[i];
                t:=t + h2;
                de( t,y1,f2 );
                for i:=1 to n do y1[i]:= y[i] + h2*f2[i];
                de( t,y1,f3 );
                for i:=1 to n do y1[i]:= y[i] + h *f3[i];
                t:=t + h2;
                de( t,y1,f4 );
                for i:=1 to n do y[i]:= y[i] + h/6*(f1[i]+2*(f2[i]+f3[i])+f4[i]);
        end;
{-------------------------------------------------------------------------}
Procedure Equations( y:extended; var w,dw :vec );
begin
{Payload Equations}
dw[1] := w[3];                  dw[2] := w[4]/w[1];
dw[3] := (w[4]*w[4]/w[1]) - (GM*1000.0*1000.0*1000.0/(w[1]*w[1])) +
        aOblRad(w[1],w[2]) + (payloadTension(w[1],w[2],w[5],w[6])*
        (XPTcen(w[1],w[2],w[5],w[6]))/(massPLact*Dist(w[1],w[2],w[5],w[6])));
dw[4] := aOblTang(w[1],w[2]) + (payloadTension(w[1],w[2],w[5],w[6])*
        (YPTcen(w[1],w[2],w[5],w[6]))/(massPLact*Dist(w[1],w[2],w[5],w[6]))) –
        (w[3]*w[4]/w[1]);
{Segment 1 Equations}
dw[5] := w[7];                  dw[6] := w[8]/w[5];
dw[7] := (w[8]*w[8]/w[5]) - (GM*1000.0*1000.0*1000.0/(w[5]*w[5])) +
        aOblRad(w[5],w[6]) + (aTenRadUp(w[5],w[6],w[9],w[10],R[1])) +
        (payloadTension(w[5],w[6],w[1],w[2])*(XPTcen(w[5],w[6],w[1],w[2]))/(rho*
        xsecArea(R[1])*SegLength*1000.0*Dist(w[5],w[6],w[1],w[2])));
dw[8] := aOblTang(w[5],w[6]) + (aTenTangUp(w[5],w[6],w[9],w[10],R[1])) –
        (w[7]*w[8]/w[5]) + aEdtTang(w[5],R[1]) +payloadTension(w[5],w[6],w[1],w[2])
        *(YPTcen(w[5],w[6],w[1],w[2]))/(rho*xsecArea(R[1])*SegLength*1000.0*Dist(
        w[5],w[6],w[1],w[2]))) - aDragTang(w[5],w[7],w[8],R[1]) ;
{Segment 2 Equations}
dw[9] := w[11];                 dw[10] := w[12]/w[9];
dw[11] := (w[12]*w[12]/w[9]) - (GM*1000.0*1000.0*1000.0/(w[9]*w[9])) +
        aTotRad(w[9],w[10],w[5],w[6],w[13],w[14],R[2]);
dw[12] := aTotTang(w[9],w[10],w[5],w[6],w[13],w[14],R[2],w[11],w[12]) –
        (w[11]*w[12]/w[9]);
{Segment 3 Equations}
dw[13] := w[15];                dw[14] := w[16]/w[13];
dw[15] := (w[16]*w[16]/w[13]) - (GM*1000.0*1000.0*1000.0/(w[13]*w[13])) +
        aTotRad(w[13],w[14],w[9],w[10],w[17],w[18],R[3]);
dw[16] := aTotTang(w[13],w[14],w[9],w[10],w[17],w[18],R[3],w[15],w[16]) –
```

```
        (w[15]*w[16]/w[13]);
{Segment 4 Equations}
dw[17] := w[19];                dw[18] := w[20]/w[17];
dw[19] := (w[20]*w[20]/w[17]) - (GM*1000.0*1000.0*1000.0/(w[17]*w[17])) +
        aTotRad(w[17],w[18],w[13],w[14],w[21],w[22],R[4]);
dw[20] := aTotTang(w[17],w[18],w[13],w[14],w[21],w[22],R[4],w[19],w[20]) –
        (w[19]*w[20]/w[17]);
{Segment 5 Equations}
dw[21] := w[23];                dw[22] := w[24]/w[21];
dw[23] := (w[24]*w[24]/w[21]) - (GM*1000.0*1000.0*1000.0/(w[21]*w[21])) +
        aTotRad(w[21],w[22],w[17],w[18],w[25],w[26],R[5]);
dw[24] := aTotTang(w[21],w[22],w[17],w[18],w[25],w[26],R[5],w[23],w[24]) –
        (w[23]*w[24]/w[21]);
{Segment 6 Equations}
dw[25] := w[27];                dw[26] := w[28]/w[25];
dw[27] := (w[28]*w[28]/w[25]) - (GM*1000.0*1000.0*1000.0/(w[25]*w[25])) +
        aTotRad(w[25],w[26],w[21],w[22],w[29],w[30],R[6]);
dw[28] := aTotTang(w[25],w[26],w[21],w[22],w[29],w[30],R[6],w[27],w[28]) –
        (w[27]*w[28]/w[25]);
{Segment 7 Equations}
dw[29] := w[31];                dw[30] := w[32]/w[29];
dw[31] := (w[32]*w[32]/w[29]) - (GM*1000.0*1000.0*1000.0/(w[29]*w[29])) +
        aTotRad(w[29],w[30],w[25],w[26],w[33],w[34],R[7]);
dw[32] := aTotTang(w[29],w[30],w[25],w[26],w[33],w[34],R[7],w[31],w[32]) –
        (w[31]*w[32]/w[29]);
{Segment 8 Equations}
dw[33] := w[35];                dw[34] := w[36]/w[33];
dw[35] := (w[36]*w[36]/w[33]) - (GM*1000.0*1000.0*1000.0/(w[33]*w[33])) +
aTotRad(w[33],w[34],w[29],w[30],w[37],w[38],R[8]);
dw[36] := aTotTang(w[33],w[34],w[29],w[30],w[37],w[38],R[8],w[35],w[36]) -
(w[35]*w[36]/w[33]);
{Segment 9 Equations}
dw[37] := w[39];                dw[38] := w[40]/w[37];
dw[39] := (w[40]*w[40]/w[37]) - (GM*1000.0*1000.0*1000.0/(w[37]*w[37])) +
aTotRad(w[37],w[38],w[33],w[34],w[41],w[42],R[9]);
dw[40] := aTotTang(w[37],w[38],w[33],w[34],w[41],w[42],R[9],w[39],w[40]) –
        (w[39]*w[40]/w[37]);
{Segment 10 Equations}
dw[41] := w[43];                dw[42] := w[44]/w[41];
dw[43] := (w[44]*w[44]/w[41]) - (GM*1000.0*1000.0*1000.0/(w[41]*w[41])) +
        aTotRad(w[41],w[42],w[37],w[38],w[45],w[46],R[10]);
dw[44] := aTotTang(w[41],w[42],w[37],w[38],w[45],w[46],R[10],w[43],w[44]) –
        (w[43]*w[44]/w[41]);
{Segment 11 Equations}
```

```
dw[45] := w[47];                dw[46] := w[48]/w[45];
dw[47] := (w[48]*w[48]/w[45]) - (GM*1000.0*1000.0*1000.0/(w[45]*w[45])) +
        aTotRad(w[45],w[46],w[41],w[42],w[49],w[50],R[11]);
dw[48] := aTotTang(w[45],w[46],w[42],w[41],w[49],w[50],R[11],w[47],w[48]) –
        (w[47]*w[48]/w[45]);
{Segment 12 Equations}
dw[49] := w[51];                dw[50] := w[52]/w[49];
dw[51] := (w[52]*w[52]/w[49]) - (GM*1000.0*1000.0*1000.0/(w[49]*w[49])) +
        aTotRad(w[49],w[50],w[45],w[46],w[53],w[54],R[12]);
dw[52] := aTotTang(w[49],w[50],w[45],w[46],w[53],w[54],R[12],w[51],w[52]) –
        (w[51]*w[52]/w[49]);
{Segment 13 Equations}
dw[53] := w[55];                dw[54] := w[56]/w[53];
dw[55] := (w[56]*w[56]/w[53]) - (GM*1000.0*1000.0*1000.0/(w[53]*w[53])) +
        aTotRad(w[53],w[54],w[49],w[50],w[57],w[58],R[13]);
dw[56] := aTotTang(w[53],w[54],w[49],w[50],w[57],w[58],R[13],w[55],w[56]) –
        (w[55]*w[56]/w[53]);
{Segment 14 Equations}
dw[57] := w[59];                dw[58] := w[60]/w[57];
dw[59] := (w[60]*w[60]/w[57]) - (GM*1000.0*1000.0*1000.0/(w[57]*w[57])) +
        aTotRad(w[57],w[58],w[53],w[54],w[61],w[62],R[14]);
dw[60] := aTotTang(w[57],w[58],w[53],w[54],w[61],w[62],R[14],w[59],w[60]) –
        (w[59]*w[60]/w[57]);
{Segment 15 Equations}
dw[61] := w[63];                dw[62] := w[64]/w[61];
dw[63] := (w[64]*w[64]/w[61]) - (GM*1000.0*1000.0*1000.0/(w[61]*w[61])) +
        aTotRad(w[61],w[62],w[57],w[58],w[65],w[66],R[15]);
dw[64] := aTotTang(w[61],w[62],w[57],w[58],w[65],w[66],R[15],w[63],w[64]) –
        (w[63]*w[64]/w[61]);
{Segment 16 Equations}
dw[65] := w[67];                dw[66] := w[68]/w[65];
dw[67] := (w[68]*w[68]/w[65]) - (GM*1000.0*1000.0*1000.0/(w[65]*w[65])) +
        aTotRad(w[65],w[66],w[61],w[62],w[69],w[70],R[16]);
dw[68] := aTotTang(w[65],w[66],w[61],w[62],w[69],w[70],R[16],w[67],w[68]) –
        (w[67]*w[68]/w[65]);
{Segment 17 Equations}
dw[69] := w[71];                dw[70] := w[72]/w[69];
dw[71] := (w[72]*w[72]/w[69]) - (GM*1000.0*1000.0*1000.0/(w[69]*w[69])) +
        aTotRad(w[69],w[70],w[65],w[66],w[73],w[74],R[17]);
dw[72] := aTotTang(w[69],w[70],w[65],w[66],w[73],w[74],R[17],w[71],w[72]) –
        (w[71]*w[72]/w[69]);
{Segment 18 Equations}
dw[73] := w[75];                dw[74] := w[76]/w[73];
dw[75] := (w[76]*w[76]/w[73]) - (GM*1000.0*1000.0*1000.0/(w[73]*w[73])) +
        aTotRad(w[73],w[74],w[69],w[70],w[77],w[78],R[18]);
```

```
dw[76] := aTotTang(w[73],w[74],w[69],w[70],w[77],w[78],R[18],w[75],w[76]) –
        (w[75]*w[76]/w[73]);
{Segment 19 Equations}
dw[77] := w[79];                dw[78] := w[80]/w[77];
dw[79] := (w[80]*w[80]/w[77]) - (GM*1000.0*1000.0*1000.0/(w[77]*w[77])) +
        aTotRad(w[77],w[78],w[73],w[74],w[81],w[82],R[19]);
dw[80] := aTotTang(w[77],w[78],w[73],w[74],w[81],w[82],R[19],w[79],w[80]) –
        (w[79]*w[80]/w[77]);
{Segment 20 Equations}
dw[81] := w[83];                dw[82] := w[84]/w[81];
dw[83] := (w[84]*w[84]/w[81]) - (GM*1000.0*1000.0*1000.0/(w[81]*w[81])) +
        aTotRad(w[81],w[82],w[77],w[78],w[85],w[86],R[20]);
dw[84] := aTotTang(w[81],w[82],w[77],w[78],w[85],w[86],R[20],w[83],w[84]) –
        (w[83]*w[84]/w[81]);
{Segment 21 Equations}
dw[85] := w[87];                dw[86] := w[88]/w[85];
dw[87] := (w[88]*w[88]/w[85]) - (GM*1000.0*1000.0*1000.0/(w[85]*w[85])) +
        aTotRad(w[85],w[86],w[81],w[82],w[89],w[90],R[21]);
dw[88] := aTotTang(w[85],w[86],w[81],w[82],w[89],w[90],R[21],w[87],w[88]) –
        (w[87]*w[88]/w[85]);
{Segment 22 Equations}
dw[89] := w[91];                dw[90] := w[92]/w[89];
dw[91] := (w[92]*w[92]/w[89]) - (GM*1000.0*1000.0*1000.0/(w[89]*w[89])) +
        aTotRad(w[89],w[90],w[85],w[86],w[93],w[94],R[22]);
dw[92] := aTotTang(w[89],w[90],w[85],w[86],w[93],w[94],R[22],w[91],w[92]) –
        (w[91]*w[92]/w[89]);
{Segment 23 Equations}
dw[93] := w[95];                dw[94] := w[96]/w[93];
dw[95] := (w[96]*w[96]/w[93]) - (GM*1000.0*1000.0*1000.0/(w[93]*w[93])) +
        aTotRad(w[93],w[94],w[89],w[90],w[97],w[98],R[23]);
dw[96] := aTotTang(w[93],w[94],w[89],w[90],w[97],w[98],R[23],w[95],w[96]) –
        (w[95]*w[96]/w[93]);
{Segment 24 Equations}
dw[97] := w[99];                dw[98] := w[100]/w[97];
dw[99] := (w[100]*w[100]/w[97]) - (GM*1000.0*1000.0*1000.0/(w[97]*w[97])) +
        aTotRad(w[97],w[98],w[93],w[94],w[101],w[102],R[24]);
dw[100] := aTotTang(w[97],w[98],w[93],w[94],w[101],w[102],R[24],w[99],w[100]) –
        (w[99]*w[100]/w[97]);
{Segment 25 Equations}
dw[101] := w[103];              dw[102] := w[104]/w[101];
dw[103] := (w[104]*w[104]/w[101]) - (GM*1000.0*1000.0*1000.0/(w[101]*w[101])) +
        aTotRad(w[101],w[102],w[97],w[98],w[105],w[106],R[25]);
dw[104] := aTotTang(w[101],w[102],w[97],w[98],w[105],w[106],R[25],w[103],w[104])
        - (w[103]*w[104]/w[101]);
{Segment 26 Equations}
```

```
dw[105] := w[107];              dw[106] := w[108]/w[105];
dw[107] := (w[108]*w[108]/w[105]) - (GM*1000.0*1000.0*1000.0/(w[105]*w[105])) +
        aTotRad(w[105],w[106],w[101],w[102],w[109],w[110],R[26]);
dw[108] := aTotTang(w[105],w[106],w[101],w[102],w[109],w[110],R[26], w[107],
        w[108]) – (w[107]*w[108]/w[105]);
{Segment 27 Equations}
dw[109] := w[111];              dw[110] := w[112]/w[109];
dw[111] := (w[112]*w[112]/w[109]) - (GM*1000.0*1000.0*1000.0/(w[109]*w[109])) +
        aTotRad(w[109],w[110],w[105],w[106],w[113],w[114],R[27]);
dw[112] := aTotTang(w[109],w[110],w[105],w[106],w[113],w[114],R[27],w[111],
        w[112]) – (w[111]*w[112]/w[109]);
{Segment 28 Equations}
dw[113] := w[115];              dw[114] := w[116]/w[113];
dw[115] := (w[116]*w[116]/w[113]) - (GM*1000.0*1000.0*1000.0/(w[113]*w[113])) +
        aTotRad(w[113],w[114],w[109],w[110],w[117],w[118],R[28]);
dw[116] := aTotTang(w[113],w[114],w[109],w[110],w[117],w[118],R[28], w[115],
        w[116]) - (w[115]*w[116]/w[113]);
{Segment 29 Equations}
dw[117] := w[119];              dw[118] := w[120]/w[117];
dw[119] := (w[120]*w[120]/w[117]) - (GM*1000.0*1000.0*1000.0/(w[117]*w[117])) +
        aTotRad(w[117],w[118],w[113],w[114],w[121],w[122],R[29]);
dw[120] := aTotTang(w[117],w[118],w[113],w[114],w[121],w[122],R[29],
        w[119],w[120]) - (w[119]*w[120]/w[117]);
{Segment 30 Equations}
dw[121] := w[123];              dw[122] := w[124]/w[121];
dw[123] := (w[124]*w[124]/w[121]) - (GM*1000.0*1000.0*1000.0/(w[121]*w[121])) +
        aTotRad(w[121],w[122],w[117],w[118],w[125],w[126],R[30]);
dw[124] := aTotTang(w[121],w[122],w[117],w[118],w[125],w[126],R[30],
        w[123],w[124]) - (w[123]*w[124]/w[121]);
{Segment 31 Equations}
dw[125] := w[127];              dw[126] := w[128]/w[125];
dw[127] := (w[128]*w[128]/w[125]) - (GM*1000.0*1000.0*1000.0/(w[125]*w[125])) +
        aTotRad(w[125],w[126],w[121],w[122],w[129],w[130],R[31]);
dw[128] := aTotTang(w[125],w[126],w[121],w[122],w[129],w[130],R[31],
        w[127],w[128]) - (w[127]*w[128]/w[125]);
{Segment 32 Equations}
dw[129] := w[131];              dw[130] := w[132]/w[129];
dw[131] := (w[132]*w[132]/w[129]) - (GM*1000.0*1000.0*1000.0/(w[129]*w[129])) +
aTotRad(w[129],w[130],w[125],w[126],w[133],w[134],R[32]);
dw[132] := aTotTang(w[129],w[130],w[125],w[126],w[133],w[134],R[32],
        w[131],w[132]) - (w[131]*w[132]/w[129]);
{Segment 33 Equations}
dw[133] := w[135];              dw[134] := w[136]/w[133];
dw[135] := (w[136]*w[136]/w[133]) - (GM*1000.0*1000.0*1000.0/(w[133]*w[133])) +
```

```
aTotRad(w[133],w[134],w[129],w[130],w[137],w[138],R[33]);
dw[136] := aTotTang(w[133],w[134],w[129],w[130],w[137],w[138],R[33],
        w[135],w[136]) - (w[135]*w[136]/w[133]);
{Segment 34 Equations}
dw[137] := w[139];              dw[138] := w[140]/w[137];
dw[139] := (w[140]*w[140]/w[137]) - (GM*1000.0*1000.0*1000.0/(w[137]*w[137])) +
        aTotRad(w[137],w[138],w[133],w[134],w[141],w[142],R[34]);
dw[140] := aTotTang(w[137],w[138],w[133],w[134],w[141],w[142],R[34],
        w[139],w[140]) - (w[139]*w[140]/w[137]);
{Segment 35 Equations}
dw[141] := w[143];              dw[142] := w[144]/w[141];
dw[143] := (w[144]*w[144]/w[141]) - (GM*1000.0*1000.0*1000.0/(w[141]*w[141])) +
        aTotRad(w[141],w[142],w[137],w[138],w[145],w[146],R[35]);
dw[144] := aTotTang(w[141],w[142],w[137],w[138],w[145],w[146],R[35],
        w[143],w[144]) - (w[143]*w[144]/w[141]);
{Segment 36 Equations}
dw[145] := w[147];              dw[146] := w[148]/w[145];
dw[147] := (w[148]*w[148]/w[145]) - (GM*1000.0*1000.0*1000.0/(w[145]*w[145])) +
        aTotRad(w[145],w[146],w[141],w[142],w[149],w[150],R[36]);
dw[148] := aTotTang(w[145],w[146],w[141],w[142],w[149],w[150],R[36],
        w[147],w[148]) - (w[147]*w[148]/w[145]);
{Segment 37 Equations}
dw[149] := w[151];              dw[150] := w[152]/w[149];
dw[151] := (w[152]*w[152]/w[149]) - (GM*1000.0*1000.0*1000.0/(w[149]*w[149])) +
        aTotRad(w[149],w[150],w[145],w[146],w[153],w[154],R[37]);
dw[152] := aTotTang(w[149],w[150],w[145],w[146],w[153],w[154],R[37],
        w[151],w[152]) - (w[151]*w[152]/w[149]);
{Segment 38 Equations}
dw[153] := w[155];              dw[154] := w[156]/w[153];
dw[155] := (w[156]*w[156]/w[153]) - (GM*1000.0*1000.0*1000.0/(w[153]*w[153])) +
        aTotRad(w[153],w[154],w[149],w[150],w[157],w[158],R[38]);
dw[156] := aTotTang(w[153],w[154],w[149],w[150],w[157],w[158],R[38],
        w[155],w[156]) - (w[155]*w[156]/w[153]);
{Segment 39 Equations}
dw[157] := w[159];              dw[158] := w[160]/w[157];
dw[159] := (w[160]*w[160]/w[157]) - (GM*1000.0*1000.0*1000.0/(w[157]*w[157])) +
aTotRad(w[157],w[158],w[153],w[154],w[161],w[162],R[39]);
dw[160] := aTotTang(w[157],w[158],w[153],w[154],w[161],w[162],R[39],
        w[159],w[160]) - (w[159]*w[160]/w[157]);
{Segment 40 Equations}
dw[161] := w[163];              dw[162] := w[164]/w[161];
dw[163] := (w[164]*w[164]/w[161]) - (GM*1000.0*1000.0*1000.0/(w[161]*w[161])) +
aTotRad(w[161],w[162],w[157],w[158],w[165],w[166],R[40]);
dw[164] := aTotTang(w[161],w[162],w[157],w[158],w[165],w[166],R[40], {tangential
acceleration equation}
```

```
{Segment 41 Equations}
dw[165] := w[167];              dw[166] := w[168]/w[165];
dw[167] := (w[168]*w[168]/w[165]) - (GM*1000.0*1000.0*1000.0/(w[165]*w[165])) +
        aTotRad(w[165],w[166],w[161],w[162],w[169],w[170],R[41]);
dw[168] := aTotTang(w[165],w[166],w[161],w[162],w[169],w[170],R[41],
        w[167],w[168]) - (w[167]*w[168]/w[165]);
{Segment 42 Equations}
dw[169] := w[171];              dw[170] := w[172]/w[169];
dw[171] := (w[172]*w[172]/w[169]) - (GM*1000.0*1000.0*1000.0/(w[169]*w[169])) +
        aTotRad(w[169],w[170],w[165],w[166],w[173],w[174],R[42]);
dw[172] := aTotTang(w[169],w[170],w[165],w[166],w[173],w[174],R[42],
        w[171],w[172]) - (w[171]*w[172]/w[169]);
{Segment 43 Equations}
dw[173] := w[175];              dw[174] := w[176]/w[173];
dw[175] := (w[176]*w[176]/w[173]) - (GM*1000.0*1000.0*1000.0/(w[173]*w[173])) +
        aTotRad(w[173],w[174],w[169],w[170],w[177],w[178],R[43]);
dw[176] := aTotTang(w[173],w[174],w[169],w[170],w[177],w[178],R[43],
        w[175],w[176]) - (w[175]*w[176]/w[173]);
{Segment 44 Equations}
dw[177] := w[179];              dw[178] := w[180]/w[177];
dw[179] := (w[180]*w[180]/w[177]) - (GM*1000.0*1000.0*1000.0/(w[177]*w[177])) +
        aTotRad(w[177],w[178],w[173],w[174],w[181],w[182],R[44]);
dw[180] := aTotTang(w[177],w[178],w[173],w[174],w[181],w[182],R[44],
        w[179],w[180]) - (w[179]*w[180]/w[177]);
{Segment 45 Equations}
dw[181] := w[183];              dw[182] := w[184]/w[181];
        dw[183] := (w[184]*w[184]/w[181]) -
(GM*1000.0*1000.0*1000.0/(w[181]*w[181]))+
        aTotRad(w[181],w[182],w[177],w[178],w[185],w[186],R[45]);
dw[184] := aTotTang(w[181],w[182],w[177],w[178],w[185],w[186],R[45],
        w[183],w[184]) - (w[183]*w[184]/w[181]);
{Segment 46 Equations}
dw[185] := w[187];              dw[186] := w[188]/w[185];
dw[187] := (w[188]*w[188]/w[185]) - (GM*1000.0*1000.0*1000.0/(w[185]*w[185])) +
        aTotRad(w[185],w[186],w[181],w[182],w[189],w[190],R[46]);
dw[188] := aTotTang(w[185],w[186],w[181],w[182],w[189],w[190],R[46],
        w[187],w[188]) - (w[187]*w[188]/w[185]);
{Segment 47 Equations}
dw[189] := w[191];              dw[190] := w[192]/w[189];
dw[191] := (w[192]*w[192]/w[189]) - (GM*1000.0*1000.0*1000.0/(w[189]*w[189])) +
        aTotRad(w[189],w[190],w[185],w[186],w[193],w[194],R[47]);
dw[192] := aTotTang(w[189],w[190],w[185],w[186],w[193],w[194],R[47],
        w[191],w[192]) - (w[191]*w[192]/w[189]);
{Segment 48 Equations}
```

```
dw[193] := w[195];              dw[194] := w[196]/w[193];
dw[195] := (w[196]*w[196]/w[193]) - (GM*1000.0*1000.0*1000.0/(w[193]*w[193])) +
        aTotRad(w[193],w[194],w[189],w[190],w[197],w[198],R[48]);
dw[196] := aTotTang(w[193],w[194],w[189],w[190],w[197],w[198],R[48],
        w[195],w[196]) - (w[195]*w[196]/w[193]);
{Segment 49 Equations}
dw[197] := w[199];              dw[198] := w[200]/w[197];
dw[199] := (w[200]*w[200]/w[197]) - (GM*1000.0*1000.0*1000.0/(w[197]*w[197])) +
        aTotRad(w[197],w[198],w[193],w[194],w[201],w[202],R[49]);
dw[200] := aTotTang(w[197],w[198],w[193],w[194],w[201],w[202],R[49],
        w[199],w[200]) - (w[199]*w[200]/w[197]);
{Segment 50 Equations}
dw[201] := w[203];              dw[202] := w[204]/w[201];
dw[203] := (w[204]*w[204]/w[201]) - (GM*1000.0*1000.0*1000.0/(w[201]*w[201])) +
        aTotRad(w[201],w[202],w[197],w[198],w[205],w[206],R[50]);
dw[204] := aTotTang(w[201],w[202],w[197],w[198],w[205],w[206],R[50],
        w[203],w[204]) - (w[203]*w[204]/w[201]);
{Segment 51 Equations}
dw[205] := w[207];              dw[206] := w[208]/w[205];
dw[207] := (w[208]*w[208]/w[205]) - (GM*1000.0*1000.0*1000.0/(w[205]*w[205])) +
        aTotRad(w[205],w[206],w[201],w[202],w[209],w[210],R[51]);
dw[208] := aTotTang(w[205],w[206],w[201],w[202],w[209],w[210],R[51],
        w[207],w[208]) - (w[207]*w[208]/w[205]);
{Segment 52 Equations}
dw[209] := w[211];              dw[210] := w[212]/w[209];
dw[211] := (w[212]*w[212]/w[209]) - (GM*1000.0*1000.0*1000.0/(w[209]*w[209])) +
        aTotRad(w[209],w[210],w[205],w[206],w[213],w[214],R[52]);
dw[212] := aTotTang(w[209],w[210],w[205],w[206],w[213],w[214],R[52],
        w[211],w[212]) - (w[211]*w[212]/w[209]);
{Segment 53 Equations}
dw[213] := w[215];              dw[214] := w[216]/w[213];
dw[215] := (w[216]*w[216]/w[213]) - (GM*1000.0*1000.0*1000.0/(w[213]*w[213])) +
        aTotRad(w[213],w[214],w[209],w[210],w[217],w[218],R[53]);
        dw[216] :=
aTotTang(w[213],w[214],w[209],w[210],w[217],w[218],R[53],w[215],w[216]) -
(w[215]*w[216]/w[213]);
{Segment 54 Equations}
dw[217] := w[219];              dw[218] := w[220]/w[217];
dw[219] := (w[220]*w[220]/w[217]) - (GM*1000.0*1000.0*1000.0/(w[217]*w[217])) +
        aTotRad(w[217],w[218],w[213],w[214],w[221],w[222],R[54]);
dw[220] := aTotTang(w[217],w[218],w[213],w[214],w[221],w[222],R[54],
        w[219],w[220]) - (w[219]*w[220]/w[217]);
{Segment 55 Equations}
dw[221] := w[223];              dw[222] := w[224]/w[221];
dw[223] := (w[224]*w[224]/w[221]) - (GM*1000.0*1000.0*1000.0/(w[221]*w[221])) +
```

```
        aTotRad(w[221],w[222],w[217],w[218],w[225],w[226],R[55]);
dw[224] := aTotTang(w[221],w[222],w[217],w[218],w[225],w[226],R[55],
        w[223],w[224]) - (w[223]*w[224]/w[221]);
{Segment 56 Equations}
dw[225] := w[227];              dw[226] := w[228]/w[225];
dw[227] := (w[228]*w[228]/w[225]) - (GM*1000.0*1000.0*1000.0/(w[225]*w[225])) +
        aTotRad(w[225],w[226],w[221],w[222],w[229],w[230],R[56]);
dw[228] := aTotTang(w[225],w[226],w[221],w[222],w[229],w[230],R[56],
        w[227],w[228]) - (w[227]*w[228]/w[225]);
{Segment 57 Equations}
dw[229] := w[231];              dw[230] := w[232]/w[229];
dw[231] := (w[232]*w[232]/w[229]) - (GM*1000.0*1000.0*1000.0/(w[229]*w[229])) +
aTotRad(w[229],w[230],w[225],w[226],w[233],w[234],R[57]);
dw[232] := aTotTang(w[229],w[230],w[225],w[226],w[233],w[234],R[57],
        w[231],w[232]) - (w[231]*w[232]/w[229]);
{Segment 58 Equations}
dw[233] := w[235];              dw[234] := w[236]/w[233];
dw[235] := (w[236]*w[236]/w[233]) - (GM*1000.0*1000.0*1000.0/(w[233]*w[233])) +
        aTotRad(w[233],w[234],w[229],w[230],w[237],w[238],R[58]);
dw[236] := aTotTang(w[233],w[234],w[229],w[230],w[237],w[238],R[58],
        w[235],w[236]) - (w[235]*w[236]/w[233]);
{Segment 59 Equations}
dw[237] := w[239];              dw[238] := w[240]/w[237];
dw[239] := (w[240]*w[240]/w[237]) - (GM*1000.0*1000.0*1000.0/(w[237]*w[237])) +
        aTotRad(w[237],w[238],w[233],w[234],w[241],w[242],R[59]);
dw[240] := aTotTang(w[237],w[238],w[233],w[234],w[241],w[242],R[59],
        w[239],w[240]) - (w[239]*w[240]/w[237]);
{Segment 60 Equations}
dw[241] := w[243];              dw[242] := w[244]/w[241];
dw[243] := (w[244]*w[244]/w[241]) - (GM*1000.0*1000.0*1000.0/(w[241]*w[241])) +
        aTotRad(w[241],w[242],w[237],w[238],w[245],w[246],R[60]);
dw[244] := aTotTang(w[241],w[242],w[237],w[238],w[245],w[246],R[60],
        w[243],w[244]) - (w[243]*w[244]/w[241]);
{Segment 61 Equations}
dw[245] := w[247];              dw[246] := w[248]/w[245];
dw[247] := (w[248]*w[248]/w[245]) - (GM*1000.0*1000.0*1000.0/(w[245]*w[245])) +
        aTotRad(w[245],w[246],w[241],w[242],w[249],w[250],R[61]);
dw[248] := aTotTang(w[245],w[246],w[241],w[242],w[249],w[250],R[61],
        w[247],w[248]) - (w[247]*w[248]/w[245]);
{Segment 62 Equations}
dw[249] := w[251];              dw[250] := w[252]/w[249];
dw[251] := (w[252]*w[252]/w[249]) - (GM*1000.0*1000.0*1000.0/(w[249]*w[249])) +
        aTotRad(w[249],w[250],w[245],w[246],w[253],w[254],R[62]);
        dw[252] := aTotTang(w[249],w[250],w[245],w[246],w[253],w[254],R[62],
```

```
        w[251],w[252]) - (w[251]*w[252]/w[249]);
{Segment 63 Equations}
dw[253] := w[255];              dw[254] := w[256]/w[253];
dw[255] := (w[256]*w[256]/w[253]) - (GM*1000.0*1000.0*1000.0/(w[253]*w[253])) +
        aTotRad(w[253],w[254],w[249],w[250],w[257],w[258],R[63]);
dw[256] := aTotTang(w[253],w[254],w[249],w[250],w[257],w[258],R[63],
        w[255],w[256]) - (w[255]*w[256]/w[253]);
{Segment 64 Equations}
dw[257] := w[259];              dw[258] := w[260]/w[257];
dw[259] := (w[260]*w[260]/w[257]) - (GM*1000.0*1000.0*1000.0/(w[257]*w[257])) +
        aTotRad(w[257],w[258],w[253],w[254],w[261],w[262],R[64]);
dw[260] := aTotTang(w[257],w[258],w[253],w[254],w[261],w[262],R[64],
        w[259],w[260]) - (w[259]*w[260]/w[257]);
{Segment 65 Equations}
dw[261] := w[263];              dw[262] := w[264]/w[261];
dw[263] := (w[264]*w[264]/w[261]) - (GM*1000.0*1000.0*1000.0/(w[261]*w[261])) +
        aTotRad(w[261],w[262],w[257],w[258],w[265],w[266],R[65]);
dw[264] := aTotTang(w[261],w[262],w[257],w[258],w[265],w[266],R[65],
        w[263],w[264]) - (w[263]*w[264]/w[261]);
{Segment 66 Equations}
dw[265] := w[267];              dw[266] := w[268]/w[265];
dw[267] := (w[268]*w[268]/w[265]) - (GM*1000.0*1000.0*1000.0/(w[265]*w[265])) +
        aTotRad(w[265],w[266],w[261],w[262],w[269],w[270],R[66]);
dw[268] := aTotTang(w[265],w[266],w[261],w[262],w[269],w[270],R[66],
        w[267],w[268]) - (w[267]*w[268]/w[265]);
{Segment 67 Equations}
dw[269] := w[271];              dw[270] := w[272]/w[269];
dw[271] := (w[272]*w[272]/w[269]) - (GM*1000.0*1000.0*1000.0/(w[269]*w[269])) +
        aTotRad(w[269],w[270],w[265],w[266],w[273],w[274],R[67]);
dw[272] := aTotTang(w[269],w[270],w[265],w[266],w[273],w[274],R[67],
        w[271],w[272]) - (w[271]*w[272]/w[269]);
{Segment 68 Equations}
dw[273] := w[275];              dw[274] := w[276]/w[273];
dw[275] := (w[276]*w[276]/w[273]) - (GM*1000.0*1000.0*1000.0/(w[273]*w[273])) +
        aTotRad(w[273],w[274],w[269],w[270],w[277],w[278],R[68]);
dw[276] := aTotTang(w[273],w[274],w[269],w[270],w[277],w[278],R[68],
        w[275],w[276]) - (w[275]*w[276]/w[273]);
{Segment 69 Equations}
dw[277] := w[279];              dw[278] := w[280]/w[277];
dw[279] := (w[280]*w[280]/w[277]) - (GM*1000.0*1000.0*1000.0/(w[277]*w[277])) +
aTotRad(w[277],w[278],w[273],w[274],w[281],w[282],R[69]);
dw[280] := aTotTang(w[277],w[278],w[273],w[274],w[281],w[282],R[69],
        w[279],w[280]) - (w[279]*w[280]/w[277]);
{Segment 70 Equations}
```

```
dw[281] := w[283];              dw[282] := w[284]/w[281];
dw[283] := (w[284]*w[284]/w[281]) - (GM*1000.0*1000.0*1000.0/(w[281]*w[281])) +
        aTotRad(w[281],w[282],w[277],w[278],w[285],w[286],R[70]);
dw[284] := aTotTang(w[281],w[282],w[277],w[278],w[285],w[286],R[70],
        w[283],w[284]) - (w[283]*w[284]/w[281]);
{Segment 71 Equations}
dw[285] := w[287];              dw[286] := w[288]/w[285];
dw[287] := (w[288]*w[288]/w[285]) - (GM*1000.0*1000.0*1000.0/(w[285]*w[285])) +
        aTotRad(w[285],w[286],w[281],w[282],w[289],w[290],R[71]);
dw[288] := aTotTang(w[285],w[286],w[281],w[282],w[289],w[290],R[71],
        w[287],w[288]) - (w[287]*w[288]/w[285]);
{Segment 72 Equations}
dw[289] := w[291];              dw[290] := w[292]/w[289];
dw[291] := (w[292]*w[292]/w[289]) - (GM*1000.0*1000.0*1000.0/(w[289]*w[289])) +
        aTotRad(w[289],w[290],w[285],w[286],w[293],w[294],R[72]);
dw[292] := aTotTang(w[289],w[290],w[285],w[286],w[293],w[294],R[72],
        w[291],w[292]) - (w[291]*w[292]/w[289]);  {tangential acceleration equation}
{Segment 73 Equations}
dw[293] := w[295];              dw[294] := w[296]/w[293];
dw[295] := (w[296]*w[296]/w[293]) - (GM*1000.0*1000.0*1000.0/(w[293]*w[293])) +
        aTotRad(w[293],w[294],w[289],w[290],w[297],w[298],R[73]);
dw[296] := aTotTang(w[293],w[294],w[289],w[290],w[297],w[298],R[73],
        w[295],w[296]) - (w[295]*w[296]/w[293]);
{Segment 74 Equations}
dw[297] := w[299];              dw[298] := w[300]/w[297];
dw[299] := (w[300]*w[300]/w[297]) - (GM*1000.0*1000.0*1000.0/(w[297]*w[297])) +
        aTotRad(w[297],w[298],w[293],w[294],w[301],w[302],R[74]);
dw[300] := aTotTang(w[297],w[298],w[293],w[294],w[301],w[302],R[74],
        w[299],w[300]) - (w[299]*w[300]/w[297]);
{Segment 75 Equations}
dw[301] := w[303];              dw[302] := w[304]/w[301];
dw[303] := (w[304]*w[304]/w[301]) - (GM*1000.0*1000.0*1000.0/(w[301]*w[301])) +
        aTotRad(w[301],w[302],w[297],w[298],w[305],w[306],R[75]);
dw[304] := aTotTang(w[301],w[302],w[297],w[298],w[305],w[306],R[75],
        w[303],w[304]) - (w[303]*w[304]/w[301]);
{Segment 76 Equations}
dw[305] := w[307];              dw[306] := w[308]/w[305];
dw[307] := (w[308]*w[308]/w[305]) - (GM*1000.0*1000.0*1000.0/(w[305]*w[305])) +
        aTotRad(w[305],w[306],w[301],w[302],w[309],w[310],R[76]);
dw[308] := aTotTang(w[305],w[306],w[301],w[302],w[309],w[310],R[76],
        w[307],w[308]) - (w[307]*w[308]/w[305]);
{Segment 77 Equations}
dw[309] := w[311];              dw[310] := w[312]/w[309];
dw[311] := (w[312]*w[312]/w[309]) - (GM*1000.0*1000.0*1000.0/(w[309]*w[309])) +
        aTotRad(w[309],w[310],w[305],w[306],w[313],w[314],R[77]);
```

```
dw[312] := aTotTang(w[309],w[310],w[305],w[306],w[313],w[314],R[77],
        w[311],w[312]) - (w[311]*w[312]/w[309]);
{Segment 78 Equations}
dw[313] := w[315];              dw[314] := w[316]/w[313];
dw[315] := (w[316]*w[316]/w[313]) - (GM*1000.0*1000.0*1000.0/(w[313]*w[313])) +
        aTotRad(w[313],w[314],w[309],w[310],w[317],w[318],R[78]);
dw[316] := aTotTang(w[313],w[314],w[309],w[310],w[317],w[318],R[78],
        w[315],w[316]) - (w[315]*w[316]/w[313]);
{Segment 79 Equations}
dw[317] := w[319];              dw[318] := w[320]/w[317];
dw[319] := (w[320]*w[320]/w[317]) - (GM*1000.0*1000.0*1000.0/(w[317]*w[317])) +
        aTotRad(w[317],w[318],w[313],w[314],w[321],w[322],R[79]);
dw[320] := aTotTang(w[317],w[318],w[313],w[314],w[321],w[322],R[79],
        w[319],w[320]) - (w[319]*w[320]/w[317]);
{Segment 80 Equations}
dw[321] := w[323];              dw[322] := w[324]/w[321];
dw[323] := (w[324]*w[324]/w[321]) - (GM*1000.0*1000.0*1000.0/(w[321]*w[321])) +
        aTotRad(w[321],w[322],w[317],w[318],w[325],w[326],R[80]);
dw[324] := aTotTang(w[321],w[322],w[317],w[318],w[325],w[326],R[80],
        w[323],w[324]) - (w[323]*w[324]/w[321]);
{Segment 81 Equations}
dw[325] := w[327];              dw[326] := w[328]/w[325];
dw[327] := (w[328]*w[328]/w[325]) - (GM*1000.0*1000.0*1000.0/(w[325]*w[325])) +
        aTotRad(w[325],w[326],w[321],w[322],w[329],w[330],R[81]);
dw[328] := aTotTang(w[325],w[326],w[321],w[322],w[329],w[330],R[81],
        w[327],w[328]) - (w[327]*w[328]/w[325]);
{Segment 82 Equations}
dw[329] := w[331];              dw[330] := w[332]/w[329];
dw[331] := (w[332]*w[332]/w[329]) - (GM*1000.0*1000.0*1000.0/(w[329]*w[329])) +
        aTotRad(w[329],w[330],w[325],w[326],w[333],w[334],R[82]);
dw[332] := aTotTang(w[329],w[330],w[325],w[326],w[333],w[334],R[82],
        w[331],w[332]) - (w[331]*w[332]/w[329]);
{Segment 83 Equations}
dw[333] := w[335];              dw[334] := w[336]/w[333];
dw[335] := (w[336]*w[336]/w[333]) - (GM*1000.0*1000.0*1000.0/(w[333]*w[333])) +
        aTotRad(w[333],w[334],w[329],w[330],w[337],w[338],R[83]);
dw[336] := aTotTang(w[333],w[334],w[329],w[330],w[337],w[338],R[83],
        w[335],w[336]) - (w[335]*w[336]/w[333]);
{Segment 84 Equations}
dw[337] := w[339];              dw[338] := w[340]/w[337];
dw[339] := (w[340]*w[340]/w[337]) - (GM*1000.0*1000.0*1000.0/(w[337]*w[337])) +
        aTotRad(w[337],w[338],w[333],w[334],w[341],w[342],R[84]);
dw[340] := aTotTang(w[337],w[338],w[333],w[334],w[341],w[342],R[84],
        w[339],w[340]) - (w[339]*w[340]/w[337]);
{Segment 85 Equations}
```

```
dw[341] := w[343];              dw[342] := w[344]/w[341];
dw[343] := (w[344]*w[344]/w[341]) - (GM*1000.0*1000.0*1000.0/(w[341]*w[341])) +
        aTotRad(w[341],w[342],w[337],w[338],w[345],w[346],R[85]);
dw[344] := aTotTang(w[341],w[342],w[337],w[338],w[345],w[346],R[85],
        w[343],w[344]) - (w[343]*w[344]/w[341]);
{Segment 86 Equations}
dw[345] := w[347];              dw[346] := w[348]/w[345];
dw[347] := (w[348]*w[348]/w[345]) - (GM*1000.0*1000.0*1000.0/(w[345]*w[345])) +
        aTotRad(w[345],w[346],w[341],w[342],w[349],w[350],R[86]);
dw[348] := aTotTang(w[345],w[346],w[341],w[342],w[349],w[350],R[86],
        w[347],w[348]) - (w[347]*w[348]/w[345]);
{Segment 87 Equations}
dw[349] := w[351];              dw[350] := w[352]/w[349];
dw[351] := (w[352]*w[352]/w[349]) - (GM*1000.0*1000.0*1000.0/(w[349]*w[349])) +
        aTotRad(w[349],w[350],w[345],w[346],w[353],w[354],R[87]);
dw[352] := aTotTang(w[349],w[350],w[345],w[346],w[353],w[354],R[87],
        w[351],w[352]) - (w[351]*w[352]/w[349]);
{Segment 88 Equations}
dw[353] := w[355];              dw[354] := w[356]/w[353];
dw[355] := (w[356]*w[356]/w[353]) - (GM*1000.0*1000.0*1000.0/(w[353]*w[353])) +
        aTotRad(w[353],w[354],w[349],w[350],w[357],w[358],R[88]);
dw[356] := aTotTang(w[353],w[354],w[349],w[350],w[357],w[358],R[88],
        w[355],w[356]) - (w[355]*w[356]/w[353]);
{Segment 89 Equations}
dw[357] := w[359];              dw[358] := w[360]/w[357];
dw[359] := (w[360]*w[360]/w[357]) - (GM*1000.0*1000.0*1000.0/(w[357]*w[357])) +
        aTotRad(w[357],w[358],w[353],w[354],w[361],w[362],R[89]);
dw[360] := aTotTang(w[357],w[358],w[353],w[354],w[361],w[362],R[89],
        w[359],w[360]) - (w[359]*w[360]/w[357]);
{Segment 90 Equations}
dw[361] := w[363];              dw[362] := w[364]/w[361];
dw[363] := (w[364]*w[364]/w[361]) - (GM*1000.0*1000.0*1000.0/(w[361]*w[361])) +
        aTotRad(w[361],w[362],w[357],w[358],w[365],w[366],R[90]);
dw[364] := aTotTang(w[361],w[362],w[357],w[358],w[365],w[366],R[90],
        w[363],w[364]) - (w[363]*w[364]/w[361]);
{Segment 91 Equations}
dw[365] := w[367];              dw[366] := w[368]/w[365];
dw[367] := (w[368]*w[368]/w[365]) - (GM*1000.0*1000.0*1000.0/(w[365]*w[365])) +
        aTotRad(w[365],w[366],w[361],w[362],w[369],w[370],R[91]);
dw[368] := aTotTang(w[365],w[366],w[361],w[362],w[369],w[370],R[91],
        w[367],w[368]) - (w[367]*w[368]/w[365]);
{Segment 92 Equations}
dw[369] := w[371];              dw[370] := w[372]/w[369];
dw[371] := (w[372]*w[372]/w[369]) - (GM*1000.0*1000.0*1000.0/(w[369]*w[369])) +
        aTotRad(w[369],w[370],w[365],w[366],w[373],w[374],R[92]);
```

```
dw[372] := aTotTang(w[369],w[370],w[365],w[366],w[373],w[374],R[92],
        w[371],w[372]) - (w[371]*w[372]/w[369]);
{Segment 93 Equations}
dw[373] := w[375];              dw[374] := w[376]/w[373];
dw[375] := (w[376]*w[376]/w[373]) - (GM*1000.0*1000.0*1000.0/(w[373]*w[373])) +
        aTotRad(w[373],w[374],w[369],w[370],w[377],w[378],R[93]);
dw[376] := aTotTang(w[373],w[374],w[369],w[370],w[377],w[378],R[93],
        w[375],w[376]) - (w[375]*w[376]/w[373]);
{Segment 94 Equations}
dw[377] := w[379];              dw[378] := w[380]/w[377];
dw[379] := (w[380]*w[380]/w[377]) - (GM*1000.0*1000.0*1000.0/(w[377]*w[377])) +
        aTotRad(w[377],w[378],w[373],w[374],w[381],w[382],R[94]);
dw[380] := aTotTang(w[377],w[378],w[373],w[374],w[381],w[382],R[94],
        w[379],w[380]) - (w[379]*w[380]/w[377]);
{Segment 95 Equations}
dw[381] := w[383];              dw[382] := w[384]/w[381];
dw[383] := (w[384]*w[384]/w[381]) - (GM*1000.0*1000.0*1000.0/(w[381]*w[381]))+
        aTotRad(w[381],w[382],w[377],w[378],w[385],w[386],R[95]);
dw[384] := aTotTang(w[381],w[382],w[377],w[378],w[385],w[386],R[95],
        w[383],w[384]) - (w[383]*w[384]/w[381]);
{Segment 96 Equations}
dw[385] := w[387];              dw[386] := w[388]/w[385];
dw[387] := (w[388]*w[388]/w[385]) - (GM*1000.0*1000.0*1000.0/(w[385]*w[385])) +
        aTotRad(w[385],w[386],w[381],w[382],w[389],w[390],R[96]);
dw[388] := aTotTang(w[385],w[386],w[381],w[382],w[389],w[390],R[96],
        w[387],w[388]) - (w[387]*w[388]/w[385]);
{Segment 97 Equations}
dw[389] := w[391];              dw[390] := w[392]/w[389];
dw[391] := (w[392]*w[392]/w[389]) - (GM*1000.0*1000.0*1000.0/(w[389]*w[389])) +
        aTotRad(w[389],w[390],w[385],w[386],w[393],w[394],R[97]);
dw[392] := aTotTang(w[389],w[390],w[385],w[386],w[393],w[394],R[97],
        w[391],w[392]) - (w[391]*w[392]/w[389]);
{Segment 98 Equations}
dw[393] := w[395];              dw[394] := w[396]/w[393];
dw[395] := (w[396]*w[396]/w[393]) - (GM*1000.0*1000.0*1000.0/(w[393]*w[393])) +
        aTotRad(w[393],w[394],w[389],w[390],w[397],w[398],R[98]);
dw[396] := aTotTang(w[393],w[394],w[389],w[390],w[397],w[398],R[98],
        w[395],w[396]) - (w[395]*w[396]/w[393]);
{Segment 99 Equations}
dw[397] := w[399];              dw[398] := w[400]/w[397];
dw[399] := (w[400]*w[400]/w[397]) - (GM*1000.0*1000.0*1000.0/(w[397]*w[397])) +
        aTotRad(w[397],w[398],w[393],w[394],w[401],w[402],R[99]);
dw[400] := aTotTang(w[397],w[398],w[393],w[394],w[401],w[402],R[99],
        w[399],w[400]) - (w[399]*w[400]/w[397]);
```

```
{Segment 100 Equations}
dw[401] := w[403];              dw[402] := w[404]/w[401];
dw[403] := (w[404]*w[404]/w[401]) - (GM*1000.0*1000.0*1000.0/(w[401]*w[401])) +
        (aTenRadDown(w[401],w[402],w[397],w[398],R[100])) +
        aOblRad(w[401],w[402]);
dw[404] := (aTenTangDown(w[401],w[402],w[397],w[398],R[100]))  -
        (w[403]*w[404]/w[401]) + aEdtTang(w[401],R[100]) +
        aOblTang(w[401],w[402]);
        end;
{-------------------------------------------------------------------------------}
Procedure Conditions;
Var a0,a1,a2,a3,a4,a5,b0,b1,b2,b3,b4,b5,Dr,Di,xi,theta,D:    extended;
begin
w[1]:=1000.0*(rEarth+aLowPt);       w[2]:=0.0;
w[3]:=0.0;                          w[4]:=1000.0*(rEarth+aLowPt)*angvelCG;
{Segment 1 Conditions}
w[5]:=R[1]*1000.0;                  w[6]:=0.0;
w[7]:=0.0;                          w[8]:=1000.0*R[1]*angvelCG;
{Segment 2 Conditions}
w[9]:=R[2]*1000.0;                  w[10]:=0.0;
w[11]:=0.0;                         w[12]:=1000.0*R[2]*angvelCG;
{Segment 3 Conditions}
w[13]:=R[3]*1000.0;                 w[14]:=0.0;
w[15]:=0.0;                         w[16]:=1000.0*R[3]*angvelCG;
{Segment 4 Conditions}
w[17]:=R[4]*1000.0;                 w[18]:=0.0;
w[19]:=0.0;                         w[20]:=1000.0*R[4]*angvelCG;
{Segment 5 Conditions}
w[21]:=R[5]*1000.0;                 w[22]:=0.0;
w[23]:=0.0;                         w[24]:=1000.0*R[5]*angvelCG;
{Segment 6 Conditions}
w[25]:=R[6]*1000.0;                 w[26]:=0.0;
w[27]:=0.0;                         w[28]:=1000.0*R[6]*angvelCG;
{Segment 7 Conditions}
w[29]:=R[7]*1000.0;                 w[30]:=0.0;
w[31]:=0.0;                         w[32]:=1000.0*R[7]*angvelCG;
{Segment 8 Conditions}
w[33]:=R[8]*1000.0;                 w[34]:=0.0;
w[35]:=0.0;                         w[36]:=1000.0*R[8]*angvelCG;
{Segment 9 Conditions}
w[37]:=R[9]*1000.0;                 w[38]:=0.0;
w[39]:=0.0;                         w[40]:=1000.0*R[9]*angvelCG;
{Segment 10 Conditions}
w[41]:=R[10]*1000.0;                w[42]:=0.0;
w[43]:=0.0;                         w[44]:=1000.0*R[10]*angvelCG;
```

```
{Segment 11 Conditions}
w[45]:=R[11]*1000.0;                w[46]:=0.0;
w[47]:=0.0;                         w[48]:=1000.0*R[11]*angvelCG;
{Segment 12 Conditions}
w[49]:=R[12]*1000.0;                w[50]:=0.0;
w[51]:=0.0;                         w[52]:=1000.0*R[12]*angvelCG;
{Segment 13 Conditions}
w[53]:=R[13]*1000.0;                w[54]:=0.0;
w[55]:=0.0;                         w[56]:=1000.0*R[13]*angvelCG;
{Segment 14 Conditions}
w[57]:=R[14]*1000.0;                w[58]:=0.0;
w[59]:=0.0;                         w[60]:=1000.0*R[14]*angvelCG;
w[61]:=R[15]*1000.0;                w[62]:=0.0;
w[63]:=0.0;                         w[64]:=1000.0*R[15]*angvelCG;
{Segment 16 Conditions}
w[65]:=R[16]*1000.0;                w[66]:=0.0;
w[67]:=0.0;                         w[68]:=1000.0*R[16]*angvelCG;
{Segment 17 Conditions}
w[69]:=R[17]*1000.0;                w[70]:=0.0;
w[71]:=0.0;                         w[72]:=1000.0*R[17]*angvelCG;
{Segment 18 Conditions}
w[73]:=R[18]*1000.0;                w[74]:=0.0;
w[75]:=0.0;                         w[76]:=1000.0*R[18]*angvelCG;
{Segment 19 Conditions}
w[77]:=R[19]*1000.0;                w[78]:=0.0;
w[79]:=0.0;                         w[80]:=1000.0*R[19]*angvelCG;
{Segment 20 Conditions}
w[81]:=R[20]*1000.0;                w[82]:=0.0;
w[83]:=0.0;                         w[84]:=1000.0*R[20]*angvelCG;
{Segment 21 Conditions}
w[85]:=R[21]*1000.0;                w[86]:=0.0;
w[87]:=0.0;                         w[88]:=1000.0*R[21]*angvelCG;
{Segment 22 Conditions}
w[89]:=R[22]*1000.0;                w[90]:=0.0;
w[91]:=0.0;                         w[92]:=1000.0*R[22]*angvelCG;
{Segment 23 Conditions}
w[93]:=R[23]*1000.0;                w[94]:=0.0;
w[95]:=0.0;                         w[96]:=1000.0*R[23]*angvelCG;
{Segment 24 Conditions}
w[97]:=R[24]*1000.0;                w[98]:=0.0;
w[99]:=0.0;                         w[100]:=1000.0*R[24]*angvelCG;
{Segment 25 Conditions}
w[101]:=R[25]*1000.0;               w[102]:=0.0;
w[103]:=0.0;                        w[104]:=1000.0*R[25]*angvelCG;
```

```
{Segment 26 Conditions}
w[105]:=R[26]*1000.0;          w[106]:=0.0;
w[107]:=0.0;                   w[108]:=1000.0*R[26]*angvelCG;
{Segment 27 Conditions}
w[109]:=R[27]*1000.0;          w[110]:=0.0;
w[111]:=0.0;                   w[112]:=1000.0*R[27]*angvelCG;
{Segment 28 Conditions}
w[113]:=R[28]*1000.0;          w[114]:=0.0;
w[115]:=0.0;                   w[116]:=1000.0*R[28]*angvelCG;
{Segment 29 Conditions}
w[117]:=R[29]*1000.0;          w[118]:=0.0;
w[119]:=0.0;                   w[120]:=1000.0*R[29]*angvelCG;
{Segment 30 Conditions}
w[121]:=R[30]*1000.0;          w[122]:=0.0;
w[123]:=0.0;                   w[124]:=1000.0*R[30]*angvelCG;
{Segment 31 Conditions}
w[125]:=R[31]*1000.0;          w[126]:=0.0;
w[127]:=0.0;                   w[128]:=1000.0*R[31]*angvelCG;
{Segment 32 Conditions}
w[129]:=R[32]*1000.0;          w[130]:=0.0;
w[131]:=0.0;                   w[132]:=1000.0*R[32]*angvelCG;
{Segment 33 Conditions}
w[133]:=R[33]*1000.0;          w[134]:=0.0;
w[135]:=0.0;                   w[136]:=1000.0*R[33]*angvelCG;
{Segment 34 Conditions}
w[137]:=R[34]*1000.0;          w[138]:=0.0;
w[139]:=0.0;                   w[140]:=1000.0*R[34]*angvelCG;
{Segment 35 Conditions}
w[141]:=R[35]*1000.0;          w[142]:=0.0;
w[143]:=0.0;                   w[144]:=1000.0*R[35]*angvelCG;
{Segment 36 Conditions}
w[145]:=R[36]*1000.0;          w[146]:=0.0;
w[147]:=0.0;                   w[148]:=1000.0*R[36]*angvelCG;
{Segment 37 Conditions}
w[149]:=R[37]*1000.0;          w[150]:=0.0;
w[151]:=0.0;                   w[152]:=1000.0*R[37]*angvelCG;
{Segment 38 Conditions}
w[153]:=R[38]*1000.0;          w[154]:=0.0;
w[155]:=0.0;                   w[156]:=1000.0*R[38]*angvelCG;
{Segment 39 Conditions}
w[157]:=R[39]*1000.0;          w[158]:=0.0;
w[159]:=0.0;                   w[160]:=1000.0*R[39]*angvelCG;
{Segment 40 Conditions}
w[161]:=R[40]*1000.0;          w[162]:=0.0;
w[163]:=0.0;                   w[164]:=1000.0*R[40]*angvelCG;
```

```
{Segment 41 Conditions}
w[165]:=R[41]*1000.0;                w[166]:=0.0;
w[167]:=0.0;                         w[168]:=1000.0*R[41]*angvelCG;
{Segment 42 Conditions}
w[169]:=R[42]*1000.0;                w[170]:=0.0;
w[171]:=0.0;                         w[172]:=1000.0*R[42]*angvelCG;
{Segment 43 Conditions}
w[173]:=R[43]*1000.0;                w[174]:=0.0;
w[175]:=0.0;                         w[176]:=1000.0*R[43]*angvelCG;
{Segment 44 Conditions}
w[177]:=R[44]*1000.0;                w[178]:=0.0;
w[179]:=0.0;                         w[180]:=1000.0*R[44]*angvelCG;
{Segment 45 Conditions}
w[181]:=R[45]*1000.0;                w[182]:=0.0;
w[183]:=0.0;                         w[184]:=1000.0*R[45]*angvelCG;
{Segment 46 Conditions}
w[185]:=R[46]*1000.0;                w[186]:=0.0;
w[187]:=0.0;                         w[188]:=1000.0*R[46]*angvelCG;
{Segment 47 Conditions}
w[189]:=R[47]*1000.0;                w[190]:=0.0;
w[191]:=0.0;                         w[192]:=1000.0*R[47]*angvelCG;
{Segment 48 Conditions}
w[193]:=R[48]*1000.0;                w[194]:=0.0;
w[195]:=0.0;                         w[196]:=1000.0*R[48]*angvelCG;
{Segment 49 Conditions}
w[197]:=R[49]*1000.0;                w[198]:=0.0;
w[199]:=0.0;                         w[200]:=1000.0*R[49]*angvelCG;
{Segment 50 Conditions}
w[201]:=R[50]*1000.0;                w[202]:=0.0;
w[203]:=0.0;                         w[204]:=1000.0*R[50]*angvelCG;
{Segment 51 Conditions}
w[205]:=R[51]*1000.0;                w[206]:=0.0;
w[207]:=0.0;                         w[208]:=1000.0*R[51]*angvelCG;
{Segment 52 Conditions}
w[209]:=R[52]*1000.0;                w[210]:=0.0;
w[211]:=0.0;                         w[212]:=1000.0*R[52]*angvelCG;
{Segment 53 Conditions}
w[213]:=R[53]*1000.0;                w[214]:=0.0;
w[215]:=0.0;                         w[216]:=1000.0*R[53]*angvelCG;
{Segment 54 Conditions}
w[217]:=R[54]*1000.0;                w[218]:=0.0;
w[219]:=0.0;                         m/s}w[220]:=1000.0*R[54]*angvelCG;
{Segment 55 Conditions}
w[221]:=R[55]*1000.0;                w[222]:=0.0;
w[223]:=0.0;                         w[224]:=1000.0*R[55]*angvelCG;
```

```
{Segment 56 Conditions}
w[225]:=R[56]*1000.0;                w[226]:=0.0;
w[227]:=0.0;                         w[228]:=1000.0*R[56]*angvelCG;
{Segment 57 Conditions}
w[229]:=R[57]*1000.0;                w[230]:=0.0;
w[231]:=0.0;                         w[232]:=1000.0*R[57]*angvelCG;
{Segment 58 Conditions}
w[233]:=R[58]*1000.0;                w[234]:=0.0;
w[235]:=0.0;                         w[236]:=1000.0*R[58]*angvelCG;
{Segment 59 Conditions}
w[237]:=R[59]*1000.0;                w[238]:=0.0;
w[239]:=0.0;                         w[240]:=1000.0*R[59]*angvelCG;
{Segment 60 Conditions}
w[241]:=R[60]*1000.0;                w[242]:=0.0;
w[243]:=0.0;                         w[244]:=1000.0*R[60]*angvelCG;
{Segment 61 Conditions}
w[245]:=R[61]*1000.0;                w[246]:=0.0;
w[247]:=0.0;                         w[248]:=1000.0*R[61]*angvelCG;
{Segment 62 Conditions}
w[249]:=R[62]*1000.0;                w[250]:=0.0;
w[251]:=0.0;                         w[252]:=1000.0*R[62]*angvelCG;
{Segment 63 Conditions}
w[253]:=R[63]*1000.0;                w[254]:=0.0;
w[255]:=0.0;                         w[256]:=1000.0*R[63]*angvelCG;
{Segment 64 Conditions}
w[257]:=R[64]*1000.0;                w[258]:=0.0;
w[259]:=0.0;                         w[260]:=1000.0*R[64]*angvelCG;
{Segment 65 Conditions}
w[261]:=R[65]*1000.0;                w[262]:=0.0;
w[263]:=0.0;                         w[264]:=1000.0*R[65]*angvelCG;
{Segment 66 Conditions}
w[265]:=R[66]*1000.0;                w[266]:=0.0;
w[267]:=0.0;                          w[268]:=1000.0*R[66]*angvelCG;
{Segment 67 Conditions}
w[269]:=R[67]*1000.0;                w[270]:=0.0;
w[271]:=0.0;                         w[272]:=1000.0*R[67]*angvelCG;
{Segment 68 Conditions}
w[273]:=R[68]*1000.0;                w[274]:=0.0;
w[275]:=0.0;                         w[276]:=1000.0*R[68]*angvelCG;
{Segment 69 Conditions}
w[277]:=R[69]*1000.0;                w[278]:=0.0;
w[279]:=0.0;                         w[280]:=1000.0*R[69]*angvelCG;
{Segment 70 Conditions}
w[281]:=R[70]*1000.0;                w[282]:=0.0;
w[283]:=0.0;                         w[284]:=1000.0*R[70]*angvelCG;
```

```
{Segment 71 Conditions}
w[285]:=R[71]*1000.0;          w[286]:=0.0;
w[287]:=0.0;                   w[288]:=1000.0*R[71]*angvelCG;
{Segment 72 Conditions}
w[289]:=R[72]*1000.0;          w[290]:=0.0;
w[291]:=0.0;                   w[292]:=1000.0*R[72]*angvelCG;
{Segment 73 Conditions}
w[293]:=R[73]*1000.0;          w[294]:=0.0;
w[295]:=0.0;                   w[296]:=1000.0*R[73]*angvelCG;
{Segment 74 Conditions}
w[297]:=R[74]*1000.0;          w[298]:=0.0;
w[299]:=0.0;                   w[300]:=1000.0*R[74]*angvelCG;
{Segment 75 Conditions}
w[301]:=R[75]*1000.0;          w[302]:=0.0;
w[303]:=0.0;                   w[304]:=1000.0*R[75]*angvelCG;
{Segment 76 Conditions}
w[305]:=R[76]*1000.0;          w[306]:=0.0;
w[307]:=0.0;                   w[308]:=1000.0*R[76]*angvelCG;
{Segment 77 Conditions}
w[309]:=R[77]*1000.0;          w[310]:=0.0;
w[311]:=0.0;                   w[312]:=1000.0*R[77]*angvelCG;
{Segment 78 Conditions}
w[313]:=R[78]*1000.0;          w[314]:=0.0;
w[315]:=0.0;                   w[316]:=1000.0*R[78]*angvelCG;
{Segment 79 Conditions}
w[317]:=R[79]*1000.0;          w[318]:=0.0;
w[319]:=0.0;                   w[320]:=1000.0*R[79]*angvelCG;
{Segment 80 Conditions}
w[321]:=R[80]*1000.0;          w[322]:=0.0;
w[323]:=0.0;                   w[324]:=1000.0*R[80]*angvelCG;
{Segment 81 Conditions}
w[325]:=R[81]*1000.0;          w[326]:=0.0;
w[327]:=0.0;                   w[328]:=1000.0*R[81]*angvelCG;
{Segment 82 Conditions}
w[329]:=R[82]*1000.0;          w[330]:=0.0;
w[331]:=0.0;                   w[332]:=1000.0*R[82]*angvelCG;
{Segment 83 Conditions}
w[333]:=R[83]*1000.0;          w[334]:=0.0;
w[335]:=0.0;                   w[336]:=1000.0*R[83]*angvelCG;
{Segment 84 Conditions}
w[337]:=R[84]*1000.0;          w[338]:=0.0;
w[339]:=0.0;                   w[340]:=1000.0*R[84]*angvelCG;
{Segment 85 Conditions}
w[341]:=R[85]*1000.0;          w[342]:=0.0;
w[343]:=0.0;                   w[344]:=1000.0*R[85]*angvelCG;
```

```
{Segment 86 Conditions}
w[345]:=R[86]*1000.0;          w[346]:=0.0;
w[347]:=0.0;                   w[348]:=1000.0*R[86]*angvelCG;
{Segment 87 Conditions}
w[349]:=R[87]*1000.0;          w[350]:=0.0;
w[351]:=0.0;                   w[352]:=1000.0*R[87]*angvelCG;
{Segment 88 Conditions}
w[353]:=R[88]*1000.0;          w[354]:=0.0;
w[355]:=0.0;                   w[356]:=1000.0*R[88]*angvelCG;
{Segment 89 Conditions}
w[357]:=R[89]*1000.0;          w[358]:=0.0;
w[359]:=0.0;                   w[360]:=1000.0*R[89]*angvelCG;
{Segment 90 Conditions}
w[361]:=R[90]*1000.0;          w[362]:=0.0;
w[363]:=0.0;                   w[364]:=1000.0*R[90]*angvelCG;
{Segment 91 Conditions}
w[365]:=R[91]*1000.0;          w[366]:=0.0;
w[367]:=0.0;                   w[368]:=1000.0*R[91]*angvelCG;
{Segment 92 Conditions}
w[369]:=R[92]*1000.0;          w[370]:=0.0;
w[371]:=0.0;                   w[372]:=1000.0*R[92]*angvelCG;
{Segment 93 Conditions}
w[373]:=R[93]*1000.0;          w[374]:=0.0;
w[375]:=0.0;                   w[376]:=1000.0*R[93]*angvelCG;
{Segment 94 Conditions}
w[377]:=R[94]*1000.0;          w[378]:=0.0;
w[379]:=0.0;                   w[380]:=1000.0*R[94]*angvelCG;
{Segment 95 Conditions}
w[381]:=R[95]*1000.0;          w[382]:=0.0;
w[383]:=0.0;                   w[384]:=1000.0*R[95]*angvelCG;
{Segment 96 Conditions}
w[385]:=R[96]*1000.0;          w[386]:=0.0;
w[387]:=0.0;                   w[388]:=1000.0*R[96]*angvelCG;
{Segment 97 Conditions}
w[389]:=R[97]*1000.0;          w[390]:=0.0;
w[391]:=0.0;                   w[392]:=1000.0*R[97]*angvelCG;
{Segment 98 Conditions}
w[393]:=R[98]*1000.0;          w[394]:=0.0;
w[395]:=0.0;                   w[396]:=1000.0*R[98]*angvelCG;
{Segment 99 Conditions}
w[397]:=R[99]*1000.0;          w[398]:=0.0;
w[399]:=0.0;                   w[400]:=1000.0*R[99]*angvelCG;
{Segment 100 Conditions}
w[401]:=R[100]*1000.0;         w[402]:=0.0;
w[403]:=0.0;                   w[404]:=1000.0*R[100]*angvelCG;
```

```
        t := 0.0;
        end;
{--------------------------    MAIN    ----------------------------------}
begin
Parameters;
Segment;
Conditions;
Time:=0.0;
                repeat;
                        Runge(Equations,404,0.05,t,w);
                until t>Time;

        writeln(t/60.0:15:10,chr(9),((w[1]/1000.0)-
        6378.0):15:10,chr(9),w[2]/(2*Pi):15:10,chr(9),w[3]:15:10,chr(9),
        w[4]:15:10,chr(9));

        Time:=Time+60.0; {second number is seconds}
                until Time>2.1*60.0*60.0; {hours*60 min*60 sec}
end.
```

Appendix B: Ascent Optimization Code

```
{-------------------------------------------------------------------------------}
program Ascent ;    {ascent problem with no throttling        Aerodynamics included}
                        {Assumes an engine cutoff at specified altitude with a
                        ballistic coast to the tether lower tip altitude
                        Assumes a vertical ascent to a specified altitude less than 11 km}

{-------------------------------------------------------------------------------}
USES SIOUX;
Type    vec = array[1..20] of extended;
                mat = array[1..20,1..20] of extended;
Var             x,z,w,dw,q,dq    : vec;
                OutputFile  : TEXT;
                i,j,ghost                                   :integer;

                Pi,             {Pi r not squared, Pi r round}
                GM,             {gravitational parameter for Earth}
                rE,             {Radius of Earth's surface 6378.135 km}
                gE,             {gravitational acceleration of the earth}
                gamma,          {specific heat of air}
                Dia,            {Vehicle Diameter}
                Area,           {Vehicle x-sectional area}
                mpl,            {mass of vehicle payload, samples and crew}
                ms,             {mass of empty spacecraft structure}
                mf,             {mass of fuel}
                m0,             {initial total mass of the vehicle}
                numeng,         {number of engines on vehicle}
                throttle,       {percent of engine thrust}
                mdot,           {mass flow rate of engines}
                Isp,            {specific impulse}
                timeempty,      {time at which fuel tank is empty}
                aT,             {Altitude of tether cg at perigee}
                Alowpt,         {Altidude of tether lower tip at perigee}
                rT,             {Radius of tether Cg}
                cg2lowpt,       {Length of tether from cg to lower tip}
                vT,             {Velocity of tether orbit}
                angvelT,        {Angular velocity of tether orbit}
                rLowpt,         {radius of tether lower point, apogee radius Vehicle}
                vLowpt,         {velocity at tether lower tip}
                rstar,          {distance scaling variable}
                vstar,          {velocity scaling variable}
                tstar,          {time scaling variable}
                pitch,          {altitude at which controlled flight begins}
```

```
rcut,          {desired engine cutoff radius}
deltaV,        {Apogee manuever used to "fine tune" LV tajectory}
oec,           {orbital energy constant}
KAC,           {Kepler Area Constant}
eccen,         {eccentricity of the orbit prior to circularization}
rp,            {perigee radius of trajectory (prior to circularization)}
a,             {semimajor axis of trajectory (prior to circularization)}
vcut,          {path velocity at engine cutoff}
vthetacut,     {tangential velocity at engine cutoff}
vrcut,         {radial velocity at engine cutoff}
altClimb,      {instantaneous Launch vehicle altitude during vertical
               climb in meters}
TClimb,        {Air temperature during vertical climb}
PClimb,        {Air pressure during vertical climb}
RhoClimb,      {Air density during vertical climb}
MClimb,        {Vehicle Mach Number during climb}
CdClimb,       {Vehicle Coefficient of Drag during climb}
DragClimb,     {Drag force on the vehicle during vertical climb}
ThrustClimb,   {Thrust force during climb}
vmagsq,        {square of the magnitude of velocity}
phi,           {angle of flight path to local horizontal}
alfa,          {angle of thrust vector to flight path}
csphal,        {cosine of phi plus alpha}
snphal,        {sine of phi plus alpha}
csphi,         {cosine of phi}
snphi,         {sine of phi}
altCon,        { Launch Vehicle Altitude during controlled flight}
TempCon,       {Air temperature during controlled flight}
PCon,          {Air pressure during controlled flight}
RhoCon,        {Air density during controlled flight}
MCon,          {Vehicle Mach Number during controlled flight}
CdCon,         {Vehicle Coefficient of Drag during controlled flight}
DragCon,       {Drag force on the vehicle during controlled flight}
ThrustCon,     {Thrust force during controlled flight}
DragConND,     {Non Dimensional Drag force on the vehicle during
               controlled flight}
ThrustConND,{Non Dimensional Thrust force during controlled flight}
accel,         {acceleration of the vehicle in g's }
mprop,         {mass of propellant consumed during ascent}
rfinal,        {radius at engine cutoff}
vrfinal,       {radial velocity at engine cutoff}
vthetafinal,{tangential velocity at engine cutoff}
phicut,        {angle to local horizontal at engine cutoff}
time,          {time during controlled flight}
t,             {time during vertically constrained flight}
```

```
                H,              {Hamiltonian of the system}
                za,             {costate variable for radius}
                zb,             {costate variable for radial velocity}
                zc,             {costate variable for tangential velocity}
                treal,          {unscaled time}
                tcon            {time during controlled flight}
                :extended;

{--------------------------------------------------------------------------------}
Procedure Parameters;
        begin
        SIOUXSettings.tabspaces := 0;
        {CONSTANTS}
        Pi:= 3.14159265358979323846 2643;
        GM:=3.98601e14;             {Grav Parameter of Earth, m3/s2}
        rE := 6378000.0;            {m, radius of Earth}
        gE:= 9.81; {m/s^2}
        gamma:=      1.4;           {Air gamma}

        {VEHICLE CONFGURATION  PLEASE SPECIFY}
        {Based on DC-Y vehicle with 1 J-2 engines}

        Dia:= 9.15;                         {Vehicle Diameter in meters}
        Area:= Pi*(Dia/2)*(Dia/2);  {Vehicle x-sectional Area in meters}
        mpl:= 10000.0;                      {kg mass payload crew and samples}
        ms:= 36000.0;                       {kg mass structure}
        mf:= 470000.0;                      {kg of fuel initial}
        m0 := mpl+mf+ms;            {46681 kg initial mass of vehicle}
        numeng:=1.0;
        throttle:=0.75;
        mdot :=1646.0*numeng*throttle; {kg/s}
        Isp:= 425.0;                {ISP of Engine}
        timeempty:=mf/mdot;

        {TETHER CONFIGURATION  PLEASE SPECIFY}
        aT := 2000000.0;                    {m}
        Alowpt := 200000.0;                 {m}
        cg2lowpt := aT - Alowpt;    {m}
        rT:= aT + rE;                       {m}
        vT:=sqrt(GM/rT);                    {m/s}
        angvelT:= vT/rT;                    {radians/second}
        rLowpt:= rE + Alowpt;               {m}
        vLowpt:= angvelT*rLowpt;    {m/s}
        {For SSTO set aT to same value as Alowpt and specify an Apogee orbit
        adjustment delta V to circularize the orbit}
```

```
        {SCALING VARIABLES}
        rstar:=rE;
        vstar:=sqrt(GM/rE);
        tstar:=sqrt(rE*rE*rE/GM);

        {FLIGHT VARIABLES}
        pitch:= 1000.0;                         {pitchover altitude in meters}
        rcut:=  rE + 100000.0;                  {engine cutoff radius  m}
        deltaV:= 0.0;                           {Apogee orbit adjustment m/s}
                {Must be set to a value >0.0 for SSTO}
        oec:= ((vLowpt-deltaV)*(vLowpt-deltaV)) - (2.0*GM/rLowpt);
        KAC:= (vLowpt-deltaV)*rLowpt;
        eccen:=sqrt(1.0 + (KAC*KAC*oec/(GM*GM)));
        rp:=rLowpt*(1.0-eccen)/(1.0+eccen);
        a:=(rLowpt+rp)/2.0;
        vcut:=sqrt(GM/rcut)*sqrt(2.0-(rcut/a));
        vthetacut:=rLowpt*(vLowpt-deltaV)/rcut;{rapogee*vapogee/r}
        vrcut:= sqrt((vcut*vcut) - (vthetacut*vthetacut));
        end;
{-------------------------------------------------------------------------}
{                          NUMERICAL ROUTINES                             }
{-------------------------------------------------------------------------}
function arctan2(r,s : extended) : extended;
        var q: extended;
        begin
                if s= 0.0 then
                        if r>0 then q:=Pi/2 else q:=-Pi/2
                else
                        q:= arctan(r/s);
                if s<0.0 then
                        if r<0.0 then q:=q-Pi else q:= q+Pi;
                if r=0.0 then q:= 0.0;
                arctan2:= q;
        end;
{-------------------------------------------------------------------------}
procedure Runge( procedure de(t:extended; var y,dy:vec); n :integer; h :extended;
                                        var t :extended; var y :vec );
        var     y1,f1,f2,f3,f4 :vec;
                i : integer;
                h2 : extended;
        begin
                h2:= h/2;

                de( t,y,f1 );
```

```
                for i:=1 to n do y1[i]:= y[i] + h2*f1[i];
                t:=t + h2;

                de( t,y1,f2 );
                for i:=1 to n do y1[i]:= y[i] + h2*f2[i];

                de( t,y1,f3 );
                for i:=1 to n do y1[i]:= y[i] + h *f3[i];
                t:=t + h2;

                de( t,y1,f4 );
                for i:=1 to n do y[i]:= y[i] + h/6*(f1[i]+2*(f2[i]+f3[i])+f4[i]);
        end;
{-------------------------------------------------------------------------}
Procedure Vecroot( procedure Vector(var x,y :vec); var x,ybase :vec;
                                        ndim :integer; delx :extended );
        type mat = array[1..20,1..20] of extended;
        var     y,x1                    :vec;
                jacob                   :mat;
                errlast,err,det  :extended;
                i,j,k                   :integer;

        procedure System(n :integer; var a :mat; var b,x :vec; var det :extended);
                var     i,j,m:  integer;
                        k:   extended;
                begin
                        det := 1.0;
                        for m := 1 to n-1 do begin
                                det := det*a[m,m];
                                for i := m+1 to n do begin
                                        k := a[i,m]/a[m,m];
                                        for j := m+1 to n do a[i,j] := a[i,j] - k * a[m,j];
                                        b[i] := b[i] - k*b[m];
                                end;
                        end;
                        det := det * a[n,n];
                        for m := n downto 1 do begin
                                x[m] := b[m]/a[m,m];
                                for i := 1 to m -1 do b[i] := b[i] - x[m]*a[i,m];
                        end;
                end;
        begin
                errlast:= inf;
                for k:= 1 to 25 do begin
                        Vector( x,ybase );
```

```
                    err:= 0;
                    for i:= 1 to ndim do err:= err + sqr(ybase[i]);
                    err:= sqrt(err);
                    {writeln('Vecroot : ', err);}
                    if (err<10) and (k>3) and (err>=errlast) then exit(Vecroot);
                    errlast:= err;

                    { Calculate Jacobian }
                    for j:= 1 to ndim do begin
                            x[j]:= x[j] + delx;
                            Vector( x,y );
                            for i:= 1 to ndim do jacob[i,j]:= (y[i]-ybase[i]) / delx;
                            x[j]:= x[j] - delx
                    end;

                    { Solve for correction vector and correct x }
                    System( ndim,jacob,ybase,x1,det );
                    for i:= 1 to ndim do x[i]:= x[i] - x1[i];
            end;
            {writeln('Solution not found in "Vecroot"')}
    end;
{-------------------------------------------------------------------------------}
Procedure Climbeqs (y:extended; var q,dq :vec);
begin

{atmosphere calculations}
    altClimb:=(q[2]*rstar)-rstar;   {altitude}
    TClimb:=15.04-(0.00649*altClimb);
    PClimb:=101.29*(exp(5.256*ln((TClimb+273.1)/288.08)));
    RhoClimb:=PClimb/(0.2869*(TClimb+273.1));

    {Mach Number Calculation}
    MClimb:=q[4]/sqrt(gamma*RhoClimb*TClimb);

    {Ceoefficient of drag}
    If MClimb < 1.0 Then CdClimb:= 0.075;
    If MClimb > 1.0 Then CdClimb:= 0.20;
    If MClimb > 1.4 Then CdClimb:= 0.18;
    If MClimb > 2.0 Then CdClimb:= 0.14;
    If MClimb > 3.0 Then CdClimb:= 0.135;
    If MClimb > 4.0 Then CdClimb:= 0.12;
    If MClimb > 5.0 Then CdClimb:= 0.11;
    If MClimb > 6.0 Then CdClimb:= 0.10;
    If MClimb > 7.0 Then CdClimb:= 0.095;
    If MClimb > 8.0 Then CdClimb:= 0.090;
```

```
        DragClimb:=CdClimb*RhoClimb*q[4]*q[4]*Area/2.0;
        ThrustClimb:=mdot*gE*Isp;           {N}

        dq[1] := -mdot*tstar/m0;                                    {mdot}
        dq[2] := q[4];                                                  {rdot}
        dq[3] := q[5]/q[2];             {thetadot}
        dq[4] := (q[5]*q[5]/q[2]) + (-1.0/(q[2]*q[2])) + ThrustClimb/(q[1]*m0*gE) –
                DragClimb/(q[1]*m0*gE);{vrdot}
        dq[5] := 0.0;                   {vthetadot}
end;
{-------------------------------------------------------------------------------}
Procedure Climb;
begin
        q[1] := 1.0;    {mass0}
        q[2] := 1.0;    {r0}
        q[3] := 0.0;    {theta0}
        q[4] := 0.0;    {vr0}
        q[5] := 0.0;    {vtheta0}


t := 0.0;
        repeat

                Runge( Climbeqs, 5, 0.001, t, q );
                writeln(t*tstar:10:5,chr(9), q[1]*m0:10:5,chr(9), (q[2]-1.0)*rstar:10:5,
                 chr(9) ,q[4]*vstar:10:5,chr(9));

        until q[2] >  (rE+pitch)/rstar;
writeln(t:10:5,chr(9),q[1]:10:5,chr(9),q[2]:10:5,chr(9),q[3]:10:5,chr(9),q[4]:10:5,chr(9),
q[5]:10:5,chr(9));
end;
{-------------------------------------------------------------------------------}
Procedure Equations( y:extended; var w,dw :vec );

        begin

        vmagsq:= (w[5]*w[5]) + (w[4]*w[4]);     {magnitude velocity squared}
        phi:= arctan2(w[4],w[5]);               {angle to local horizon}
        alfa:= arctan2(w[7],w[8])-phi;          {control law}
        csphal:= cos(alfa + phi);
        snphal:= sin(alfa + phi);
        csphi:=cos(phi);
        snphi:=sin(phi);
```

```
{atmosphere calculations}
altCon:=(w[2]*rstar)-rstar;     {altitude}

If altCon < 11000.0 Then begin
TempCon:=15.04-(0.00649*altCon);
PCon:=101.29*(exp(5.256*ln((TempCon+273.1)/288.08)));
end;

If altCon > 11000.0 then begin
TempCon:=-56.46;
PCon:=22.65*(exp(1.73 - (0.000157*altCon)));
end;

If altCon > 25000.0 then begin
TempCon:=(0.00299*altCon) - 131.21;
PCon:=2.488*(exp(-11.388*ln((TempCon+273.1)/216.6)));
end;

{Density and Mach Number Calculation}
RhoCon:=PCon/(0.2869*(TempCon+273.1));
MCon:=sqrt(vmagsq)/sqrt(gamma*RhoCon*TempCon);

{Ceoefficient of drag}
If MCon < 1.0 Then CdCon:= 0.075;
If MCon > 1.0 Then CdCon:= 0.20;
If MCon > 1.4 Then CdCon:= 0.18;
If MCon > 2.0 Then CdCon:= 0.14;
If MCon > 3.0 Then CdCon:= 0.135;
If MCon > 4.0 Then CdCon:= 0.12;
If MCon > 5.0 Then CdCon:= 0.11;
If MCon > 6.0 Then CdCon:= 0.10;
If MCon > 7.0 Then CdCon:= 0.095;
If MCon > 8.0 Then CdCon:= 0.090;

DragCon:=CdCon*RhoCon*vmagsq*Area/2.0;
ThrustCon:=mdot*gE*Isp;
ThrustConND:=ThrustCon/(w[1]*m0*gE);
DragConND:=DragCon/(w[1]*m0*gE);

accel:= (ThrustCon-DragCon)/(w[1]*m0*gE);                    {F/m*go}


dw[1] := -mdot*tstar/m0;          {mdot}
dw[2] := w[4];                    {rdot}
dw[3] := w[5]/w[2];               {thetadot}
```

```
        dw[4] := (w[5]*w[5]/w[2]) - (1.0/(w[2]*w[2])) + (ThrustConND*snphal) –
        (DragConND*snphi);                      {vrdot}
        dw[5] := (-w[4]*w[5]/w[2]) + (ThrustConND*csphal) - (DragConND*csphi);
        {vthetadot}
        dw[6] := (w[7]*( (w[5]*w[5]/(w[2]*w[2])) - (2.0/(w[2]*w[2]*w[2])) )) + w[8]*(
                -w[4]*w[5]/(w[2]*w[2]) );                               {zrdot}
        dw[7] := -w[6] + (w[7]*((-ThrustConND*csphal*w[5]/vmagsq) +
                (CdCon*RhoCon*Area*((2.0*w[4]*snphi)+(w[5]*csphi))/
                (2.0*w[1]*m0*gE)))) + (w[8]*( (w[5]/w[2]) +
                (ThrustConND*snphal*w[5]/vmagsq) + (CdCon*RhoCon*Area*
                ((2.0*w[4]*csphi)-(w[5]*snphi))/(2.0*w[1]*m0*gE))));
                        {zvrdot}
        dw[8] := (w[7]*( (-2.0*w[5]/w[2]) + (ThrustConND*csphal*w[4]/vmagsq) +
                (CdCon*RhoCon*Area*((2.0*w[5]*snphi)-(w[4]*csphi))/
                (2.0*w[1]*m0*gE)))) + (w[8]*( (w[4]/w[2]) – (ThrustConND*snphal*
                w[4] / vmagsq) +(CdCon*RhoCon*Area*((2.0*w[5]*csphi)
                +(w[4]*snphi))/(2.0*w[1]*m0*gE))));          {zvthetadot}

        end;
{-------------------------------------------------------------------------------}
Procedure Solve;
Var a0,a1,a2,a3,a4,a5,b0,b1,b2,b3,b4,b5,Dr,Di,xi,theta,D:    extended;
        begin

        {Initial Conditions}
        w[1] := q[1];   {mass0}
        w[2] := q[2];   {r0}
        w[3] := q[3];   {Theta0}
        w[4] := q[4];   {vr0}
        w[5] := q[5];   {vtheta0}
        w[6] := x[1];
        w[7] := x[2];
        w[8] := x[3];

        tcon := t;

        repeat
                Runge( Equations, 8, 0.001, tcon, w );

        until tcon > time;


H:= -1.0 + (w[6]*w[4]) + (w[7]*( (w[5]*w[5]/w[2]) - (1.0/(w[2]*w[2])) +
(ThrustConND*snphal) - (DragConND*snphi) ) ) + (w[8]*( (-w[4]*w[5]/w[2]) +
(ThrustConND*csphal) - (DragConND*csphi) ) );
```

```
end;
{-------------------------------------------------------------------------------}
procedure Vecset( var x,z :vec);
        begin
                Solve;
                z[1]:= H;
                z[2]:= (w[2]*rstar) - rcut;
                z[3]:= (w[4]*vstar) - vrcut;
        end;
{-----------------------------------------------------}
Procedure Search;
        begin
                x[1] := 0.5;            {guess conditions of costate vector}
                x[2] := 0.5;
                x[3] := 0.5;

                Vecroot(Vecset, x,z,3,1e-5);
        end;
{---------------------------  MAIN  ----------------------------------}
begin
Parameters;
        Climb;
time:=(timeempty-50.0)/tstar; {t}
Repeat
                Search;
                treal:=tcon*tstar;
                mprop := m0*(w[1]);
                rfinal := (w[2]*rstar)-rE;
                vrfinal := w[4]*vstar;
                vthetafinal := w[5]*vstar;
                za:= x[1];
                zb:= x[2];
                zc:= x[3];
                phicut:=arctan2(vrcut,vthetacut);

writeln( treal:15:5, chr(9), (w[1]*m0)-(ms+mpl):15:10, chr(9), vrfinal:15:10, chr(9),
        vthetafinal:15:10, chr(9), H:15:5, chr(9), phi:15:10, chr(9), accel:15:10, chr(9));
writeln(  vcut:15:10, chr(9), rcut-rE:15:10, chr(9), vrcut:15:10,chr(9), vthetacut:15:10,
        chr(9), H:15:5,chr(9), phicut:15:10, chr(9));
writeln( za:15:5,chr(9),zb:15:10,chr(9),zc:15:10,chr(9));

time := time + 0.001;
        until time >timeempty/tstar;
end.
```

Appendix C: Rendezvous Code

```
{--------------------------------------------------------------------------------}
program rend3;
{Goal: Calculates first and second delta V need to effect rendezvous if the launch
vehicle arrives at apogee at a different time then the tether

Assumptions:  Tether vertically oriented in an circular orbit
              Launch vehicle on ballistic trajectory
              Rendezvous should occur at launch vehicle apogee
              Noncoplanar orbits
              Intersection of orbital planes occuring at the rendezvous point
              Analysis starts with Launchvehicle at 9 degrees of true anomaly before
              rendezvous (appox 100 km altitude)
{--------------------------------------------------------------------------------}

USES SIOUX;
Type    vec = array[1..20] of extended;
              mat = array[1..20,1..20] of extended;
Var
              x,z,w,dw    : vec;
              OutputFile  : TEXT;
              {Tether coordinate system centered on tether Cg}
              GM,           {Gravitational parameter of the Earth}
              Pi,           {Pi are round}
              rEarth,       {Radius of the Earth}
              aT,           {Altitude of tether cg at perigee}
              Alowpt,       {Altidude of tether lower tip at perigee}
              rT,           {Radius of tether Cg}
              error,        {Amount of true anomaly that the tether is off by at
                            point of rendezvous}
              nuT,          {Initial tether cg true anomaly}
              cg2lowpt,     {Length of tether from cg to lower tip}
              vT,           {Velocity of tether orbit}
              angvelT,      {Angular velocity of tether orbit}
              gT,           {Gravity at tether center}
              rTtime,       {time varying tether radius}
              nuTdoubdot,   {time varying tether nu double dot}
              incLV,        {Rocket trajectory inclination relative to tether orbit}
              nuLV,         {initial true anomaly of Launch Vehicle}
              raLV,         {Apogee radius of Launch Vehicle}
              vaLV,         {Apogee velocity of Launch Vehicle}
              CLV,          {Kepler Area constant of Launch Vehicle Trajectory}
              hLV,          {Orbital energy constant of Launch Vehicle Trajectory}
```

pLV, {Parameter of Launch Vehicle Trajectory}
eLV, {Eccentricity of Launch Vehicle Trajectory}
aLV, {Semimajor axis of Launch Vehicle Trajectory}
rLV, {Launch Vehicle initial radial position}
gLV, {gravity at Launch Vehicle altitude}
nudotLV, {Initial Launch Vehicle true anomaly rate of change}
pathangLV, {Initial Launch Vehicle Path angle}
vLV, {Initial Launch Vehicle Velocity}
EaLV, {Launch Vehicle Eccentric anomaly at start of analysis}
Tstarttoapogee, {Time from start of analysis to Launch vehicle apogee}
x0, {x coordinate initial relative distance in tether coord system}
y0, {y coordinate initial relative distance in tether coord system}
z0, {z coordinate initial relative distance in tether coord system}
dist, {distance from launch vehicle to tether end}
fx, {x coordinate external acceleration applied to launch vehicle in tether coordinate system}
fy, {y coordinate external acceleration applied to launch vehicle in tether coordinate system}
fz, {x coordinate external acceleration applied to launch vehicle in tether coordinate system}
xTpc, {Tether cg x coordinate in planetocentric coord system}
yTpc, {Tether cg y coordinate in planetocentric coord system}
zTpc, {Tether cg z coordinate in planetocentric coord system}
xLVpc, {Launch Vehicle x coordinate in planetocentric coord system}
yLVpc, {Launch Vehicle y coordinate in planetocentric coord system}
zLVpc, {Launch Vehicle z coordinate in planetocentric coord system}
xdot0, {initial x relative volcity coordinate in tether coordinate system}
ydot0, {initial y relative volcity coordinate in tether coordinate system}
zdot0, {initial z relative volcity coordinate in tether coordinate system}
vTx, {Tether velocity x coordinate in tether coord system}
vTy, {Tether velocity y coordinate in tether coord system}
vTz, {Tether velocity z coordinate in tether coord system}
vLVx, {Launch Vehicle x velocity in LV frame}
vLVy, {Launch Vehicle y velocity in LV frame}
vLVxPCLV, {Launch Vehicle x velocity in PC frame aligned to LV orbital plane}
vLVyPCLV, {Launch Vehicle y velocity in PC frame aligned to LV orbital plane}
vLVzPCLV, {Launch Vehicle z velocity in PC frame aligned to LV orbital plane}
vLVxPC, {Launch Vehicle velocity x coordinate in planetocentric coord system aligned to Tether orbital plane}
vLVyPC, {Launch Vehicle velocity y coordinate in planetocentric coord system aligned to Tether orbital plane}
vLVzPC, {Launch Vehicle velocity z coordinate in planetocentric

```
                                coord system aligned to Tether orbital plane}
            vLVxTC,{Launch Vehicle velocity x coordinate in tether coord system}
            vLVyTC,{Launch Vehicle velocity y coordinate in tether coord system}
            vLVzTC,{Launch Vehicle velocity z coordinate in tether coord system}
            relvelx,        {Relative velocity x component in tether coord system}
            relvely,        {Relative velocity y component in tether coord system}
            relvelz,        {Relative velocity z component in tether coord system}
            DelVx1,         {Required x Delta V for maneuver 1}
            DelVy1,         {Required y Delta V for maneuver 1}
            DelVz1,         {Required z Delta V for maneuver 1}
            DelV1,          {Total required delta V for maneuver 1}
            DelVx2,         {Required x Delta V for maneuver 2}
            DelVy2,         {Required y Delta V for maneuver 2}
            DelVz2,         {Required z Delta V for maneuver 2}
            DelV2,          {Total required delta V for maneuver 2}
            test,
            rtime,          {time varying radius}
            t,              {time in R-K interation}
            Time,
            rho,            {Time varying magnitude of distance vector from tether cg
                            to launch vehicle}
            phi,            {Angle between y axis and rho vector}
            rLVtime         {Time varying Launch vehicle radius}
            :extended;
{-------------------------------------------------------------------------}
function arctan2(r,s : extended) : extended;
    var q: extended;
    begin
        if s= 0.0 then
            if r>0 then q:=3.14159265358979323846264 3/2
            else q:=-3.14159265358979323846264 3/2
        else
            q:= arctan(r/s);
        if s<0.0 then
            if r<0.0 then q:=q-3.14159265358979323846264 3
            else q:= q+3.14159265358979323846264 3;
        if r=0.0 then q:= 0.0;
        arctan2:= q;
    end;
{-------------------------------------------------------------------------------}
function arcsin(r : extended) : extended;
    var q: extended;
    begin
        if r= 0.0 then q:=0.0
        else
```

```
                    if r = 1.0 then q:=3.14159265358979323846264 3/2
                    else
                    if r =-1.0 then q:=-3.14159265358979323846264 3/2
                    else q:= arctan(r/sqrt (1-(r*r)));
                if r=0.0 then q:= 0.0;
                arcsin:= q;
        end;
{-------------------------------------------------------------------------------}
Procedure Parameters;
        begin
        SIOUXSettings.tabspaces := 0;
        Pi := 3.14159265358979323846264 3;
        GM := 398601.0;  {Gravitational Parameter (Earth), km3/s2}
        rEarth := 6378.0;       {Radius of Earth, km}
        {Tether Cg Orbital characteristics}
        {SPECIFY}
        aT := 2100.0;                   {km}
        Alowpt := 200.0;                {km}
        error:= 0.1;{degrees of true anomaly that the tether end misses the rendezvous}
        {Positive degrees means the tether end is behind the LV at apogee}
        {Negative degrees means the tether end is ahead of the LV at apogee}

        cg2lowpt := aT - Alowpt;        {km}
        rT:= aT + rEarth;       {km}
        vT:=sqrt(GM/rT);                {km/s}
        angvelT:= vT/rT;                {radians/second}

        {Launch Vehicle Trajectory Charachteristics}
        {SPECIFY}
        incLV:=         0.0*Pi/180.0;           {radians}
        {positive angle means launch takes place south of orbital plane of tether
         negative angle means launch takes place north of orbital plane of tether}
        nuLV:=          171.0*Pi/180.0;                 {radians}

        raLV:=rEarth+Alowpt;                    {km}
        vaLV:=angvelT*raLV;                             {km/s}
        CLV:=raLV*vaLV;                                 {km^2/s}
        hLV:=(vaLV*vaLV)-(2*GM/raLV);  {(km/s)^2)}
        pLV:=CLV*CLV/GM;                                {km}
        eLV:=sqrt(1+(CLV*CLV*hLV/(GM*GM)));
        aLV:=GM/abs(hLV);                       {km}
        rLV:=pLV/(1+(eLV*cos(nuLV)));{km}
        nudotLV:=CLV/(rLV*rLV);         {Radians per second}

        {Kepler equation analysis to calculate initial true anamaly of tether}
```

```
EaLV:=(Pi/2.0)-arcsin((aLV-rLV)/(aLV*eLV));
Tstarttoapogee:= (Pi-EaLV-(eLV*-sin(EaLV)))/(sqrt(GM/(aLV*aLV*aLV)));
nuT:= Pi-(Tstarttoapogee*angvelT)-(error*Pi/180.0);
{Calculate initial relative distances}
{Tether coord in planetocentric coord sys}
xTpc:=rT*sin(Pi-nuT);                                          {km}
yTpc:=rT*cos(Pi-nuT);                                          {km}
zTpc:=0.0;                                                     {km}
{Launch Vehicle coord in planetocentric coord sys}
xLVpc:=      rLV*sin(Pi-nuLV)*cos(incLV);      {km}
yLVpc:=      rLV*cos(Pi-nuLV);   {km}
zLVpc:=      rLV*sin(Pi-nuLV)*-sin(incLV);
{wrong km}
{Relative Distance in Tether coordinate system centered on tether end}
x0:=   ((xLVpc-xTpc)*cos(Pi-nuT))-((yLVpc-yTpc)*sin(Pi-nuT));
{km}
y0:=   ((xLVpc-xTpc)*sin(Pi-nuT))+((yLVpc-yTpc)*cos(Pi-nuT));        {km}
z0:=   zLVpc-zTpc;  {km}
dist:=sqrt((x0*x0)+(y0*y0)+(z0*z0));

{CALCULATE INITIAL RELATIVE VELOCITIES}
vTx:=-vT;
vTy:=0.0;
vTz:=0.0;

pathangLV:=arctan2(eLV*sin(nuLV),(1+(eLV*cos(nuLV))));
vLV:=sqrt((GM*2.0/rLV)-(GM/aLV));
vLVx:=-vLV*cos(pathangLV);
vLVy:=vLV*sin(pathangLV);

vLVxPCLV:=(vLVx*cos(Pi-nuLV))+(vLVy*sin(Pi-nuLV));
vLVyPCLV:=(vLVy*cos(Pi-nuLV))-(vLVx*sin(Pi-nuLV));
vLVzPCLV:= 0.0;

vLVxPC:=cos(incLV)*vLVxPCLV;
vLVyPC:=vLVyPCLV;
vLVzPC:=-sin(incLV)*vLVxPCLV;

vLVxTC:=(vLVxPC*cos(Pi-nuT))-(vLVyPC*sin(pi-nuT));
vLVyTC:=(vLVyPC*cos(Pi-nuT))+(vLVxPC*sin(pi-nuT));
vLVzTC:=vLVzPC;

relvelx:=vLVxTC-vTx+(angvelT*y0);
relvely:=vLVyTC-vTy-(angvelT*x0);
relvelz:=vLVzTC-vTz;
```

```
        end;
{-------------------------------------------------------------------}
procedure Vecroot( procedure Vector(var x,y :vec); var x,ybase :vec;
                                        ndim :integer; delx :extended );
        type mat = array[1..20,1..20] of extended;
        var     y,x1                    :vec;
                jacob                   :mat;
                errlast,err,det  :extended;
                i,j,k                   :integer;

        procedure System(n :integer; var a :mat; var b,x :vec; var det :extended);
                var     i,j,m:  integer;
                        k:   extended;
                begin
                        det := 1.0;
                        for m := 1 to n-1 do begin
                                det := det*a[m,m];
                                for i := m+1 to n do begin
                                        k := a[i,m]/a[m,m];
                                        for j := m+1 to n do a[i,j] := a[i,j] - k * a[m,j];
                                        b[i] := b[i] - k*b[m];
                                end;
                        end;
                        det := det * a[n,n];
                        for m := n downto 1 do begin
                                x[m] := b[m]/a[m,m];
                                for i := 1 to m -1 do b[i] := b[i] - x[m]*a[i,m];
                        end;
                end;

        begin
                errlast:= inf;
                for k:= 1 to 25 do begin
                        Vector( x,ybase );
                        err:= 0;
                        for i:= 1 to ndim do err:= err + sqr(ybase[i]);
                        err:= sqrt(err);
                        {writeln('Vecroot : ', err);}
                        if (err<10) and (k>3) and (err>=errlast) then exit(Vecroot);
                        errlast:= err;

                        { Calculate Jacobian }
                        for j:= 1 to ndim do begin
                                x[j]:= x[j] + delx;
```

```
                        Vector( x,y );
                        for i:= 1 to ndim do jacob[i,j]:= (y[i]-ybase[i]) / delx;
                        x[j]:= x[j] - delx
                    end;

                    { Solve for correction vector and correct x }
                    System( ndim,jacob,ybase,x1,det );
                    for i:= 1 to ndim do x[i]:= x[i] - x1[i];
                end;
                writeln('Solution not found in "Vecroot"')
        end;
{-------------------------------------------------------------------------------}
procedure Runge( procedure de(t:extended; var y,dy:vec); n :integer; h :extended;
                                        var t :extended; var y :vec );
        var     y1,f1,f2,f3,f4 :vec;
                i : integer;
                h2 : extended;
        begin
                h2:= h/2;

                de( t,y,f1 );
                for i:=1 to n do y1[i]:= y[i] + h2*f1[i];
                t:=t + h2;

                de( t,y1,f2 );
                for i:=1 to n do y1[i]:= y[i] + h2*f2[i];

                de( t,y1,f3 );
                for i:=1 to n do y1[i]:= y[i] + h *f3[i];
                t:=t + h2;

                de( t,y1,f4 );
                for i:=1 to n do y[i]:= y[i] + h/6*(f1[i]+2*(f2[i]+f3[i])+f4[i]);
        end;
{-------------------------------------------------------------------------}
Procedure Equations( y:extended; var w,dw :vec );

        begin

        gT:=GM/(rT*rT);                         {km/s^2}
        rho:=   sqrt((w[1]*w[1])+(w[3]*w[3])+(w[5]*w[5]));
        phi:=   (Pi/2.0)-arcsin(-w[3]/rho);
        rLVtime:=sqrt((rT*rT)+(rho*rho)-(2.0*rT*rho*cos(phi)));
        gLV:=GM/((rLVtime)*(rLVtime));              {km/s^2}
```

```
        dw[1] := w[2];                  {x dot equation}
        dw[2] := (-gLV*w[1]/(rLVtime)) + fx + (2.0*angvelT*w[4]) +
                 (angvelT*angvelT*w[3]);          {x double dot equation}
        dw[3] := w[4];                  {y dot equation}
        dw[4] := (-gLV*(w[3]+rT)/(rLVtime)) + fy + gT - (2.0*angvelT*w[2]) +
                 (angvelT*angvelT*w[3]);    {y double dot equation}
        dw[5] := w[6];                  {z dot equation}
        dw[6] := (-gLV*w[5]/(rLVtime)) + fz;       {z double dot equation}

        end;
{-------------------------------------------------------------------------------}
Procedure Solve;
Var a0,a1,a2,a3,a4,a5,b0,b1,b2,b3,b4,b5,Dr,Di,xi,theta,D:    extended;
        begin
        w[1]:=x0;                               {x distance}
        w[2]:=x[1];                             {x velocity}
        w[3]:=y0;                               {y distance}
        w[4]:=x[2];                             {y velocity}
        w[5]:=z0;                               {z distance}
        w[6]:=x[3];                             {z velocity}

        t := 0.0;

        repeat
                Runge( Equations, 6, 0.01, t, w );
        {writeln(t:15:10,chr(9),w[1]:15:10,chr(9),w[2]:15:10,chr(9),w[3]:15:10,chr(9),
                w[4]:15:10,chr(9),w[5]:15:10,chr(9),w[6]:15:10,chr(9));}
        until t > Time;

end;
{---------------------------------------------}
procedure Vecset( var x,z :vec);
        begin
                Solve;
                 z[1]:= w[1];
                 z[2]:= w[3] + cg2lowpt;        {Equal to zero at final time}
                 z[3]:= w[5];
        end;
{-----------------------------------------------------}
Procedure Search;
        begin
                x[1] := 0.0;
                x[2] := 0.5;      {Initial Guess}
                x[3] := 0.0;
                Vecroot(Vecset, x,z,3,1e-5);
```

```
end;
{--------------------------   MAIN   ----------------------------------}
begin

Parameters;
writeln(Tstarttoapogee:15:10,chr(9));

writeln(relvelx:15:10,chr(9),relvely:15:10,chr(9),relvelz:15:10,chr(9));
writeln(x0:15:10,chr(9),y0:15:10,chr(9),z0:15:10,chr(9));

Time:=100.0;
        Repeat
                Search;
                xdot0:=x[1];
                ydot0:=x[2];
                zdot0:=x[3];

                {CALCULATE INITIAL RELATIVE VELOCITIES}
                DelVx1:=xdot0-relvelx;
                DelVy1:=ydot0-relvely;
                DelVz1:=zdot0-relvelz;
                DelV1:=sqrt((DelVx1*DelVx1)+(DelVy1*DelVy1)+(DelVz1*DelVz1));

                DelVx2:=w[2];{Why do this need to come out}
                DelVy2:=w[4];
                DelVz2:=w[6];
                DelV2:=sqrt((DelVx1*DelVx1)+(DelVy1*DelVy1)+(DelVz1*DelVz1));

        writeln(t:15:10,chr(9),w[1]:15:10,chr(9),w[3]:15:10,chr(9),w[5]:15:10,chr(9));
        {distances}
        writeln(t:15:10,chr(9),DelVx1:15:10,chr(9),DelVy1:15:10,chr(9),
                DelVz1:15:10,chr(9));
        writeln(t:15:10,chr(9),DelVx2:15:10,chr(9),DelVy2:15:10,chr(9),
                DelVz2:15:10,chr(9));
        {writeln(t:15:10,chr(9),relvelx:15:10,chr(9),relvely:15:10,chr(9),
                relvelz:15:10,chr(9));}

                Time:=Time+10.0; {time step in 10 seconds}
        until Time>200.0;

end.
```

Vita

Stephen Edward Stasko was born on May 31, 1976 in Portsmouth, Virginia, the son of Edward and Marie Stasko. Soon after his birth his family moved to Philadelphia, Pennsylvania, where he received he graduated from Archbishop Ryan High School in June of 1994. He entered Drexel University in September of 1994, where, as a cooperative student, he held several jobs in the course of his undergraduate education, both in the university as a teaching assistant and in the VIZ Corporation as a design engineer. In June of 1999 he graduated Magna Cum Laude from Drexel with a Bachelor of Science in mechanical engineering. Shortly afterwards, in August of 1999, he entered graduate study working towards a Masters Degree in Aerospace Engineering at the University of Tennessee Space Institute under Dr. Gary Flandro. His research area included orbital mechanics and trajectory optimization. He received his Master of Science degree in December of 2001. Immediately following that he began pursuing his Doctor of Philosophy degree in Aerospace Engineering, continuing to work under Dr. Gary Flandro.